

# Geometry-based structural analysis and design via discrete stress functions



**Marina Konstantatou**

Supervisor: Prof. Allan McRobie

Department of Engineering  
University of Cambridge

This dissertation is submitted for the degree of  
*Doctor of Philosophy*





To Max,



## **Declaration**

I hereby declare that except where specific reference is made to the work of others, the contents of this dissertation are original and have not been submitted in whole or in part for consideration for any other degree or qualification in this, or any other university. This dissertation is my own work and contains nothing which is the outcome of work done in collaboration with others, except as specified in the text and Acknowledgements. This dissertation contains fewer than 65,000 words including appendices, bibliography, footnotes, tables and equations and has fewer than 150 figures.

Marina Konstantatou  
September 2019



## Acknowledgements

Firstly, I would like to thank my supervisor Prof. Allan McRobie and Bill Baker. I am grateful to Allan for all his support and input in my five years in Cambridge, our numerous discussions, the intellectual wondering in the Inglis building and the catastrophe theory sculptures in his back garden. I am grateful to Bill for initiating this PhD research 5 years ago in an ad-hoc meeting at Bishopsgate, before I even started my studies at Cambridge and before I even knew what a reciprocal diagram is, and for our exciting collaborations and stimulating discussions ever since in Cambridge and Chicago. This thesis would not have been possible without them.

I would also like to thank Prof. Chris Calladine for giving me the opportunity to work with him and learn from his research style and experience – it was invaluable. These collaborations have been a privilege and I cannot overstate their importance for my academic and personal development.

I would like to acknowledge all my friends at the department of engineering, particularly from the CDT FIBE, for our nice times together and for creating a supportive atmosphere for each other. Also, I would like to thank my friends from Corpus Christi College – I will cherish our long-lasting friendships and always remember our days and nights at Leckhampton gardens.

I would like to thank my colleagues at ETH Zürich and at the University of Pennsylvania for being so hospitable during my academic secondments there. Specifically, I want to thank Dr. Pierluigi D’Acunto at the Chair of Structural Design of Prof. Joseph Schwartz for our fruitful collaborations over the last years and Dr. Masoud Akbarzadeh at Penn Design for a productive term in Philly. Also, I would like to thank the structures team at SOM Chicago for their input and support in my two visits – summer of 2014 and spring of 2019.

Lastly, I would like to thank my family for their unconditional love and support, my partner for lightening up the dark patches and my friends from Athens for our shared experiences from 2005 onward.



## **Abstract**

This PhD thesis proposes a direct and unified method for generating global static equilibrium for 2D and 3D reciprocal form and force diagrams based on reciprocal discrete stress functions. This research combines and reinterprets knowledge from Maxwell's 19th century graphic statics, projective geometry and rigidity theory to provide an interactive design and analysis framework through which information about designed structural performance can be geometrically encoded in the form of the characteristics of the stress function. This method results in novel, intuitive design and analysis freedoms.

In contrast to contemporary computational frameworks, this method is direct and analytical. In this way, there is no need for iteration, the designer operates by default within the equilibrium space and the mathematically elegant nature of this framework results in its wide applicability as well as in added educational value. Moreover, it provides the designers with the agility to start from any one of the four interlinked reciprocal objects (form diagram, force diagram, corresponding stress functions).

This method has the potential to be applied in a wide range of case studies and fields. Specifically, it leads to the design, analysis and load-path optimisation of tension-and-compression 2D and 3D trusses, tensegrities, the exoskeletons of towers, and in conjunction with force density, to tension-and-compression grid-shells, shells and vaults. Moreover, the abstract nature of this method leads to wide cross-disciplinary applicability, such as 2D and 3D discrete stress fields in structural concrete and to a geometrical interpretation of yield line theory.





# Table of contents

<b>List of figures</b>	<b>xv</b>
<b>1 Introduction</b>	<b>1</b>
1.1 Research statement . . . . .	2
1.2 Objectives . . . . .	2
1.3 Methodology . . . . .	3
1.4 Outline of Chapters . . . . .	4
<b>2 Literature review</b>	<b>7</b>
2.1 Graphic statics . . . . .	7
2.1.1 Maxwell's contribution to graphic statics . . . . .	12
2.2 Projective Geometry . . . . .	14
2.2.1 Pole and polar reciprocals . . . . .	17
2.3 N-polytopes and planarity . . . . .	22
2.4 Reciprocal diagrams and Airy stress functions . . . . .	24
2.5 Polarities as a tool for deriving reciprocal polyhedra . . . . .	32
2.6 The role of polarities in structural analysis . . . . .	38
2.7 Minkowski sums . . . . .	42
2.8 Summary . . . . .	44
<b>3 Geometry-based structural analysis</b>	<b>45</b>
3.1 Introduction . . . . .	45
3.2 Graphic statics . . . . .	47
3.2.1 Counting the states of self-stress . . . . .	47
3.2.2 2D global static equilibrium . . . . .	62
3.2.3 3D global static equilibrium . . . . .	64
3.2.4 N-connected reciprocal diagrams . . . . .	68
3.3 Graphic kinematics . . . . .	72

3.3.1	Introduction . . . . .	72
3.3.2	2D and 3D graphic kinematics . . . . .	72
3.4	Summary . . . . .	74
<b>4</b>	<b>Geometry-based optimisation</b>	<b>77</b>
4.1	Introduction . . . . .	77
4.2	Optimal trusses . . . . .	77
4.3	Method . . . . .	81
4.4	Summary . . . . .	84
<b>5</b>	<b>Geometry-based design</b>	<b>85</b>
5.1	Truss design by analysis . . . . .	85
5.2	Vault, shell and grid-shell design via the Airy stress function . . . . .	86
5.2.1	Force Density Method . . . . .	91
5.2.2	Methodology . . . . .	92
5.3	Summary . . . . .	98
<b>6</b>	<b>Applications</b>	<b>99</b>
6.1	Implementation and case studies . . . . .	100
6.1.1	2D trusses . . . . .	102
6.1.2	3D trusses and polyhedral spatial structures . . . . .	108
6.1.3	Statically balanced tensegrity mechanisms . . . . .	112
6.1.4	Large infrastructure: Towers . . . . .	114
6.1.5	Large infrastructure: Vaults, shells and grid-shells . . . . .	119
6.2	Summary . . . . .	130
<b>7</b>	<b>Impact study and cross-disciplinary applications</b>	<b>131</b>
7.1	Introduction . . . . .	131
7.2	Discrete stress fields in reinforced concrete . . . . .	132
7.2.1	Methodology . . . . .	136
7.2.2	Practical interpretation and considerations . . . . .	138
7.2.3	Implementation and results . . . . .	143
7.3	Yield line mechanisms . . . . .	149
7.3.1	Methodology . . . . .	150
7.3.2	Implementation and results . . . . .	152
7.4	Summary . . . . .	152

<b>8</b>	<b>Conclusions</b>	<b>155</b>
8.1	Discussion . . . . .	155
8.2	Contributions . . . . .	155
8.3	Impact . . . . .	157
8.4	Future work . . . . .	158
8.5	Personal Reflection . . . . .	158
	<b>References</b>	<b>161</b>
	<b>Appendix A Algebraic description of Lemma.01</b>	<b>171</b>



# List of figures

2.1	Varignon's introduction of the polygon of forces and funicular polygon . . .	8
2.2	Table of standardised form and force diagrams for 2D trusses . . . . .	9
2.3	Graphic statics hand drawings of elaborated 2D trusses in Wolfe . . . . .	11
2.4	Projective-Affine-Euclidean geometry – primitive concepts and metrics . .	15
2.5	Conics In Projective Geometry . . . . .	15
2.6	Cremona's dual configuration . . . . .	16
2.7	Poncelet Duality of Projective Geometry . . . . .	18
2.8	Pole and Polar construction on the plane - Case 1 . . . . .	20
2.9	Pole and Polar construction in 3-space - Case 1 . . . . .	20
2.10	Pole and Polar construction on the plane - Case 2 . . . . .	21
2.11	Pole and Polar construction in 3-space - Case 2 . . . . .	21
2.12	Desargues configuration . . . . .	23
2.13	Constituent geometrical elements of a regular K5 . . . . .	27
2.14	Construction of Rankine reciprocal for a K5 through spheres . . . . .	28
2.15	Cremona 3D reciprocal diagrams . . . . .	29
2.16	Vector 3D reciprocal diagrams . . . . .	30
2.17	Spiderwebs: Schlegel diagrams as projections on polyhedra . . . . .	31
2.18	Geometrical correspondence of reciprocal tetrahedra . . . . .	33
2.19	Polarity induced by a paraboloid of revolution . . . . .	34
2.20	Equivalent mathematical descriptions of polarities . . . . .	35
2.21	Duality between spatial trusses and hinged sheetworks . . . . .	40
2.22	The application of polarities in structural analysis and design . . . . .	41
2.23	2D and 3D Minkowski sums . . . . .	43
3.1	Icosahedral (Jessen's) Tensegrity . . . . .	48
3.2	Steffen Polyhedron . . . . .	48
3.3	Geometrical interpretation of states of self-stress: a triangulated structure .	50

3.4	Geometrical interpretation of states of self-stress: dependent and independent elements . . . . .	51
3.5	Lemma.01 . . . . .	52
3.6	Lemma.02 . . . . .	54
3.7	Summary of states of self-stress of Maxwell Figure 3 . . . . .	55
3.8	States of self-stress of Maxwell Figure 3 . . . . .	56
3.9	Self-stressed tensile structure $F(71, 133, 64)$ . . . . .	59
3.10	Self-stressed tensile structure $F(71, 133, 64)$ : Geometrical constraint 1 . . .	60
3.11	Self-stressed tensile structure $F(71, 133, 64)$ : Geometrical constraint 2 . . .	61
3.12	Reciprocal tetrahedra induced by a paraboloid of revolution . . . . .	63
3.13	Polarity induced by a hyper-paraboloid of revolution . . . . .	65
3.14	Rankine reciprocals induced by a hyper-paraboloid of revolution . . . . .	67
3.15	2-connected form and force diagrams . . . . .	70
3.16	2-connected reciprocal polyhedra . . . . .	71
3.17	The parallelogram of virtual work joining the force and displacement polygons	73
3.18	Graphic kinematics in 2D and 3D . . . . .	74
3.19	Graphic kinematics in 3D for a spoked cube . . . . .	75
4.1	Optimum trusses: Michell torsion ball . . . . .	78
4.2	Optimum trusses: Michell 2D optimum truss . . . . .	79
4.3	Geometry-based optimisation for the 2D case . . . . .	83
4.4	Geometry-based optimisation for the 3D case . . . . .	84
5.1	The Airy stress function <i>correcting</i> a truss towards static equilibrium . . . .	87
5.2	User-friendly interface of the Airy force density tool . . . . .	94
5.3	Flow chart of the Airy force density tool . . . . .	95
5.4	The Airy force density tool can be used both for compression-only and compression-and-tension structures . . . . .	96
5.5	The Airy force density tool provides design freedoms . . . . .	97
6.1	Reciprocal Airy stress functions for Maxwell Figure IV and 4 . . . . .	101
6.2	Reciprocal Airy stress functions for a Pratt truss . . . . .	102
6.3	Reciprocal Airy stress functions for a Pratt truss - Global and local transfor- mations . . . . .	103
6.4	Incorporation of boundary conditions and external forces in the form diagram	104
6.5	Pairs of spatial reciprocal diagrams in a Rankine 3D configuration - Global and local transformations . . . . .	105

6.6	Designing a tensile stadium roof in static equilibrium via an Airy stress function - Case 1 . . . . .	106
6.7	Designing a tensile stadium roof in static equilibrium via an Airy stress function - Case 2 . . . . .	107
6.8	Graphic statics and kinematics analysis of a 3-Prism tensegrity . . . . .	110
6.9	Graphic statics and kinematics analysis of a Jessen icosahedron . . . . .	111
6.10	Graphic statics and kinematics analysis for the Steffen flexible polyhedron .	112
6.11	Dynamic Minkowski sums for a statically balanced tensegrity mechanism .	113
6.12	Polyhedral lifting of Maxwell's Figure IV and generalisation in the 4 <sup>th</sup> dimension . . . . .	115
6.13	Rankine force reciprocal of a self-stressed tower in static equilibrium . . . .	116
6.14	Various typologies of trusses of towers in static equilibrium . . . . .	117
6.15	CAD and CAM fabrication of a tower prototype . . . . .	118
6.16	Reciprocal form and force diagrams of the Great Court Roof (GCR) of the British Museum . . . . .	121
6.17	Minkowski sum of a grid-shell resulting from a 2-connected stress function	122
6.18	Minkowski sum of a grid-shell resulting from a 1-connected stress function	123
6.19	Resulting grid-shell of the GCR by using two different versions of a 2-connected Airy stress functions . . . . .	124
6.20	Resulting grid-shell of the GCR by using two different versions of a 1-connected Airy stress functions . . . . .	125
6.21	2-connected reciprocal polyhedral Airy stress function of the GCR . . . . .	126
6.22	Resulting grid-shell of the GCR by using 2-connected Airy stress functions and force density . . . . .	127
6.23	1-connected reciprocal polyhedral Airy stress function of the GCR . . . . .	128
6.24	Resulting grid-shell of the GCR by using 1-connected Airy stress functions and force density . . . . .	129
7.1	Topology of a strut-and-tie model and corresponding Airy stress function .	139
7.2	Minkowski sum as a stress field . . . . .	140
7.3	Compatible stress field generated via the Airy stress function . . . . .	141
7.4	Geometrical interpretation of continuous loading . . . . .	144
7.5	Graphic statics generated stress field - 2D Case 1 . . . . .	145
7.6	Graphic statics generated stress field - 2D Cases 2 and 3 . . . . .	146
7.7	Graphic statics generated stress field - 2D Cases 4 and 5 . . . . .	147
7.8	Graphic statics generated stress field - 3D Case . . . . .	148
7.9	Common cases of yield line patterns and their graphic statics interpretation	153





# Chapter 1

## Introduction

Graphic statics is a 19<sup>th</sup> century design and analysis methodology for structures in static equilibrium. After a 20<sup>th</sup> century decline, they are back largely due to great advances in Computer Aided Design (CAD). They hold the promise of bridging the increasingly large gap between structural and architectural design, between architects and engineers, through the universal language of geometry. As a result, they contribute to a shift towards materially efficient structures where the structural performance informs the early conceptual design stages. Graphic statics is often praised for the intrinsic visual and intuitive nature, specifically, with regard to the output – reciprocal form and force diagrams where geometrical elements represent structural members or their internal forces.

CAD developments have opened the door to the revival of graphic statics, to their generalisation in the 3<sup>rd</sup> dimension and to their development as computational design and analysis frameworks for a wide range of case studies. At the same time, this computational power has also affected the way in which graphic statics is being developed, *viz.*, through iterative optimisation algorithms which converge towards the wanted output rather than analytical and direct methods. This can limit the potential of graphic statics in terms of their applicability and educational value. This is not to say that contemporary computational frameworks are not useful – they are valuable form-finding design and analysis tools. However, current advancements in CAD, computational power and visualisation provide us with the valuable opportunity to develop rigorous theoretical frameworks in conjunction with their computational implementation. Thus, it is possible to combine the best of both worlds, analytical, direct and mathematically elegant theory within interactive, visual and computational environments. This holds promise for:

- Increasing the educational value of graphic statics where the geometrical, visual and intuitive nature holds both about the output and the method.

- Increasing the applicability of graphic statics where the users (architects, engineers and designers) are able to understand and reproduce the methods while interacting with them throughout the process.
- Introducing profound design and analysis freedoms with regards to the structure and its performance.
- Some limitations of iterative algorithms can be lifted and their applicability can be enhanced and expanded to other fields of engineering.

This PhD research started with Maxwell's papers (Maxwell, 1864a, 1870). As a result, explanations, references and visualisations are provided that relate to Maxwell's original ideas which influenced this thesis.

## 1.1 Research statement

The contemporary built environment industry is characterised by a lack of effective communication between those who design forms and those who analyse them and by a need for material efficiency in how we build our structures. As a result, there is a need to shift towards interactive design and analysis tools which can inform conceptual design stages with structural performance while talking a language common to a wide range of researchers and practitioners.

This PhD research aims to develop geometry-based, direct -as opposed to iterative-analytical and unified design and analysis tools for compression-and-tension 2D and 3D pin-jointed structures while introducing design and analysis freedoms in an interactive framework. In particular, this will be achieved by using reciprocal stress functions which embed in an explicit way the structural behaviour of the structure while ensuring the form exploration is within equilibrium space.

## 1.2 Objectives

The objectives of this thesis can be divided into four categories:

- Historical research: this thesis seeks to explain, visualise and discuss Maxwell's approach in relation to the contemporary graphic statics research. This will be achieved by highlighting Maxwell's contribution to the field within the scientific context of his time, and moreover, by discussing the central role of projective geometry in his methods and how these can benefit designers today.

- Development of new theory: based on Maxwell's abstract and fundamentally geometrical approach, a direct and unified method will be developed for generating global static equilibrium for 2D as well as 3D reciprocal form and force diagrams based on reciprocal stress functions.
- Application thereof in design and analysis tools: based on this theory an interactive design and analysis framework will be developed where geometrical observations with regards to the form and force diagrams and their corresponding stress functions constitute intuitive design and analysis freedoms. In particular, this will be applied to tension-and-compression 2D and 3D trusses, tensegrities, exoskeletons of towers and in conjunction to force density, to grid-shells, shells and vaults.
- Impact on other disciplines: this research seeks to provide designers with a geometrical and intuitive language for a wide range of structural analysis and design notions. Applications include truss design via reciprocal stress functions, load-path optimisation and grid-shell design, as well as uses in representing discrete stress fields for 2D and 3D reinforced concrete structures and yield line patterns.

This thesis aims to contribute towards a new design paradigm where the space of forces can be explicitly 'sculpted' using stress functions, resulting in structures in static equilibrium. In other words, instead of freely designing the form and then analysing the resulting structural behaviour, the designer can freely design the stress function - hence the wanted structural performance - and then see the form emerging in a bi-directional interactive framework.

## 1.3 Methodology

The methodology developed here is based on the introduction of reciprocal stress functions. These exist one dimension up from the reciprocal diagrams, namely, in 3-dimensional space for 2-dimensional form and force diagrams and in 4-dimensional space for 3-dimensional reciprocals. This approach provides agility to the designer to start from any one of the reciprocal objects (form, force, or stress functions) while designing within equilibrium space.

The main idea is that reciprocal stress functions can be derived from one another and can be subsequently projected one dimension down to produce reciprocal form and force diagrams. Thus, a direct way to obtain global static equilibrium can be introduced. This results in a mathematically elegant method which has no need for iterative convergence to derive form and force diagrams. Moreover, the geometry of stress functions holds all the information of the structural behaviour of the corresponding truss: which members are in

tension, which are in compression, by how much, and how many are the states of self-stress and thus of possible design and analysis freedoms.

This method is applicable to any 2D truss geometry and to any polyhedral 3D geometry which has plane faces, each one of which belongs to two cells. For these cases the method is equally applicable to tension-only, compression-only, and tension-and-compression structures of any topology and, potentially intersecting, geometry. Moreover, it is applicable both to self-stressed and externally loaded structures.

Maxwell's convention is followed where the role of reciprocal diagrams (form and force) are interchangeable, and edges in a diagram can signify structural members or external forces. As a result, a truss with external loading can be also seen as an equivalent self-stressed geometry. This approach is fundamental and agile and makes the need for special treatment of different geometrical objects redundant.

## 1.4 Outline of Chapters

The second Chapter comprises an in-depth literature review from the 19<sup>th</sup> century to today of fundamentals such as, graphic statics, reciprocal diagrams, stress functions, N-polytopes and Minkowski sums. Maxwell's contribution is highlighted and discussed with regards to today's research scene.

The third Chapter introduces a direct, geometrical and unified graphic statics methodology for 2D and 3D tension-and-compression trusses based on the concept of reciprocal stress functions.

The fourth Chapter presents a geometry-based, visual, optimisation method based on the load path theorem and volume minimisation for 2D and 3D trusses through the construction of Minkowski sums.

The fifth Chapter introduces design by analysis methodologies for 2D and 3D trusses in static equilibrium by using reciprocal stress functions. This method is also combined with the force density method for the design and analysis of tension-and-compression shells, grid-shells and vaults.

The sixth Chapter presents applications and case studies in design, analysis and transformations for a number of case studies:

- 2D and 3D (polyhedral) trusses;
- Interlinked graphic statics and kinematics study of tensegrities with infinitesimal mechanisms and flexible polyhedra with finite mechanisms;

- Introduction of the dynamic Minkowski sum for statically balanced tensegrity mechanisms;
- Design and analysis of large infrastructure such as tensile nets, shells and tension-and-compression grid-shells;
- Structural morphogenesis of exoskeletons and trusses of towers.

The seventh Chapter presents cross-disciplinary applications on the automatic generation of 2D and 3D discrete stress fields as well as geometrical criteria for admissibility of yield line patterns and geometrical representations of internal and external work.

Lastly, in the eighth and final Chapter conclusions are drawn and the applicability, limitations, impact and possible future directions of this PhD research are discussed.



# Chapter 2

## Literature review

This Chapter provides an in-depth literature review of graphic statics, reciprocal diagrams and reciprocal stress functions from the 19<sup>th</sup> century to today. Fundamental notions for this PhD research are discussed such as N-polytopes and Minkowski sums. Maxwell's fundamental, but largely unknown or inaccessible, contribution is particularly highlighted as well as the benefits of re-introducing analytical and direct graphic statics methods.

Most parts of this Chapter have been published in the International Journal of Solids and Structures in (Konstantatou et al., 2018).

### 2.1 Graphic statics

Graphic statics can provide a visual, intuitive and geometrical framework both for the design and analysis of trusses in static equilibrium and for other fields of structural engineering. The scientific context that gave rise to the development of graphic statics is grounded on the legacy of Da Vinci, Galilei, Newton (Zalewski and Allen, 1998), Hooke, Poleni and Stevin (Heyman, 1995). Cremona (Cremona, 1872) traces back the foundation of graphic statics to the 18<sup>th</sup> century, when Varignon used the funicular polygon and the polygon of forces to calculate and visualize the equilibrium of a system of forces on a plane (Varignon, 1725) (Figure 2.1). According to Maxwell and Cremona, Rankine was the first to propose a consistent graphical methodology for the analysis of bar frameworks in his 'A Manual of Applied Mechanics' (Rankine, 1858). The earliest systematisation of the theory of graphic statics can be attributed to Cullman, in his seminal monograph 'Die Graphische Statik' (Culmann, 1875). Rankine's, Maxwell's, Cremona's and Cullman's methods were then further extended by various scientists and practitioners of engineering at the end of the 19<sup>th</sup> century, such as Bow. In 1873 Bow (Bow, 1873) with his monograph 'The economics of construction in relation to framed structures' categorised 2-dimensional truss geometries into

four different types and derived their reciprocal force diagrams. In this, 136 truss geometries and corresponding form and force diagrams were standardised (Figure 2.2) for structural engineers and designers to use (Kurrer, 2008). However, it is Maxwell who is credited as the originator of the notion of reciprocity between form and force diagrams (Charlton, 1982; Kurrer, 2008; Zalewski and Allen, 1998) and who suggested a methodology to construct the diagrams within the context of projective geometry. Relevant work in this direction was also undertaken by Cremona (Cremona, 1872), who introduced an alternative approach to that of Maxwell in the construction of reciprocal diagrams.

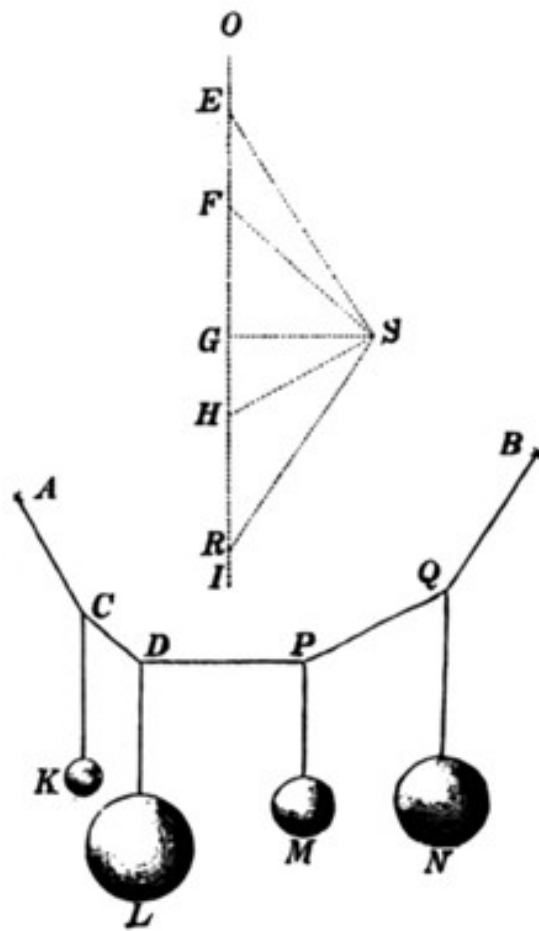


Fig. 2.1 Varignon's introduction of the polygon of forces and funicular polygon in (Varignon, 1725).

The design and analysis procedures of graphic statics were particularly relevant in the late 19<sup>th</sup> century, when they were regarded, along with the notions of projective geometry, as essential elements in the education of young engineers (Charlton, 1982). At that time, graphic statics, and more generally graphical analysis, was used as the conventional approach



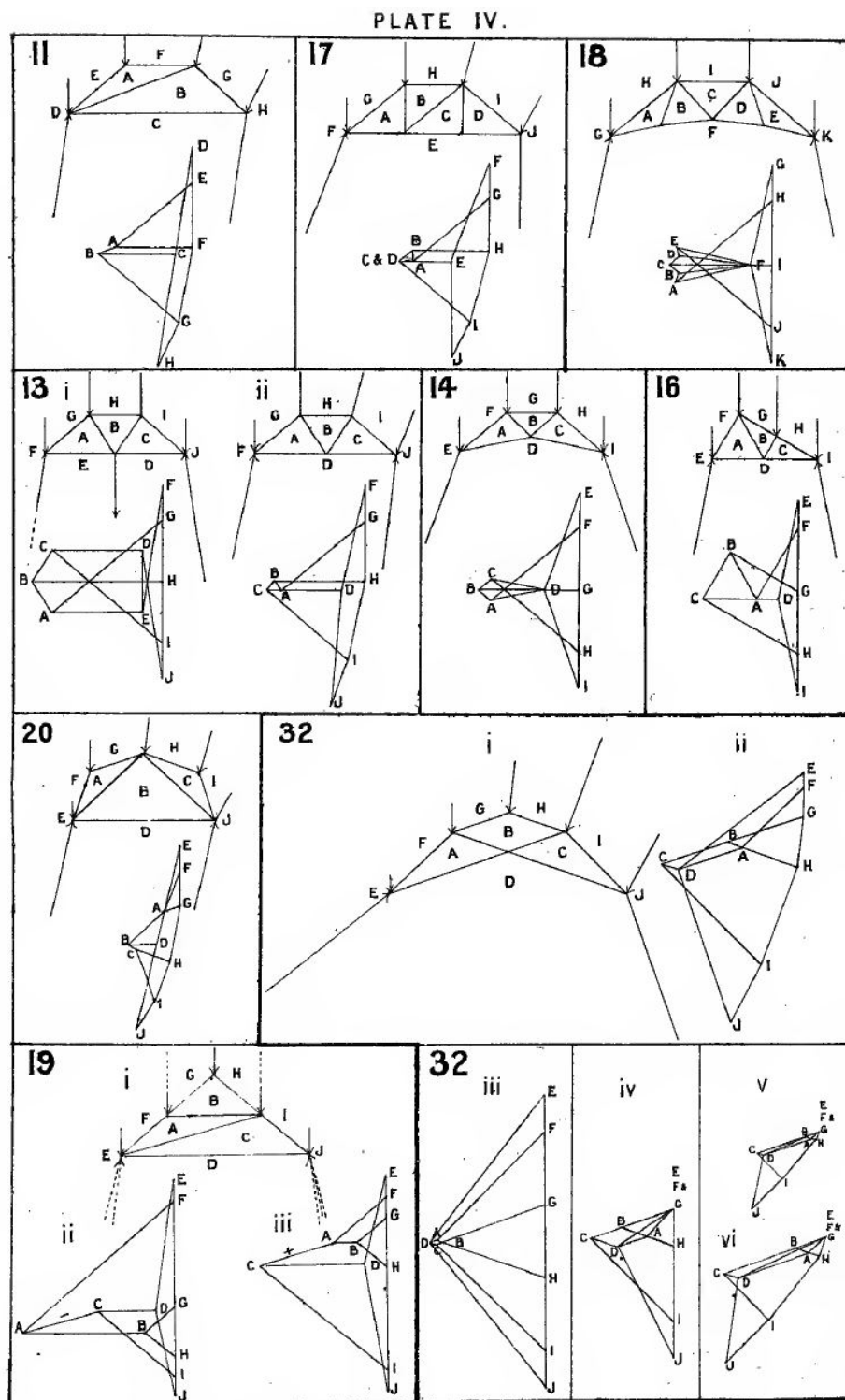


Fig. 2.2 Table of standardised 2D truss geometries and their force diagrams in Bow (Bow, 1873).

to solving engineering problems, including safety assessment of masonry vaults, arches and domes. However, most of the applications were largely limited to the standardised analysis of 2-dimensional trusses and required a considerable number of hours of draughtsmanship. In the early 20<sup>th</sup> century Wolfe (Wolfe, 1921) wrote one of the most concise textbooks on graphical analysis and 2D reciprocal diagrams. 'Graphical analysis: A Text Book on Graphic Statics' exemplifies a number of elaborate constructions based on parallel drawing (Figure 2.3) as well as the limitations of these methods since solving complicated structures, even 2-dimensional, requires tedious line hand drawing and draughtsmanship. At the same time (early 20<sup>th</sup> century), the interest in and research on graphic statics went through a rapid decline. The developments in analytical statics led engineers away from the subject, where no significant progress was made after the late 19<sup>th</sup> century (Kurrer, 2008). By the second quarter of 20<sup>th</sup> century, graphic statics was almost entirely replaced by the analytical approaches of elasticity theory, which relied on the solution of equations rather than the construction of time-consuming hand drawing. The fast advances in analytical statics and the introduction of numerical methods such as the finite element method in the second half of the 20<sup>th</sup> century, led to the widespread situation where in the curricula of young engineers and architects, the study of geometry, let alone projective geometry, and its relation to graphic statics gradually declined. In the field of theoretical research, an exception is represented by the work of the structural topology group at the University of Montreal on reciprocal diagrams among others. There, following Maxwell's legacy, the application of projective geometry and higher-dimensional duality between stress functions was developed from a general and mathematical point of view within the context of rigidity theory (Crapo, 1979; Crapo and Whiteley, 1994). In the field of applied research, graphic statics has been proposed, within the domain of plasticity theory, for the design of reinforced concrete structures (Muttoni et al., 1997).

Over the last few decades, graphic statics has seen a renewed interest. This directly reflects the increasing demand for the construction of material efficient structures, which in turn calls for the use of synthetic and intuitive tools that allow the designers to take advantage of the relationship between form and forces from the early stages of the design process. In this context, there is a current trend to reintroduce graphic statics within the engineering and architectural education (Allen and Zalewski, 2010; Muttoni, A., 2011; Zalewski and Allen, 1998). Recent applications of graphic statics are underpinned by the computational and visualization capabilities offered by contemporary computer aided design tools. As a result, a lot of research, methodologies and computational frameworks have emerged recently. These can be found, among others, in: the design of compression-only or tension-only spatial funicular structures by means of the Thrust Network Analysis (TNA) (Block

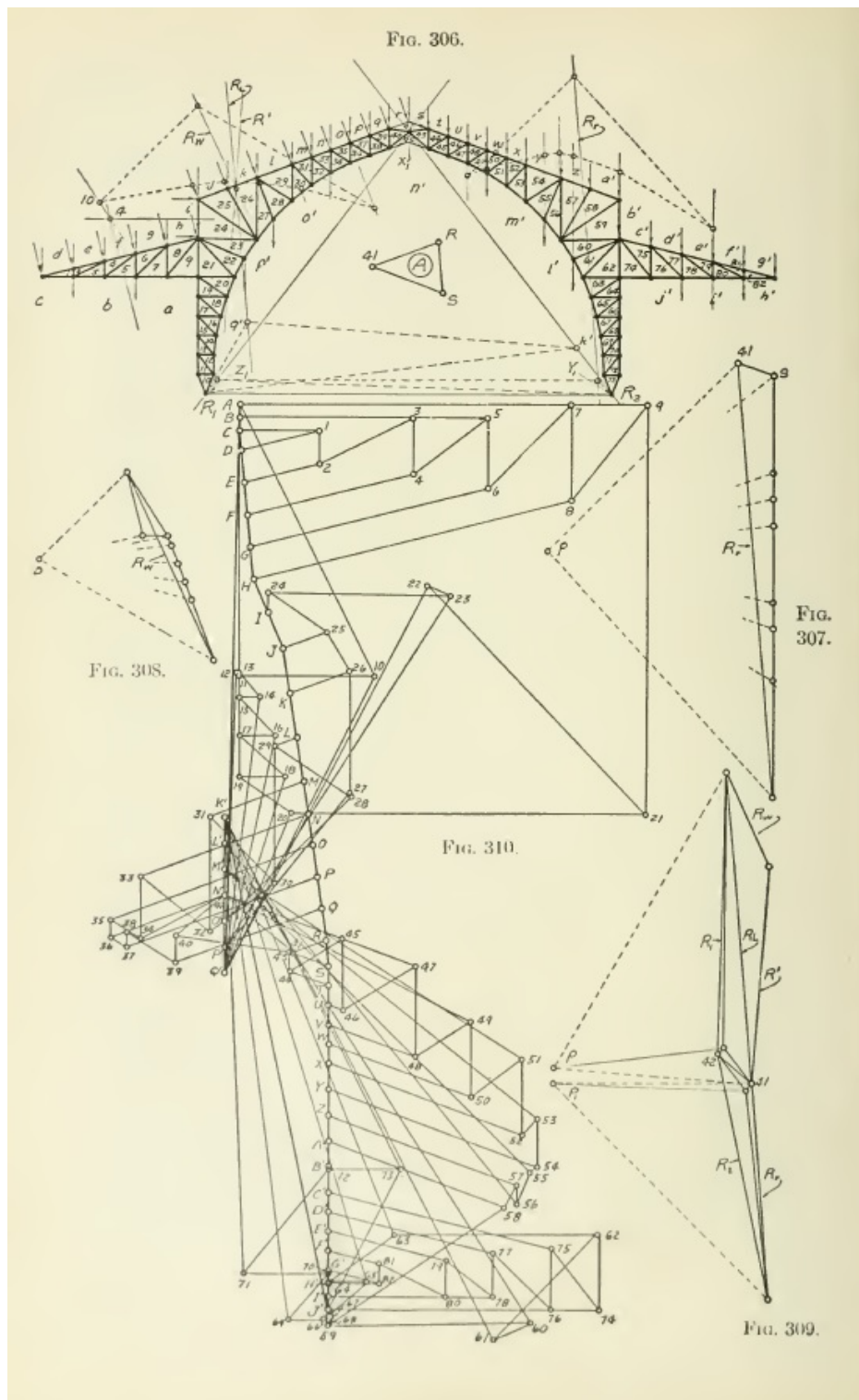


Fig. 2.3 Graphic statics hand drawings of elaborated 2D trusses in Wolfe (Wolfe, 1921).

and Ochsendorf, 2007) which combines 2D graphic statics with the force density method (Block and Ochsendorf, 2007); the computational framework for analysing and designing compression-only or tension-only plane-faced polyhedral structures based on subdivisions and manipulations of spatial force diagrams (Rankine 3D) (Akbarzadeh et al., 2015); the extension of this method to compression and tension cases through matrix analysis (Hablicsek et al., 2019) based on the principles of the Singular Value Decomposition (SVD) (Pellegrino, 1993). Moreover, another computational framework has been recently developed for the analysis of spatial structures in static equilibrium which is not confined to plane-faced cases and can input target values of the external forces (Lee et al., 2018).

Graphic statics can be also used in the context of transformations of form diagrams in static equilibrium (Fivet, 2016). Other recent contributions in the study and generalization of graphical analysis include publications from (Fraternali and Carpentieri, 2014; Micheletti, 2008; Zanni and Pennock, 2009). Graphic statics has also regained popularity in the engineering industry as a design and optimisation tool (Beghini et al., 2014; Mazurek et al., 2016). Most of the current graphic statics approaches for the construction and transformation of 3D form and force diagrams rely on the use of iterative algorithms or procedural reconstruction techniques, such as the *polyhedral* one (Akbarzadeh et al., 2015; Lee et al., 2018), the *vector-based* one (D'Acunto et al., 2017), and operate on a local node-by-node basis. A direct global implementation, which is grounded on the definition of higher dimensional reciprocal stress functions as a tool for generating pairs of reciprocal form and force diagrams, has been also suggested (Konstantatou and McRobie, 2016; McRobie, 2016). A theoretical framework based on Clifford Algebra has been introduced by McRobie (McRobie, 2017a) for the analysis of the general case of plane and spatial frames in static equilibrium. This utilizes the concept of zero-oriented area auxiliary geometrical elements and results in the analysis of all six stress resultants (axial and shear forces, bending and torsion moments). This method is applicable to general cases of spatial structures where faces need not lie on a plane and are thus *gauche*<sup>1</sup>.

### 2.1.1 Maxwell's contribution to graphic statics

Maxwell was interested in the concept of analogies in science from a very young age. He was particularly intrigued by the relation between beautiful forms and mathematics (Harman, 2004); from how the underlying geometrical principles can act as a morphological mould. That idea was explored conceptually in his essay 'Analogies in Nature', which he wrote for the student society 'Cambridge Apostles' in 1856 (Harman, 1990). In this work, he

<sup>1</sup>Gauche is a term used by Maxwell to denote polygons which do not lie on a plane. Thus, the surface that spans them is curved.

mentioned reciprocity which would be a key idea in his seminal papers on structures and electromagnetism (Harman, 1990). Also, a few months earlier, he published his famous paper ‘On Faraday’s lines of force’ (Maxwell, 1855) where he related magnetic forces with electric currents through a geometrical construction of lines of force which run on a surface in an analogous way to how incompressible fluids flow (Harman, 2004). Maxwell’s fascination with analogies and reciprocity was heavily influenced from his contemporaries and took form through the mathematical theories of his time.

The mathematics of late 19<sup>th</sup> century were characterized not only from projective geometry, the ‘modern geometry’ of the time, but also from the newly formed topology. Maxwell was familiar with the work of Carnot, Chasles and Poncelet with respect to the former and the work of Gauss, Listing, Euler, Riemann, Leibniz and Cayley with regards to the latter (Harman, 1998; Maxwell, 1870). His mathematical physics framework was heavily influenced by Gauss’ ‘*Geometria Situs*’ and Listing’s topology, which shaped his ‘knotted curves’ discussion, his theory on translations and rotations of spatial motions, and fed his electromagnetic analogies and relations between electrical circuits and lines of force (Harman, 1998; Maxwell, 1855). Moreover, Maxwell also used projective geometry as a tool of geometrical analogy; in his point of view, projective geometry could express the supremacy of the geometrical over the analytical way of thinking (Harman, 1998). This can be seen clearly in his theory of reciprocity between geometrical elements if placed within a projective geometry framework. Maxwell wrote on this: ‘The study of corresponding elements in two figures has led to the establishment of a geometry of position by which results are obtained by pure reasoning without calculation, the verification of which by the Cartesian analysis would fill many pages with symbols’ (Harman, 1998). As a result, projective geometry and its underlying notion of duality was the tool used by Maxwell to express the reciprocity between not only form and force diagrams in the context of graphical analysis but also, of ‘geometrical optics, electrical circuits, and the kinetic theory of gases’ (Harman, 1998).

Maxwell’s graphical analysis of trusses (Maxwell, 1864b, 1867, 1870) was particularly influenced by Chasles’, Monge’s and Poncelet’s pole and polar construction and duality principle, which expressed the reciprocity between form and force diagrams. As he characteristically put it in 1873: ‘[...] principle of duality ... the leading idea of modern geometry’ (Harman, 1998). Maxwell combined the projective geometry duality with Euler’s work on polyhedral counting to develop his theory of reciprocal diagrams in statics. He observed that two-dimensional reciprocal diagrams follow the counting rules of polyhedra when it comes to their constituent geometrical elements (points, edges, faces) and that a 2-dimensional form diagram has a force reciprocal when it is a projection of a polyhedron (Maxwell, 1864b). At that point, he would derive reciprocal diagrams by using geometrical constructions with

circles, for the 2D, and spheres, for the 3D case, which would ensure that corresponding reciprocal elements were perpendicular. However, it is not until few years later that he placed his constructions one dimension up, and entirely in the space of the reciprocal polyhedra following Poncelet's and Monge's theory of polar figures (Charlton, 1982). Maxwell was also familiar with the work of Airy (Airy, 1862) since he was keeping a regular communication with the Astronomer Royal on all sorts of scientific matters and he was a reviewer for some of his work. In particular, Maxwell along with Rankine were the reviewers of Airy's 1862 paper on structural analysis and the Airy stress function (Harman, 1990) which he considered as a significant simplification of the already existing theories and he later developed and applied himself in his graphical analysis of trusses. A number of his contemporaries, (such as Cremona, Rankine and Cullman) adopted, generalized, or standardized his methods. However, most of them did not grasp or consider reciprocal diagrams in the deep geometrical way Maxwell did. An exception was Cremona, who as a geometer, was also familiar with polarities, and who discussed and applied Möbius' null-system methods. As a result, Maxwell is credited with making the biggest intellectual contribution in the context of graphic statics (Kurrer, 2008).

## 2.2 Projective Geometry

Projective geometry is a system of geometric prepositions that does not include any of the familiar Euclidean notions of parallelism, intermediacy, angle and length measurement (Figure 2.4). Its origins can be traced back to Pappus of Alexandria (4<sup>th</sup> century) as well as the French architect Desargues (16<sup>th</sup> century) and the French philosopher and mathematician Pascal (17<sup>th</sup> century) (Coxeter, 1969; Rosenfeld, 1988). On the projective plane, two lines always meet in a point, either an ordinary point or a point at infinity (Coxeter, 1974). The set of all the points at infinity constitutes the line at infinity, which together with the Euclidean plane defines the projective plane. On the projective plane, there is only one type of conic, or conic section; it is its position with respect to the line at infinity that gives rise to the different embeddings (circle, ellipse, parabola, hyperbola) when seen from a Euclidean point of view (Coxeter, 1974; Rosenfeld, 1988) (Figure 2.5).

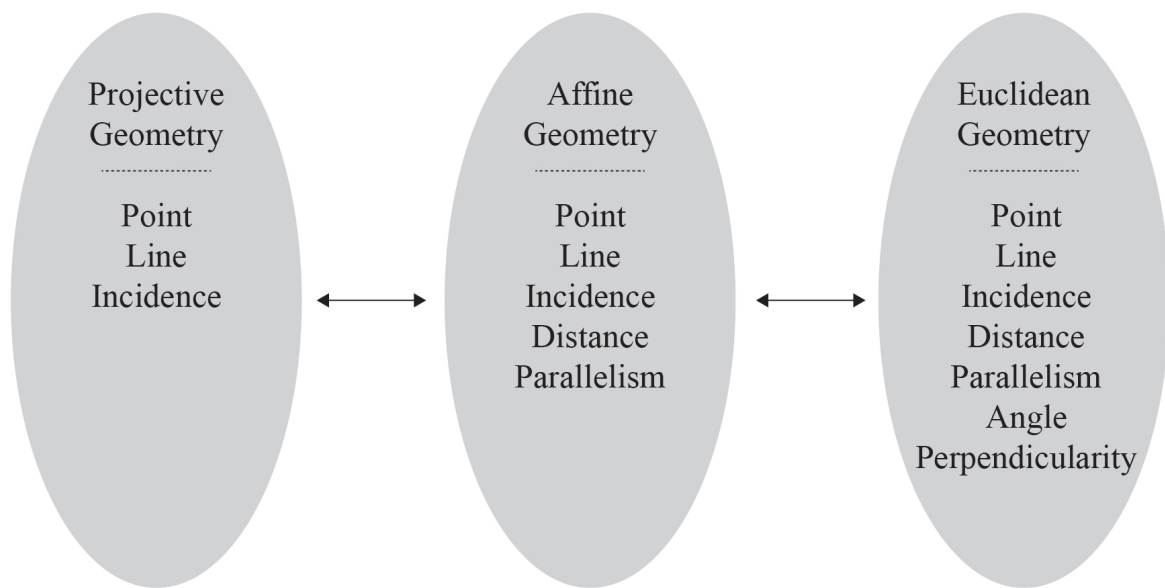


Fig. 2.4 Projective-Affine-Euclidean geometry – primitive concepts and metrics

Following the principle of duality in 2D projective geometry any proposition that is true on the projective plane for points and lines can be dualised to an equivalently true proposition for lines and points as showed by Cremona (Cremona, 1885) (Figure 2.6). The principle of duality thus works by interchanging primitive geometrical elements of the projective plane. This can be extended to higher spatial dimensions by taking into account the primitive elements of the specific projective space under consideration (Figure 2.7) (i.e. the point and the line in 2D; the point, the line and the plane in 3D; the point, the line, the plane and the hyperplane in 4D).

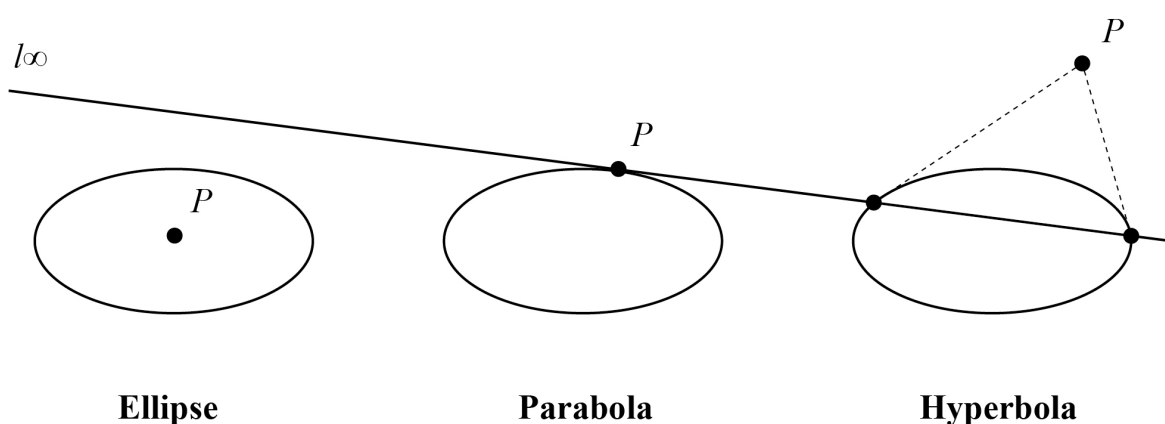


Fig. 2.5 Conics in relation to the line at infinity of the projective plane.

1. Two points  $A, B$  determine a straight line (viz. the straight line  $AB$  which passes through the given points) which contains an infinite number of other points.

2. A straight line  $a$  and a point  $B$  (not lying on the line) determine a plane, viz. the plane  $aB$  which connects the line with the point.

3. Three points  $A, B, C$  which are not collinear determine a plane, viz. the plane  $ABC$  which passes through the three points.

4. Two straight lines which cut one another lie in the same plane.

5. Given four points  $A, B, C, D$ ; if the straight lines  $AB, CD$  meet, the four points will lie in a plane, and consequently the straight lines  $BC$  and  $AD, CA$  and  $BD$  will also meet two and two.

6. Given any number of straight lines; if each meets all the others, while the lines do not all pass through a point, then they must lie all in the same plane (and constitute a plane of lines)\*.

1. Two planes  $\alpha, \beta$  determine a straight line (viz. the straight line  $\alpha\beta$ , the intersection of the given planes), through which pass an infinite number of other planes.

2. A straight line  $a$  and a plane  $\beta$  (not passing through the line) determine a point, viz. the point  $a\beta$  where the line cuts the plane.

3. Three planes  $\alpha, \beta, \gamma$  which do not pass through the same line determine a point, viz. the point  $\alpha\beta\gamma$  where the three planes meet each other.

4. Two straight lines which lie in the same plane intersect in a point.

5. Given four planes  $\alpha, \beta, \gamma, \delta$ ; if the straight lines  $\alpha\beta, \gamma\delta$  meet, the four planes will meet in a point, and consequently the straight lines  $\beta\gamma$  and  $\alpha\delta, \gamma\alpha$  and  $\beta\delta$ , will also meet two and two.

6. Given any number of straight lines; if each meets all the others, while the lines do not all lie in the same plane, then they must pass all through the same point (and constitute a sheaf of lines)†.

Fig. 2.6 Dual propositions, definitions, theorems and true statements of 3D projective geometry can be arranged in a 'parallel column' configuration in Cremona's Elements of Projective Geometry (Cremona, 1885). Specifically, this 3D duality between points and planes is important since it underpins the study of 2D trusses.


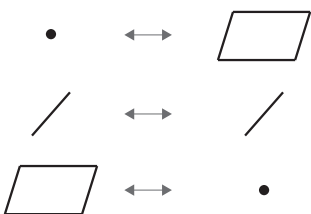
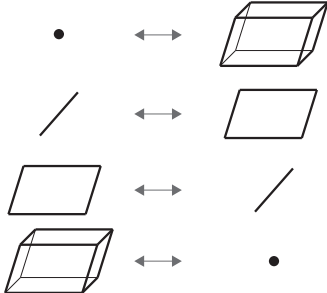


Considering that a pair of  $n$ -dimensional form diagram and its reciprocal force diagram are projections of  $(n+1)$ -dimensional stress functions, then this reciprocal pair also obeys the counting rules and connectivity of their higher-dimensional stress functions (Figure 2.7). The reciprocity between geometrical elements also applies to their connectivity matrices. For example,  $C_p, C_l, C_{pl}, C_{h-pl}$  are the connectivity matrices between points, lines, planes and hyper-planes of a form diagram, and  $C_{p'}, C_{l'}, C_{pl'}, C_{h-pl'}$  the corresponding connectivity matrices of its reciprocal. These matrices are symmetric and their entries are either 1, if two elements are adjacent (for instance, two points in  $C_p$  are connected from an edge or two planes in  $C_{pl}$  share an edge), or 0 if they are not. For example, a 2D truss and its 2D force reciprocal are projections of 3D polyhedral stress functions and they thus obey the connectivity and counting rules of these polyhedra: points map to planes, lines to lines, with the connectivity remaining fixed; if two points of the form diagram are connected via an edge then the corresponding faces of the force reciprocal share a common edge.

### 2.2.1 Pole and polar reciprocals

The concept of pole and polar reciprocals were central to 19<sup>th</sup> century projective geometry. Pole and polar constructions or ‘polarities’ are transformations which map geometrical elements to each other according to the principle of duality (Figure 2.7). On the plane, a polarity maps points to lines and dually lines to points, in 3-dimensional space a polarity maps planes to points and vice versa. They have degree 2 since the image of transforming an element twice is the element per se and they preserve incidence (Coxeter, 1969). In a 2-dimensional geometry the former means that a point  $A$  maps to a line  $a$  which maps back to point  $A$ , and the latter that if three lines  $A, B, C$  on the plane are concurrent on a point  $d$ , then after the polar transformation points  $a, b, c$  lie on the line  $D$  (Coxeter, 1969).

Desargues was the first to come up with the concept of polar transformations in 2-dimensional space induced by a conic (Rosenfeld, 1988) - although Brianchon is also credited with the discovery of mapping a point to a plane through a line (Gray, 2010). Moreover, Monge was the one to generalize Desargues’ pole and polar construction in 3-dimensional space. Given a generic point  $P$  (pole) and a conic  $\gamma$  on the projective plane, in such a way that  $P$  is outside  $\gamma$ , the two lines  $a$  and  $b$  incident to  $P$  and tangent to  $\gamma$  meet the conic in two intersection points  $A$  and  $B$ ; the chord through  $A$  and  $B$  defines the polar line  $p$  (Figure 2.8). Equivalently, given any pole  $P$  outside of a quadric  $\Gamma$  in the projective 3-space, the cone with vertex in  $P$  and tangent to  $\Gamma$ , intersects the quadric in a plane curve  $\gamma$  (a conic), which lies in the polar plane  $\pi$  (Amir-Moez, 1973) (Figure 2.9). The fact that the curve  $\gamma$  lies on a plane can be also deduced from a geometrical point of view. Specifically, if we apply the above construction to a sphere it is trivial to see how  $\gamma$  is a circle on a plane. If we

Projective Geometry Duality (Dimension of Stress Function)		
2D	3D	4D
		
1D	2D	3D
Corresponding Truss Dimension		

Duality between Connectivity Matrices of Geometrical Elements		
$C_p = C_{l'}$ $C_l = C_{p'}$	$C_p = C_{pl'}$ $C_l = C_{l'}$ $C_{pl} = C_{p'}$	$C_p = C_{h-pl'}$ $C_l = C_{pl'}$ $C_{pl} = C_{l'}$ $C_{h-pl} = C_{p'}$




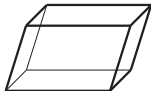
0D, 1D, 2D, 3D Geometrical Elements			
 0D - Point	 1D - Line	 2D - Plane	 3D - Hyper-plane

Fig. 2.7 Summary of duality principles between geometrical elements in projective geometry and correspondence between  $n$ -dimensional structures and their  $(n+1)$ -dimensional stress functions.

now apply a projective transformation to this model we can transform the sphere to other quadrics (ellipsoid, paraboloid of revolution, etc.) while the transformation of the polar plane retains its planarity and thus the fact that  $\gamma$  lies on a plane. We should note that these constructions readily apply on the Euclidean plane and space for any embedding of a conic (circle, parabola, ellipse, hyperbola) and real non-degenerate quadric (sphere, paraboloid, ellipsoid, hyperboloid), in this section we use as a 2D example an ellipse and as a 3D example an ellipsoid. When the pole  $P$  is inside the conic  $\gamma$  on the projective plane, the polar line  $p$  can be found as follows (Figure 2.10): from  $P$  take any two arbitrary lines  $p_1, p_2$  which will intersect  $\gamma$  in points  $A, B$  and  $C, D$  respectively; from these two pairs of points take the corresponding pairs of tangent lines  $a, b$  and  $c, d$  with regards to  $\gamma$ ; these two pairs of lines will intersect in points  $AB$  and  $CD$ . These two points define the polar line  $p$ . Equivalently, in projective 3-space for a pole  $P$  inside a quadric  $\Gamma$  the polar plane  $\pi$  can be found as follows (Figure 2.11): from  $P$  take any three arbitrary planes  $\pi_1, \pi_2, \pi_3$ , which intersect  $\Gamma$  in the plane curves  $\gamma_1, \gamma_2, \gamma_3$  respectively; from these three curves take the corresponding tangent cones which define points  $P_1, P_2, P_3$ . These three points define the polar plane  $\pi$ .

Von Staudt observed that the conic and the quadric are essentially the locus of self-conjugate points on the plane and in space respectively; that is, self-conjugate are points which lie on their polar lines, or planes, which in turn are tangent to the conic, or quadric. Monge applied this construction, using a paraboloid of revolution as a quadric, to derive reciprocal polyhedra (Chasles, 1875). However, Monge's notes on this did not survive (Chasles, 1875) and his student Poncelet developed his theories, formally established the principle of duality and through it polar reciprocation (Cremona, 1885; Maxwell, 1870; Poncelet, 1822; Rosenfeld, 1988) which utilized such a pole and polar reciprocal construction based on a paraboloid of revolution to map nodes (poles) and faces (polar planes) of a polyhedron to the faces and nodes of its reciprocal (Konstantatou et al., 2018). Maxwell's construction of reciprocal polyhedra was an elegant and abstract geometrical toolkit to produce a corresponding pair of 2D reciprocal form and force diagrams of trusses in static equilibrium through projection. Moreover, other types of polar transformations were explored at the time, most notably Möbius' Null-polarity, which was not based on transformations induced by quadrics and where all poles, and polar planes, are self-conjugate (Cremona, 1885).

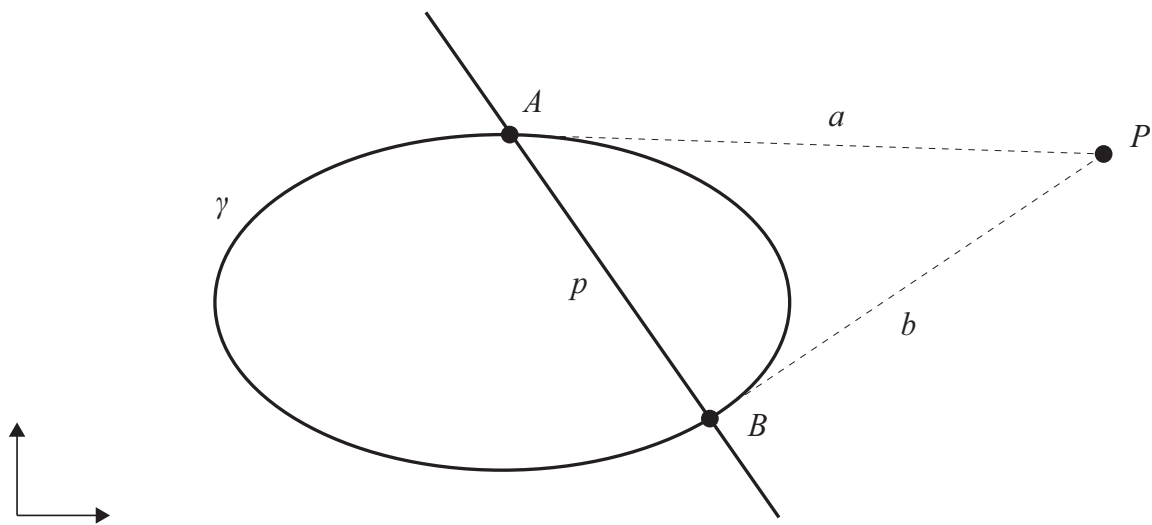


Fig. 2.8 Polarity on the plane induced by a conic - Pole outside the conic.

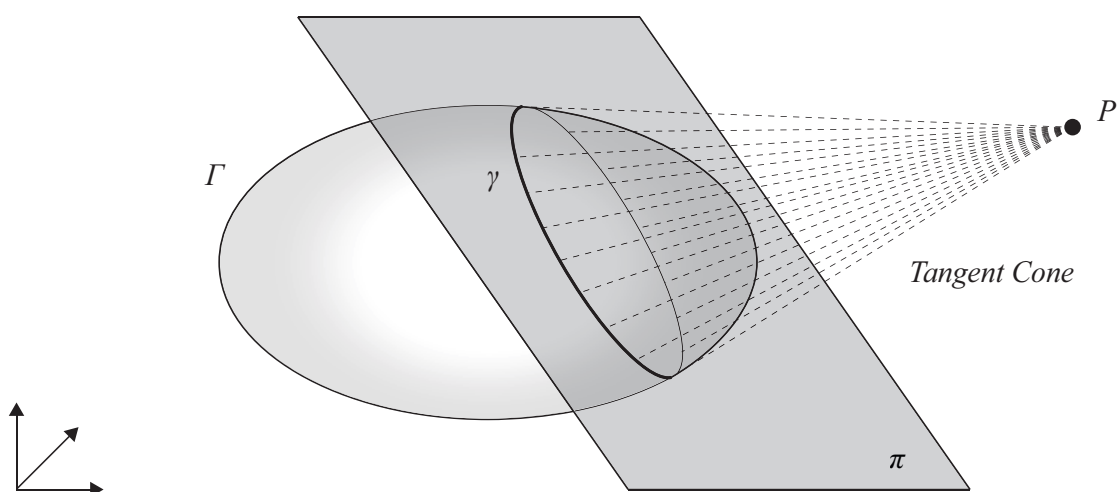


Fig. 2.9 Polarity in 3-space induced by a quadric - Pole outside the quadric.

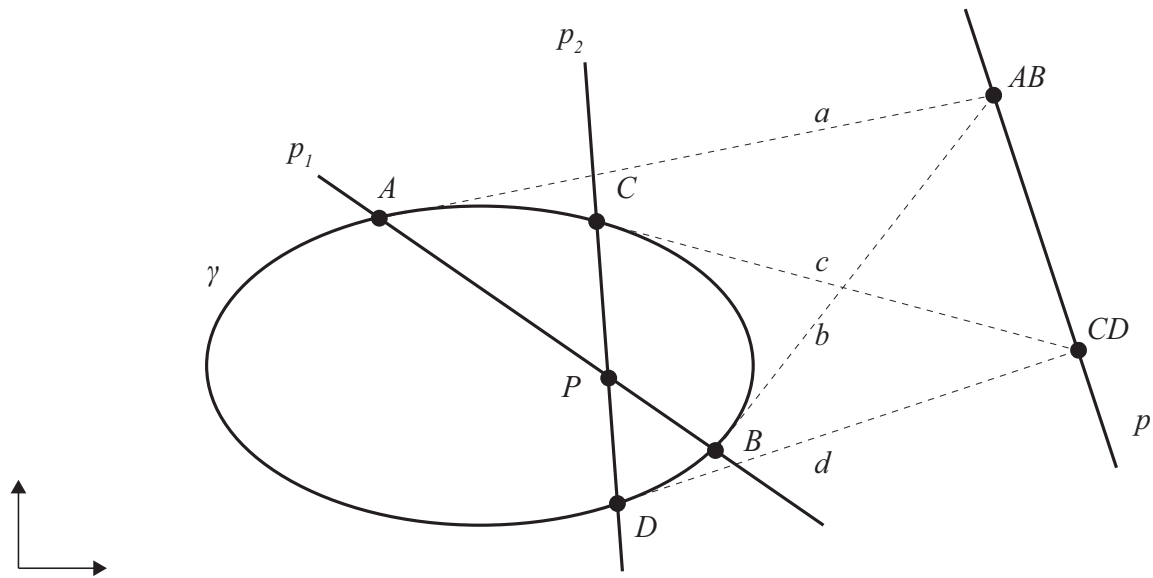


Fig. 2.10 Polarity on the plane induced by a conic - Pole inside the conic.

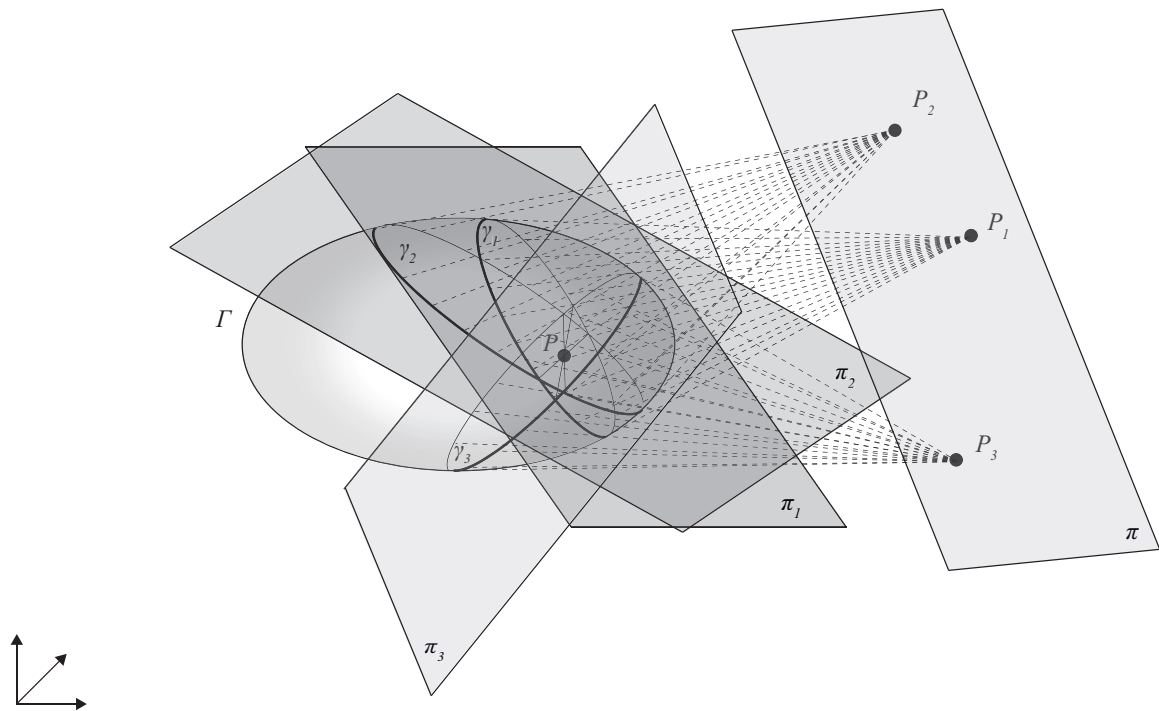


Fig. 2.11 Polarity in 3-space induced by a quadric - Pole inside the quadric.

## 2.3 N-polytopes and planarity

The frameworks we analyse here are self-stressed, pin-jointed structures. We will denote such a 2D framework  $F$  as a set of vertices  $v$ , edges  $e$  and faces  $f$ :  $F(v, e, f)$  and its reciprocal to be  $F'(v', e', f')$ . This pair of 2D form and force diagrams can be lifted in 3-space to a pair of reciprocal polyhedra  $P(v, e, f)$ ,  $P'(v', e', f')$ . Equivalently, we denote 3D frameworks of polyhedral structures  $P$  as a set of vertices  $v$ , edges  $e$ , faces  $f$  and cells  $c$ :  $P(v, e, f, c)$  and its reciprocal to be  $P'(v', e', f', c')$ . These can also be lifted in 4-dimensional space to a pair of reciprocal 4-polytopes. It should be noted that 4-polytopes are the equivalent of polyhedra in the 4-dimensional space where the cells lie on hyper-planes in the same way that faces lie on planes; hyper-planes constitute 3-dimensional subspaces in 4-dimensional space in the same way that planes constitute 2-dimensional sub-spaces in 3-dimensional space.

A planar graph  $G(v, e)$  is a set of vertices  $v$  and edges  $e$ , which can be drawn topologically on a 2D Euclidean plane without any edge crossing. This can be extended to spatial trusses, which are projections of 4-polytopes and have an underlying spatial planar graph. A spatial planar graph  $G(v, e, f)$  is a set of vertices  $v$ , edges  $e$  and faces  $f$ , which can be drawn topologically in a 3D Euclidean space without any edges or faces crossing (Crapo, 1979).

The condition of possessing a planar graph is considered in the literature a necessary, but not sufficient, condition for a 2D truss to have a reciprocal - although as we will see in section 3.2.4 there are some special cases for which this is not the case. Together with the additional requirement that the 2D truss has a state of self-stress, these conditions imply that the 2D truss is an accurate picture on the Euclidean plane of a projection of the corresponding polyhedron (Crapo, 1979). As a result, a 2D truss without external loading, which is a projection of a polyhedron, is necessarily self-stressed (Micheletti, 2008). At the same time, given a diagram of a 2D truss with a planar graph the question arises of how to assess whether this diagram corresponds to a projection of a polyhedron. An example is (Figure 2.12) where Maxwell's Figure IV (Maxwell, 1864a) is not self-stressed in the general position even though it possesses a planar graph. The special case where the truss has one state of self-stress is when it is a projection of a polyhedron - specifically, when it is in a Desargues configuration.

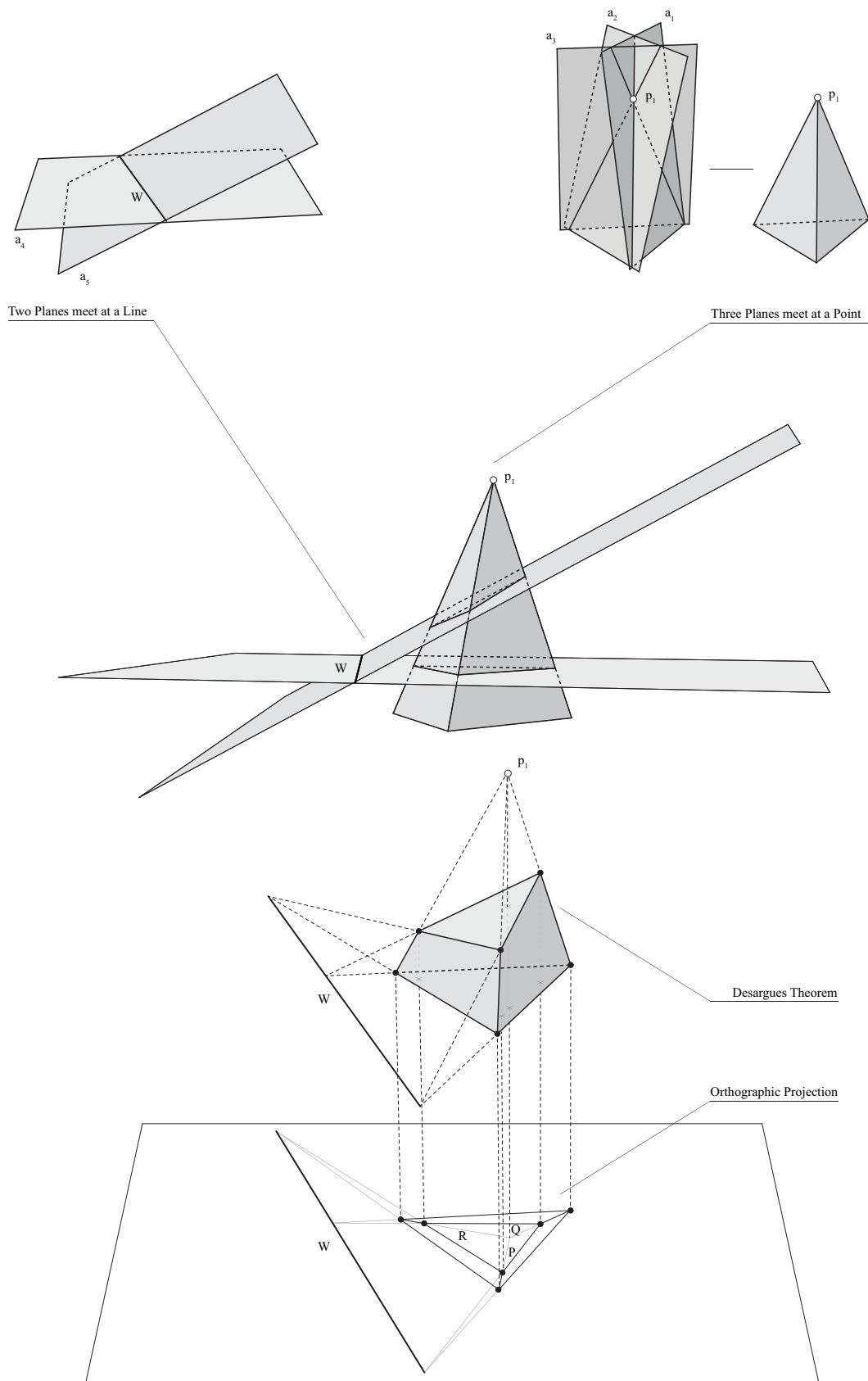


Fig. 2.12 Maxwell's Figure IV as a projection of a polyhedron in a Desargues configuration.

## 2.4 Reciprocal diagrams and Airy stress functions

Reciprocal form and force diagrams, were used in the context of graphic statics from as early as Hooke's era (17<sup>th</sup> century) for the assessment of masonry structures (for a detailed historical overview on graphic statics the reader can see (Charlton, 1982; Kurrer, 2008); however, the formal conception of these dual figures, and the definition we will be using here, can be largely attributed to Maxwell for the 2D case (Maxwell, 1864b, 1870) and Rankine (Rankine, 1864) for the 3D case. In 2D reciprocal diagrams, form edges map to force edges and form nodes to closed force polygons – thus, obeying a 3D duality (Figure 2.7). These reciprocal diagrams are projections of polyhedral Airy stress functions which are reciprocal as well. Maxwell (Maxwell, 1870) succinctly mentioned that this reciprocity between polyhedra can be obtained through a polar transformation, or polarity, using a paraboloid of revolution. The change of slope between adjacent faces of the Airy stress function defines the axial force of the corresponding structural member of the 2D truss (McRobie et al., 2016; Mitchell et al., 2016). In 3D reciprocal diagrams, form edges correspond this time to force faces, and nodes to closed polyhedral cells. Thus, obeying a 4D duality. As per the 2-dimensional case, reciprocal self-stressed 3-dimensional figures can also be seen as projections of 4-polytopes, which Maxwell defined in equation form (Maxwell, 1870) and in contemporary nomenclature are called Maxwell-Rankine stress functions (McRobie, 2016).

Moreover, the roles of reciprocal form and force diagrams are interchangeable and there is no distinction between lines of action of the applied forces and structural members. This has been explained in detail in (McRobie et al., 2016; Mitchell et al., 2016) where external forces, which can be applied on the structural perimeter as well as on internal nodes, can be combined with the form diagram to make a projection of a single polyhedron, possibly with the use of an extra portion of a funicular polygon. Thus, this polyhedron can be also seen as the Airy stress function of an equivalent self-stressed truss. As a result, there is no distinction between these two cases (self-stressed, with external loading) since they are geometrically equivalent.

Already in the (Maxwell, 1864a) paper, Maxwell establishes the correspondence of geometrical elements between 2D reciprocal diagrams. In particular, for a form diagram  $F(v, e, f)$  we have that for its reciprocal  $F'(v', e', f')$ :  $v = f'$ ,  $e = e'$ ,  $f = v'$ . Moreover,  $e = v + f - 2$  and  $e' = v' + f' - 2$  which is Euler's formula for counting the geometrical elements of polyhedra. Also, a necessary condition for the existence of two reciprocal figures is that every  $e, e'$  belongs only to two polygons from  $f, f'$ .

At the same time there are exceptions to this general rule. For example, Figure 7 in (Maxwell, 1864a) is a case of a 2D truss which does have a state of self-stress without being



a projection of a polyhedron and thus without obeying Euler's counting rule. This is because the underlying graph of this truss geometry is non-planar.

There are two ways to solve this: Maxwell suggested that a corresponding force diagram can be constructed by repeating some of its edges – consequently, the resulting pair of form and force figures are not reciprocal since they cannot be derived from each other in a non-ambiguous way. Alternatively, Bow (Bow, 1873) suggested that this issue can be addressed by adding an extra node at the point of intersection of two overlapping edges which are thus split. In this way, the resulting diagram is a projection of a polyhedron and its constituent geometrical elements do obey Euler's rule. The force reciprocal can be now derived following Maxwell's standard methods in (Maxwell, 1864a, 1870). We should note that the extra added node will correspond to a parallelepiped quad in the force diagram created from two pairs of duplicated force edges. These correspond to the two split form edges. However, this construction does not apply to the 3D case. It should be noticed that for spatial trusses, cases can be found where trusses are not projections of 4-polytopes and nonetheless, they do possess states of self-stress. In contemporary nomenclature this is called 'Rankine incompleteness' and has been discussed recently in the graphic statics literature (McRobie, 2016, 2017b).

For spatial, 3D, structures the reciprocity is between form edges  $e$  and force faces  $f'$ . Moreover, points  $v$  are mapped to reciprocal cells  $c'$  indicating a Poncelet 4D duality where  $v = c'$ ,  $e = f'$ ,  $f = e'$ ,  $c = v'$  and thus  $F(v, e, f, c)$  maps to  $F'(v', e', f', c')$ . Also, Maxwell highlights how spatial reciprocal figures  $F(v, e, f, c)$ ,  $F'(v', e', f', c')$  obey the counting rules of 4-polytopes, *i.e.*, each face of the polyhedral diagram belongs only to two polyhedral cells, every line is the intersection of at least three faces and there are no free edges, faces, or points. This type of reciprocal geometrical construction was firstly described by Rankine (Rankine, 1864).

Maxwell solved the simple case of a spatial form diagram the geometry of which is a spoked tetrahedron (Figure 2.13) - or in mathematical terms a 4-simplex or 5-cell in two ways:

- Firstly, since the 5-cell comprises 5 tetrahedra this is a trivial case where a sphere construction can be applied. This is a generalisation of the circle construction used in 2D examples. In this way, it is ensured that edges are perpendicular to reciprocal faces (Figure 2.14) and the line connecting the centres of two spheres is always perpendicular to their common intersection plane. As a result, Rankine 3D reciprocals are derived where for each form edge the corresponding internal forces are proportional to the surface area of the reciprocal triangular faces.

- Secondly, an alternative construction is also proposed, where for every point, and its concurrent edges, a ‘local’ force diagram is created where form edges correspond force edges which form closed spatial force polygons (Figure 2.16). In this way, the static equilibrium of the node is guaranteed, however; in order to assemble these local force polygons in one global force diagram, it is very likely that a number of edges should be repeated (Figure 2.16).

Depending on their spatial dimension and the geometrical relationship between corresponding members, reciprocal diagrams can be categorised as follows:

- *Maxwell 2D reciprocals*, where edges in the 2D form diagram correspond to perpendicular edges in the reciprocal 2D force diagram.
- *Cremona 2D reciprocals*, where corresponding edges between 2D form and force diagrams are parallel.
- *Rankine 3D reciprocals*, where form edges correspond to reciprocal perpendicular force faces.
- *Cremona 3D reciprocals*, where edges in the 3D form diagram correspond to parallel edges in the reciprocal 3D force diagram.

We should note that Maxwell 2D and Cremona 2D diagrams are identical up to a 90 degrees rotation, whereas Rankine 3D and Cremona 3D are geometrically distinct since in the former forces are expressed by surface areas and in the latter by edge lengths.

For a given 3D form diagram with underlying 2D planar graph and a state of self-stress, it is possible to derive a Cremona 3D reciprocal force diagram (Crapo, 1979), where spatial form edges correspond to reciprocal parallel force edges (Figure 2.15). Contrary to the Cremona 2D case however, these 3-dimensional reciprocal diagrams are not projections of 4D reciprocal stress functions through a null-polarity, which is not defined mathematically in even dimensions (Baer, 1945). Cremona 3D reciprocals have been investigated in the work of Sauer (Sauer, 1970) and more recently in Micheletti (Micheletti, 2008), Wallner and Pottmann (Wallner and Pottman, 2008), and Tachi (Tachi, 2012).

More generally, since the 2D graphs of 3D form and force diagrams are usually non-planar, edge-to-edge reciprocity between the 3D diagrams is not possible in such cases (Jasienski et al., 2016). Different solutions to derive reciprocal form and force diagrams with corresponding edges parallel and with underlying non-planar graphs can be found in literature for these cases: Maxwell observed that the static equilibrium of a spatial structure can be evaluated using 2D graphic statics by studying its three orthogonal 2-dimensional

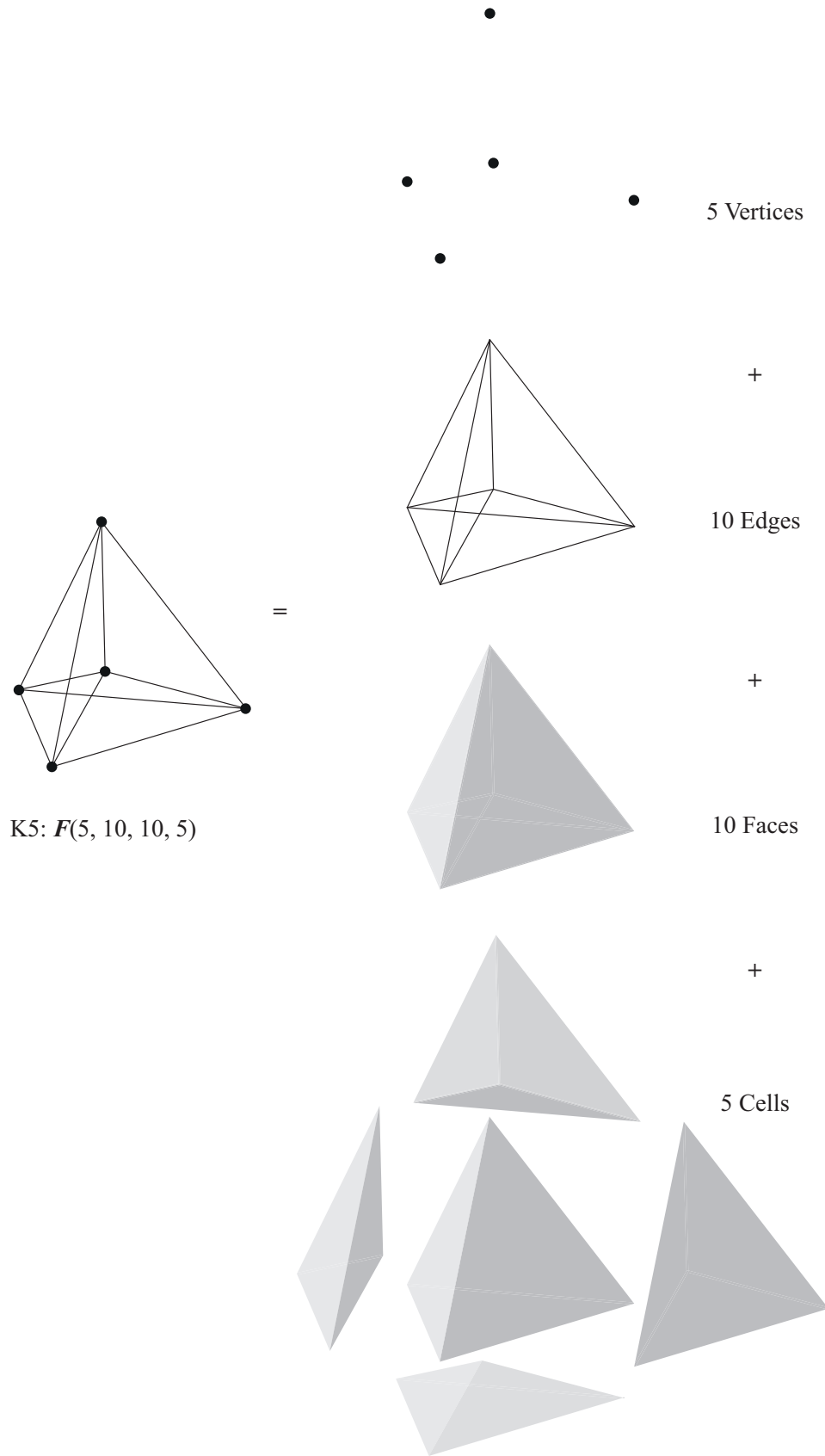


Fig. 2.13 Constituent geometrical elements of a regular K5.

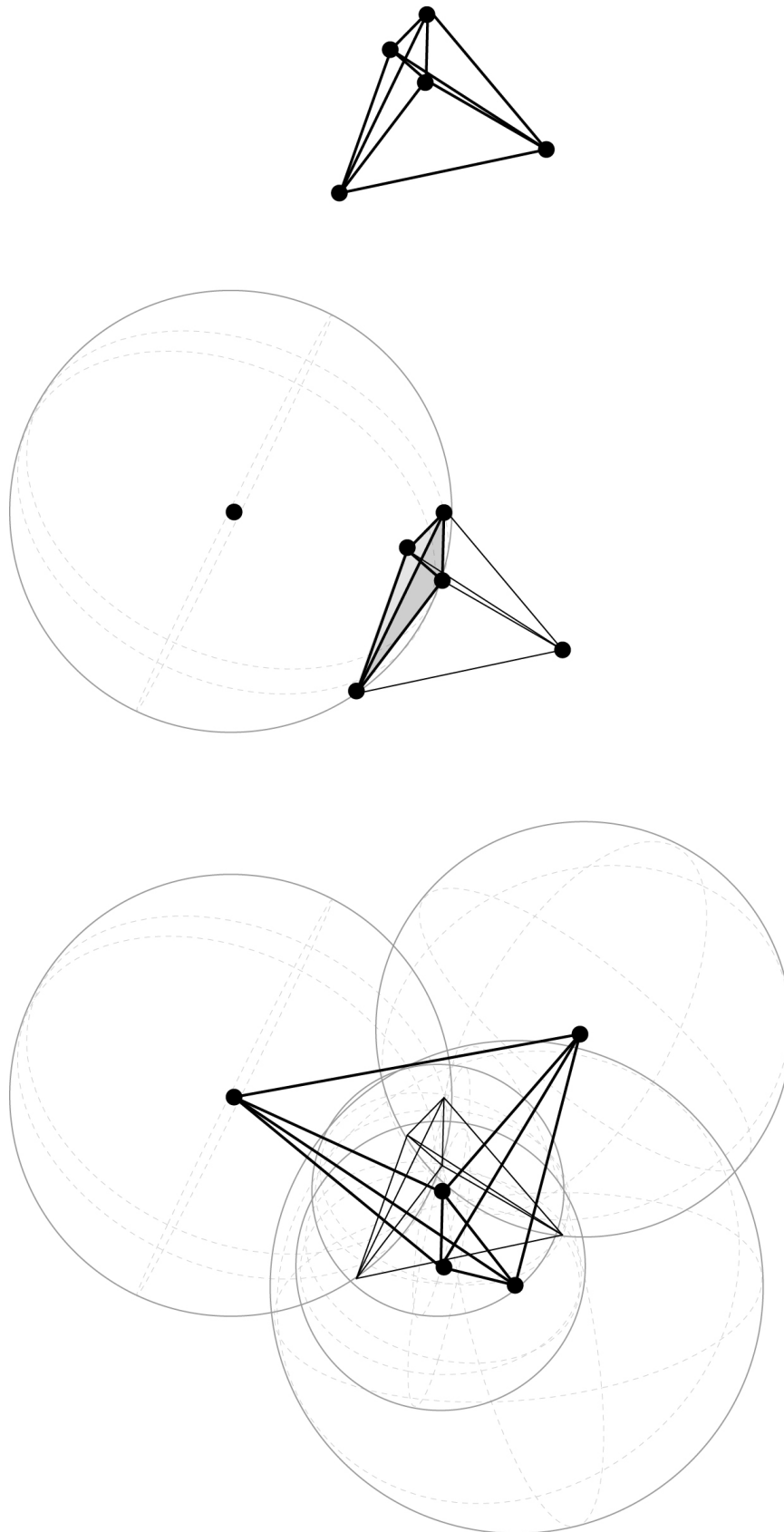


Fig. 2.14 Construction of Rankine reciprocal for a K5 through spheres.

projections and their corresponding Airy stress functions, and more recently, Micheletti proposed a matrix-based procedure for the construction of point-symmetric reciprocal force diagrams for some 3D self-stressed networks (Micheletti, 2008).

Given a generic 3D form diagram in static equilibrium, various possible configurations of 3D force diagrams with corresponding edges parallel can be generated and transformed using the vector-based approach to 3D graphic statics (D'Acunto et al., 2017, 2019), (Figure 2.16). Unlike Rankine 3D diagrams (Figure 2.15), vector-based 3D diagrams do not obey a 4D duality between their geometrical elements. In particular, they follow a rather 3D duality in the sense that form edges  $e$  map to force edges  $e'$  and form vertices  $v$  to force faces  $f'$ ; however, they generally have duplicate edges (Figure 2.16). As a result, vector-based diagrams are in general not reciprocal.

The methodologies developed in this thesis correspond to Maxwell 2D diagrams for the 2D case and to Rankine 3D diagrams for the 3D case.

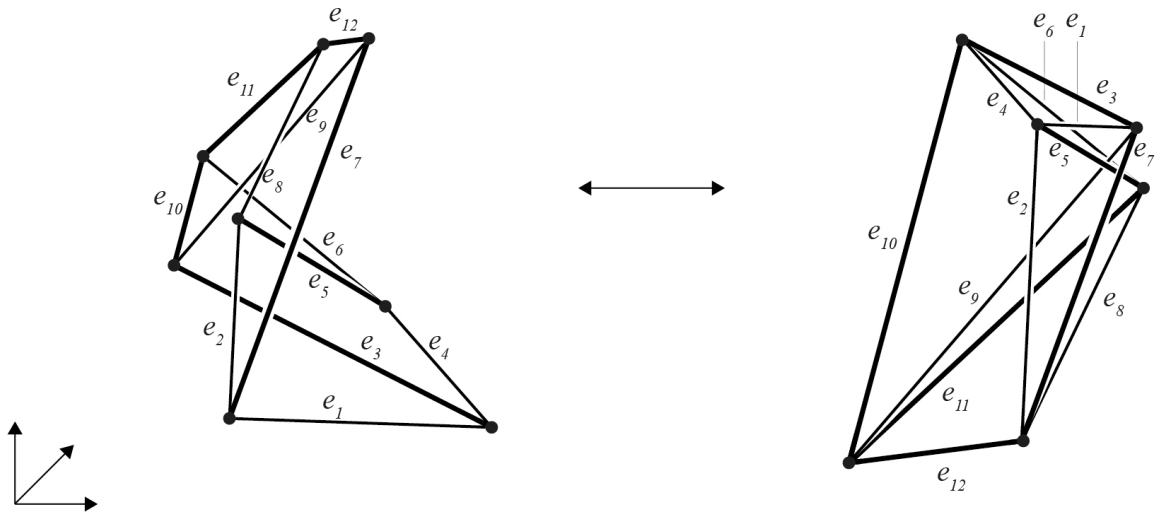


Fig. 2.15 Cremona 3D reciprocals. Left: Spatial form diagram which is topologically a cube. Right: Reciprocal force diagram which is topologically an octahedron with corresponding edges parallel.

A type of diagrams which is of particular importance is spiderwebs (Whiteley et al., 2013). These derive their name from the homonymous insect's elaborate tensile structures which can be observed in nature. In the context of structural engineering and rigidity theory a spiderweb can be thought of as a cable-only structure which is fixed to some points. A spiderweb with non-slack edges has a positive self-stress (is in tension without the presence of external forces) in all its cables and is attached on a compressive hoop. A 2D spiderweb is self-stressed if and only if it is the orthogonal projection of a convex polyhedron (Connelly, 1993; Whiteley et al., 2013). The fact that spiderwebs comprise tensile elements fully

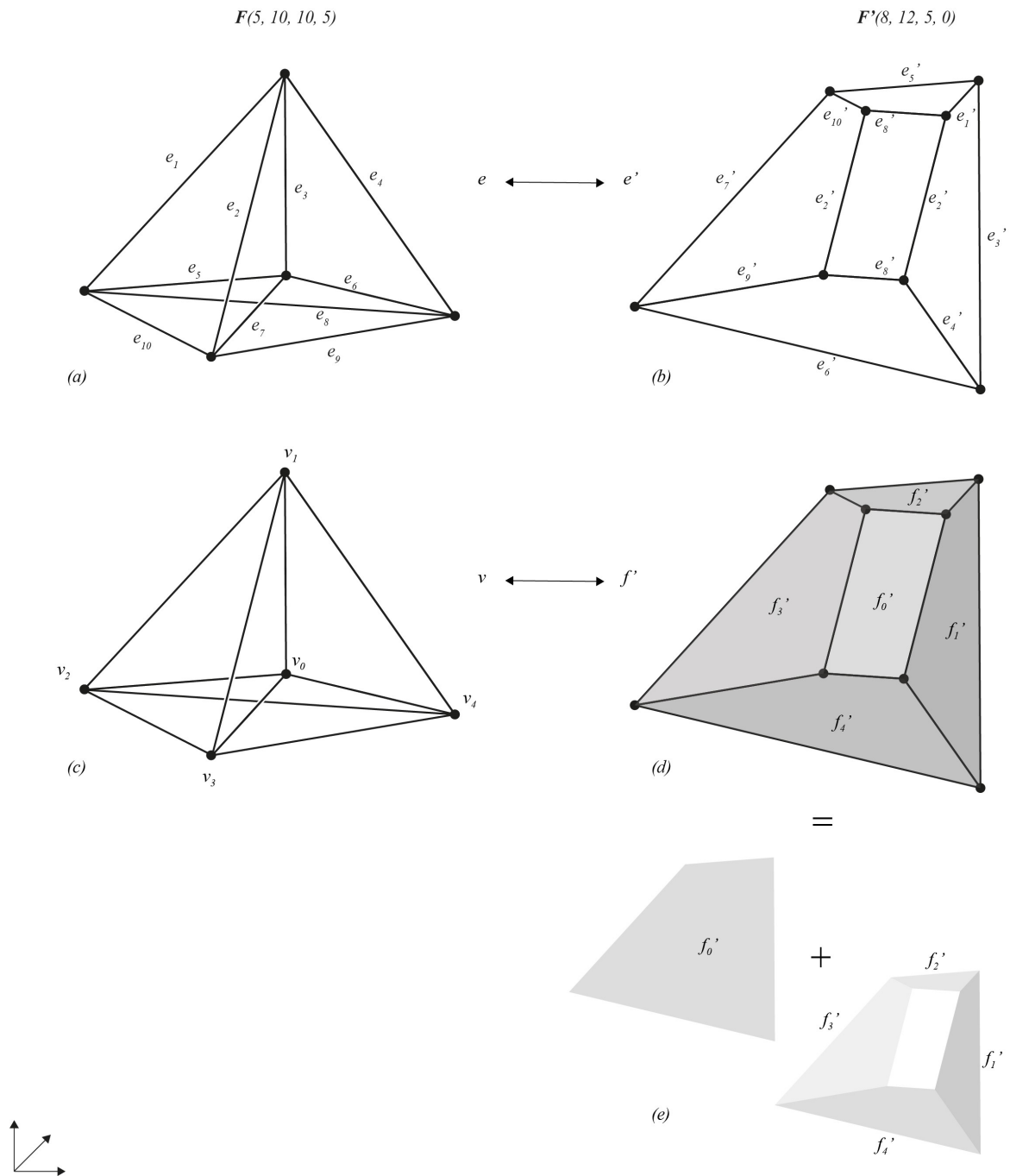


Fig. 2.16 (a): 3D form diagram of a spatial truss with a 5-simplex geometry  $F(5, 10, 10, 5)$ ; (b): 3D force diagram with corresponding force edges  $e'$  parallel to the form edges  $e$ ; (c, d, e): The form vertices  $v$  map to force faces  $f'$  following a 3D duality, however; the resulting force diagram  $F'(8, 12, 5, 0)$  has duplicate edges.

enclosed in a single compressive hoop can also readily relate to the geometric construction of Schlegel diagrams.

Schlegel diagrams are perspective projections (in  $\mathbb{R}^{d-1}$ ) of convex polytopes (in  $\mathbb{R}^d$ ) from a point just outside one of their faces. For example, for a 2D Schlegel diagram the geometric construction is as follows: for a given convex polyhedron (3-polytope) we take a point just outside of the centroid of one of its faces and apply a perspective projection from there onto a projection plane. The resulting 2D diagram will consist of the outer boundary – the edges of the face picked initially – and all the internal edges which are the projections of all the remaining polyhedral faces, edges and vertices (Loeb, 1991) (Figure 2.17). Interestingly, we can find some Schlegel diagrams in Maxwell, 1864 – like Figure 5 (Maxwell, 1864a) (Figure 2.17). It follows that a Schlegel diagram is a spiderweb where the outer boundary (compressive hoop) is the projection of the face which fully contains the projections of the remaining geometrical elements of the polyhedron. Moreover, spiderwebs have planar graphs since topologically they have non-crossing edges for the  $\mathbb{R}^2$  case and non-intersecting faces for the  $\mathbb{R}^3$  case (Crapo, 1979).

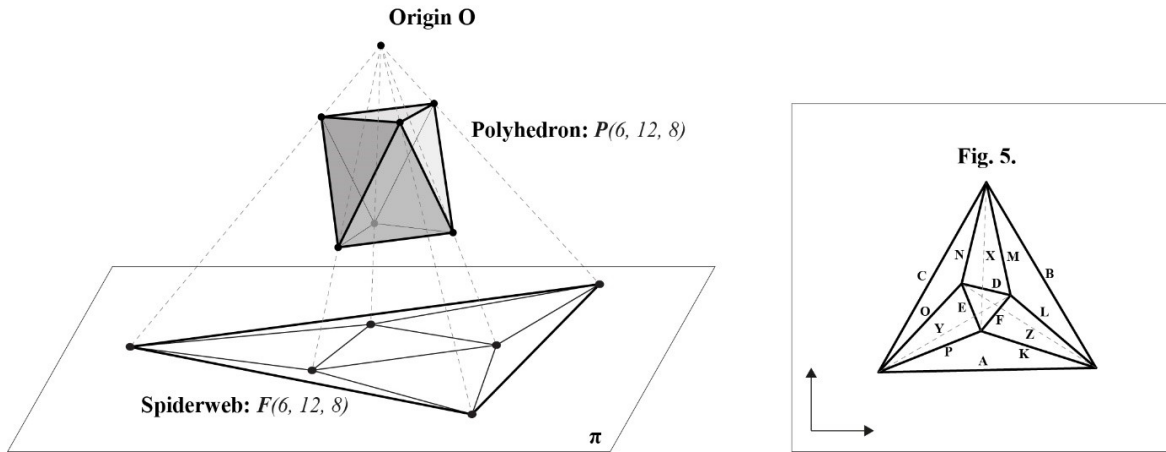


Fig. 2.17 Left: Schlegel projection of a polyhedron resulting in a 2D spiderweb structure. Right: a 2D truss with a spiderweb geometry as found in Maxwell's 19<sup>th</sup> century paper.

Lastly, it should be highlighted that we can talk about reciprocity and duality in very general and topological terms, namely, two reciprocal or dual geometries need not necessarily conform to the rules of perpendicularity outlined above (McRobie, 2017a). For instance, in the case of a 2D pair of reciprocal diagrams, we can have reciprocal form and force edges which are not perpendicular. The diagrams are still topologically reciprocal or dual with each other, they just not represent structures with purely axial loads. For example, it has been showed (Konstantatou et al., 2018) that general reciprocals can be produced by using polar transformations based on quadrics other than the paraboloid of revolution or the sphere. The

latter are two special cases which can directly produce through projection (orthogonal or central) pairs of reciprocal 2D diagrams of trusses in static equilibrium with purely axial forces – the case which is of interest in graphic statics and of the applications addressed here. Nonetheless, general reciprocal polyhedra obtained in a general manner can still be transformed to the special cases of interest.

## 2.5 Polarities as a tool for deriving reciprocal polyhedra

Since polarities are global transformations mapping every element in space to another they are a useful tool for generating global force reciprocals of structures in static equilibrium as well as for transforming structures from one typology to another.

As discussed in section 2.2.1, in a 3D geometry, a polyhedron can be mapped to its reciprocal polyhedron through a polar transformation, or polarity. As a result, for every polyhedron  $P$  the planes (polar planes) on which its faces lie on can be transformed to the vertices (poles) of its reciprocal polyhedron. If this geometrical procedure is followed for every plane of the faces of the given polyhedron then all the reciprocal vertices are found. These can now be connected following the connectivity of the given faces ( $C_{pl}$ ) to construct the reciprocal polyhedron. More generally, planes can map to points using a range of polarities. These transformations, or mappings between reciprocal geometrical elements, can be achieved in several equivalent ways. These were known and used by Maxwell (Maxwell, 1870); however, they were not acknowledged or employed from most contemporary graphic statics methods.

Considering these geometric constructions from a Euclidean perspective and reclaiming the distinction between various non-degenerate conics and quadrics, the relations between dual elements can be expressed in analytical form, using Cartesian coordinates (Smith, 1886). These were already studied in Maxwell's time in the 19<sup>th</sup> century. For the general equation of a quadric:

$$ax^2 + by^2 + cz^2 + 2fyz + 2gzx + 2hxy + 2ux + 2vy + 2wz + d = 0 \quad (2.1)$$

Given a pole  $P(x', y', z')$ , the corresponding polar plane  $\pi$  is described by the following equation:

$$x(ax' + hy' + gz' + u) + y(hx' + by' + fz' + v) + z(gx' + fy' + cz' + w) + ux' + vy' + wz' + d = 0 \quad (2.2)$$



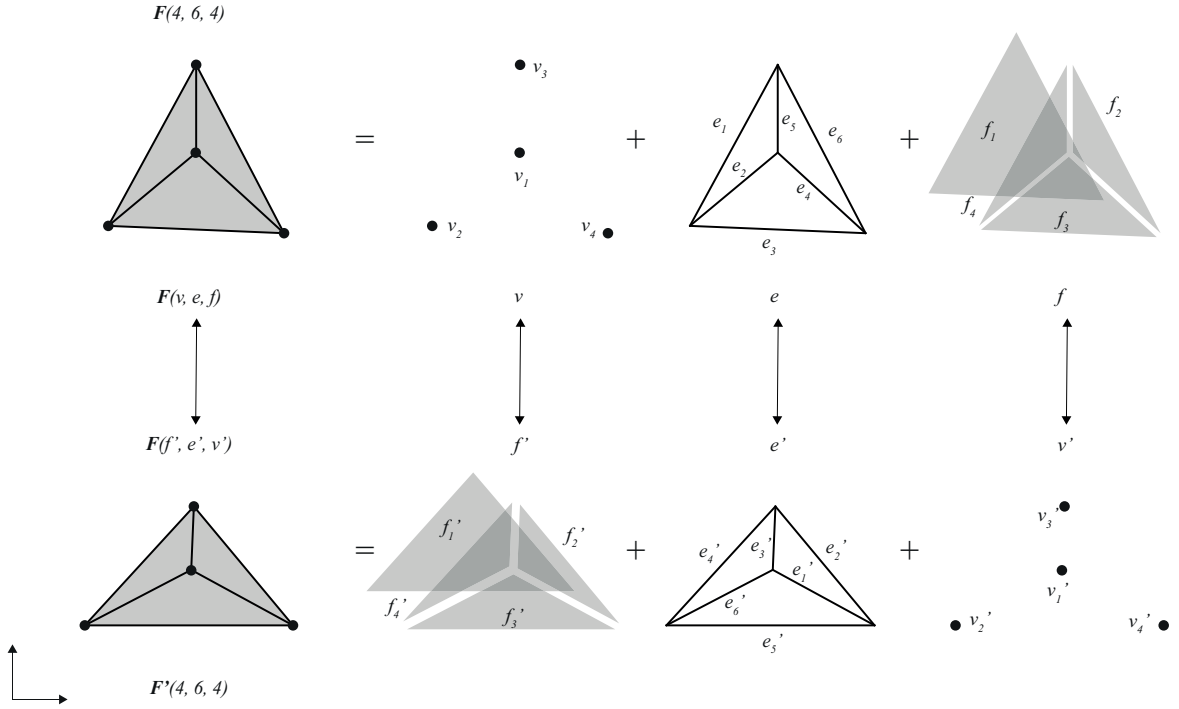


Fig. 2.18 Reciprocal 2D form and force diagrams showing the correspondence between their geometrical elements which follows a 3D projective geometry duality.

Polarities can be thought of as pairs of transformations  $L, L^{-1}$  that map a plane  $\pi$ , defined in equation form as  $Ax + By + Cz + D = 0$  and described by the corresponding quadruples  $(A, B, C, D)$ , to a point  $P$  described from the triple  $(x', y', z')$  and vice versa.

Using, for example, a paraboloid of revolution (Figure 2.19) with equation  $x^2 + y^2 - 2cz = 0$  as the quadric of the polarity, for a point  $P(x', y', z')$  and its polar plane  $\pi$  described by the equation  $z = Ax + By + D$ , we have that

$$L^{-1}(P) = \pi \quad (2.3)$$

$$L^{-1}(x', y', z') = (A, B, -1, D) \quad (2.4)$$

then by using equation (2.2), we have that for this particular quadric, the plane  $\pi$  is given by

$$x(x') + y(y') + z(-c) - cz' = 0$$

which rearranges to

$$z = \frac{x'}{c}x + \frac{y'}{c}y - z' \quad (2.5)$$

which, when expressed in the  $(A, B, -1, D)$  form has

$$A = \frac{x'}{c}, \quad B = \frac{y'}{c}, \quad D = -z' \quad (2.6)$$

These equations can be readily inverted to give

$$x' = cA, \quad y' = cB, \quad z' = -D \quad (2.7)$$

which is thus the mapping  $L$ :

$$L(\pi) = P \quad (2.8)$$

$$L(A, B, -1, D) = (x', y', z') = (cA, cB, -D) \quad (2.9)$$

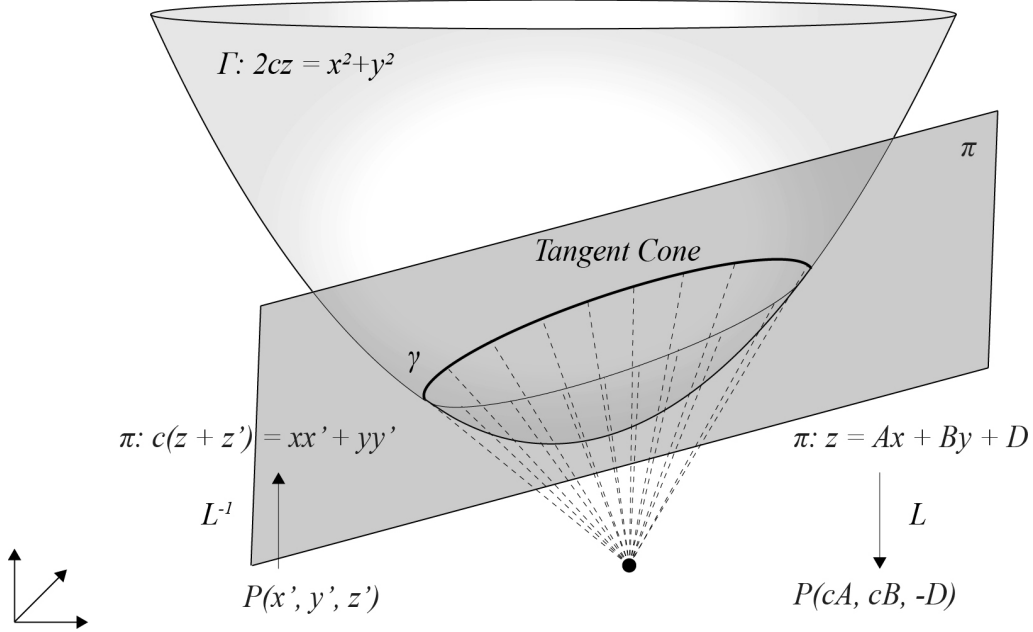


Fig. 2.19 Polarity in 3-space induced by a paraboloid of revolution.

Polarities and projective geometry in the context of graphic statics have not only been explored from a geometrical point of view but also from an algebraic one; the latter following a matrix approach (Figure 2.20). In the first case, the geometrical constructions are based on the notion of conics, quadrics and their higher-dimensional analogues and they apply to both 2D and 3D graphic statics, whereas in the latter case they are based on the notion of

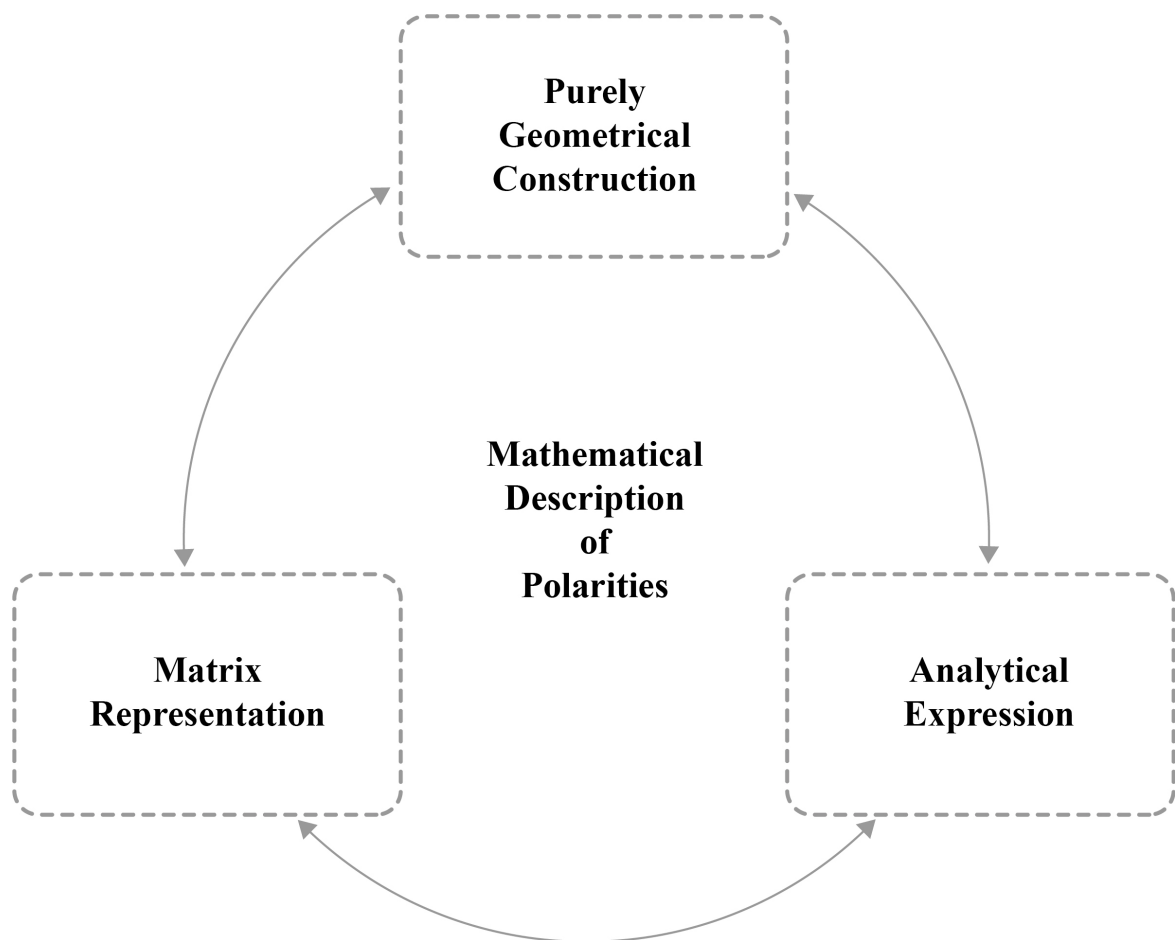


Fig. 2.20 Equivalent mathematical descriptions of polarities.

null-polarity which applies only to 2D graphic statics (since it cannot be defined in even dimensions). In (Konstantatou et al., 2018) is highlighted how the matrix approach can be used for any polar transformation and how the geometrical approach can be used for the null-polarity. Thus, ultimately the two approaches (projective geometry constructions and matrix transformations) are equivalent with respect to constructing reciprocal diagrams.

A non-degenerate quadric, described in its general equation form in (Vaisman, 1997), can be represented in matrix form (Amir-Moez, 1973) as:  $\mathbf{x}^t \mathbf{S} \mathbf{x} = 0$ .

where  $\mathbf{x} = \begin{bmatrix} x \\ y \\ z \\ 1 \end{bmatrix}$ , and the symmetric matrix associated to the quadric is:

$$\mathbf{S} = \begin{bmatrix} a_{11} & a_{12} & a_{13} & a_{14} \\ a_{21} & a_{22} & a_{23} & a_{24} \\ a_{31} & a_{32} & a_{33} & a_{34} \\ a_{41} & a_{42} & a_{43} & a_{44} \end{bmatrix}$$

A point  $P = (x_p, y_p, z_p, 1)$  is then mapped to its polar plane  $\pi$  through the polar transformation (in homogeneous coordinates)  $P^t \mathbf{S} \mathbf{x} = 0$ .

This relation holds not only for points that lie on the quadric but more generally for any point in space. If the point lies on the quadric, then the polar plane is the tangent plane on that point. As a result, the point lies on its polar plane. If the point does not lie on the quadric, the equation for its polar plane can be obtained which this time does not include the point.

For example, considering as the quadric of the polarity a paraboloid of revolution with canonical equation (in Cartesian coordinates):

$$x^2 + y^2 - 2z = 0 \quad (2.10)$$

A point  $P = (x_p, y_p, z_p)$  is mapped to its polar plane  $\pi$ :

$$xx_p + yy_p - z - z_p = 0 \quad (2.11)$$

through the transformation (in homogeneous coordinates):

$$\begin{bmatrix} x_p & y_p & z_p & 1 \end{bmatrix} \begin{bmatrix} 1 & 0 & 0 & 0 \\ 0 & 1 & 0 & 0 \\ 0 & 0 & 0 & -1 \\ 0 & 0 & -1 & 0 \end{bmatrix} \begin{bmatrix} x \\ y \\ z \\ 1 \end{bmatrix} = 0$$

We should note that by using a polarity induced by a paraboloid of revolution this implies an orthographic projection of the reciprocal polyhedra. However, other polarities and projections can be used too. In which case transformations are needed to ‘correct’ the reciprocal form and force diagrams into a perpendicular/ or parallel configuration for trusses in static equilibrium.

The matrices associated to non-degenerate quadrics and null-polarity can be converted to each other through affine (reflection, scaling, shear, rotation, etc.) or more generally projective transformations using corresponding transformations matrices  $\mathbf{T}$  (Konstantatou et al., 2018). For instance, in order to convert the matrix  $\mathbf{S}$  of a real ellipsoid to the matrix  $\mathbf{S}'$  of an elliptic hyperboloid, it is possible to multiply the former with the following transformation matrix:

$$\mathbf{T} = \begin{bmatrix} 1 & 0 & 0 & 0 \\ 0 & 1 & 0 & 0 \\ 0 & 0 & -1 & 0 \\ 0 & 0 & 0 & 1 \end{bmatrix}$$

which corresponds to an affine transformation representing a reflection along the  $z$ -axis. As a result, any type of quadric or null-polarity can be used as described above to obtain a reciprocal polar plane for a given point  $P$  and then by using a suitable matrix  $\mathbf{T}$  convert it to any other polar construction. At the same time, these non-specific polarities could be useful for generating topological reciprocals where reciprocal edges need not be perpendicular or parallel. All the above apply to  $n$ -dimensional spaces and can be used for 2D, 3D and  $n$ D graphic statics where reciprocal elements map to each other following the principle of duality for the corresponding space.

The polarities approach followed here can be applied to any 2D self-stressed truss, to any 3D self-stressed truss which is a projection of a 4-polytope, and to rotationally symmetric spatial self-stressed structures (such as tensegrities) through the technique of coning. Following this method, spatial structures which have just one cell, which would otherwise map to just a single point, can be further subdivided to numerous cells which in turn can produce a geometrically richer force reciprocal (McRobie, 2016).

Polarities, which are applicable in the context of graphic statics as discussed above, are also closely related to the mathematical tool of Legendre transforms, which is widely used in a range of contemporary scientific fields. These are interconnected from a mathematical and historical point of view. In particular, Legendre transforms are a very useful mathematical tool which is underpinned from the concept of duality. Like polarities a key property is that they have period 2. They can be particularly useful in cases where thinking, measuring or

controlling the derivative of a function with respect to a point is easier than doing so about the point itself. Historically, polarities and Legendre transforms are also interlinked. Legendre transforms were introduced by Andrien-Marie Legendre (1752-1833) to solve a minimal surface problem given by Monge (Barbaresco, 2018). Moreover, ‘Chasles and Darboux interpreted Legendre Transforms in a geometrical way using reciprocal polars with respect to a paraboloid of revolution, a construction which was later re-used by Hadamard and Frechet in calculus of variations’ (Barbaresco, 2018). This type of reciprocation, seen in Legendre transforms and polarities, which is underpinned from projective geometry duality and has period 2 is a fundamental and far reaching, in terms of applications, geometrical construction and mathematical tool. With a starting point in the 18<sup>th</sup> century has gained popularity in multiple and diverse fields in the 20<sup>th</sup> and 21<sup>st</sup> century.

Examples of the applicability of Legendre transforms include (Baierlein, 1999; Callen, 1985; Houlsby and Puzrin, 2007; Shell, 2015): the relation between the Lagrangian and Hamiltonian functions in analytical mechanics; between strain energy and complementary energy in elasticity theory; between the various potentials that occur in thermodynamics (internal energy, Helmholtz free energy, Gibbs free energy, enthalpy); between the physical and hodograph planes occurring in the theories of the flow of compressive fluids and perfectly plastic solids. Moreover, they play a central role in the general theory of complementary variational and extremum principles. These transformations have also been widely employed in rate formulations of elastic/ plastic materials to transfer between stress-rate and deformation-rate potentials. Furthermore, Legendre transforms have been shown to play a role to conventional plasticity as well as to the hyperplasticity approach (Houlsby and Puzrin, 2007). As a result, Legendre transforms are very closely related to polarities. In fact, they are equivalent for mapping points to their tangent planes given a smooth and convex function of a surface. A detailed geometrical description of the Legendre transforms which underlines their connection to polarities can be found in Callen (Callen, 1985).

## 2.6 The role of polarities in structural analysis

In the context of structural engineering theory, polar transformations have not only been used in relation to graphic statics. Tarnai (Tarnai, 1989) used polarities in the projective 2-space to establish transformations between 2D tensegrity structures and grillages<sup>2</sup> in a projective geometry framework that guarantees duality. These two types of structures obey a 2D duality principle with the number of joints and bars of the tensegrity corresponding to the

---

<sup>2</sup>Grillages in the work of Tarnai are plane beam grids with simple joints which can carry forces only perpendicularly to the plane of the grillage.

number of beams and joints of the grillage. As observed by Rankine (Rankine, 1864) and Whiteley (Whiteley, 1987) the static and kinematic properties of a structure, including its stiffness, are preserved under projective transformations. Moreover, Tarnai (Tarnai, 1989) proved algebraically that the rank of the equilibrium matrix is preserved under a polarity which maps tensegrities to grillages and vice versa. As a result, these types of structures can be transformed into each other while maintaining their basic properties such as infinitesimal rigidity (Tarnai, 1989).

In the projective 3-space, polarities can be applied for the construction of lattice (truss) and dual plate structures (*hinged sheetworks*), where plates rigid in their planes are connected through shear-resistant edges. This has been studied in detail by Wester (Wester, 1989, 2011) as well as by rigidity theorists such as Whiteley (Whiteley, 1987). Following this 3D dualism (Figure 2.7), truss nodes map to plate faces, truss bars to shear-resistant edges, and consequently axial forces to shear forces. The two structures obey Euler's polyhedral formula, have the same Gaussian curvature (Wester, 1989), static and infinitesimal behaviour, rigidity properties and degrees of freedom (Whiteley, 1987). The construction proposed by Wester for deriving dual lattice and plate structures is essentially a polarity induced by a sphere (Figure 2.21). In this way, the axial loads in the lattice structure regarded as force vectors are transformed into moment vectors that produce shear forces in the edges of the plate structure. The shear forces relate to the axial forces by a ratio  $r_f$  which is calculated as  $r_f = l/\sin(a)$ , where  $l$  is the length of the reciprocal truss bar and  $a$  is the angle between the position vectors of the nodes of the bar regarding the centre of the sphere as the origin  $O$  (Wester, 1989). As a result, the structural and geometrical analysis and design of a plate structure can be performed on the reciprocal truss and then mapped back to the original structure and vice versa (Wester, 2011) – potentially simplifying the structural problem, when the reciprocal structure is easier to solve.

The work of Tarnai and Wester meets and can be generalized through rigidity theory. Whiteley (Whiteley, 1987), extended spatial trusses to become spatial tensegrities and discusses how they can be transformed under a polarity to special cases of hinged sheetworks, (*slotted sheetworks*) in which plates meeting at an edge can not only rotate but also slide with respect to each other on one direction along the slotted hinge. This result, even though not commonly used, generalises Tarnai's tensegrity – grillage polar correspondence in two-dimensions to its 3-dimensional analogue. Thus, for the same structure the dimension of the polar transformation can give different insights; for a spatial tensegrity a 4D polarity can give a reciprocal Rankine force diagram and a 3D polarity can transform the tensegrity to a completely different type of structure which is also in static equilibrium. Consequently,

polarities can provide a very elegant, useful and unified framework for applications in design, analysis, and structural transformations (Figure 2.22).

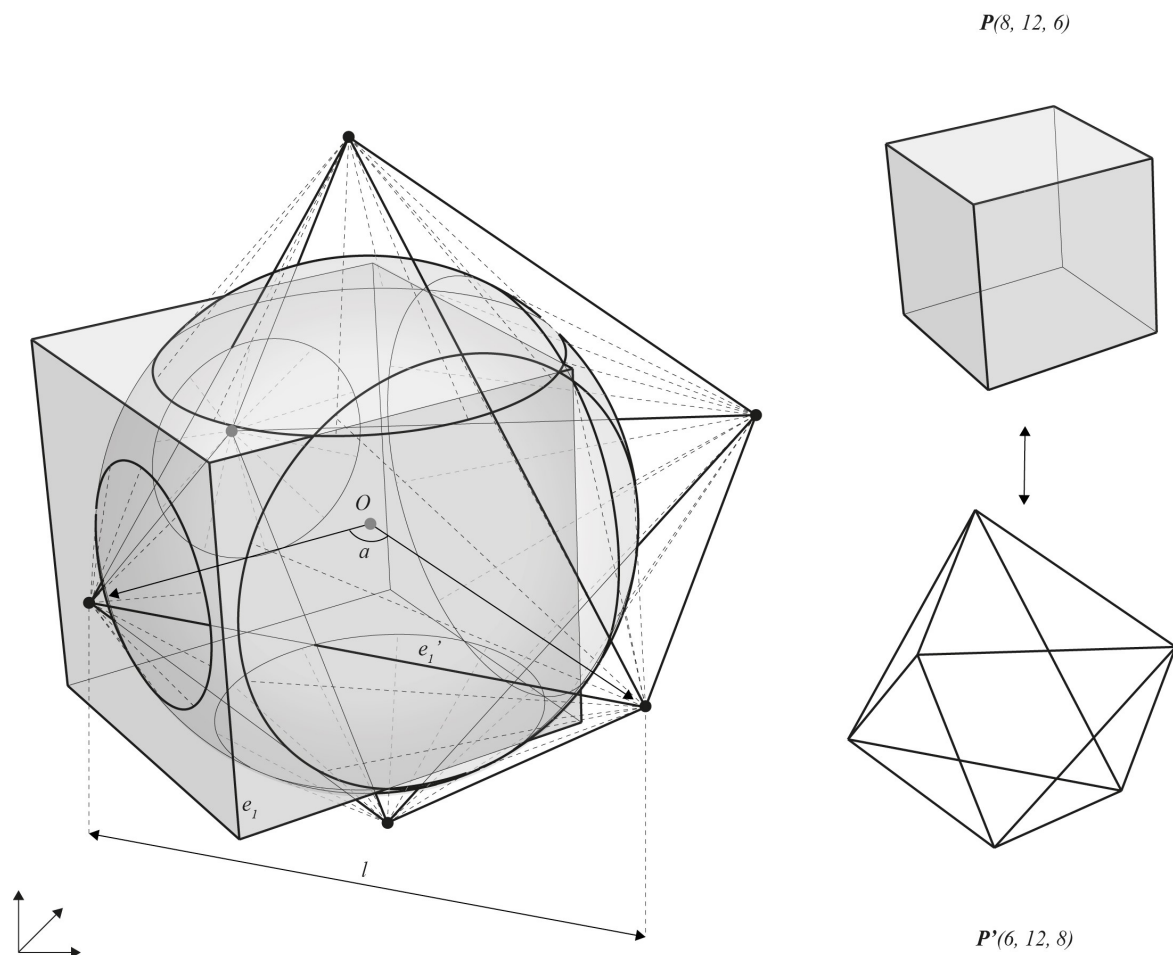


Fig. 2.21 Reciprocal spatial truss and hinged sheetwork on the right, induced by a polar transformation using a sphere on the left as described in the work of Wester (Wester, 1989).



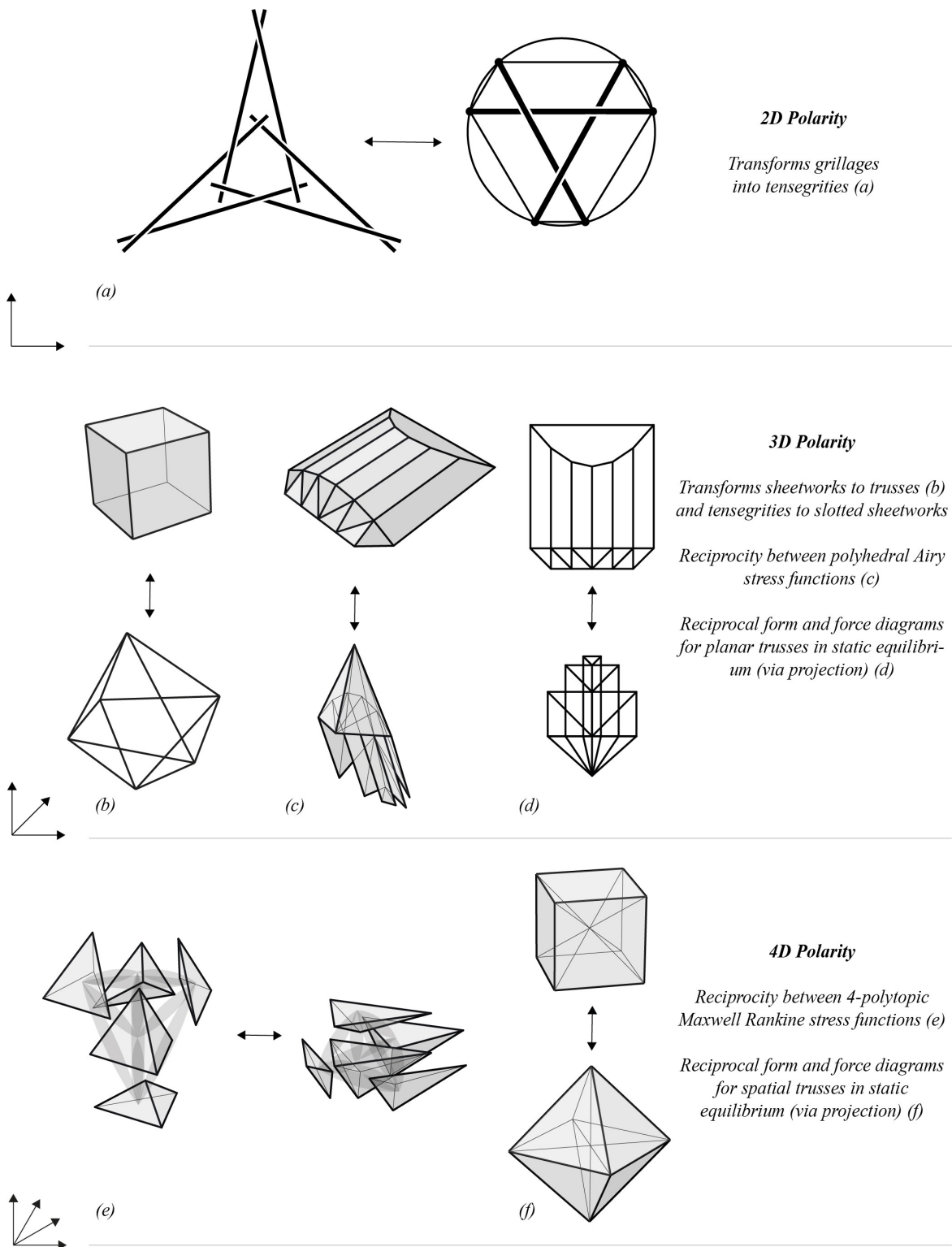


Fig. 2.22 The application of polarities in structural analysis and design.

## 2.7 Minkowski sums

Reciprocal form and force diagrams can be synthesized geometrically in one object (McRobie, 2016; Zanni and Pennock, 2009), named ‘Minkowski sum’ in contemporary graphic statics nomenclature. Thus, Minkowski sums embed visually the information for both form and force. For two sets of vectors  $\mathbf{A}$  and  $\mathbf{B}$ , we define the Minkowski sum to be the set:

$$\mathbf{A} + \mathbf{B} = \{a\mathbf{A}_i + b\mathbf{B}_i | \mathbf{A}_i \in \mathbf{A}, \mathbf{B}_i \in \mathbf{B}, a, b \text{ scalars}\} \quad (2.12)$$

Which is a vectorial addition of the coordinates for the two sets  $\mathbf{A}$ ,  $\mathbf{B}$  (Figure 2.23). For example, in a pair of 2D reciprocal diagrams  $\mathbf{F}(v, e, f)$ ,  $\mathbf{F}'(v', e', f')$ , we can take  $\mathbf{B}$  to be the set of vertices  $v$  of  $\mathbf{F}$  and  $\mathbf{A}$  the set of faces  $f'$  of  $\mathbf{F}'$ . Thus, the Minkowski sum will be an object resulting from the faces  $f'$  being added on the vertices  $v$  and the created parallelepipeds defined from form edges  $e$  and their reciprocal force edges  $e'$ . The inclusion of the scalars  $a$ ,  $b$  in the equation leads to different visual interpretations of the Minkowski sum: if  $b = (a-1)$ , then for  $a \approx 0$  the prominent geometry is the one of  $\mathbf{F}$ , whereas for  $a \approx 1$  the prominent geometry is the one of  $\mathbf{F}'$ . For values between 0 and 1 the Minkowski sum shows the transition between the two diagrams. Equivalently, for 3D reciprocal diagrams  $\mathbf{F}(v, e, f, c)$ ,  $\mathbf{F}'(v', e', f', c')$ ,  $\mathbf{B}$  can be seen as the set of vertices  $v$  of  $\mathbf{F}$  and  $\mathbf{A}$  as the corresponding set of reciprocal cells  $c'$  of  $\mathbf{F}'$ . For the spatial case, the parallelepipeds become volumetric prisms created from the faces of the cells  $c'$  extruded over the edges  $e$ . Given that the form diagram has units of length ( $L$ ) and the force diagram units of force ( $F$ ), it follows that their Minkowski sum has units of ( $FL$ ). Thus, it can provide intuitive and visual information on Maxwell’s load path theorem as well as on the volume of material required for constant stress design of the structure (McRobie, 2016).

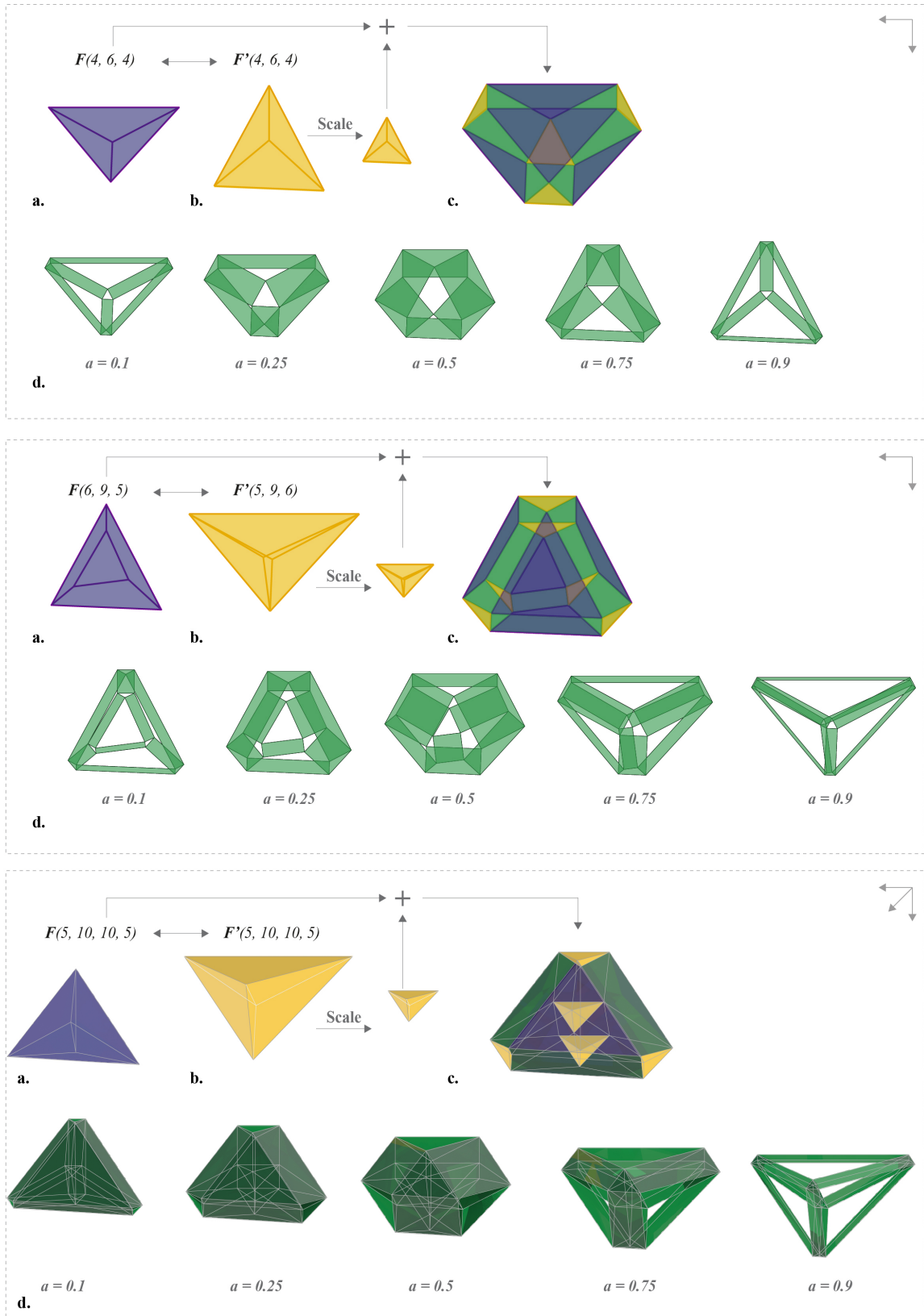


Fig. 2.23 Top and middle: two 2D examples of reciprocal diagrams and their Minkowski sums for various values of  $a$ . Bottom: Spatial example of reciprocal examples and Minkowski sum for a 5-simplex.

## 2.8 Summary

This Chapter reviewed the history of graphic statics, reciprocal diagrams and stress functions from their infancy to today, while highlighting the influential but comparatively unknown contribution of Maxwell. Specifically, by explaining and visualising Maxwell's reciprocal constructions while placing them in the scientific context of the time (late 19<sup>th</sup> century) through an in-depth literature review. Moreover, the role of polarities was presented as a tool for deriving 2D form and force diagrams by reciprocating their corresponding polyhedral stress functions. The importance of this method is based on the following facts:

- It is a direct method for deriving global static equilibrium.
- All four reciprocal objects (form diagram, force diagram, corresponding stress functions) are interlinked and the designer can start designing with any one of these - the rest will be automatically updated.
- This method has a rigorous and elegant three-fold equivalent description in terms of purely geometrical construction, matrix description and analytical expression.
- The use of the Airy stress function makes sure that any design and transformation operations are performed within the equilibrium space.

Furthermore, the fundamental role of polarities in other fields of engineering (transformations between 2D grillages and tensegrities, transformations between 3D sheetworks and trusses as well as 3D tensegrities to slotted sheetworks) was underlined and thus the far-reaching and cross-disciplinary applicability of this method. Lastly, key notions that will be used in the next Chapters were reviewed such as N-polytopes and Minkowski sums.

# Chapter 3

## Geometry-based structural analysis

This Chapter introduces a direct, geometrical, graphic statics methodology, which is unified for 2D and 3D tension-and-compression trusses based on the concept of reciprocal stress functions. This methodology has an equivalent three-fold mathematical description (geometrical construction, matrix representation and analytical expression) and enables designers to work with any one of four interlinked reciprocal objects: the form and force diagrams and their corresponding stress functions. This introduces significant design and analysis freedoms.

The parts of this Chapter concerning global static equilibrium (subsections 3.2.2 and 3.2.3) have been published in the *International Journal of Solids and Structures* (Konstantatou et al., 2018) and presented in the Symposium for the International Association of Shell and Spatial Structures - Tokyo, September 2016 (Konstantatou and McRobie, 2016).

### 3.1 Introduction

Existing computational frameworks in the contemporary graphic statics community are valuable tools for the design and analysis of structures in static equilibrium. However, many of these are based on iterative/ node-by-node (local)/ brute force/ matrix analysis approaches to solve the problem and do not take into consideration the reciprocal stress functions but solely the reciprocal form and force diagrams. As a result, they lose valuable insight as well as design and analysis freedom capabilities. Moreover, they do not take advantage of the underlying fundamental geometrical principles and projective geometry framework introduced by Maxwell (Maxwell, 1870). It should also be highlighted that the method and its output (reciprocal form and force diagrams) are distinct. The visual and intuitive nature of the output is independent from the less intuitive and less visual computational implementation of the method which is inaccessible to most users. Graphic statics are praised

for their intuitive nature but most of the times the methods to obtain them do not necessarily follow suit.

A direct and unified methodology for 2D and 3D trusses in static equilibrium has been developed as a result of this PhD research (Konstantatou et al., 2018) in the context of projective geometry. This method directly generates global static equilibrium, has no need for iterative/ reconstructive procedures, and is based on the reciprocity between stress functions – the projections of which are reciprocal form and force diagrams. This method can be used to derive any type of 2D (Maxwell or Cremona) and 3D (Rankine) force reciprocals for trusses in static equilibrium when these are projections of 3D and respectively 4D plane-faced stress functions. This approach has the following characteristics:

- The structures need not be compression-only/ tension-only.
- The structures can be either self-stressed or loaded with external forces.
- There is no distinction or special treatment between form and force diagrams.
- It works for all cases of 2D structures (with the possible addition of extra vertices in the case of non-planar graphs<sup>1</sup>),
- and for spatial plane-faced polyhedral structures which obey the counting rules of 4-polytopes (every face belongs to two cells, every edge to at least three cells).

This framework interlinks and gives direct insight to the designer over all four reciprocal objects: form diagram, force diagram and their corresponding stress functions. The latter prove to be powerful design tools. They are intuitive representations of the structural properties of the form diagram, and they have cross-disciplinary applications to other fields of structural engineering and science.

In this Chapter a number of geometrical tools are presented for the visual and intuitive analysis of structures in static equilibrium. Specifically it addresses the following questions:

- How global static equilibrium can be derived for 2D and 3D cases by using a direct and unified method?
- What insight does this method add to the already existing literature?
- What is the role and what are the benefits of stress functions when used in the context of structural analysis and design?

---

<sup>1</sup>If the graph of a diagram is non-planar topologically, there are special cases when this is not necessarily a problem as we will see in section 3.2.4. In particular, this special case is of diagrams which are projections of  $n$ -connected polyhedra with  $n > 1$  like a faceted torus.

Moreover, a twofold structural analysis framework comprising statics and kinematics is discussed. This reflects recent progress (McRobie et al., 2017) on extending the graphic statics theory and applying it, in conjunction with virtual work, to derive a kinematic analysis by geometrical manipulations of the force reciprocal.

## 3.2 Graphic statics

### 3.2.1 Counting the states of self-stress

Maxwell (Maxwell, 1864a,b, 1870) introduced counting rules which aimed to provide a general framework for the study of the rigidity of plane and spatial trusses and the analysis of their internal mechanisms and states of self-stress. He described sequential constructions of *stiff* trusses which are essentially a forerunner of minimally rigid graphs as described by Henneberg in 1911 (Henneberg, 1911) and formally defined by Laman almost a century later (Laman, 1970) in the field of graph theory.

In his 1870 paper, Maxwell discusses his rigidity rules, counting rules and their relation to the number of mechanisms and states of self-stress.

For the 2D case, Maxwell states that if  $2s - e - 3 = p > 0$ , where  $s$  is the number of points and  $e$  is the number of edges, then the system has  $p$  degrees of freedom (mechanisms).

For the 3D case, Maxwell observes that if  $3s - e - 6 = p > 0$  and if that also applies for every subsystem of points and edges, then the system has  $p$  degrees of freedom (mechanisms). On the other hand, if  $3s - e - 6 = q < 0$  then there are  $q$  independent possible states of self-stress.

Advancements in rigidity counting rules (Calladine, 1978) have improved and formalised the above. The generalised rule proved by Calladine states that for the 2D case:  $2s - e - 3 = p - q$ , and for the spatial case:  $3s - e - 6 = p - q$ . Specifically, for systems which satisfy Maxwell's rule we have that  $p = q$  thus they can either be rigid and have no mechanisms and self-stresses or have an equal number of mechanisms and states of self-stresses (Calladine, 1978). An example of the latter case is tensegrity structures (Figure 3.1), which obey Maxwell's rule on rigidity, but exhibit infinitesimal mechanisms which are stabilised from corresponding states of self-stress.

Moreover, Maxwell assumed that all triangulated polyhedra are rigid. Specifically, in Maxwell's time (second half of 19<sup>th</sup> century) Cauchy had already proved, in 1831, that *all convex* polyhedra are rigid and Euler conjectured that *all triangulated* polyhedra were rigid (Cromwell, 1997). However, the dawn of the 20<sup>th</sup> century witnessed the first flexible triangulated polyhedron example by Bricard. This was followed by research and counter-

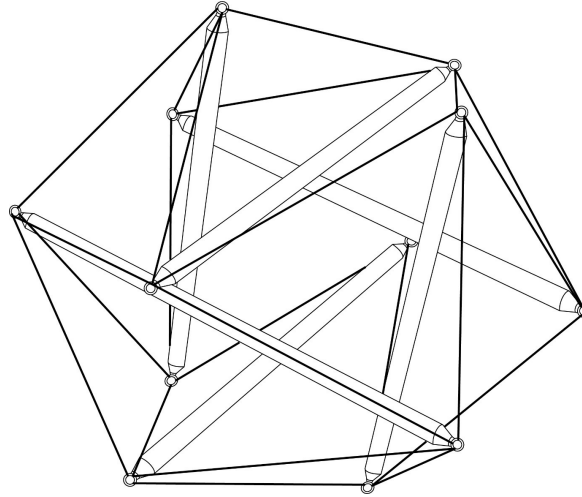


Fig. 3.1 A tensegrity structure which has 1 state of self-stress and 1 infinitesimal mechanism even though it satisfies Maxwell's rule.

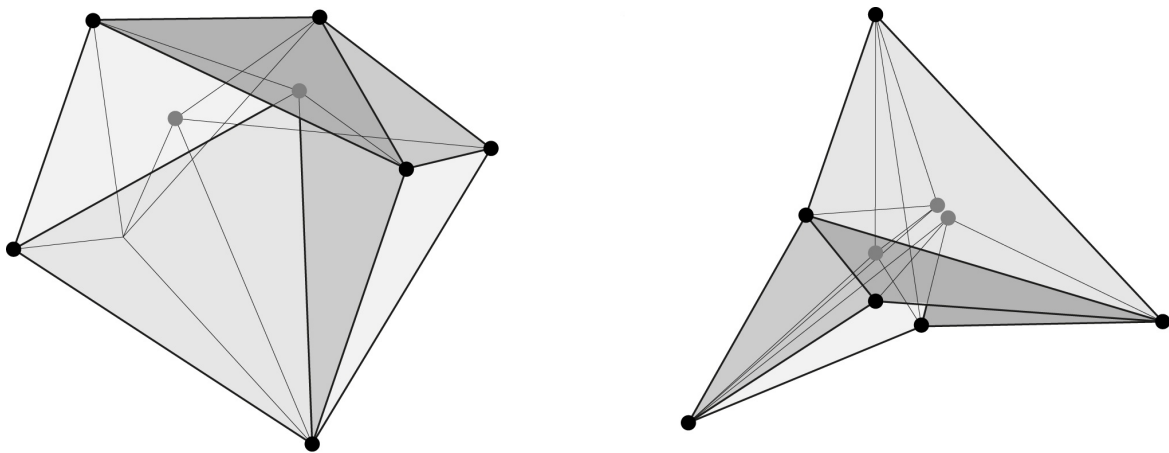


Fig. 3.2 The Steffen flexible polyhedron: a triangulated topological sphere with 1 state of self-stress and 1 finite mechanism.



examples on the rigidity of polyhedra by Bruckner, Connelly, Kuiper, Deligne and Steffen (Cromwell, 1997) who came up with a triangulated non-intersecting polyhedron of 9 vertices and 21 edges (Figure 3.2) which has one finite mechanism and one state of self-stress as  $p = q = 1$ . These type of flexible polyhedra are extremely rare though. In particular, they are very specific embeddings of topologically triangulated spheres in  $\mathbb{R}^3$  which are ‘generically rigid’. That is, Gluck proved in 1975 that almost any geometric manifestation with such a topology is rigid, but there are some specific geometries which are not (Cromwell, 1997).

Calladine’s counting rules give a complete algebraic description of the relation between edges and nodes of a pin-jointed structure and the number of its states of self-stresses and mechanisms. Moreover, by using matrix analysis and specifically Singular Value Decomposition (Pellegrino, 1993) the designer can have a full detailed analysis of the structural behaviour of the truss. However, there are no visual ways and guidelines with which practitioners could assess geometrically the number of states of self-stress of a structure. Such guidelines would be useful since they would provide an estimate of the design and analysis freedoms available with regards to constructing the stress function and subsequently the possible forms of a truss in static equilibrium. In this section such visual rules and guidelines are introduced. The example used here is a self-stressed 2D tensile net structure with numerous faces of irregular geometry. This geometry is similar to a large-scale art installation designed by Janet Echelman and analysed structurally by Skidmore, Owings and Merrill (SOM) (Vansice et al., 2018).

What is examined here is: given an initial 2-dimensional form diagram in static equilibrium how many nodes can be lifted individually in the  $z$ -direction to construct a plane-faced polyhedron? An initial discussion on the equivalence of independent states of self-stress and polyhedral liftings of a given form diagram was presented at the International Association for Shell and Spatial Structures (IASS) symposium in Amsterdam (McRobie et al., 2015). There, it was shown (Figure 3.3) that for a triangulated form diagram every internal node (apart from the ones belonging to a bottom boundary face which remains fixed on the  $z$ -plane) can be lifted independently and thus corresponds to an independent state of self-stress. However, in the case of non-triangulated structures which have polygonal faces with more than three vertices, the number of nodes that can be lifted independently can be greatly reduced. This is because every plane, which contains a face of the resulting polyhedron, is defined solely by three points. As a result, the remaining nodes belonging to that face are automatically fixed.

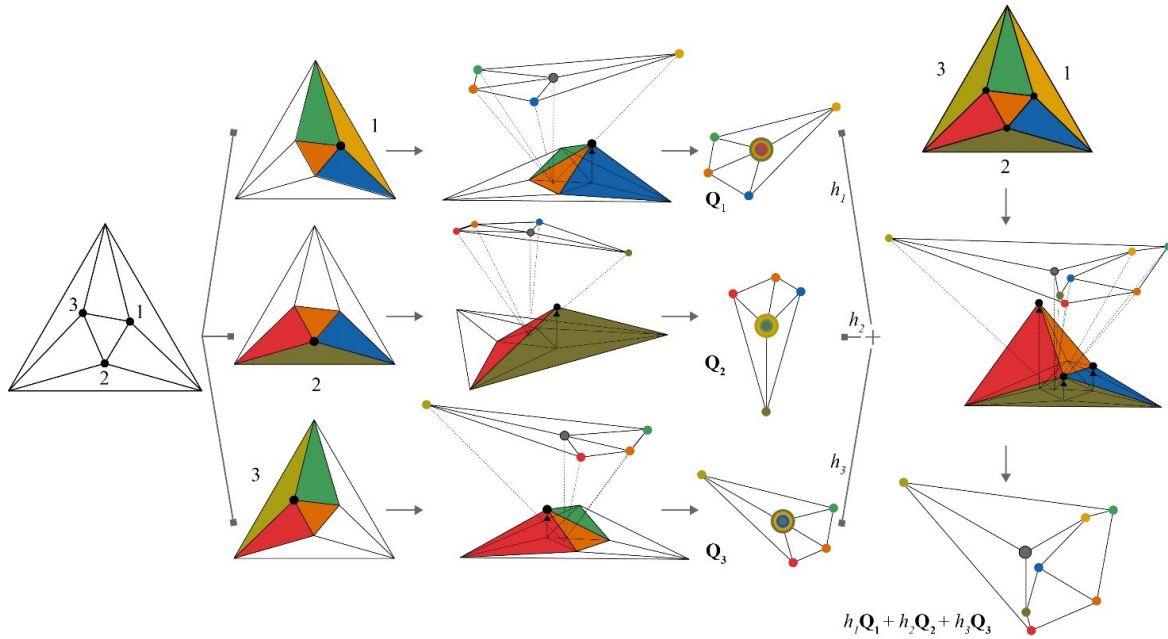


Fig. 3.3 Reciprocal basis diagrams from local Airy polyhedra. The original supports three independent local stress functions since it has three internal nodes (1, 2, 3) that can be lifted independently. The linear combinations of these three lead to more general reciprocals.

Let's take the example of an irregular, non-triangulated structure. We want to develop a visual algorithm which identifies the minimum number of nodes that can be lifted individually. Each one of them corresponds to an independent state of self-stress:

- Suppose that the boundary is spanned by a fixed face on the plane which includes all the other internal faces and internal vertices  $V_{in}$ . In the initial flat configuration all vertices have a  $z$ -coordinate equal to zero.
- From the faces adjacent to the boundary, we choose the face  $f_a$  which has the maximum number of vertices  $v_{ai}$ . We lift in the  $z$ -direction one of them which does not belong to the boundary. As a result, now three vertices are fixed and thus, the plane of  $f_a$  and all the  $z$ -coordinates of the remaining vertices in  $v_{ai}$  can be calculated.

- The lifting of this face may result in more faces and vertices being fixed. Let's name this set of faces  $F_a$  and the corresponding set of vertices  $V_a$ .
- If  $V_a \subset V_{in}$  continue:

For the faces adjacent to  $F_a$  which are not yet lifted pick the one  $f_b$  with the maximum number of vertices  $v_{bi}$ .

In order to lift  $f_b$  only one new non-fixed vertex is needed (we already have two fixed vertices from the adjacency to  $F_a$ ).

\* If  $V_a \cup V_b \subset V_{in}$  repeat until all vertices in  $V_{in}$  are fixed.

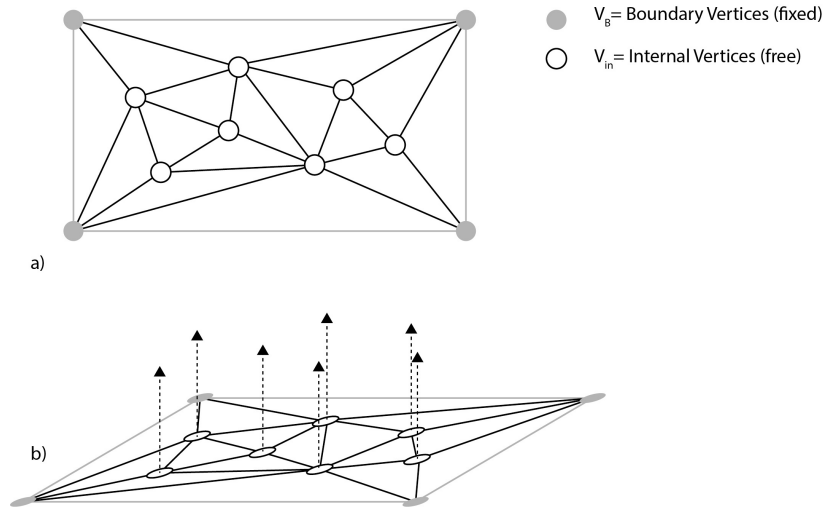


Fig. 3.4 a) The vertices in grey  $V_B$  belong to the boundary and are fixed (their  $z$ -coordinate equals zero), whereas the vertices in white  $V_{in}$  are free to move; b)  $V_{in}$  are free to move in the  $z$ -direction.

The above construction is based exclusively on the number of vertices of each face and the adjacency between them. However, for non-triangulated nets some of the nodes that the algorithm indicates that they are free to move, are actually fixed due to geometrical constraints. Let us now define two such constraints which can provide visual geometrical restrictions to the number of independent polyhedral liftings.

**Lemma.01:** let's suppose that we have two planes  $\pi_1, \pi_2$ . These planes intersect in a line  $l_3$  the projection of which  $l_{3pr}$  is given by two fixed points  $P_{1pr}(x_1, y_1, 0), P_{2pr}(x_2, y_2, 0)$ . Given that the planes go through lines  $l_1, l_2$  respectively, we seek to find the possible solutions of the  $z$ -coordinate of the point  $P_1(x_1, y_1, z_1)$  which satisfy the fixed elements:  $l_1, l_2, P_{1pr}$  and  $P_{2pr}$ . If the two sets of lines  $l_1, l_2, l_3$  and  $l_{1pr}, l_{2pr}, l_{3pr}$  are not in a perspective configuration (they do not meet at a point or they are not parallel) then point  $P_1(x_1, y_1, z_1)$  is fixed from the particular geometry (Figure 3.5-Bottom, Appendix.01). If they are in a perspective configuration then  $P_1(x_1, y_1, z_1)$  is not fixed and can move freely on the  $z$ -axis (Figure 3.5-Top).

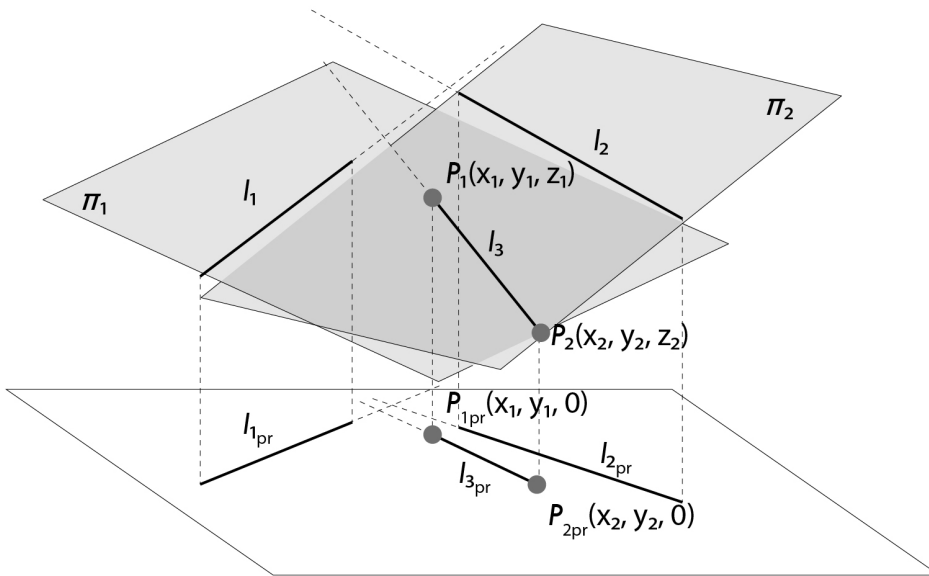
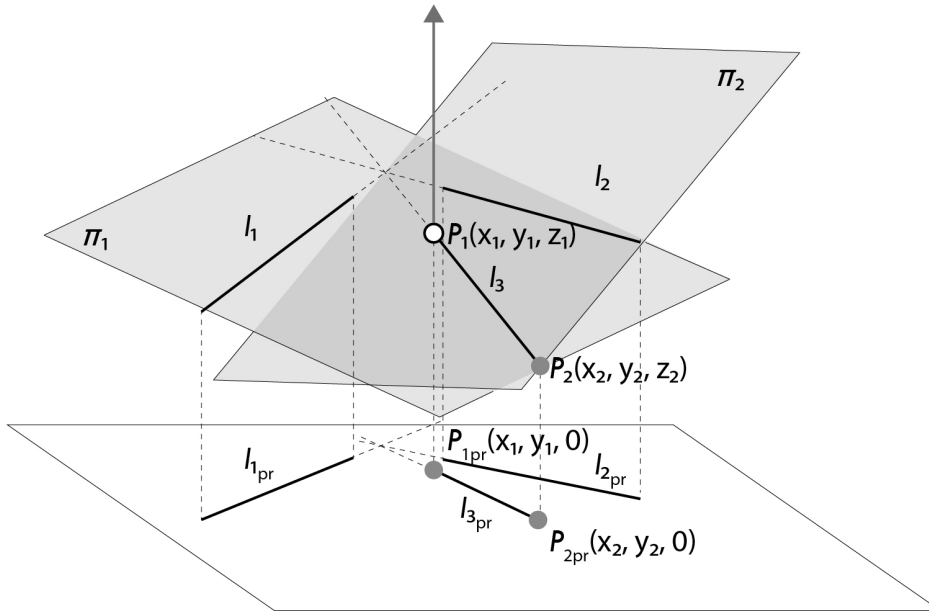


Fig. 3.5 Top: The three sets of lines  $l_1, l_2, l_3$  and  $l_{1pr}, l_{2pr}, l_{3pr}$  are in a perspective configuration (they meet at a point) – the  $z$ -coordinate of point  $P_1(x_1, y_1, z_1)$  does not depend on the fixed elements  $l_1, l_2, P_{1pr}$  and  $P_{2pr}$  – it can slide on the  $z$ -axis; Bottom: The two sets of lines  $l_1, l_2, l_3$  and  $l_{1pr}, l_{2pr}, l_{3pr}$  are not in a perspective configuration – the  $z$ -coordinate of point  $P_1(x_1, y_1, z_1)$  depends on the fixed elements  $l_1, l_2, P_{1pr}$  and  $P_{2pr}$ .

The above lemma concerned two adjacent faces, we now introduce a further geometrical restriction with regards to a series of adjacent faces. Firstly, we define a cyclic polygonal ribbon  $F : f_i(v_i, e_i), i \in 1, \dots, k$  to be a subset of faces in  $P(e, v, f)$  such that:

- $f_i$  is adjacent to  $f_{i+1}$ . Also,  $f_1$  is adjacent to  $f_k$
- The lifting of  $f_i$  in  $\mathbb{R}^3$  results also in  $f_{i+1}$  being fixed in  $\mathbb{R}^3$

**Lemma.02:** Given a cyclic polygonal ribbon  $F : f_i(v_i, e_i), i \in 1, \dots, k$ , the equation of planes  $\pi_i$  (on which  $f_i$  lie on) will be defined from a line and a point (or equivalently from three points). If we fix  $f_1, \pi_1$  by choosing one point  $P_{1i}$  we observe that the adjacent face  $f_2$  in  $F$  is fixed as well. Also,  $f_k$  is fixed from  $f_{k-1}$ , which in turn is fixed from  $f_{k-2} \dots$  and ultimately from  $f_1$ . Thus, the equation of  $\pi_k$ , and hence the  $z$ -coordinate of  $P_{ki}$ , depends on the selection of  $P_{1i}$ . However, we want  $F$  to be continuous for the truss to be self-stressed. As a result, point  $P_{ki}$  should coincide with point  $P_{1i}$ . Thus, the  $z$ -coordinate of  $P_{1i}$  is dependent.

In the example of Figure 3.6, we have a ribbon of four 4-gons enclosed from a fixed boundary. If we lift point  $P_{1ipr}$ , then face  $f_1$  will be lifted on plane  $\pi_1$ . Then, we proceed to face  $f_2$ : point  $P_{2i}$  has been already defined from the equation of  $\pi_1$  and  $e_{21}$  is fixed. Thus, we can define plane  $\pi_2$ . In the same sequential fashion, we lift all the planes up to the last plane  $\pi_4$ .

We observe that, since this ribbon is cyclic, the last lifted face  $f_4$  is adjacent to face  $f_1$  with which it shares a common edge and thus two common vertices - including  $P_{1ipr}$ . If this polygonal ribbon corresponds to a continuous closed ribbon in space (which is part of a closed polyhedron), then we know that there is at least one  $z$ -coordinate for  $P_{1ipr}$  such that  $P_{1i}$  lies on both planes  $\pi_1$  and  $\pi_4$ .

In fact, by sliding  $P_{1i}$  on the  $z$ -axis, we observe that the ribbon is generally not continuous in space since the projections of the point  $P_{1ipr}(x, y, 0)$  on plane  $\pi_1$ :  $P_{1i}(x, y, z)$  and on plane  $\pi_4$ :  $P'_{1i}(x, y, z')$  do not coincide anymore. As a result, we have no freedom with respect to the polyhedral lifting of the ribbon in the general configuration and all the points, including  $P_{1i}(x, y, z)$ , are fixed.

An alternative method to validate the findings of the geometry-based structural analysis is through Singular Value Decomposition. In this matrix-analysis method, the rank of the Equilibrium matrix can be found for the particular geometry and thus the exact number of states of self-stress.

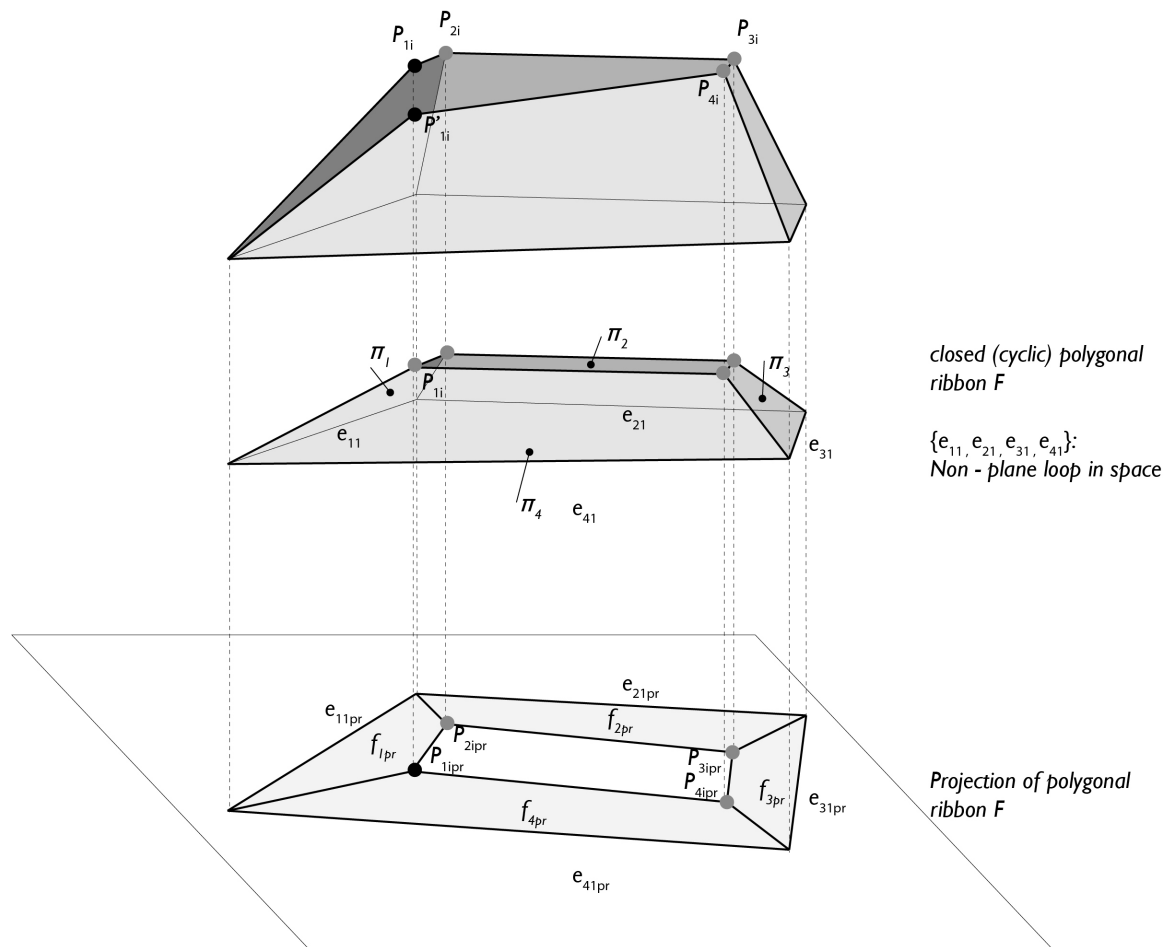


Fig. 3.6 A polygonal ribbon with a non - plane boundary: point  $P_{1i}$  is fixed and cannot slide on the  $z$ -axis whilst the ribbon remains continuous.

Let us now examine two examples: Maxwell's (1864) Figure 3 and a tensile net similar to Janet Echelman's installation mentioned above.

The geometry of Maxwell's Figure 3 (Figure 3.8) has potentially two underlying Desargues configurations for a special geometrical embedding, or none for the general position. Thus, this topology can have a number of interpretations (Figure 3.7):

1. In the general position, we have zero Desargues configurations, the boundary ABCD is not on the plane and we have now one state of self-stress/ polyhedral lifting which fixes all faces in space. By fixing three of the boundary vertices (in grey) we proceed by lifting the fourth boundary vertex in the  $z$ -axis (in red). It follows from Lemma.01 that all the other vertices (in blue) and faces are then fixed. For example, if we take quads LTQD and MBPT, and their corresponding planes  $\pi_1$  and  $\pi_2$ , then if we take  $l_1$  to be D,  $l_2$  to be B, and  $l_3$  to be T, we can use the Lemma.01 to find the  $z$ -coordinates of the vertices along T (as D, B, T do not meet at a point).
2. Moreover, there is a special position that we have one Desargues configuration. Then, we have one state of self-stress/ polyhedral lifting from this Desargues 'roof'. However, the second roof, since it is not in Desargues configuration, cannot leave the plane and we have only a partial polyhedral lifting
3. In another special position we have two Desargues configurations, a plane boundary ABCD, and both roofs can slide independently on the  $z$ -axis. Thus, we have a full polyhedral lifting with two independent states of self-stress.

Case	Number of Desargues configurations	How many faces lift?	Is boundary ABCD planar in space?	Number of polyhedral liftings/ states of self-stress
a	0	All	no	1
b	1	Half	yes	1
c	2	All	yes	2

Fig. 3.7 Table of the various possible configurations of the geometry of Maxwell Figure 3.

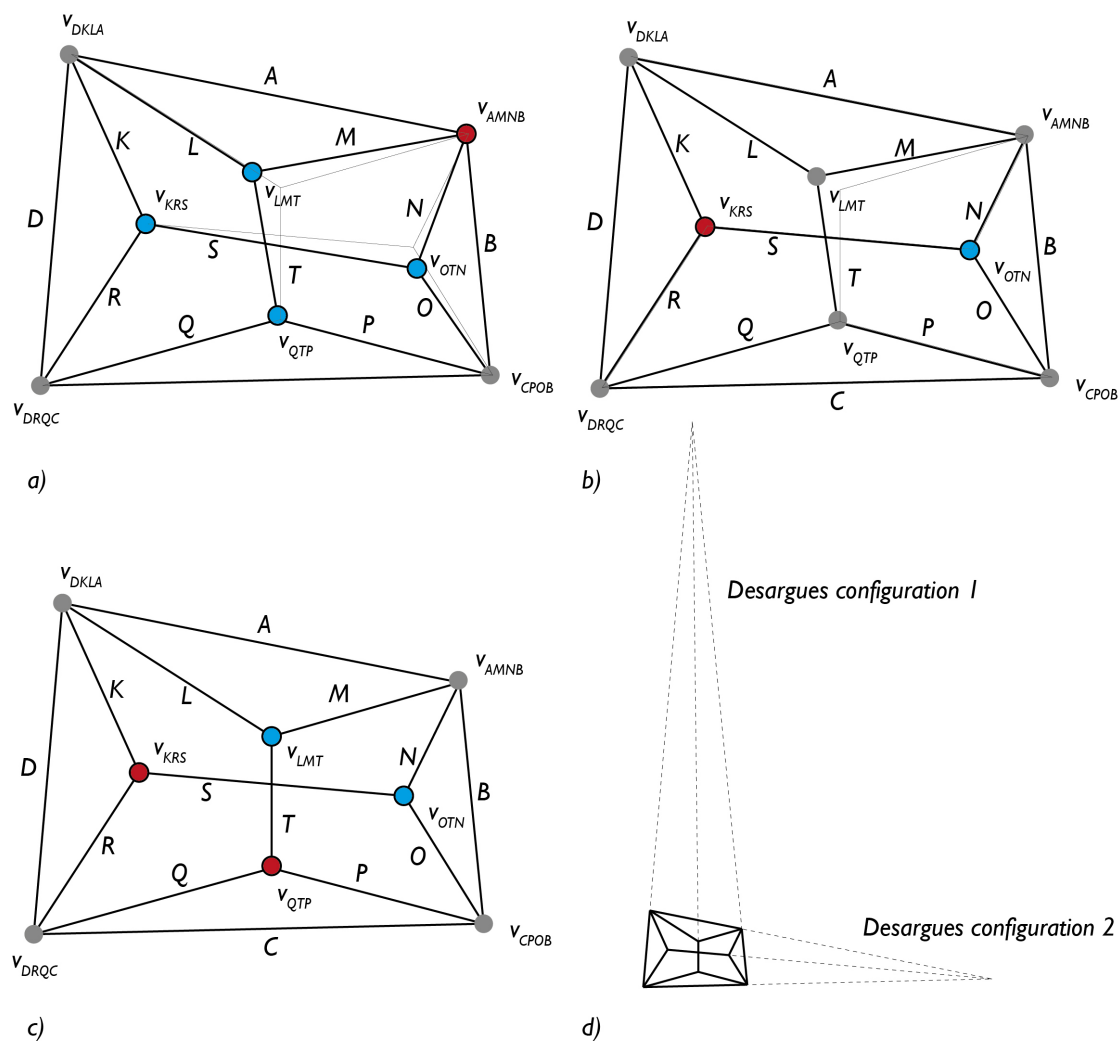


Fig. 3.8 Three configurations of Maxwell Figure 3: a) Zero Desargues configurations, one state of self-stress, non-plane boundary; b) One Desargues configuration, one state of self-stress, plane boundary; c) Two Desargues configurations, two states of self-stress, plane boundary; d) The two underlying Desargues configurations.



Moving to the second example (Figure 3.9) of  $F(71, 133, 64)$ , from Calladine's rule we have that  $p - q = 6$ . Firstly, we apply a visual algorithm based only on adjacency of faces and the number of their vertices (Figure 3.9): We lift one initial face  $f_a$  adjacent to the boundary (shares a common edge and thus two vertices). Note that the boundary/ bottom face is fixed and will remain flat on  $z=0$  throughout the construction. Observe that at this step no matter which one of the four faces, which are adjacent to the boundary, we take, the same number of faces and vertices will be fixed. This is because the four faces adjacent to the boundary are also adjacent to one another; if any one lifts the others will be fixed in response. Since the boundary is fixed we need only one internal node to lift  $f_a$  (first state of self-stress). Observe that several extra faces and vertices ( $F_a/V_a$ ) get fixed too.

Let's now pick a face adjacent to  $F_a$  with the maximum number of vertices -  $f_b$ . Since  $f_b$  already shares an edge (and two vertices) with  $F_a$  we only need one new internal node to lift it (second state of self-stress). Observe that several extra faces and vertices ( $F_b/V_b$ ) get fixed too. At this step we observe that there are two adjacent faces  $f_c, f_d$  which are not fully fixed yet, but they each have one edge fixed:  $e_{cl}, e_{dl}$  and share a common edge  $e_{cd}$  (Figure 3.10). We notice that lines  $e_{cl}, e_{dl}, e_{cd}$  are not in a perspective configuration (they do not meet at a point and they are not parallel). As a result, from lemma.01 we have that node  $v_{cd}$  is fixed and is not free to move.

By fixing  $v_{cd}$  we observe that all the vertices are now fixed (Figure 3.9-d). The structure has thus a maximum of two independent polyhedral liftings / states of self-stress. Let's now check for any other geometrical constraints which will result in reducing the number of states of self-stress to one. Taking as a starting position (Figure 3.9-b), we observe that we can make a cyclic polygonal ribbon which starts from an internal face  $f_l$  and ends in  $f_k$  (Figure 3.11). As a result, vertex  $v_{lk}$  belongs both to faces  $f_l$  and  $f_k$  and gets lifted from both corresponding planes. Since we want the ribbon to be continuous we need  $v_{lk}$  to have the same  $z$ -coordinate both on plane  $\pi_l$  and  $\pi_k$ . From Lemma.02 we thus have that the vertices of the ribbon are fixed. Consequently, the net has only one state of self-stress.

Thus the structure has 7 mechanisms and 1 state of self-stress.

$$p - q = 6$$

$$p = 1$$

$$q = 7$$

The result of the geometrical analysis is validated from the Singular Value Decomposition (Pellegrino, 1993) or the Equilibrium matrix of the net's geometry. As a result, this geometrical embedding of the topology of net  $F(71, 133, 64)$  has one state of self-stress. We should note that it is expected that in the general configuration this net will have one state of self-stress. It will be for special geometries that can have up to three states of self-stress. So, we could say that this net has 'generically' (in almost every configuration) one state of self-stress.

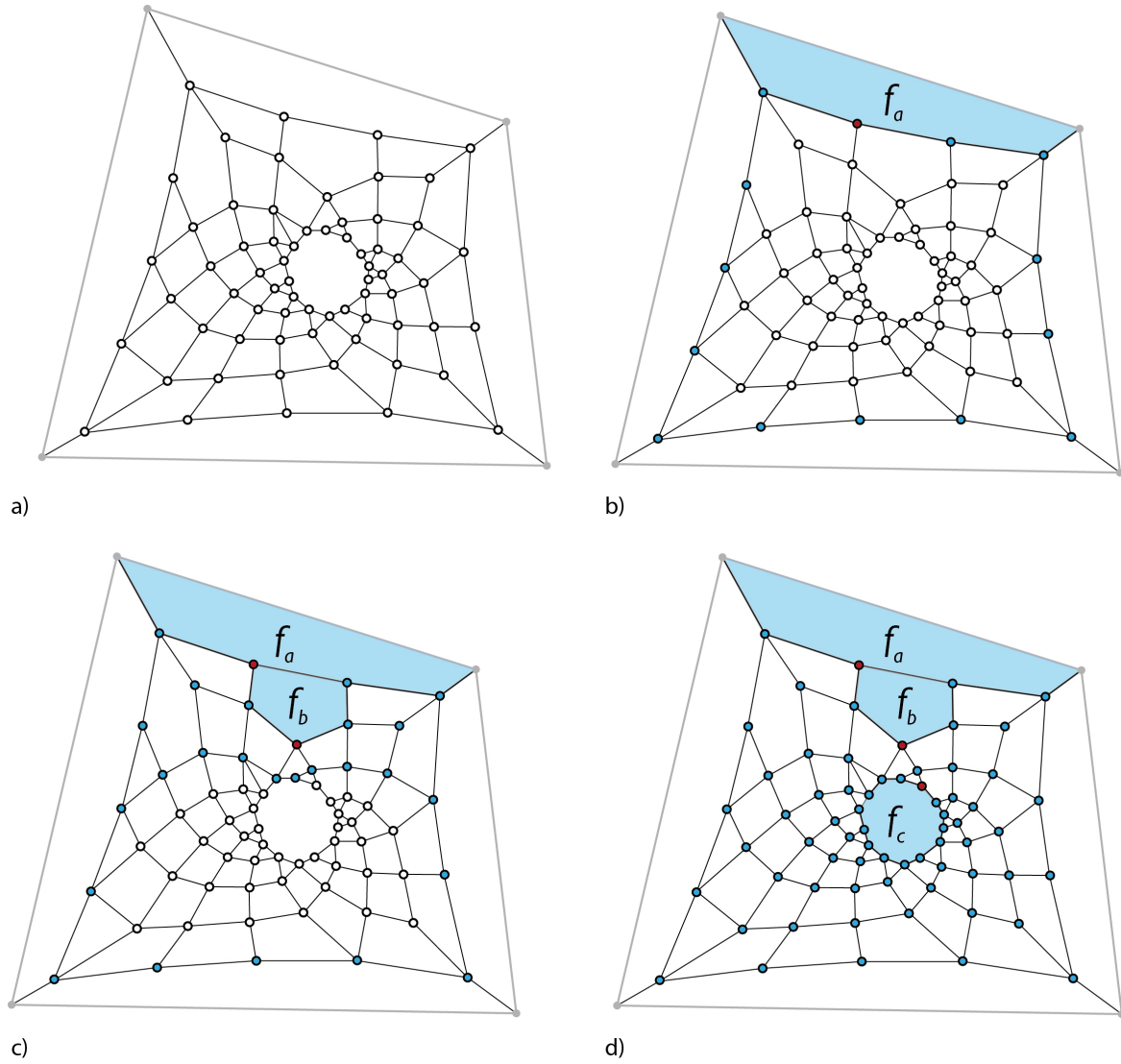


Fig. 3.9 a) The topology of the 2D net with  $F(71, 133, 64)$ ; b) Lifting of the first face  $f_a$  adjacent to the boundary by lifting one internal vertex; c) Lifting of face  $f_b$  also fixes several other faces and vertices; d) The lifting of face  $f_c$  by fixing a third node completes the polyhedral lifting.

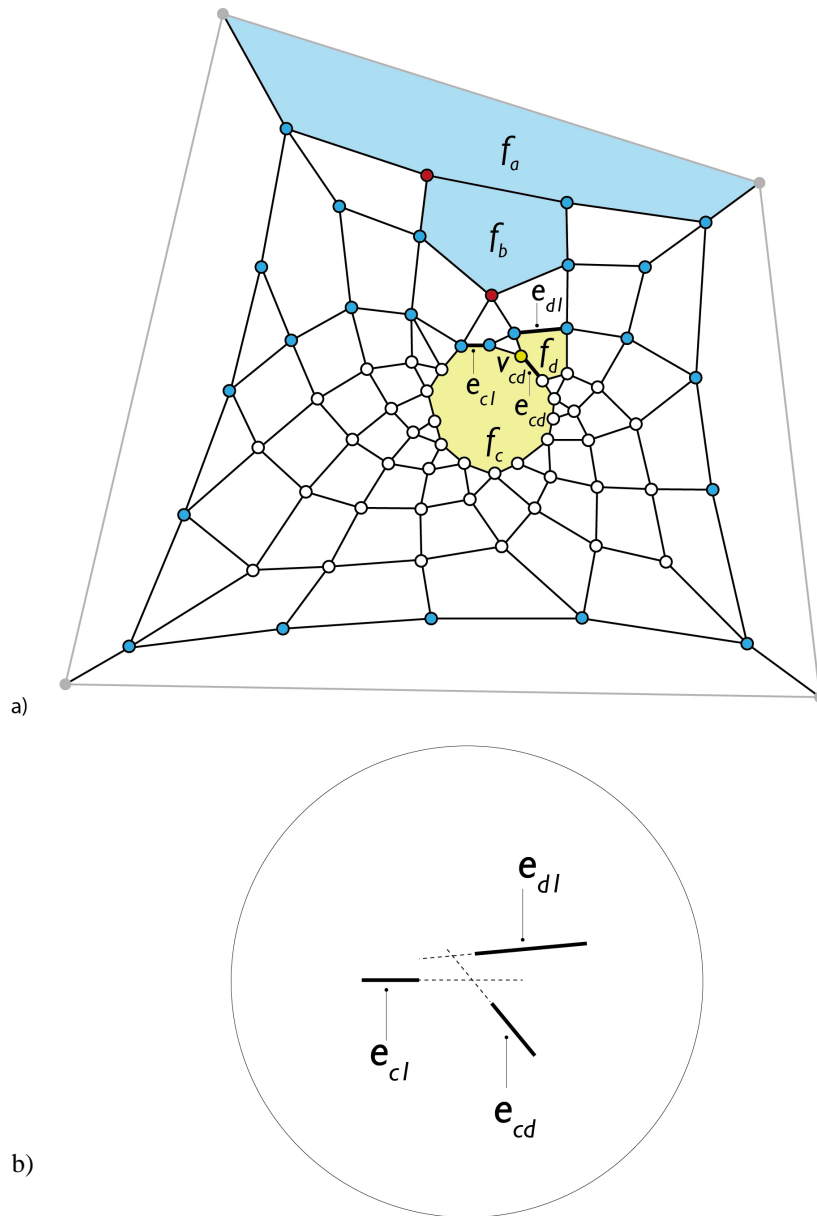
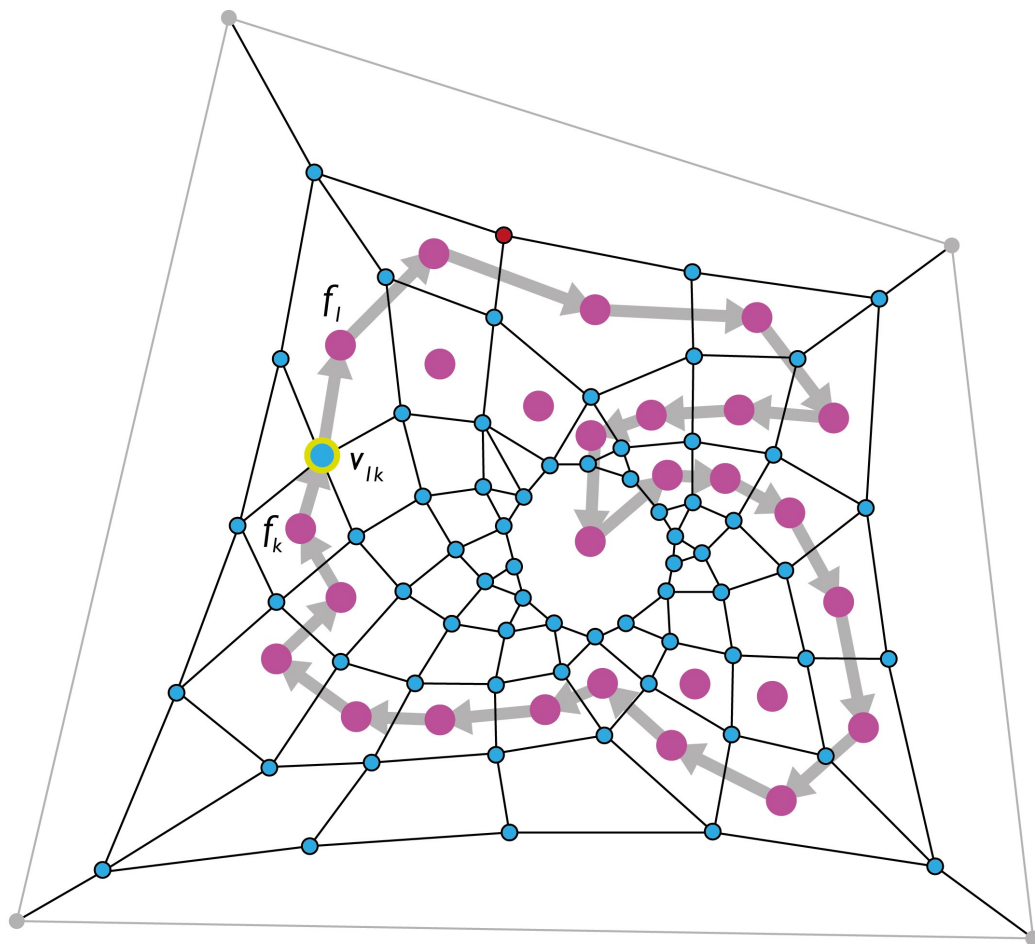


Fig. 3.10 a) Semi defined faces  $f_c$  and  $f_d$  fix node  $v_{cd}$  since edges  $e_{cl}$ ,  $e_{dl}$  and  $e_{cd}$  are not in perspective/parallel; b) Edges  $e_{cl}$ ,  $e_{dl}$ ,  $e_{cd}$  do not meet at a point and are not parallel.



a)

Fig. 3.11 a) A second geometrical constraint deriving from Lemma.02 results in only one state of self-stress for the net.

### 3.2.2 2D global static equilibrium

In this section, we apply the theoretical framework of polarities as discussed in Chapter 2 to derive global static equilibrium for 2D trusses. These can be seen as form diagrams  $\mathbf{F}(v, e, f)$  comprising vertices, edges and faces where the edges correspond to the members of the truss and the vertices to its nodes. When a form diagram is a projection of a plane-faced polyhedron  $\mathbf{P}(v, e, f)$  it is in static equilibrium and its reciprocal force diagram  $\mathbf{F}'(v', e', f')$ , where the length of the edges  $e'$  corresponds to the axial forces of  $e$ , can be derived through the method of polarities. As a result, the pair of reciprocal form and force diagrams are projections of reciprocal polyhedral stress functions. As already mentioned, their role is interchangeable - either one can be seen as the form or the force. Also, the form diagrams need not be tension-only or compression-only and can represent structures which are either self-stressed or under external loading. For the 2D case, reciprocal diagrams can be produced from any polarity induced by a non-degenerate quadric or from the Null-polarity (an alternative construction investigated by Möbius and referenced by Cremona (Cremona, 1890)). For the examples visualised here, the simplest case is used (i.e. this of the paraboloid of revolution). The constructions are developed using the CAD platform *McNeel Rhino*, together with the plug-in the *Grasshopper* and customised *Python* codes.

The advantages of using a polar transformation through a paraboloid of revolution are:

- This is a direct method (no need for transforming or ‘correcting’ the reciprocal geometries).
- With this transformation the form diagram is an orthogonal projection of the polyhedral Airy stress function the designer can clearly inspect the latter and draw insights for the structural performance and geometrical properties of the truss.
- Polarities have a degree-2 (transforming an element twice results to the element itself). As a result, the designer can directly move in a bidirectional way from the one polyhedron to its reciprocal.

For a given tetrahedral Airy stress function  $\mathbf{P}(v, e, f)$ , the planes, on which the faces  $f$  lie on, are mapped to their reciprocal vertices  $v'$  through a paraboloid of revolution (Figure 3.12). Considering that the connectivity of the vertices  $C_{v'}$  follows the connectivity of the faces  $C_f$ , a reciprocal tetrahedron  $\mathbf{P}'(v', e', f')$  can be constructed. Applying an orthographic projection of these dual tetrahedra along the axis of the paraboloid yields a reciprocal 2D form  $\mathbf{F}(v, e, f)$  and force  $\mathbf{F}'(v', e', f')$  pair, where the force diagram is an instance of a Maxwell 2D diagram with edges being perpendicular to the corresponding ones in the form diagram.

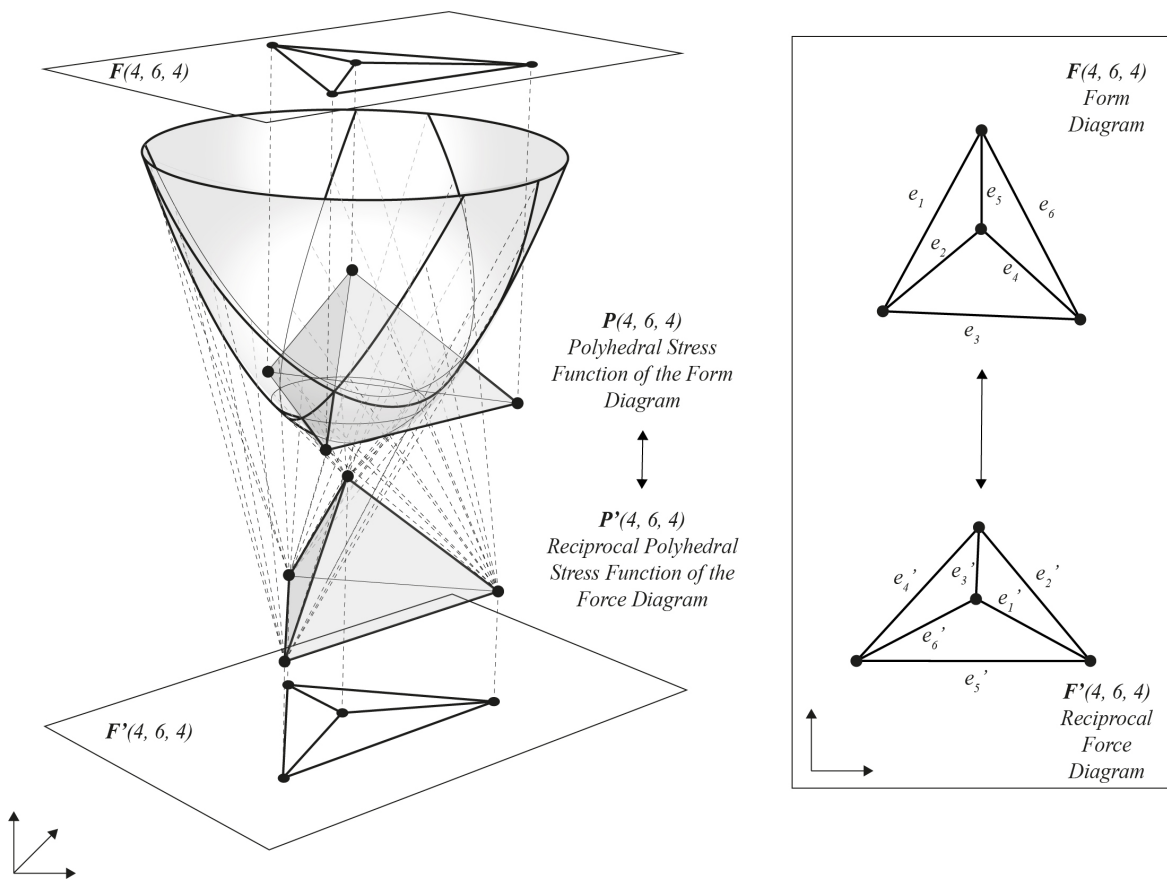


Fig. 3.12 Left: Reciprocal polyhedral Airy stress functions ( $P, P^*$ ) through a polarity induced by a paraboloid of revolution. Right: The orthographic projections of the reciprocal polyhedra produce a pair of reciprocal form and force diagrams ( $F, F^*$ ).

### 3.2.3 3D global static equilibrium

Maxwell did discuss about the graphical analysis of spatial trusses as well. However, not in the great length he did for the 2D case. At the same time, he did observe (Maxwell, 1864a) that self-stressed spatial trusses obey the counting rules of, what we would call today, 4-polytopes. Nonetheless, he did not generalise and apply the reciprocal constructions of the paragraphs discussed here for 3D trusses which are projections of 4-polytopes even though intuitively he had grasped it. The reason for this may lie in the history of mathematics of his time. Geometrical language and concepts were not abstracted to  $n$ -dimensions before the 1840s (James, 1999). Even after that and until the end of the 19<sup>th</sup> century, geometry was largely the 3-dimensional world inherited from the last two millennia. As a result, Maxwell did not explicitly talk of 4D duality and 4D reciprocity because in a sense, 4-polytopes were not really known at the time. He did know intuitively that self-stressed spatial structures obey the counting rules of higher-dimensional objects, but at the time the statement ‘a 3D truss is a projection of a 4-polytope’ could not be articulated with the ease of today, in contrast to the statement ‘a 2D truss is a projection of a polyhedron’.

Polarities in the context of contemporary graphic statics were introduced in (Konstantatou et al., 2018) for the design and analysis of 3D structures. It should be noted that these constructions were mentioned in the context of rigidity theory in the 90s (Crapo and Whiteley, 1994). In the 4-dimensional space, following the duality principle, a polar hyper-plane  $\pi$  defined in equation form as  $Ax + By + Cz + Dw + E = 0$  and described by the corresponding quadruples  $(A, B, C, D, E)$ , is mapped to a point  $P$  described from the quadruple  $(x', y', z', w')$  (and vice versa) through transformations  $L, L^{-1}$ . Specifically, given a point  $P$  outside a hyper-quadric  $\Gamma$  (i.e. a 4-dimensional generalisation of a 3-dimensional quadric), the hyper-cone with vertex in  $P$  and tangent to  $\Gamma$ , intersects  $\Gamma$  in a quadric that lies on the hyper-plane  $\pi$ . Using, for example, a hyper-paraboloid of revolution (Figure 3.13) with equation  $2cw = x^2 + y^2 + z^2$  as the quadric of the polarity, for a point  $P(x', y', z', w')$  and its polar plane  $\pi$  described by the equation  $w = Ax + By + Cz + D$ , we have that

$$L^{-1}(P) = \pi \quad (3.1)$$

$$L^{-1}(x', y', z', w') = (A, B, C, -1, E) \quad (3.2)$$

the by following the methodology of section (2.5), we have that for this particular hyper-quadric, the hyper-plane  $\pi$  is given by

$$x(x') + y(y') + z(z') + w(-c) - cw' = 0$$



which rearranges to

$$w = \frac{x'}{c}x + \frac{y'}{c}y + \frac{z'}{c}z - w' \quad (3.3)$$

which, when expressed in the  $(A, B, C, -I, E)$  form has

$$A = \frac{x'}{c}, \quad B = \frac{y'}{c}, \quad C = \frac{z'}{c}, \quad E = -w' \quad (3.4)$$

These equations can be readily inverted to give

$$x' = cA, \quad y' = cB, \quad z' = cC, \quad w' = -E \quad (3.5)$$

which is thus the mapping  $L$ :

$$L(\pi) = P \quad (3.6)$$

$$L(A, B, C, -1, E) = (x', y', z', w') = (cA, cB, cC, -E) \quad (3.7)$$

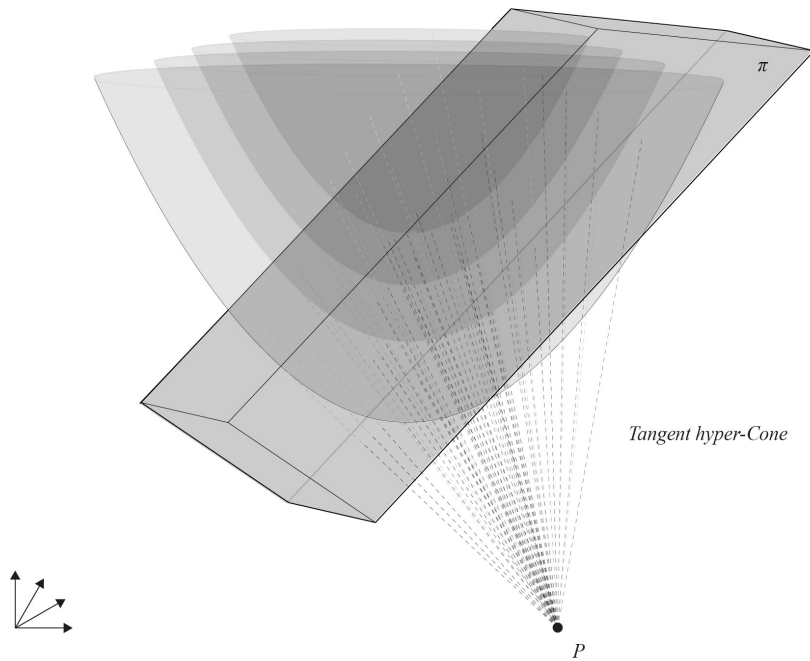


Fig. 3.13 Polarity in 4-space induced by a hyper-paraboloid of revolution (in a schematic representation here).

Following the above construction, it is possible to directly obtain force reciprocals when the form diagrams are projections of 4D stress functions  $P(v, e, f, c)$ ,  $P'(v', e', f', c')$ . These are spatial polyhedral geometries with plane faces, each one of which belongs to exactly two cells, for example the structures discussed in (Akbarzadeh et al., 2015). Essentially, the constructions are exactly the same as with the 2D case, just one dimension up. Topologically, this type of structures comprise internal cells enclosed by an external boundary and in 3-space they look like cellular or polyhedral structures. In this case, vertices  $v$  of a 4-polytope map to hyperplanes  $c'$  which intersect to produce reciprocal force cells (in the same fashion as for 2D trusses where the polar planes of the polyhedral Airy stress function intersect and to faces). Thus, a reciprocal 4-polytope is created. The 3D projections of this higher-dimensional pair will result in a pair of spatial reciprocal form and force diagrams  $F(v, e, f, c)$ ,  $F'(v', e', f', c')$  where form edges ( $e$ ) correspond to reciprocal perpendicular force faces ( $f'$ )

Some spatial frameworks have a state of self-stress even though they are not projections of 4D Maxwell-Rankine stress functions. For instance, the Steffen polyhedron and several tensegrities comprise solely one internal space/ cell. Thus, if we were to map that cell to obtain the Rankine reciprocal we would end up with solely one reciprocal vertex. One geometrical construction that can be used in this case is coning (McRobie, 2016). Coning is a technique that adds one extra vertex one dimension up (so in 4D for 3D structures) from which we take edges to the initial set of vertices  $v$ . As a result, for an initial spatial framework  $F(v, e, f, c)$  the coned structure  $F_c(v_c, e_c, f_c, c_c)$  will have  $v+1$  number of vertices ( $v_c$ ),  $v+e$  number of edges ( $e_c$ ),  $e+f$  number of edges ( $f_c$ ) and  $f+c$  number of cells ( $c_c$ ).

For the simplest case of a simply connected 4-polytope  $P(5, 10, 10, 5)$  (5-simplex), a polarity is used to map it to its reciprocal  $P'(5, 10, 10, 5)$  (Figure 3.14). After projecting the 4-polytopes back to 3-space, the 3-dimensional form and force diagrams are obtained.

As mentioned in Chapter 2, force reciprocals for spatial trusses can be of different kinds (Rankine 3D, Cremona 3D, Vector-based 3D). Each one of these types can be applied, and is more suitable, to different kind of geometries. The Rankine 3D force reciprocals used here are applicable to tension-and-compression spatial polyhedral structures; through coning to rotationally-symmetric 1-cell structures, such as tensegrities, and are particularly useful for constant-stress design through the application of Minkowski sums as well as for applications such as 3D discrete stress fields (which we will develop in Chapter 7).

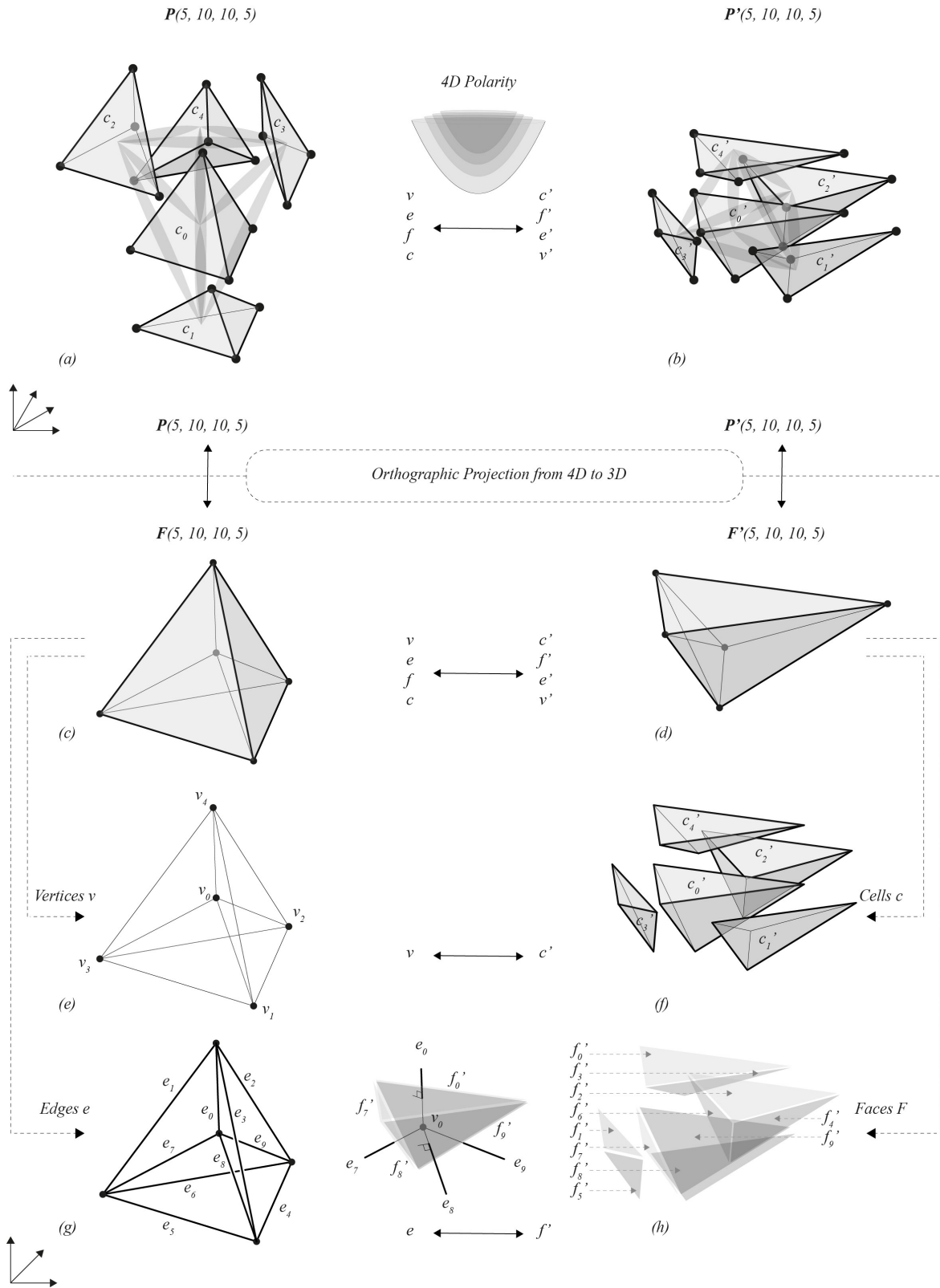


Fig. 3.14 (a, b): Topology of two reciprocal 4-polytopes ( $P, P'$ ), constructed through a polarity induced by a hyper-paraboloid of revolution; (c, d): The orthographic projection of the 4-polytopes produces a pair of reciprocal form and force diagrams ( $F, F'$ ) which follow 4D duality between their geometrical elements; (e, f): form vertices  $v$  map to reciprocal cells  $c$ ; (g, h): form edges  $e$  map to reciprocal and perpendicular force faces  $f$ .

### 3.2.4 N-connected reciprocal diagrams

The theory of polarities can be also applied to  $n$ -connected polyhedra. In fact, in order to solve some complicated cases such as Figure 3.15 via polyhedral stress functions it is necessary to do so (unless extra nodes are added). For example, Figure 3.15 can be lifted to a polyhedron only if the central quad is assumed to be a hole (Figure 3.16). As a result, the non-planarity does not always constitute a problem. Specifically, if a form diagram does not have a topologically planar graph but is a projection of an  $n$ -connected, plane-faced polyhedron then it can actually be solved in a straightforward way without the addition of extra nodes by the polarities method.

For a  $n$ -connected (one that has  $n-1$  number of holes though it) diagram  $P(v, e, f)$  Maxwell (Maxwell, 1870) states that  $v + f - e = 2 - 2(n - 1) = 2n - 4$ . We should note that  $n - 1 = g$ , with  $g$  being the genus (a sphere has genus 0, a torus genus 2, etc.). The above formula is also known as the Euler characteristic or Poincare formula for  $n$ -connected surfaces. This generalisation of the Euler polyhedral formula for  $n$ -connected surfaces was developed by Lhuillier (Lhuillier, 1812). However, the full generalization of the formula for polytopes of any dimension was proved by Poincaré (Poincare, 1895).

From Poncelet duality we have that for reciprocal polyhedra  $P(v, e, f)$ ,  $P'(v', e', f')$  the number of edges ( $e, e'$ ) are the same, and since nodes ( $v, v'$ ) go to faces ( $f', f$ ) and vice versa, then the sum  $v + f$  is constant ( $v + f - e = v' + f' - e'$ ). It follows that the quantity  $v + f - e$  is the same for both diagrams  $P, P'$ . Since this equals  $2n-4$ , where  $n$  is the connectedness, Maxwell infers that the reciprocal of an  $n$ -connected polyhedron is an  $n$ -connected polyhedron.

For the case of polyhedral stress functions, lets start with a polyhedron with genus 0 (topologically a sphere,  $n=1$ ) for which  $v + f - e = 2$

Lets now make a hole by connecting two identical faces  $f_1, f_2$  which have  $v_1, v_2$  number of vertices and  $e_1, e_2$  number of edges. The faces  $f_1, f_2$  are polygons so trivially  $v_1 = e_1, v_2 = e_2$

The resulting geometry will have:

$$v - v_1 + f - 2 - e - e_1 = v + f - e - v_1 + e_1 - 2 = 2 - 2 = 0$$

Consequently, every new hole decreases the sum by 2 and the reciprocity retains the genus.

We should highlight that when a polyhedron of genus  $g > 0$  has a single flat face enclosing a hole, that bottom face will map to only one point in the reciprocal. Consequently, the reciprocal will not be of the same genus as the original polyhedron since the hole of the reciprocal has been contracted to a point.

For the case of 4-polytopic stress functions, let's start with a 4-polytope  $P(v, e, f, c)$  for which (through the Schälfi formula)

$$v - e + f - c = 0$$

let's now make a hole by connecting two identical cells  $c_1, c_2$ , which have  $v_1, v_2$  number of vertices,  $e_1, e_2$  number of edges, and  $f_1, f_2$  number of faces. The cells are closed polyhedra so we have

$$v_1 + f_1 - e_1 = 2$$

The resulting geometry will have

$$v - v_1 - e - e_1 + f - f_1 - c - 2 = v - e + f - c + 2 - v_1 + e_1 - f_1 = v - e + f - c + 2 - 2 = v - e + f - c$$

We observe that the addition of holes does not give us information on the genus of the 4-polytope for the 4D case through the generalized Schälfi formula.

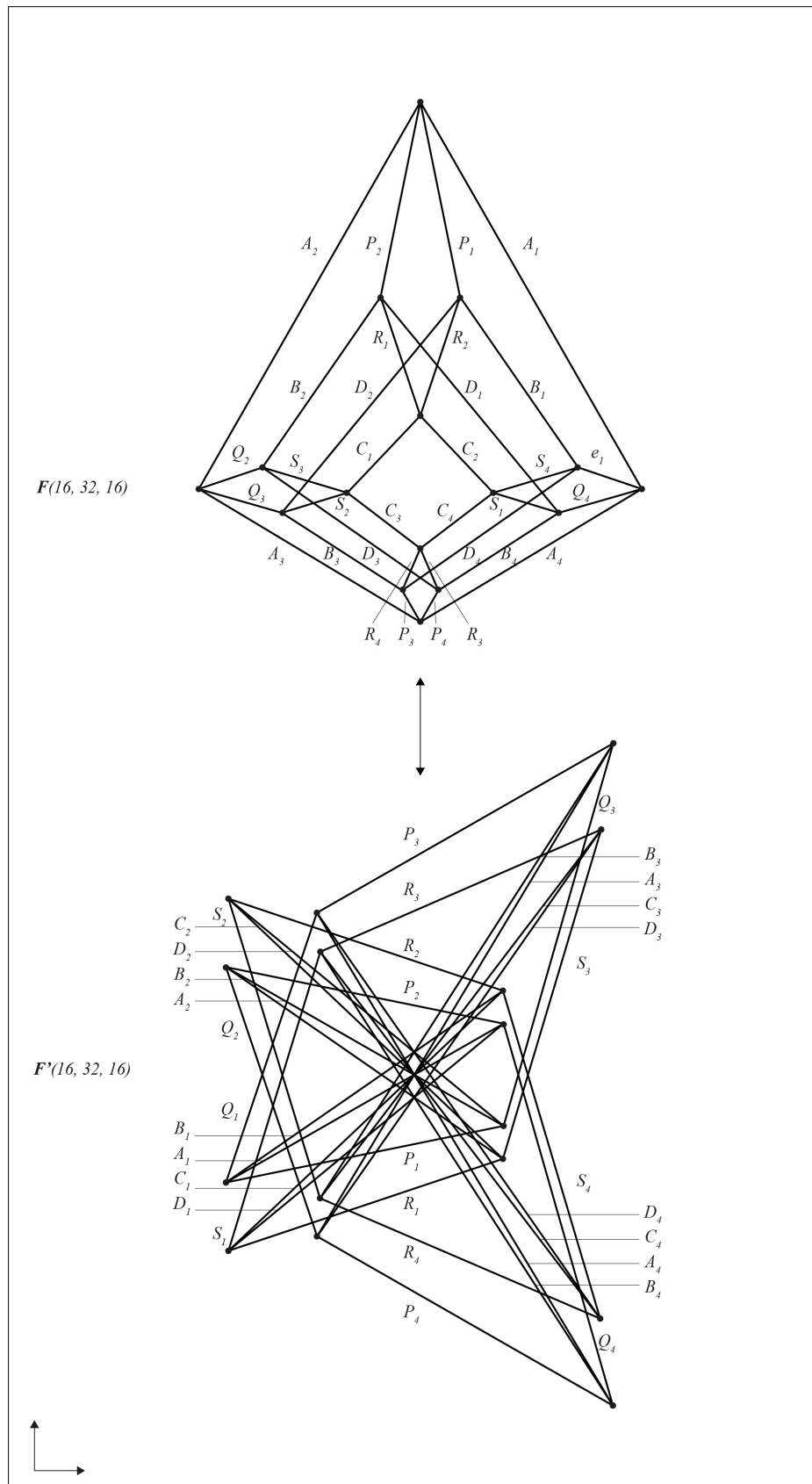


Fig. 3.15 Reciprocal 2-connected form and force diagrams from (Maxwell, 1870).

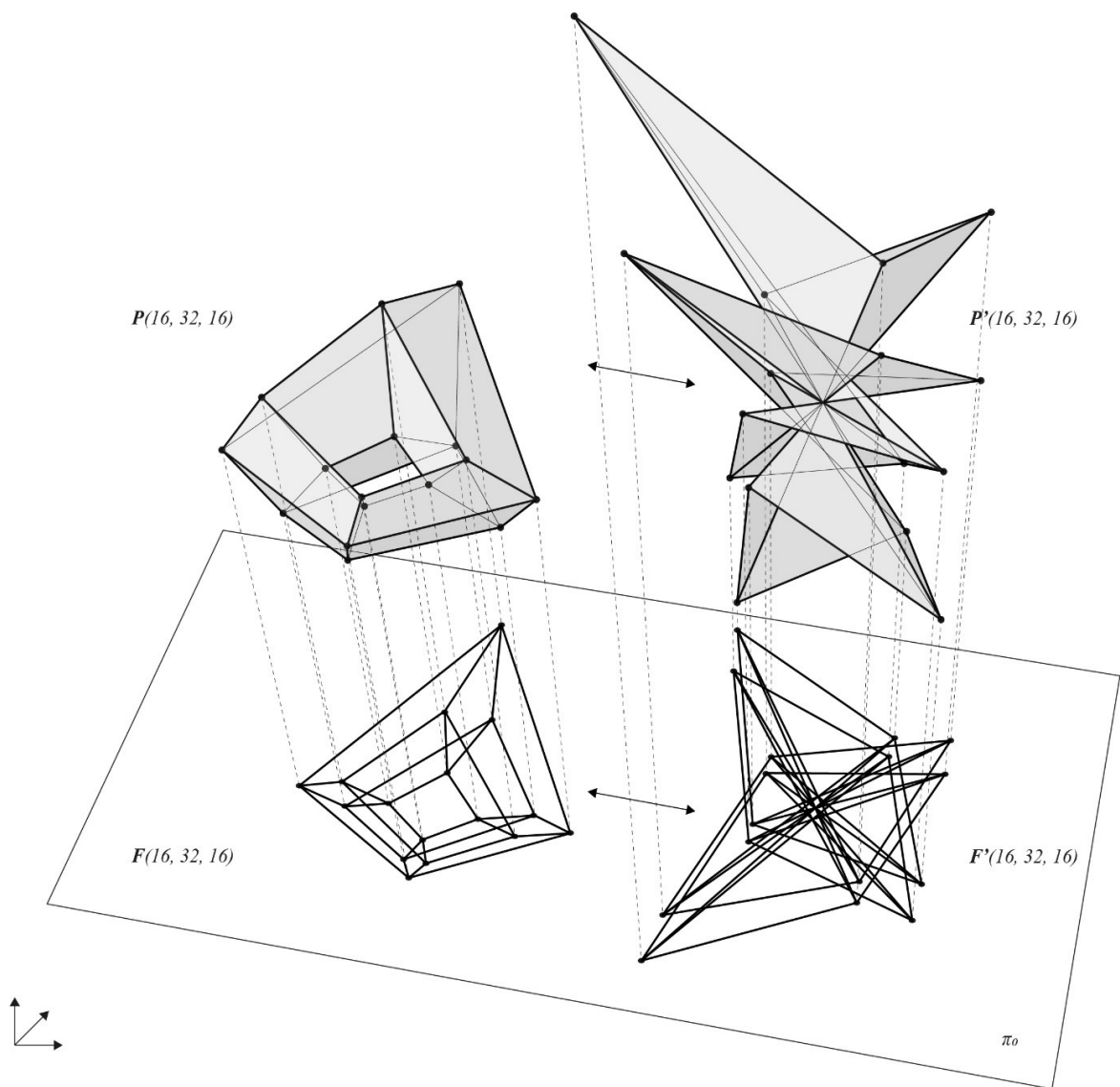


Fig. 3.16 Reciprocal 2-connected polyhedra.

### 3.3 Graphic kinematics

#### 3.3.1 Introduction

Graphic statics offers design and analysis methodologies for plane and spatial structures in static equilibrium via the reciprocity between form and force diagrams. However, graphical analysis of structures holds the promise of encompassing more fields than statics. Graphic kinematics can be derived from graphic statics using purely geometrical manipulations of the reciprocal form and force diagrams (McRobie et al., 2017). In this paragraph, we outline the principles of this type of twofold graphical analysis (static and kinematic) to derive the mechanisms and states of self-stress of both 2D and 3D structures.

#### 3.3.2 2D and 3D graphic kinematics

McRobie et al. (McRobie et al., 2017) showed how to combine force and displacement through visual virtual work while incorporating a material law in a Maxwell-Williot diagram Figure 3.17. From this, it derives that if the parallelogram has zero width, it corresponds to a bar that does not extend. As a result, in this case the displacements are that of a finite or infinite mechanism and the force polygons (or cells for the 3D case) slide with respect to each other while adjacent edges (or faces) remain 'glued' together. It should be mentioned that a similar method has been developed by (Zanni and Pennock, 2009) for the 2D case.

The simplest example on the plane is that of the 4-simplex  $F(4, 6, 4)$ . This 2D truss has one state of self-stress. As discussed, 2D reciprocals have perpendicular corresponding form and force edges. Moreover, the tetrahedron is self-dual, *i.e.*, the force reciprocal has the same topology and geometry. Following the Poncelet duality approach, the vertices  $v_i$  of  $P$  will map to faces  $f'_i$  in  $P'$  (Figure 3.18). These reciprocal faces can now slide as follows: common edges of adjacent faces should remain in contact, *i.e.*, keep lying at the same line while they slide. Also, the geometry of the faces and thus the distance between vertices is fixed. We also notice that the inner three faces share edges with the outer face and should therefore slide along those corresponding common edges. The resulting displacement vectors  $u_i$  correspond to the mechanism of the form diagram which in this case is a rigid framework and thus we obtained a rotation on the plane which is a trivial rigid body motion (Figure 3.18) (McRobie et al., 2017).

Equivalently, the simplest example in 3-space is that of the 5-simplex  $F(5, 10, 10, 5)$  which can also be seen the 3D projection of 4-polytope, which is its corresponding Maxwell-Rankine stress function. The 5-simplex is also self-dual with the 4D Poncelet duality mapping vertices  $v_i$  to cells  $c_i$  and edges to perpendicular faces (Figure 3.18). Note that vertex  $v_5$  will



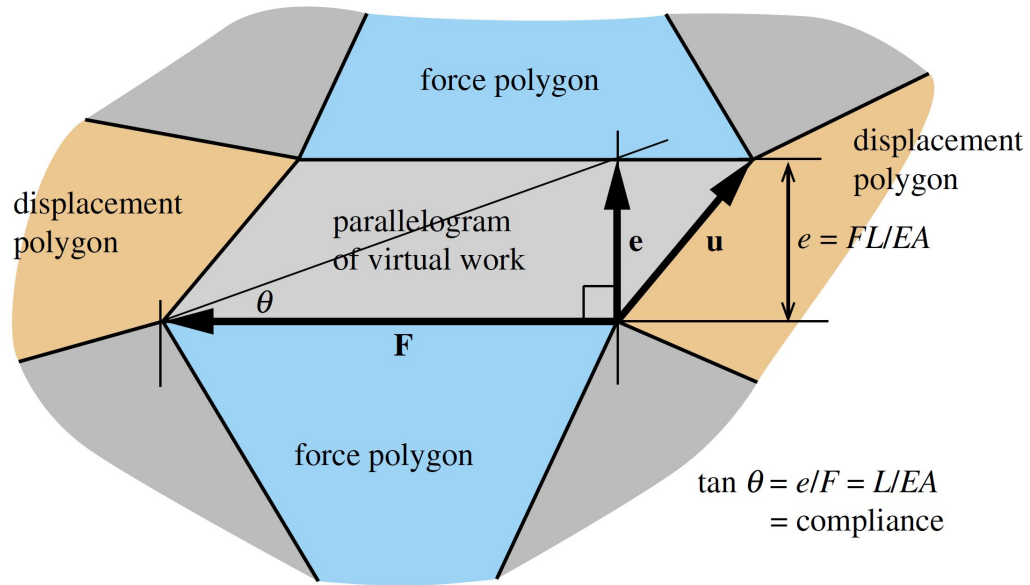


Fig. 3.17 The parallelogram of virtual work joining the force and displacement polygons from (McRobie et al., 2017).

map to the external cell  $c_5$  which encloses all the other internal tetrahedral cells. If we now start sliding the internal force cells by retaining shared faces on the same plane and edge lengths fixed, we obtain the nodal displacement vectors  $u_i$  of the form diagram (Figure 3.18). As expected, these also correspond to a rotation which is a rigid body motion since the 5-simplex is self-stressed but does not possess a mechanism.

More generally, for 3D trusses with Rankine reciprocals, the force cells can slide with respect to each other revealing the mechanisms such as in the case of the spoked cube (Figure 3.19). However, edges can also be auxiliary and have infinite flexibility. In this case, these edges can be ignored geometrically - as they can extend infinitely - but their initial inclusion leads to the potential of addressing a plethora of truss geometries which were previously inaccessible (McRobie et al., 2017). For example in Figure 3.19 if the radial edges are assumed to have infinite flexibility, and thus the corresponding adjacent faces need not be in contact during sliding, then the mechanisms which are derived correspond to a cubical truss rather than to a spoked cube.

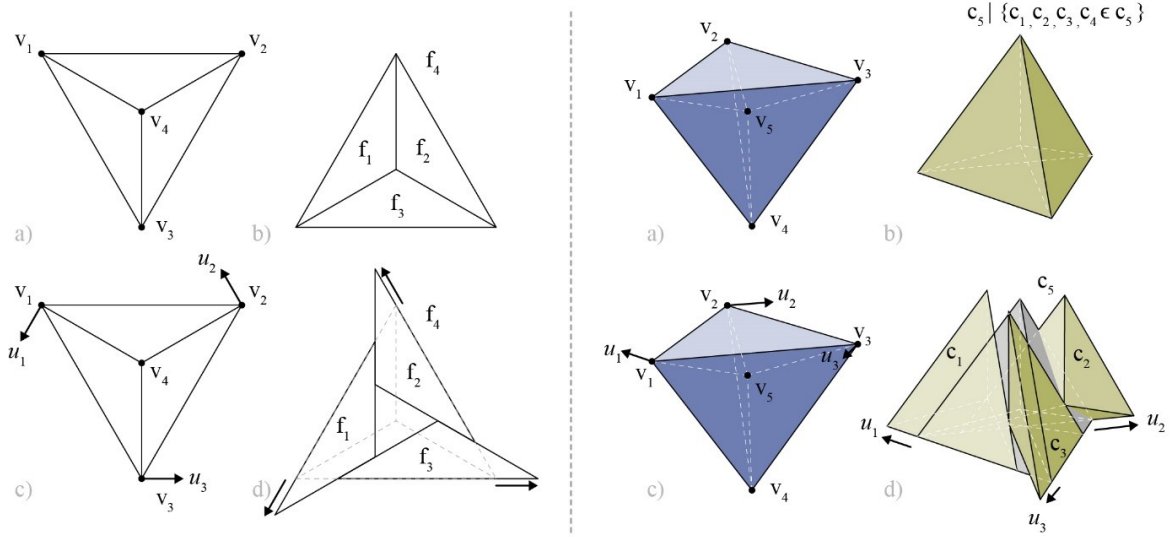


Fig. 3.18 Left: Graphic statics and kinematics for the 4-simplex in 2D, Right: Graphic kinematics for the 5-simplex in 3D.

### 3.4 Summary

In this Chapter we introduced a direct, unified, visual and intuitive graphic statics framework for global static equilibrium of 2D and 3D trusses which are projections of discrete stress functions. This was achieved by generalising Maxwell's reciprocal constructions in the 4th dimension. This applies to any 2D truss (resulting in Maxwell 2D/ Cremona 2D force reciprocals) and to polyhedral spatial trusses with plane faces (resulting in Rankine 3D force reciprocals). This works for any loading case (tension-, compression-only as well as for tension-and-compression structures) for self-stressed structures or equivalent ones with external loading. Within this direct and interactive framework the designer has access, and can start from any reciprocal object - form, force, or stress functions. In particular, the notion of stress functions guarantees that the design is performed within equilibrium space and thus there is no need for iterative converging algorithms in every step like in most approaches. Furthermore, the geometrical characteristics of stress functions introduce novel design and analysis freedoms. Specifically, through the connection to the various states of self-stress which through the lower bound theorem can equip the designers with creative form-finding capabilities. This connection is particularly useful for 2D trusses, for example large-scale tensile installations, and in conjunction to force density for the design and analysis of tension-and-compression shells, grid-shells and vaults. Lastly, graphic statics for N-connected reciprocal diagrams are presented following Maxwell's work and a two-fold purely geometrical static and kinematics framework is discussed.

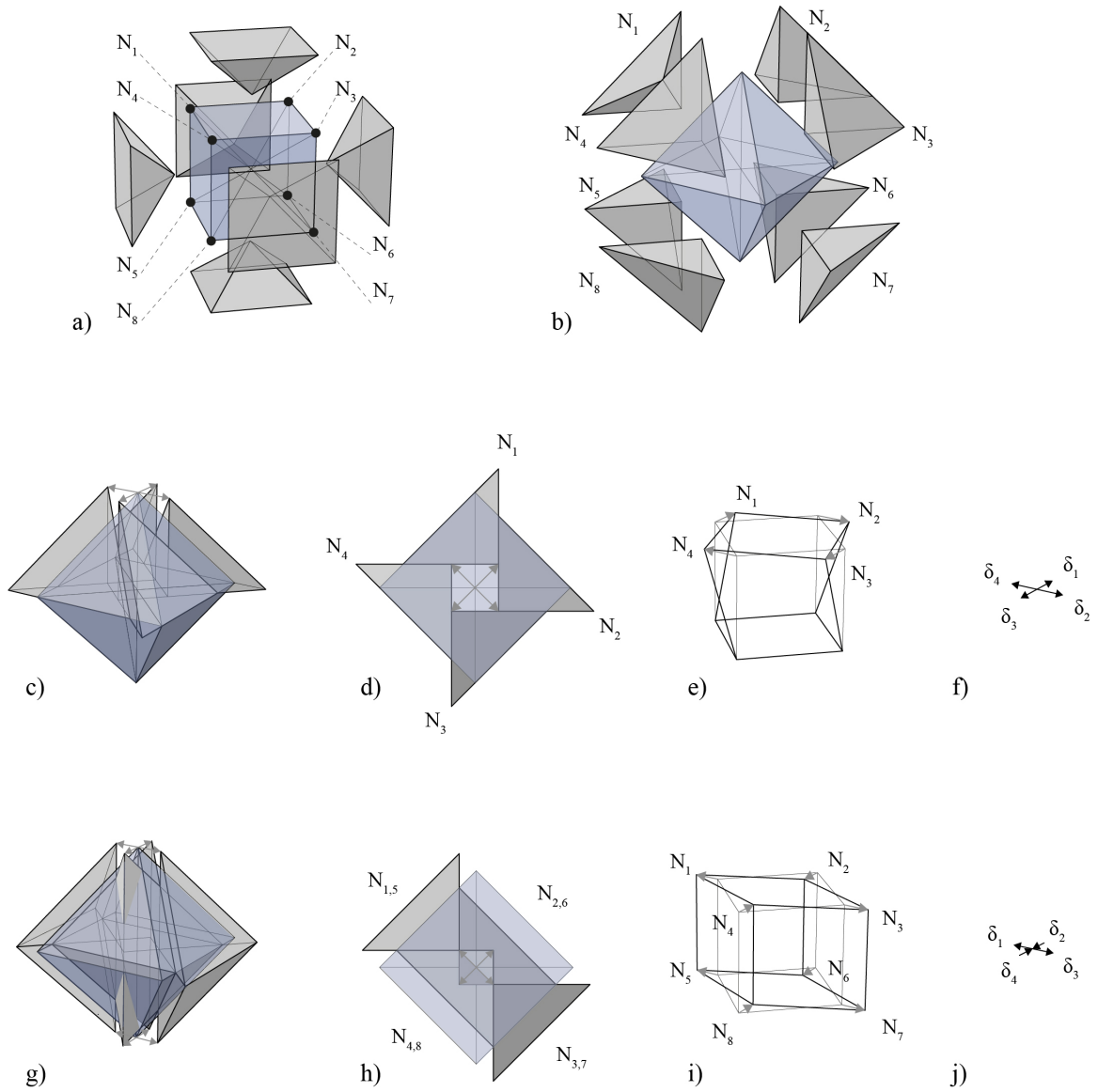


Fig. 3.19 a) The form diagram of a spoked cube; b) The force diagram is a spoked octahedron; c) A mechanism of the spoked cube; d) A mechanism of the unspoked cube from (McRobie et al., 2017).



# Chapter 4

## Geometry-based optimisation

This Chapter presents a geometry-based, visual method of optimisation based on the load path theorem and volume minimisation. This is based on the construction of the Minkowski sum of 2D and 3D trusses and their corresponding force diagram. This research has been presented in the Symposium for the International Association of Shell and Spatial Structures - Boston, July 2018 (Konstantatou and McRobie, 2018).

### 4.1 Introduction

Graphic statics can provide a framework not only for the static and kinematic analysis of plane and spatial trusses but also for their optimisation. Specifically, graphic statics have already been proposed as a structural optimisation framework and applied to plane truss optimisation problems due to their comparative advantages to other methods. From this standpoint we revisit optimal trusses and gain insights with regards to geometry-based optimisation. We show how the objective function in a truss optimisation problem can be essentially expressed and geometrically embedded by the geometry of the Minkowski sum: the total surface area of its parallelepipeds, for 2D trusses; and the total volume of its prisms, for the 3D case.

### 4.2 Optimal trusses

Currently, there is great interest from engineers and architects alike in material-efficient and sustainable designs, especially for large infrastructure projects. As a result, cost and material efficiency considerations lead designers to develop frameworks where structural performance is embedded in the early design stages. Thus, the role of geometry is of paramount importance. Optimal geometries can be characterized by a number of advantages,

such as least volume of material or decreased deflections. In this context, the seminal work of Michell (Michell, 1904) of early 20<sup>th</sup> century is of great significance since it provides benchmark solutions of trusses with least volume, and thus material cost, for a number of cases (Figure 4.1, Figure 4.2).

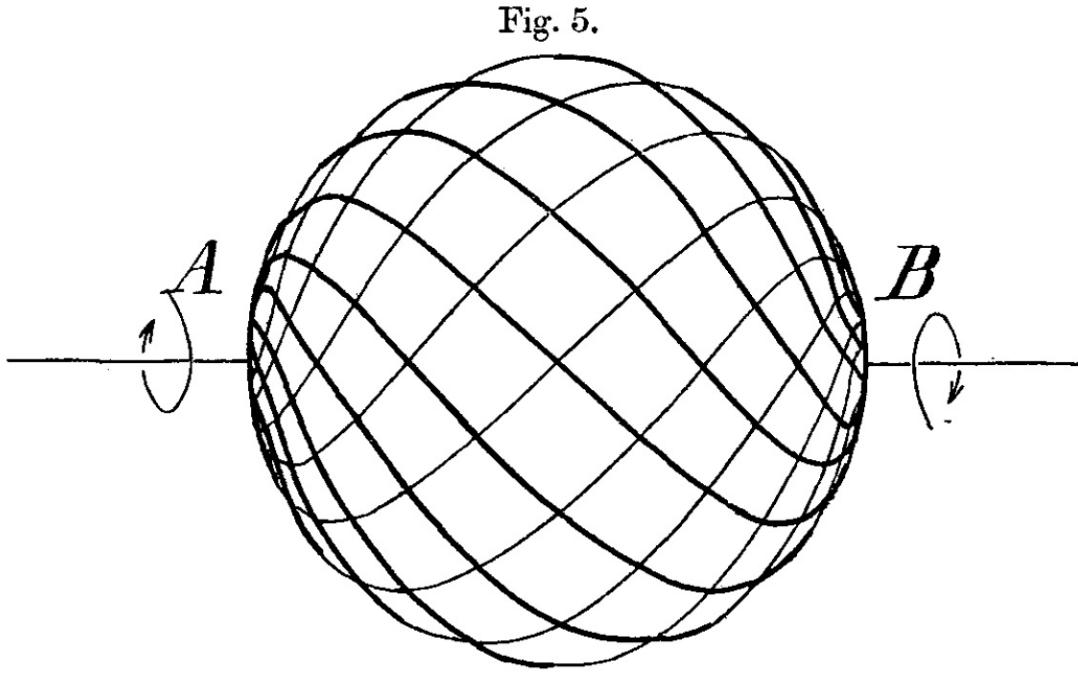


Fig. 4.1 Optimum trusses: Michell torsion ball from (Michell, 1904).

Michell's structural solutions were heavily influenced by Maxwell's work on structural theory and reciprocity in the context of graphic statics. In particular, Michell's paper starts with Maxwell's theorem on load paths which are formulated as follows:

$$\sum F_T L_T - \sum |F_C| L_C = \sum \mathbf{F} \cdot \mathbf{r} \quad (4.1)$$

with  $F_T$  being the axial forces of a truss' members in tension,  $L_T$  their length,  $F_C$ ,  $L_C$  the corresponding values for the members in compression,  $\mathbf{F}$  the applied external forces - including reactions - and  $\mathbf{r}$  the corresponding position vectors (Beghini et al., 2014). Specifically, the dot product on the right of the equation is the value of the applied forces  $\mathbf{F}$ , multiplied by the position vectors  $\mathbf{r}$  with regards to an arbitrary origin (Baker et al., 2015). This theorem essentially states that for a given system of external applied forces the length of the total load path in tension is related to the length of the total load path in compression. In particular, if one of the two load paths is longer than the optimum solution then the truss will pay this twice; once in tension and once in compression (Baker et al., 2013). Conversely, a structure

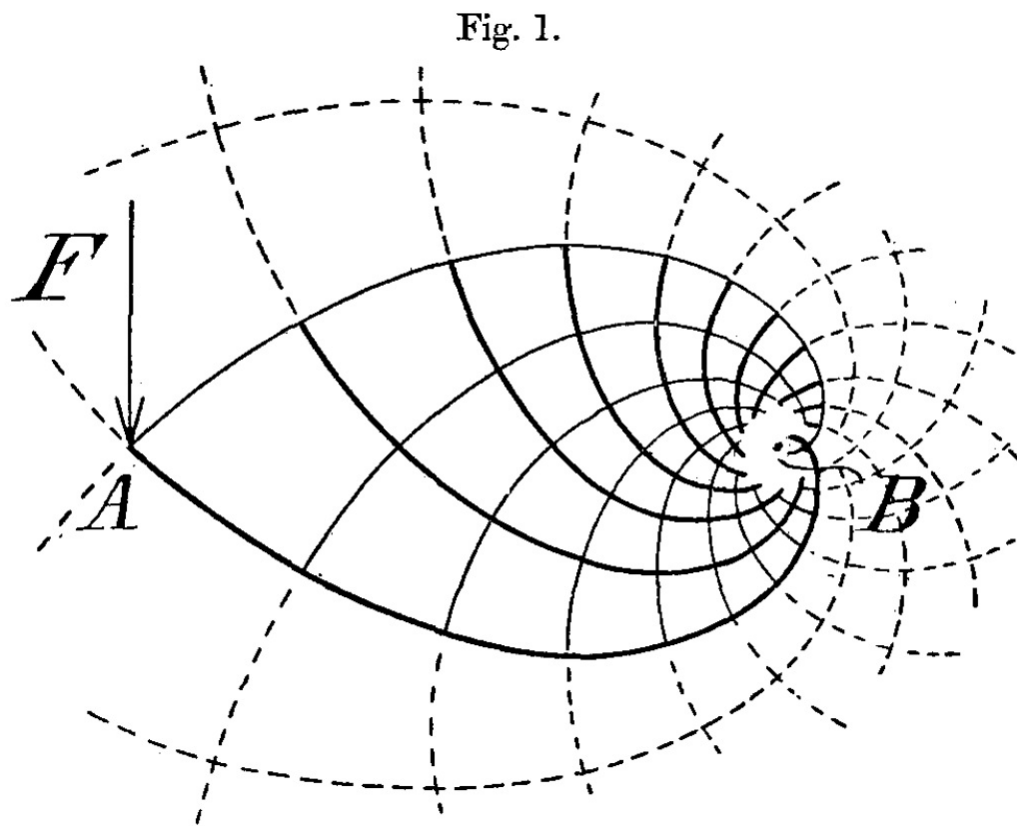


Fig. 4.2 Optimum trusses: Michell 2D optimum truss from (Michell, 1904).

which is optimized solely with respect to its tension (or compression) load path is automatically optimized regarding its compression (or tension) load path as well. Moreover, by dividing the load paths of tension and compression with the allowable stress  $\sigma$  of structural members of the truss can be derived as follows (Hemp, 1973):

$$V_{TOT} = V_T + V_C = \sum \frac{F_T L_T}{\sigma} + \sum \frac{|F_C| L_C}{\sigma} \quad (4.2)$$

with  $V$  being the volume of the structure; specifically,  $V_{TOT}$  the total volume,  $V_T$  the volume corresponding to the tension load path and  $V_C$  the volume corresponding to the compression load path. By applying Maxwell's theorem on load paths Michell derived trusses which are not only of least volume and least material but also of aesthetic significance through their regular, simple, and organic forms. As a result, these trusses, the discrete versions of which can be derived, are the absolute optima and 'ideal' structures in relation to which all other structural solutions can be compared in terms of efficiency (Hemp, 1973). Moreover, Michell proved that, under appropriate conditions, a truss of maximum stiffness is actually a truss of minimum weight and volume (Beghini et al., 2014). Specifically, that its deflection will decrease when removing rather than adding structural members (Baker et al., 2013). A remarkable result, which contributes greatly to material efficiency being analogous to structural performance. In particular, the objective function that needs to be minimized to obtain a solution of minimum volume is:

$$\min_{\mathbf{x}} V = \min_{\mathbf{x}} \frac{1}{\sigma} \sum |F| L \quad (4.3)$$

where  $\mathbf{x}$  corresponds to the vector coordinates of the structural nodes that can be altered. It follows, that this equation is geometrically described from the Minkowski sum. Discrete optimum trusses combined with graphic statics have proved to be important influences on fundamental structural research (Baker et al., 2013, 2015) and important paradigms in real-life structural design of landmark structures (Beghini et al., 2014) due to a number of advantages (Beghini et al., 2014; Mazurek, 2012; Mazurek et al., 2010):

- They provide absolute minima benchmarks with regards to volume and total load path for truss layouts.
- They provide visual insight in the structural behavior of the structure.
- They provide the possibility for defining geometrical characteristics and variables of the truss in question.
- They provide the ability to study and optimize the reciprocal problem instead, in the case that the truss is under-defined or more complicated than its dual.



- They provide great simplification of calculations: no need for deriving and using a stiffness matrix or analytical/ numerical optimisation techniques.

### 4.3 Method

For a pin-jointed structure of applicable geometry <sup>1</sup> in static equilibrium, we include in the form diagram any external forces. Then, the resulting geometry can be thought of as an equivalent self-stressed system which is thus a projection of a plane-faced polyhedral or 4-polytopic stress function. If there are no external forces to add then the structure is self-stressed. Using polarities, as shown in Chapter 3, we map the stress function to its reciprocal. The pair of reciprocal  $(n+1)$ -dimensional stress functions is projected orthogonally one dimension lower to create a pair of reciprocal  $n$ -dimensional form and force diagrams. Then both diagrams can be combined into a Minkowski sum - the parallelepipeds or prisms of which reveal the  $FL$  terms of the structure's load path which need to be minimized for material efficiency. We should highlight that this approach gives insight and direct control to any one of the reciprocal objects and as a result the designer can design with the form or with its forces – the roles of which are interchangeable.

In the process of lifting a form diagram to its 3D stress function we identify a number of nodes that can be independently lifted one dimension up. For example, in a triangulated structure enclosed by a fixed boundary, these would be all the nodes apart from the ones belonging to the boundary. For structures which are not triangulated, this number, as shown in section 3.2.1, would decrease. This is because a plane face needs only three points to be defined in 3-space. Consequently, if the polygonal face has more than three nodes, the extra ones will be dependent on the three which define the plane. Similarly, in a 3D structure comprising exclusively of tetrahedral cells enclosed by a fixed boundary, all the nodes can be lifted - apart from the fixed ones belonging to the boundary. However, if there are cells with more than four nodes then, the number of nodes that can be independently lifted will decrease since each hyper-plane, on which a cell lies on, needs only four nodes to be defined in 4-space. We should highlight that it is possible for 3D structures to have more states of self-stress than can be revealed through this geometrical approach (what is known as Rankine incompleteness (McRobie, 2016)). Nonetheless, if a geometry can be found for which the structure is in static equilibrium, then, via the lower bound theorem of plasticity the particular

<sup>1</sup>These are the geometries addressed in this PhD thesis as described in section 3.1: for the 2D case, they comprise any 2D diagram in static equilibrium - with the possible addition of extra nodes; for the 3D case, they comprise plane-faced polyhedral structures which obey the counting rules of 4-polytopes.

structure is safe and will not collapse - given that appropriate conditions are met <sup>2</sup>. When an initial stress function has been created, the nodal location of the vertices can be adjusted iteratively until the solution converges to a minimum load path and thus minimum volume. During that process, the imposed condition of the faces remaining plane of the stress function will add geometrical constraints which lead to the optimisation process being performed within equilibrium space.

We implement the above methodology for 2D and 3D cases using as a CAD platform the McNeel Rhino software, in conjunction with the Grasshopper plug-in and custom Python scripts. For example, in Figure 4.3 we see a 2D example in which the three internal nodes of the structure are allowed to move. We observe the changes in all four reciprocal diagrams (form, force, and polyhedral stress functions) and the corresponding Minkowski sums. We highlight how the forces (in dotted lines) are incorporated in a unified geometry of an equivalent self-stressed truss. The total surface area of the rectangles, corresponding to structural members, readily gives the  $FL$  terms of the total load path of the structure, which we schematically represent with bars (Figure 4.3). As a result, these bars give an intuitive and visual representation of the objective function that needs to be minimized in a structural optimisation problem. Consequently, a designer can easily grasp when a truss is optimized: when geometrically the sum of the form and its forces is minimized too. Moreover, after the structure is optimised, the graphic kinematics method described in section 3.3 can be used to check for mechanisms.

Similarly, in 3D (Figure 4.4) a spatial truss and its external forces are combined in a single geometrical object (forces in dotted lines) of an equivalent self-stressed spatial truss. The form diagram is lifted to the 4<sup>th</sup> dimension and subsequently mapped to its force reciprocal. Note how the forces are concurrent to point  $v_f$  of the form diagram and map to the force cell  $c_f$  in the reciprocal force diagram which remains fixed throughout the displacement of the internal nodes. The two geometries are then combined in a spatial Minkowski sum. We allow for the two internal nodes to move and thus the geometry can be optimized by minimizing the total volume of the prisms of its Minkowski sum which correspond to structural members (in green in Figure 4.4).

---

<sup>2</sup>It should be noted that the local and global buckling behaviour of the structure is not addressed here and should always be examined in detail. This has special importance for structures with subtle buckling behaviour such as shells and grid-shells.

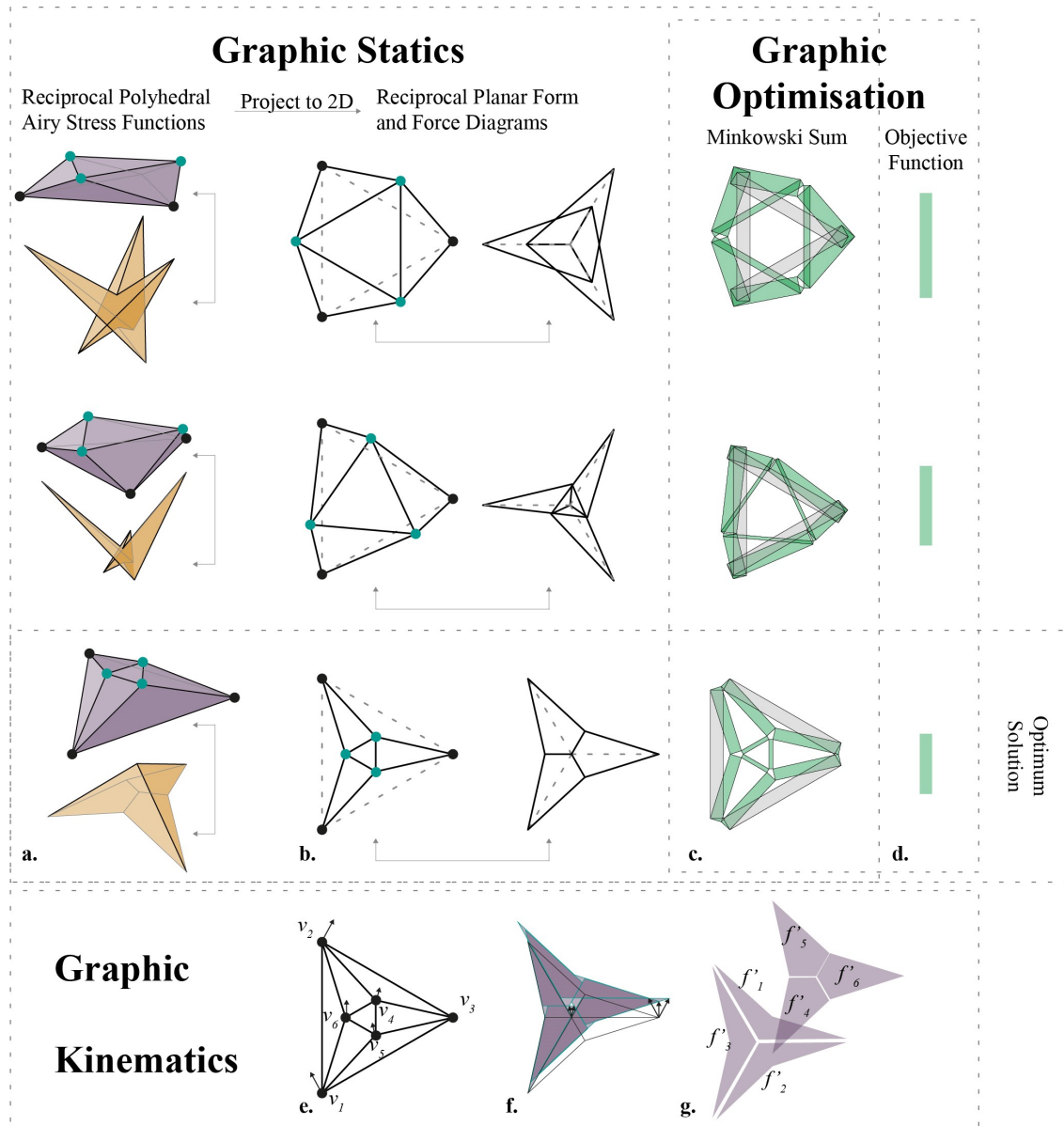


Fig. 4.3 a) Pairs of reciprocal polyhedral Airy stress functions; b) Pairs of plane form and force diagrams resulting as a projection of stress functions, the location of the three internal nodes in blue can change to find the optimum configuration; c) Combination of form and force diagrams in a Minkowski sum - the surface areas correspond to the  $FL$  terms of the structure's load path; d) The resulting area of the rectangles is the geometrical manifestation of the total load path and the objective function of the structural optimisation problem; e,f,g) After the structure is optimised, graphic kinematics can be used to check for mechanisms.

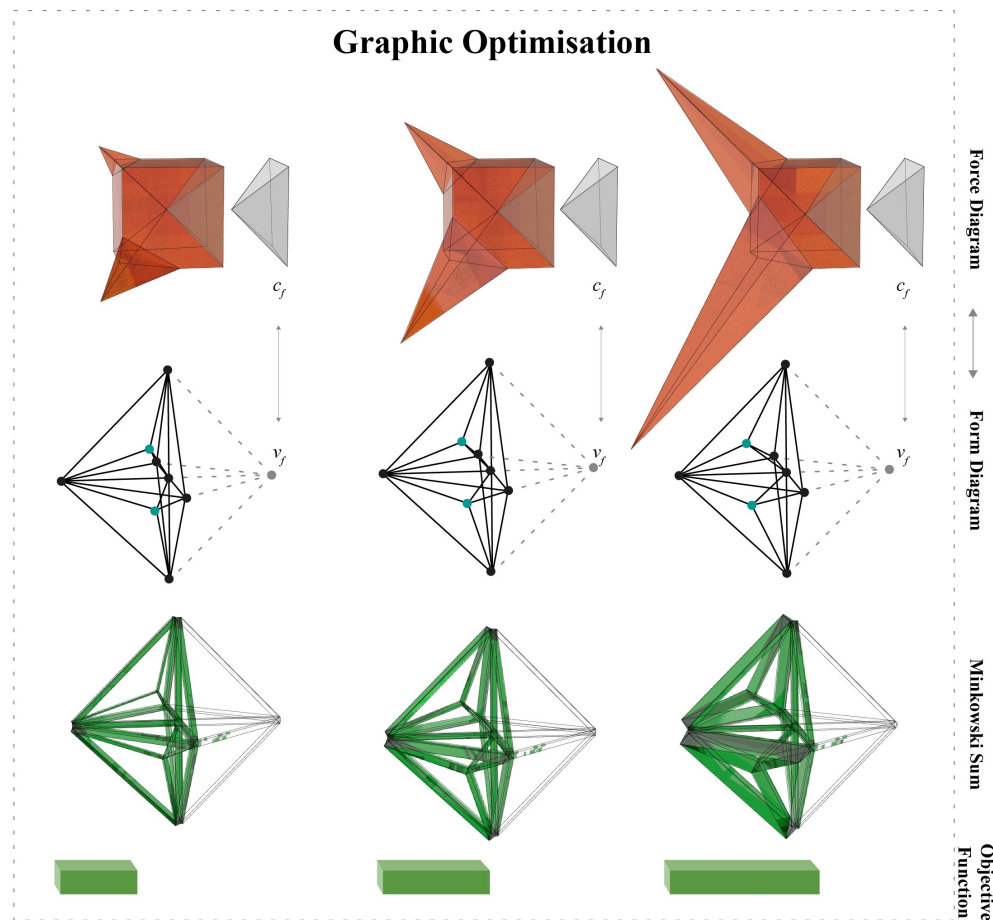


Fig. 4.4 Examples of different geometries (form diagrams), their corresponding force reciprocals (in Rankine 3D configuration), Minkowski sum, and total load path in visual terms of volume (the green prisms correspond to structural members and the white ones to edges which represent the lines of action of the forces). The moving nodes are in blue and the diagrams are in order of reducing material efficiency from left to right.

## 4.4 Summary

In this Chapter we showed how a geometrical and unified (for the 2D and 3D case) graphic statics framework can be applied not only for structural analysis (static and kinematic) and design, but also as a visualisation method of optimisation. This results in an intuitive way of minimising a structures volume via the application of Minkowski sums. Due to the visual nature of this method, it is intended to be accessible and user-friendly both for engineers and architects.

# Chapter 5

## Geometry-based design

This Chapter presents design-by-analysis methodologies for 2D and 3D trusses based on the polarities graphic statics method outlined in Chapter 3. In particular, it discusses how to design structures in static equilibrium by using reciprocal stress functions. This method is also combined with the force density method for tension-and-compression shells, grid-shells, and vaults. This last part, on which we will expand in Chapter 6, started as an industry secondment at SOM Chicago in spring 2018 with Bill Baker and the structures team. Also, the Airy stress function as a *correction* tool of trusses which are not in static equilibrium is the contribution of the author to the research paper 'A 3D Airy Stress Function Tool for Reciprocal Graphic Statics' (Vansice et al., 2018) presented at the Symposium for the International Association of Shell and Spatial Structures - Boston, July 2018.

### 5.1 Truss design by analysis

The polarities graphic statics framework which was introduced in Chapter 3 has a number of design and analysis advantages. Since all four reciprocal objects are interlinked and all of them can be altered while updating the rest, the designer has the option of choosing the starting point: form, force, or reciprocal stress functions. Each one of these starting points has different capabilities but all result in statically equilibrated structures. By starting with the force diagram as an input the designer can essentially design with the forces and observe interactively the form as an output of the process. Specifically, by working with the force stress function, or by imposing the corresponding geometrical constraints on its projection (the force diagram), a structural morphogenesis method can be obtained where the resulting form diagram is guaranteed to be in static equilibrium. For the 2D case, the force diagram should be a projection of a polyhedron, and for the 3D a projection of a 4-polytope. This latter condition is essentially what is already known in the literature as plane-faced

(non-intersecting) Rankine reciprocals which produce compression-/tension-only polyhedral spatial structures (Akbarzadeh et al., 2015). This methodology includes subdivisions of the force diagrams which result in different topologies of the spatial truss. By using the polarities approach this structural morphogenesis approach can be generalised for tension and compression structures, where the geometry of the faces (in terms of intersections, or complexity) is not limited. This is because something wrapped and complicated in 3D can unravel and inflate in 4D. Moreover, by controlling the curvature of the stress function the designer can control the areas of tension and compression. It should be highlighted that form, force diagrams and stress functions have an interchangeable character. The same applies to truss members and the lines of action of external forces. As a result, no special treatment is needed for any of these.

Alternatively, the designer can choose to work directly in the form space. In this case, by following the geometrical constraints imposed by the projective interlink of the form diagram and its corresponding stress function one can be sure that the designed form is structurally sound and not merely a free-form design with no structural performance considerations. What is more, even if the designer starts to draw a truss in a free-form manner then the resulting geometry can be *corrected* by the ensuring it is a projection of a higher dimensional stress function. For example, a polyhedral lifting can be performed on a 2D truss which will check if it is a projection of a plane-faced polyhedron. In this process, the location of a number of nodes can be corrected until the geometrical constraint is satisfied and the resulting truss is in static equilibrium (Figure 5.1). Moreover, the fact that these geometrical objects are interlinked through a direct transformation ensures global static equilibrium in every step and there is no need for iterative node-by-node reconstructions and imposed approximations between the form and force reciprocals.

## 5.2 Vault, shell and grid-shell design via the Airy stress function

Contemporary computational frameworks for the design and analysis of self-supporting surfaces are valuable tools for form explorations but they also have drawbacks. Specifically, they work only for compression-only shells/ vaults and they do not exploit a plethora of design and analysis freedoms that derive from graphic statics methods, most notably from the use of the Airy stress function. As a result, these methods are case specific and cannot solve the general case of tension-and-compression grid-shells which are self-supporting without the application of external lateral forces. In response to this, we introduce here an

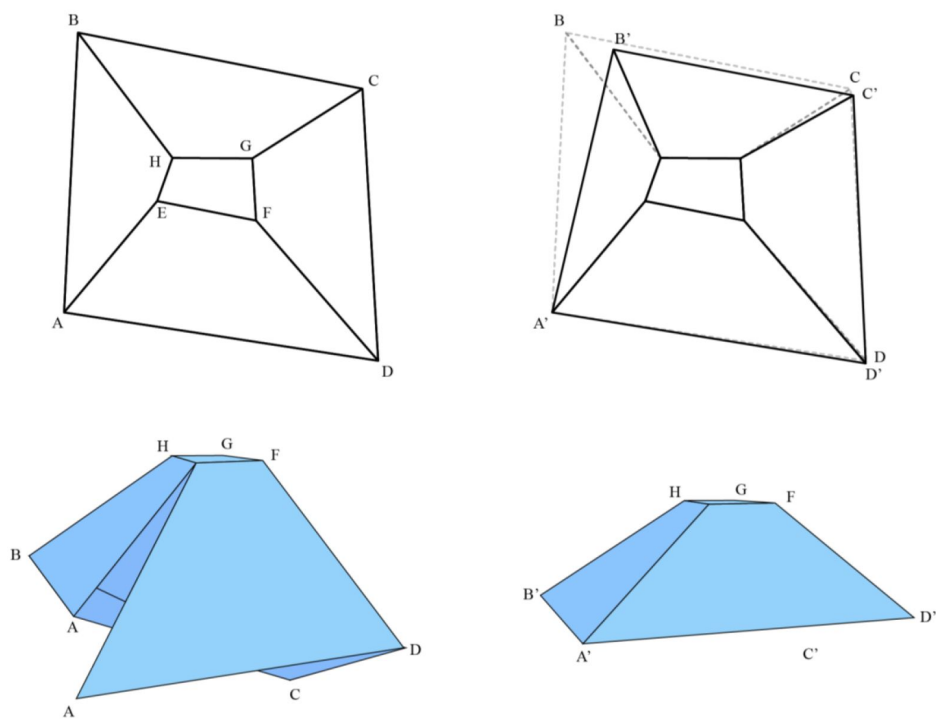


Fig. 5.1 The Airy stress function *correcting* a truss towards static equilibrium from (Vansice et al., 2018).

interactive form-finding method for tension-and-compression structures which is based on the reciprocity between polyhedral Airy stress functions for the generation of horizontal equilibrium in conjunction with the force density method.

Contemporary research on the design and analysis of spatial structures acknowledges the advantages and insights gained from bi-directional, geometry-based methodologies. These include: a shift towards material efficient structures by incorporating structural performance in the early conceptual design stages; an interactive approach where designers have more leverage, design and analysis freedoms on the outcome of the model; structural morphogenesis opportunities by manipulating reciprocal diagrams; a new approach of free form design for structures which are by definition in static equilibrium (as opposed to conventional free-form, structurally-irrational design); facilitating communication between architects, engineers, and generally specialists in design and analysis of the built environment by re-introducing the unified language of geometry.

As summarized in Lachauer (Lachauer, 2015) contemporary structural design approaches can be generative or interactive. The former comprises an algorithm which given a user input, outputs a resulting form while having limited and not explicit interaction possibilities throughout the process. The latter comprises a hybrid methodology in which modelling and computation phases can alternate in the pursuit of a satisfying form. Thus, it provides explicit interaction between the design and the analysis of the model. Numerous such form-finding methods have been developed in the context of graphic statics and the force density method.

In the last two decades there are several contributions related to hybrid graphic statics and force density methods for the design and analysis of spatial forms in static equilibrium. Lachauer (Lachauer and Block, 2014; Lachauer, 2015) introduced an interactive computational framework which when applicable combines force density and optimisation routines to produce compression-and-tension spatial structures while imposing geometrical and force constraints. Rippmann and Block (Rippmann and Block, 2013; Rippmann et al., 2012) introduced the computational framework of RhinoVault, based on the Thrust Network Approach (Block and Ochsendorf, 2007), for form-finding of compression-only vaults. In this method, the force and form diagrams can be altered interactively while optimisation routines converge the result to an equilibrium solution. This works for diagrams consisting of regular quad networks of curves and includes the possible addition of continuous tension ties. Bahr (Bahr, 2017) introduced a method to generate strut-and-tie spatial networks in static equilibrium by transforming an initial kinematic system into a structure in static equilibrium for specific loading. This works mainly for simple arrangements by solving the non-linear equation systems with the Newton-Raphson method given an initial guess of the unknown parameters. Similarly, by defining a loading-bearing mechanism and a load case, Ohlbrock



et al. (Ohlbrock et al., 2017; Ohlbrock and Schwartz, 2016) introduced an interactive computational form-finding framework which employs gradient-based optimisation techniques to converge to an equilibrium state of a spatial strut-and-tie network given user-specified constraints.

As a result, there seems to be a shift towards geometry-based structural and architectural design methods in which:

- Analysis and design have a bidirectional relationship.
- Geometrical language is preferred.
- Interaction between the designer and the form throughout the process is steadily enhanced.
- The analysis can be seen as an indispensable design tool in the early conceptual design stages rather than as an independent post-process after the form has been decided.

The above methods are valuable computational frameworks and contributions towards this direction. However, they do not make use of the full potential given from the inherent structural indeterminacy of the structure, and they use iterative routines and optimisation algorithms which are opaque to the users. Specifically, by imposing/ updating geometrical and other constraints in every step, the structure will get out of equilibrium which results in the need to run iterative/ optimisation algorithms in every step to converge again to a configuration of static equilibrium. As a result, there is still unexplored potential in employing graphic statics methods for developing interactive, direct methods where structural analysis is both an explicit design tool and part of the method per se, in a visual, intuitive, and inherently geometrical framework. Specifically, if the analysis part does not only have a bidirectional relationship with the design process but is an integral part of the design method, there is no need for reconstruction or convergence in every interaction since by construction the allowed changes result in a structure in static equilibrium.

The method presented here takes advantage of the direct generation of global equilibrium which can be achieved through polarities between reciprocal polyhedral stress functions. The applicable geometries are envelopes, which topologically are polyhedra. Thus, they obey their counting rules: every edge belongs to two faces, each node to at least three faces, as well as Euler's polyhedral formula. As such, this method is about discrete versions of the Airy stress function which correspond to strut-and-tie networks. We should highlight that any horizontal reactions are incorporated in the geometry of the truss resulting in an equivalent self-stressed truss as per Maxwell's approach where structural members and lines of action of external forces are not distinguished. As a result, this method can be applied to

compression-only vaults and tension-only membranes in the same way that it can be applied to compression-and-tension grid-shells. There is no limitation in the geometry of the faces or a geometrical constraint on the faces being enclosed from a structural boundary.

By using the Airy stress function as the centre of the method and generator of horizontal equilibrium, several advantages are gained:

- The structure is always in static equilibrium while the designer interacts with it.
- Local and global transformations can be made in any one of the four reciprocal objects (form diagram, force diagram, form Airy stress function, force Airy stress function) while the rest update automatically and directly.
- The Airy stress function is a powerful design tool. By sculpting its curvature and carving its geometry, the designer can introduce openings, control which edges are in tension, which in compression, by how much, and which have axial loads at all. Moreover, all this information, which designers were mainly sourcing from the force reciprocal, is directly and intuitively visible on the geometry of the Airy stress function which has the same topology with the form diagram (which is its orthographic projection).
- The Airy stress function gives insight to the states of self-stress in a more explicit and intuitive way than the force diagram for two reasons. Firstly, it has the same topology as the form diagram (which is its orthographic projection) so for every edge in the form diagram the designer can have a full picture of its structural behavior just by interrogating visually its two adjacent faces in the Airy stress function: the magnitude of their kink corresponds to the magnitude of axial loading, their curvature (valley or ridge) to whether it is a tie or a strut; if they lie on the same plane the particular edge has no axial load at all. Secondly, the number of polyhedral liftings, namely, of how many nodes can be lifted independently for the polyhedral stress function to form in 3-space, are equal to the number of self-stresses in the system. These self-stresses are design freedoms in the sense that each one of them will output a different form. This is particularly useful for grid-shells or discrete structures in which the tessellation pattern needs to be exact and reconfiguration of the form diagram is not desirable.
- This method, based on the polarities framework, is direct and produces global equilibrium without the need for iterative node-by-node algorithms or reconstructions of the diagrams after a change is made. Moreover, the polarities graphic statics framework applies the same methodology both for 2D and 3D structures (by outputting Rankine force reciprocals in the latter case). As a result, 2D graphic statics via polyhedral stress

functions can be used to obtain a spatial strut-and-tie network in static equilibrium and subsequently 3D graphic statics via 4-polytopic stress functions can be used to produce spatial Minkowski sums of the structure. These prismatic structures are useful to designers as they visually represent the size of each one of the structural members under a constant-state design as well as the terms of Maxwell's load path theorem which can be used for optimisation purposes.

### 5.2.1 Force Density Method

The force density method (Schek, 1974), or 'Stuttgart direct approach' was primarily used for form-finding and design explorations of prestressed spatial tension-only structures, such as hanging cable nets and membranes (Linkwitz in (Adriaenssens et al., 2014)). For this type of funicular structures, the form is interlinked to the internal forces and greatly affects the load-bearing behavior (Linkwitz in (Adriaenssens et al., 2014)). Relating geometry and static equilibrium results in a non-linear problem. This can be converted to a linear one by introducing force densities, namely, the ratios of axial forces over lengths of a strut or tie. In particular, for a given 2D self-stressed form diagram, for which the boundary heights  $\mathbf{z}_F$  are fixed, the height of the internal nodes  $\mathbf{z}_N$  can be found:

$$\mathbf{z}_N = \mathbf{D}_N^{-1}(\mathbf{p} - \mathbf{D}_F \mathbf{z}_F)$$

where  $\mathbf{p}$  is the vertical loading,  $\mathbf{D} = \mathbf{C}^T \mathbf{Q} \mathbf{C}$ , with  $\mathbf{C}$  being the directed branch-node connectivity matrix of the form diagram and  $\mathbf{Q}$  the diagonal matrix of force densities (Linkwitz in (Adriaenssens et al., 2014)).

This method, which was developed in the 1970s, was used for the form-finding of some eminent structures such as the Mannheim Multihalle and the Olympic roofs of Munich. Apart from calculating spatial forms in static equilibrium without the need for specific material information, it can also incorporate geometrical constraints such as boundary conditions and equal lengths of the structural members. Moreover, it can be used for mixed compression and tension structures by introducing positive (tension) and negative (compression) force densities.

The input of the force density method is a 2D diagram of the topology and projected geometry of the spatial structure, vertical point loads for every node, and the force density values for each edge. The role of the states of self-stress as a design and analysis freedom are implicit in the force density method as different sets of force densities will output different geometries. The tension-only outputs of the force density method can also be seen as their compression-only equivalents following Hooke's analogy between a hanging chain (purely

in tension) and an equivalent inverted chain as a purely compressive arch. This has been used in the Thrust Network Analysis and its computational implementation (RhinoVault). In these frameworks, the force density method is coupled with an iterative algorithm, which calculates horizontal equilibrium in terms of a graphic statics force diagram, for the form-finding of compression-only vaults.

Research has been done in extending the potential and robustness of this method to the form-finding of compression-and-tension structures such as tensegrities (Miki and Kawaguchi, 2010; Zhang and Ohsaki, 2006), suspended membranes with bars (Miki and Kawaguchi, 2010) and spatial combinations of cables and struts (Malerba et al., 2012). Also, there is relevant research in applying the force density method in interactive design and analysis frameworks where the user has more active role in intermediate steps of the process than solely defining the initial input parameters. This has been most notably developed in the context of tensegrity structures (Tachi, 2012; Zhang and Ohsaki, 2006). The Airy stress function has been used in the context of graphic statics for the generation of self-supporting compression-only structures. Specifically, the discrete polyhedral stress function has been introduced (Fraternali, 2010) for the analysis of unreinforced masonry vaults and for the prediction of fracture-prone regions. Moreover, a continuous approach has been developed in Miki (Miki et al., 2015) in which the geometry is represented by parametric NURBS surface rather than discrete networks.

### 5.2.2 Methodology

This form-finding method for spatial tension-and-compression structures such as vaults, shells and grid-shells, in static equilibrium uses reciprocal polyhedral Airy stress functions both as design freedoms and for generating horizontal equilibrium which then is the input of the force density method. As in the literature, negative force densities are used for compression and positive for tension.

Given an initial 2D closed boundary curve of the structure, the enclosed space can be tessellated in several ways such as a regular triangulation which is convenient for the purposes of the method. Triangulation results in the maximum number of polyhedral liftings of the form diagram/ states of self-stress. Thus, it highlights the potential of the Airy stress function as a design freedom. Of course other patterns with  $n$ -gons can produce patterns that are projections of polyhedra; however, these will require an extra layer of analysis (since then not all the vertices can be lifted independently). Now, this tessellation is a 2D truss which is trivially a projection of a polyhedron (since all the faces are triangular). We should note that this type of diagram is a Schlegel diagram, *viz.*, an outer (bottom) face which encloses all the other (upper) ones. This type of diagram includes all the topologies found in (Rippmann et al.,

2012). However, following the approach outlined here, we need not be constrained to this. The structure can also have a non-trivial ‘bottom layer’ which is also a part of the structure in static equilibrium. After the initial tessellation is decided, all the internal nodes are lifted to create the polyhedral Airy stress function of the 2D truss. Since by construction we have freedom to move every one of the internal nodes in the  $z$ -direction there are an infinite number of possible polyhedra which live on top of the truss. The number of independent states of self-stress equals the number of internal nodes. Moreover, the tessellation can also happen directly as a discretization of the surface of an Airy stress function in 3-space so potentially the designer does not even need the form diagram as a starting point.

The choice of the polyhedron reflects the wanted structural behaviour and is a design and analysis freedom. For example, the choice of a strictly convex (concave) polyhedron produces a tension (compression)-only 2D truss enclosed by a compression (tension) boundary. This makes sense for a compression/ tension only structure such as self-supporting masonry vaults or nets. From Heyman’s plasticity theory and the lower bound theorem, we know that one solution suffices for our structural analysis and design purpose. However, the multiple solutions that are readily available through the Airy stress function approach can give us more insight. Every different choice of an Airy polyhedron will lead to a different shell/ grid-shell spatial geometry. As a result, by combining the lower bound theorem and Airy stress functions the designer has more freedom with regards to structural design. The chosen Airy polyhedron can now be mapped to its reciprocal using polarities and subsequently projected on the plane to derive the force reciprocal of the initial 2D truss in a Maxwell configuration. The two diagrams can be combined in a Minkowski sum with the aspect ratio of each of the rectangles readily giving the value of force density for each one of the bars. Then the vertical loads can be assigned to each one of the internal nodes. The values can just be a constant or more generally defined by the user at will. Moreover, as an approximation for dead load a Voronoi pattern on the internal nodes can be used for the tributary areas. Now that we have horizontal equilibrium, force density values, and vertical loads we can lift the 2D diagram to a spatial shell/ grid-shell in static equilibrium. We should note that the 2D truss, its Airy polyhedron, and the final spatial grid-shell/ shell have exactly the same topology but different geometry. The 2D static equilibrium is combined with the force density method and vertical point loading to produce 3D vaults in static equilibrium. We should note that this method can be readily applied to  $n$ -connected polyhedra too (with  $n > 1$ ).

This methodology is implemented in the Rhino/ Grasshopper environment. The python code which includes a matrix solver for the force density method was implemented using the MathNet.Numerics library. Moreover, a user-friendly interface was developed through the Human UI plug-in for Grasshopper Figure 5.2. With this, a number of important input parameters are presented in a window where the user can define the values without the need to delve into the code. Also, since this is written as Grasshopper code, it can be readily added or extended within the Grasshopper environment.

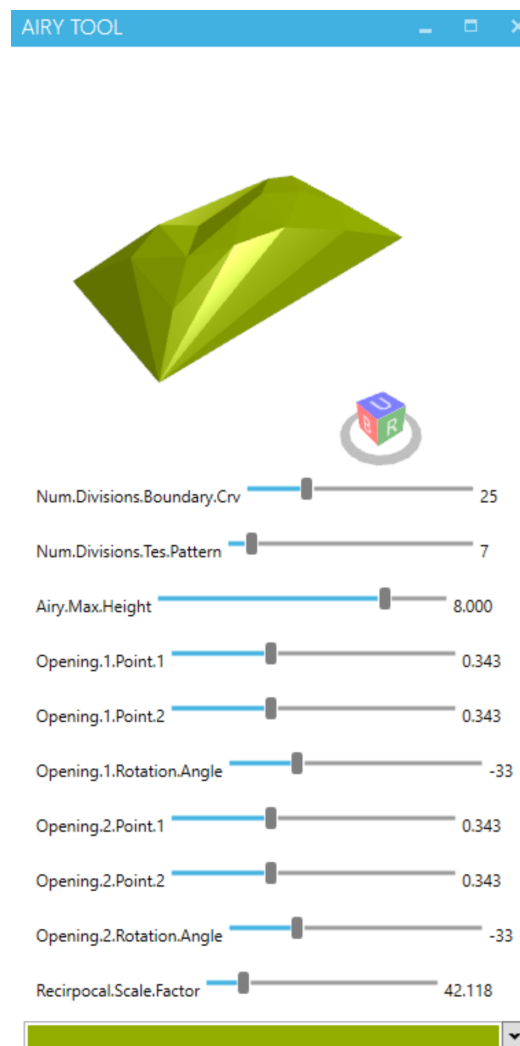


Fig. 5.2 User-friendly interface of the Airy force density tool which presents to the user a window with key parameters which can be controlled.

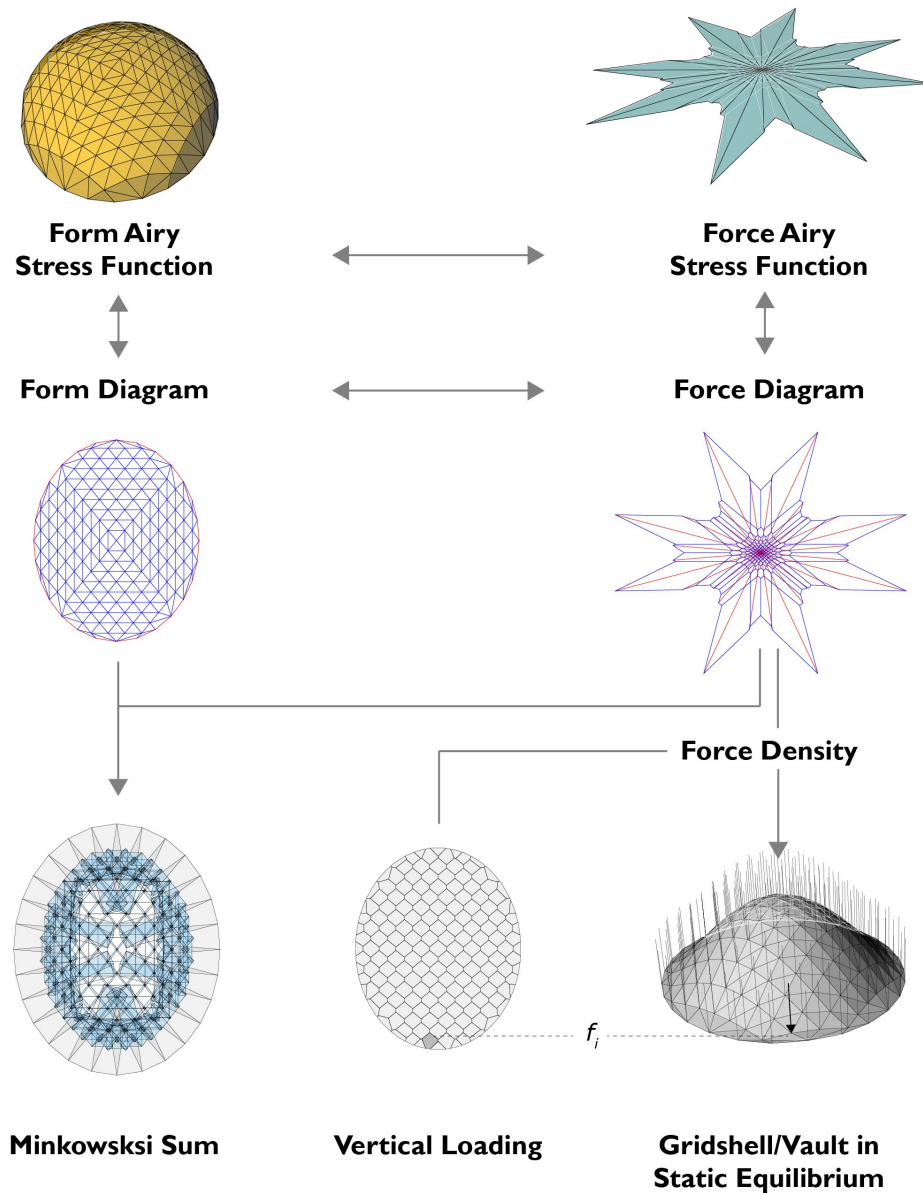


Fig. 5.3 A polyhedral Airy stress function follows the tessellation of the form diagram and provides global horizontal equilibrium. When this is combined with force density for given vertical loads, it results in a spatial shell/ grid-shell in static equilibrium. In this case a convex Airy stress function was used resulting in a compression-only shell. The vertical loading can be defined by the user. For the example used here, the weight of the tributary area of the shell is approximated from a Voronoi pattern. 2D form and force diagrams can be combined in a Minkowski sum.

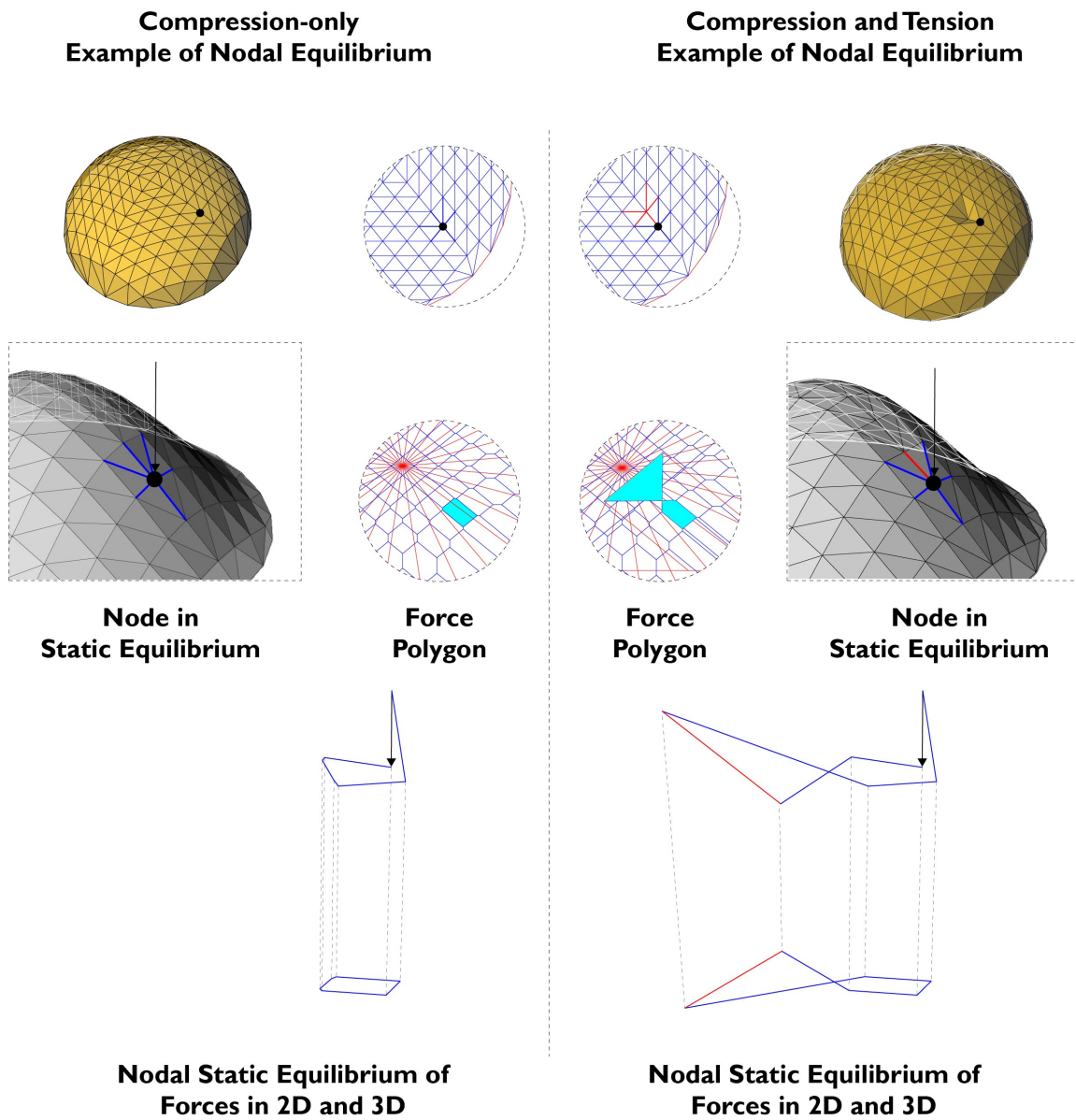


Fig. 5.4 This method based on polarities can work both for tension-only, compression-only and compression-and-tension structures.



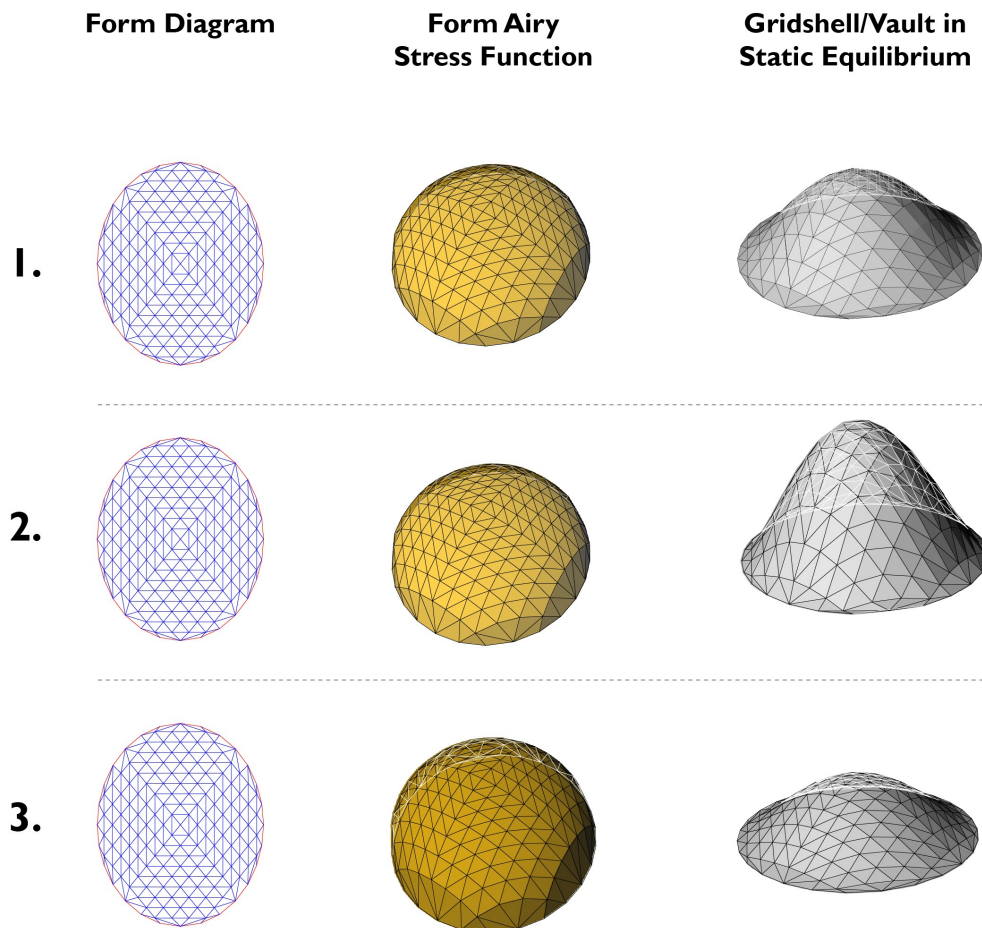


Fig. 5.5 The Airy stress function as a design freedom: different polyhedral liftings (admissible states of self-stress) of the same form diagram result in different spatial forms in static equilibrium.

## 5.3 Summary

In this Chapter, a direct design-by-analysis framework was introduced for 2D and 3D trusses, as well as for the development of tension-and-compression shells, grid-shells and vaults. For the latter case, this was based on combining global horizontal static equilibrium and the force density method. It was highlighted how the stress function is useful not only for designing structures within static equilibrium but also as an intuitive and geometrical way to correct form diagrams should the designer decide to start a *free-form* design exploration of the geometry.

With regards to the shell, grid-shell and vault design and analysis method introduced here, the main advantages include:

- Direct transformation (as opposed to iterative approximations).
- Elegant mathematical graphic statics framework which includes algebraic and matrix descriptions next to the fundamental geometrical construction.
- Not only the outputs (reciprocal diagrams) but also part of the toolkit (Airy stress function) is purely geometrical and has a physical meaning which greatly adds to its education value.
- It is not limited to compression-only structures (it can as well analyse and design self-supporting tension-and-compression grid-shells without external lateral loads).
- Incorporation of n-connected Airy stress functions.
- This method allows internal courtyards and openings rather than just oculus-sky lights.
- The Airy stress function approach gives control and insight in 4 reciprocal and interactive objects (reciprocal diagrams and corresponding stress functions).
- As an approach it gives insight and explicitly uses the states of self-stress as design and analysis freedoms rather than merely local/ affine transformations of the form / force diagram. This is crucial for structural design since it enables a more fundamental understanding of structural analysis and enables a purely geometrical design by analysis via the lower bound plasticity theorem.
- In this approach external forces can also be introduced, via an equivalent self-stressed structure.
- Form and force features can be introduced by sculpting, transforming, and carving locally and globally the polyhedral Airy stress function.

# Chapter 6

## Applications

This Chapter presents applications of the theoretical framework presented in the previous Chapters. In particular, it illustrates methods of design, analysis and transformations of 2D and 3D (polyhedral) trusses (Konstantatou et al., 2018) which can start either from the form diagram, force diagram, or corresponding stress functions - highlighting the different advantages. In particular, the case studies developed here are:

- Study of interlinked graphic statics and kinematics for tensegrities with infinitesimal mechanisms and flexible polyhedra with finite mechanisms (Konstantatou and McRobie, 2017);
- Introduction of the dynamic Minkowski sum for statically balanced tensegrity mechanisms (Konstantatou and McRobie, 2017);
- Design and analysis of large infrastructure: tensile net as a stadium roof;
- Structural morphogenesis of large infrastructure - exoskeletons and trusses of towers;
- Design through analysis of large infrastructure: tension-and-compression shells, grid-shells, and vaults.

The above case studies have been published in journal articles and conference proceedings as indicated. The project on structural morphogenesis of towers started during an academic secondment at the Polyhedral Structures Laboratory at the University of Pennsylvania in spring 2018 with Dr. Masoud Akbarzadeh. The project on design through analysis of large infrastructure - tension-and-compression shells, grid-shells, and vaults - started as an industry secondment at SOM Chicago in spring 2018 with Bill Baker and the structures team.

## 6.1 Implementation and case studies

Following the constructions described in the previous Chapters, we present several case studies. For the 2-dimensional case, we start with the Maxwell 2D reciprocals and the corresponding Airy stress functions for two of the figures found in Maxwell (Maxwell, 1864a) (Figure 6.1). We then show the reciprocal polyhedral Airy stress function and the 2D projections in terms of a pair of form and force diagrams of a Pratt truss under external loading, and the equivalent self-stressed truss (Figure 6.2). For the same case, we then apply polar transformations for the analysis and design of the geometry and we highlight how this framework can incorporate several transformations and their combinations, (Figure 6.3) such as: local transformations induced by moving individual nodes; global affine transformations (scaling, shearing, rotating, etc.); as well as local and global transformations of the polyhedral Airy stress function. The latter can be particularly useful for cases where the external boundaries of a structure should remain fixed and the designer wants to change only the geometry of the internal structural members. Since in Maxwell's approach reciprocal form and force diagrams can interchange roles, it is important to notice that the transformations can equivalently happen in the form or force diagram, or their corresponding stress functions in which case the other three reciprocal objects are directly updated. As a result, the designer can directly design and control the force diagram by changing the location of its vertices or equivalently control the polyhedral force Airy stress function by changing its planes. These changes correspond to altering force edge lengths for the 2D case and force face surface areas for the 3D case. Then the designer can visually inspect and interact with the updated form. Moreover, after transforming the force diagram or any of the polyhedral stress functions, the result will be a new geometry under static equilibrium. In the case of local transformations and when the geometrical objects under transformation are not triangulated, the constraint should be imposed that the polyhedral stress functions remains plane-faced. Lastly, as a known result in rigidity theory (Whiteley, 1982), convex Airy stress functions project to 2-dimensional spiderweb structures (see section 2.4). As a result, by manipulating the polyhedral Airy stress function it is possible to produce tension-only/compression-only, or tension-and-compression structures. Furthermore, we should highlight how any boundary conditions/ external forces can be incorporated in the initial geometry, which can be subsequently seen and analysed as an equivalent self-stressed truss (Figure 6.4). Any external concurrent forces in equilibrium can be applied either on the structural boundary or on internal nodes of the structure and they result in a further subdivided equivalent self-stressed truss. In the general case of non-concurrent external forces in equilibrium a funicular structure can be also added to produce a diagram which is a projection of a connected stress function as explained in detail in (McRobie et al., 2016) (Figure 6.2).

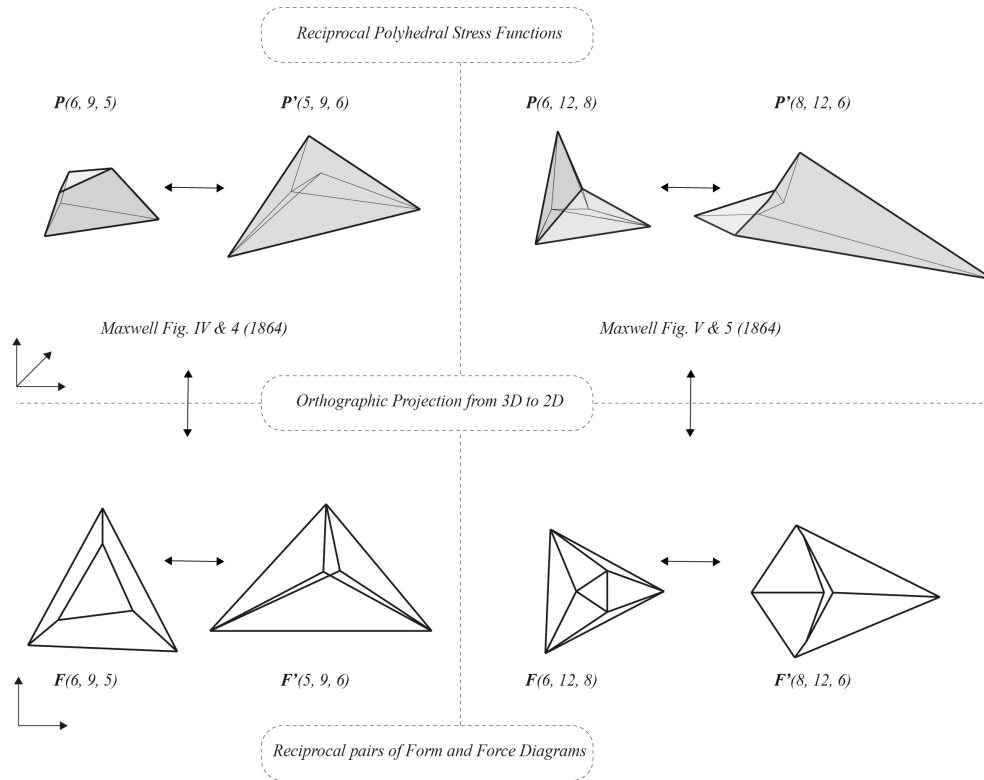


Fig. 6.1 Reciprocal polyhedral Airy stress functions ( $P, P'$ ) and resulting pairs of form and force diagrams ( $F, F'$ ) in Maxwell 2D configuration for Maxwell's Figures IV and 4 (left) and Figures V and 5 (right) (Maxwell, 1864a).

For the spatial case, we apply the constructions to trusses which are projections of simply connected 4-polytopes, such as the spoked cube, and rotationally symmetric tensegrity structures (the Jessen icosahedron and the 3-prism) for which we obtain their Rankine 3D reciprocals (Figure 6.5) through coning (by adding an internal node and thus creating several internal cells in these otherwise 1-cell structures). Furthermore, similar to the Pratt truss we apply this framework to the design and analysis of spatial trusses allowing for local and global transformations of the form or force geometries. A polyhedral spatial truss with three internal nodes (Figure 6.5), and thus three states of self-stress, can undergo local transformations by moving external or internal nodes. Moreover, global projective transformations can be applied on its form diagram, force diagram, or corresponding stress functions, and can be combined with local transformations. As in the 2D case, these transformations always result in a new spatial geometry in static equilibrium.

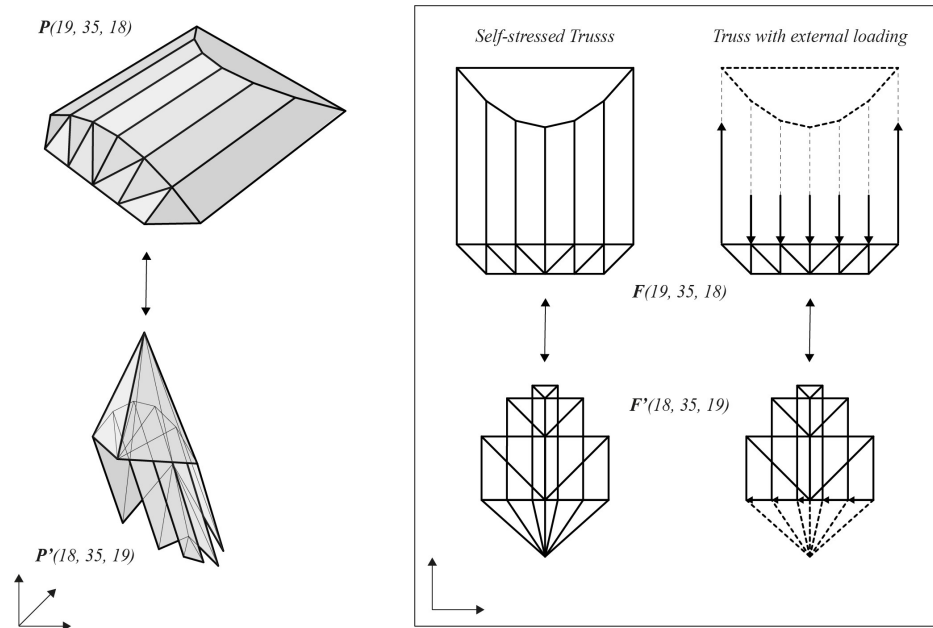


Fig. 6.2 Reciprocal polyhedral Airy stress functions ( $P$ ,  $P'$ ) for a Pratt truss ( $F$ ) (top) and its force reciprocal ( $F'$ ) (bottom). We highlight how the same Airy stress function can correspond to a Pratt truss with external loading (top right) and a self-stressed truss with an equivalent geometry (top middle).

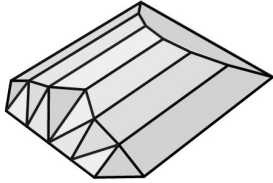
### 6.1.1 2D trusses

#### Large infrastructure: Tensile structures

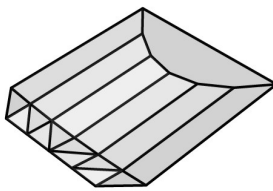
Tensile nets can be useful geometries in the design of structures such as stadium roofs. Conventional design methods start with a target geometry which is then optimised in order to converge to a solution which is in static equilibrium. By using the graphic statics framework presented here, the designer can directly design a form which is by definition in static equilibrium. For example, a polyhedral Airy stress function can be defined given the footprint of the roof, which is then projected on the plane resulting in a tensile 2D truss in static equilibrium enclosed by a compression hoop. This stress function is then mapped to its reciprocal which in turn results to the force diagram. In the example of Figure 6.6 the geometry of the polyhedron, and hence of the form diagram, can be changed in terms of: footprint curve; number of subdivisions; apex coordinates of the faceted pyramid and cutting plane resulting in an oculus in the centre of the roof. In this example we observe that the axial tension forces can vary considerably for the ties of the roof. A more even set of axial forces can be achieved by altering geometrically the polyhedral stress function (Figure 6.7) which it turn can be reciprocated to give the updated form diagram. All these transformations happen in the space of the stress functions; as a result, the form-finding is performed within

equilibrium space and there is no need for extra algorithmic steps of converting this to an equilibrated structure.

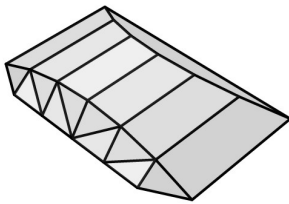
*Local Truss Transformation*



*Global Airy Transformation*



*Global Truss Transformation*



*Combination of Transformations*

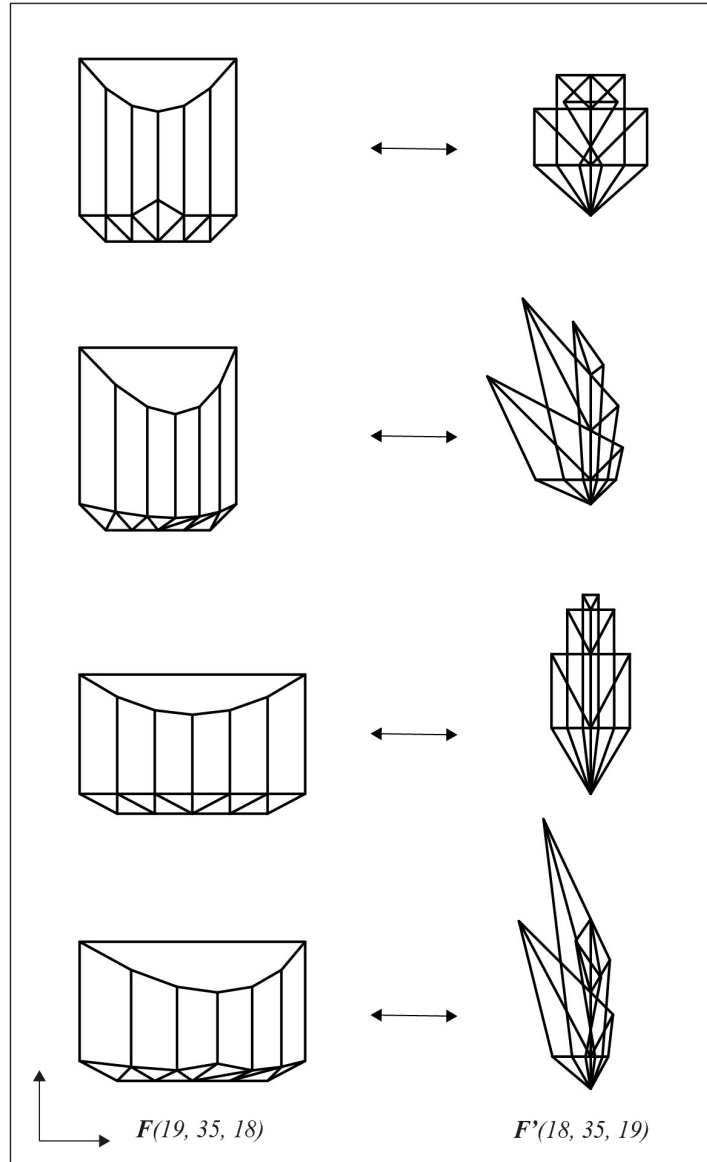
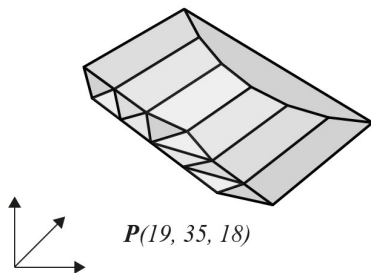


Fig. 6.3 Polyhedral Airy stress function ( $P$ ) and plane form and force diagrams ( $F$ ,  $F'$ ) for a Pratt truss under local and global transformations, from top to bottom: local transformation by moving a truss node; global transformation by shearing the Airy stress function; global transformation by scaling the form diagram; combination of the above transformations. Equivalently,  $F$  can be seen as a force diagram and  $F'$  as a reciprocal form diagram.

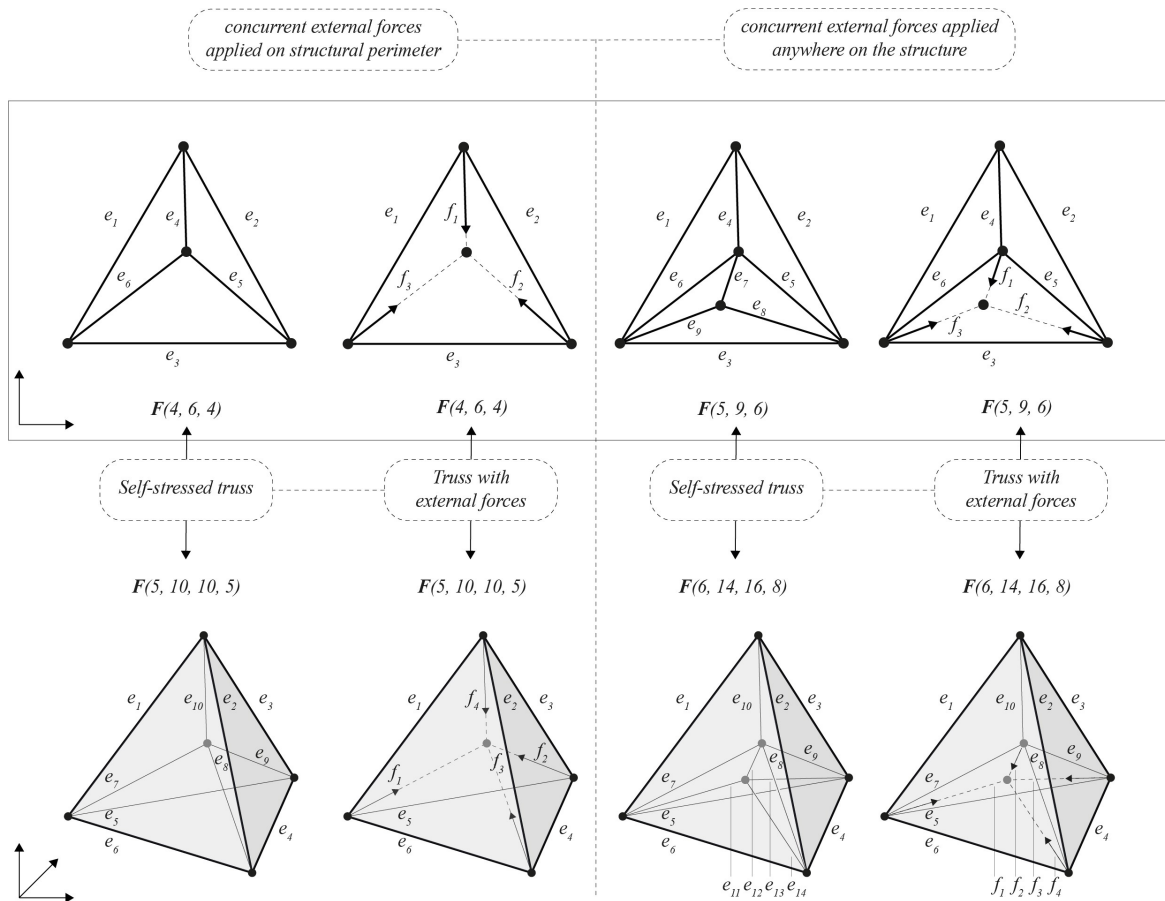


Fig. 6.4 Incorporation of boundary conditions / external forces in the form diagram. Left: adding concurrent forces on the structural boundary for a 2D (top) and 3D (bottom) truss and equivalent self-stressed form diagrams. Right: adding concurrent forces anywhere in the structure.



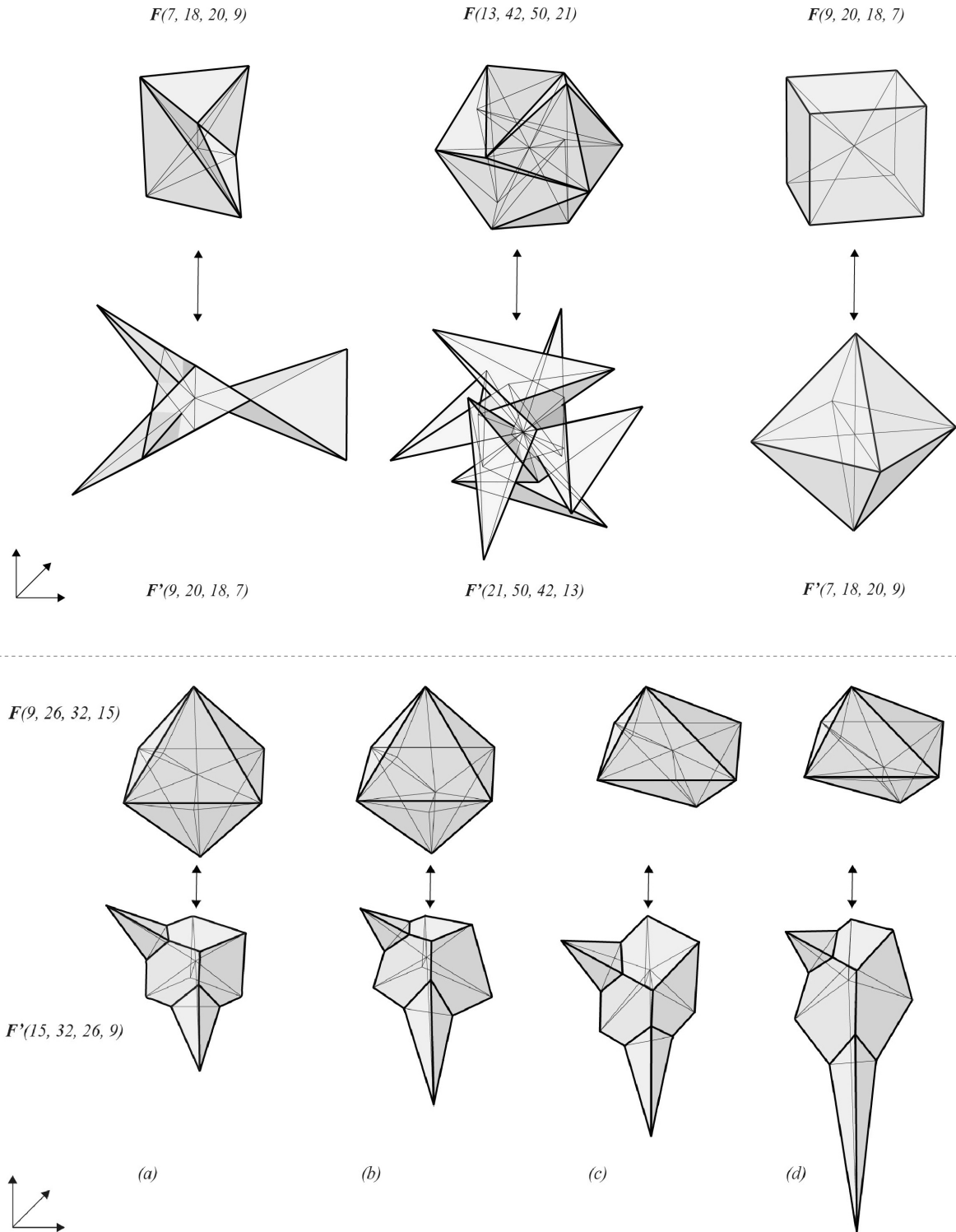


Fig. 6.5 Top: Pairs of spatial reciprocal diagrams in a Rankine 3D configuration: Tensegrity 3-prism. Jessen icosahedral tensegrity, Spoked cube. Bottom: (a): A polyhedral spatial truss ( $F$ ) with three states of self-stress (top) and its corresponding Rankine 3D force diagram ( $F'$ ) (bottom) or equivalently a polyhedral spatial truss ( $F'$ ) and a Rankine 3D force diagram ( $F$ ); (b): Local transformation by moving an internal node of  $F$ ; (c): Global projective transformations (non-uniform scaling and shearing) applied on  $F$ ; (d): Combinations of local and global transformations.

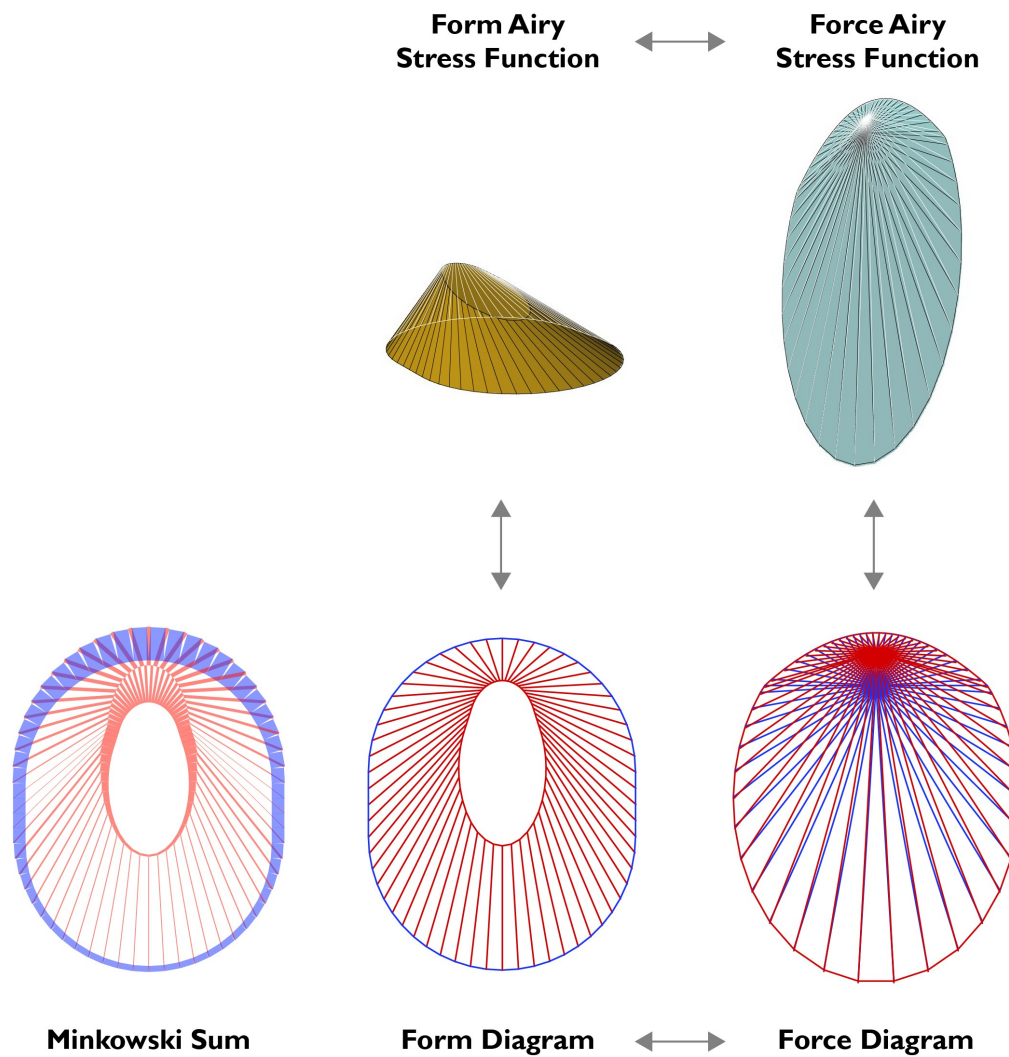


Fig. 6.6 Designing a tensile stadium roof in static equilibrium: The form diagram is a projection of a polyhedral Airy stress function so it is by definition in static equilibrium. The four reciprocal geometries are presented (form, force diagram, reciprocal stress functions) as well as the Minkowski sum of the resulting net.

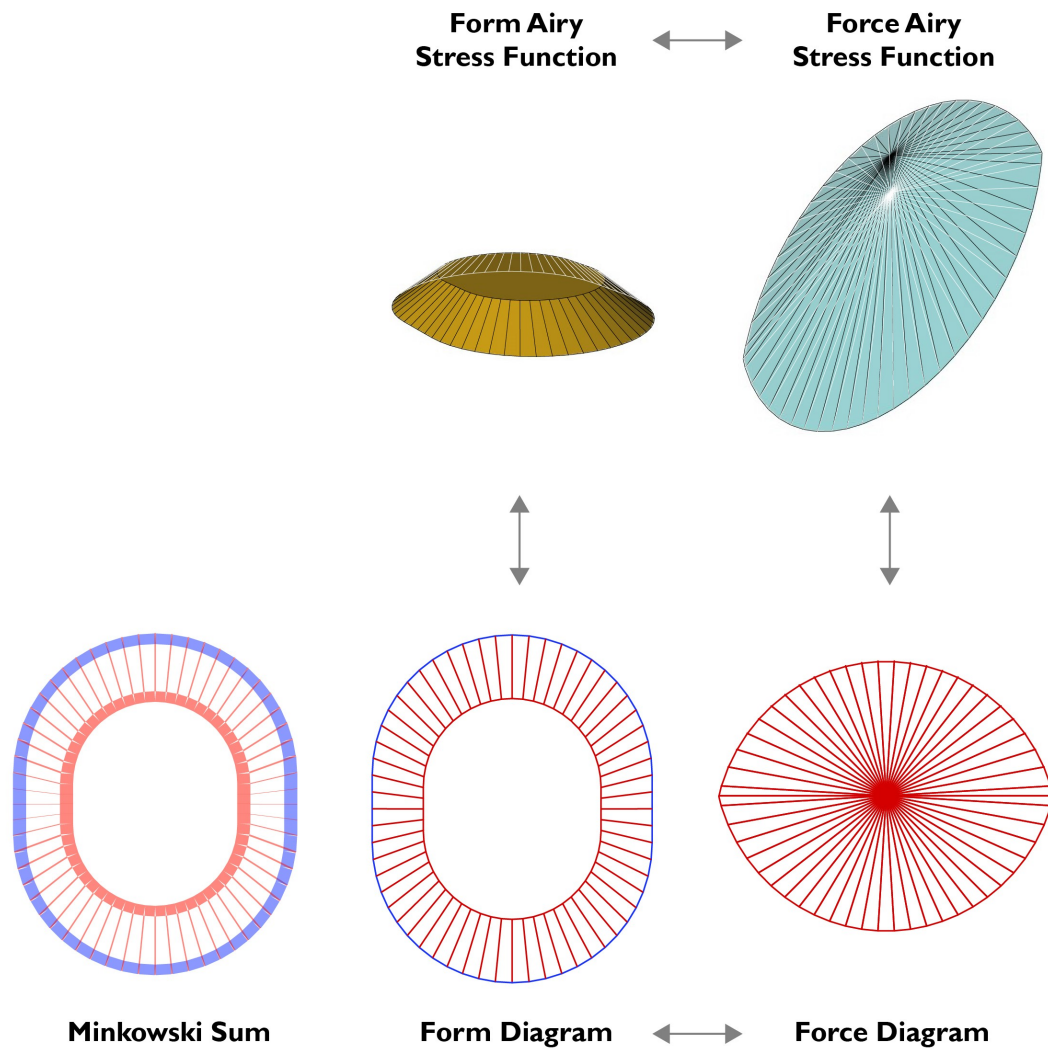


Fig. 6.7 Designing a tensile stadium roof in static equilibrium: The form diagram is a projection of a polyhedral Airy stress function so it is by definition in static equilibrium. The four reciprocal geometries are presented (form, force diagram, reciprocal stress functions) as well as the Minkowski sum of the resulting net. In this second case the reciprocal stress functions are altered geometrically to produce a more even distribution of tensile axial forces.

### 6.1.2 3D trusses and polyhedral spatial structures

#### Tensegrities

Drawing analogues and using results from rigidity theory, projective geometry and structural mechanics we apply a graphic statics and kinematics analysis to trusses, tensegrities and flexible polyhedra, extending the definition to study graphically the redistribution of internal forces in statically balanced tensegrity mechanisms.

Tensegrities can be defined as a rigid configuration of an ‘ordered finite collection of points in Euclidean space’ comprising inextendable cables and incompressible struts (Connelly and Whiteley, 1996). The tensegrities we will analyse here also have the property of their compressed elements being a discontinuous set whereas their tensioned elements are a continuous set (Motro, 2003). Tensegrities are essentially self-stressed, reticulated, rigid structures which can be traced back to the patents of Emmerich, Fuller and Snelson (1950s and 1960s) and before them to a few prototype structural sculptures developed amidst the Russian avant-garde as described by Laszlo Moholy Nagy (Motro, 2003).

The 3-prism  $F(6, 12, 8, 1)$  is the simplest prismatic spatial tensegrity and is an example of a pre-stress stable structure. It is a triangulated 2-surface in  $\mathbf{R}^3$  and has an underlying generically rigid graph for the corresponding bar framework. As the 3-prism has only one internal cell, we cone it (Figure 6.8-a) resulting in its coned/ spoked version  $F_c(7, 18, 20, 9)$ . If we now lift the newly created 8 internal cells one dimension up, we obtain a Maxwell-Rankine stress function through which we can easily derive the Rankine reciprocal (Figure 6.8-b). We observe that the faces of the force cells which correspond to the internal spokes of the structure (connecting the added vertex  $v_0$  with  $V$ ) have zero oriented area – meaning that they are not load-bearing; an expected result since those spokes are just a geometrical construction and not real edges per se – in contemporary nomenclature they are also called zero bars (McRobie, 2016). Moreover, from the counting rule we have that  $p=q$  and thus since we have one state of self-stress we will also have one, infinitesimal in this case, mechanism. As a matter of fact, the force cells can slide relative to each other in a unique way (Figure 6.8-d) revealing the infinitesimal mechanism (Figure 6.8-c). This slide corresponds to the rotation on the  $z$ -axis and the translation on the  $xy$  plane of the upper three internal cells  $c_1, c_2, c_3$  relative to the lower three internal cells  $c_4, c_5, c_6$ . We should note that the faces corresponding to the internal spokes can separate, albeit retaining their parallelism, since they have infinite flexibility/ zero stiffness.

The Jessen icosahedral tensegrity  $F(12, 30, 20, 1)$  analysed statically and kinematically (Konstantatou and McRobie, 2017; McRobie et al., 2017), is also an example of a spherical, triangulated, 1-cell, pre-stress stable tensegrity which possesses one state of self-stress

and one infinitesimal mechanism. As for the 3-prism, we cone it (Figure 6.9), obtain the reciprocal Rankine reciprocal through a 4D polarity (Figure 6.9) and slide the force cells (which we show in detail in Figure 6.9), revealing the displacement vectors of the mechanism (Figure 6.9). As above the internal spokes correspond to faces of zero oriented area and the corresponding faces are free to separate.

Some of the special cases which deviate from Maxwell's counting rules as well as from his assumption on the rigidity of triangulated surfaces are tensegrities and flexible polyhedra. By synthesizing Maxwell's approach on form and force diagrams based on polarities, Calladine's generalised counting rules, as well as newly formed theory on graphic kinematics (McRobie et al., 2017) it is possible to study these interesting spatial geometries both statically and kinematically (Konstantatou and McRobie, 2017). The Jessen icosahedral tensegrity  $F(12, 30, 20, 1)$ , is an example of a spatial structure which possesses one state of self-stress ( $q$ ) and one infinitesimal mechanism ( $p$ ). Since this polyhedral structure is essentially just a single faceted cell, it can be coned to derive a richer geometrical structure with numerous cells. Then the 3D Rankine reciprocal can be obtained through a 4D polarity and the *compatible sliding* of the resulting force cells (McRobie et al., 2017) will reveal the displacement vectors of the mechanism (Figure 6.9). As a result, a purely geometrical two-fold structural analysis can be used to derive the static and kinematic behaviour of this tensegrity structure.

### Flexible Polyhedra

The Steffen flexible polyhedron  $F(9, 21, 14, 1)$  (Figure 6.10) is a generically rigid, triangulated polyhedron, which in this particular geometrical embedding is not rigid, exhibiting a range of motion of  $\pi/6 \rightarrow \pi/60$  while flexing. From Calladine's counting rules we have that  $p=q$  (where  $p$  is the number of mechanisms and  $q$  the number of states of self-stress) which equals to zero for the general case of a triangulated polyhedron, being an isostatic structure, but in the special case of the Steffen polyhedron  $p=q=1$  with the corresponding spatial truss possessing one state of self-stress and one finite mechanism. As above, the Steffen has only one cell so we cone it and lift it in a Maxwell-Rankine stress function to obtain the Rankine reciprocal (Figure 6.10). We then observe that the sliding of the force cells is unique, revealing the nodal vectors for the finite mechanism of the form polyhedron (Figure 6.10), which do coincide with the applications in literature (McClure, 2005). Interestingly, we observe that this time the internal spokes do not correspond to force faces of zero oriented area (Figure 6.10) - even though we assumed that they have infinite flexibility and they do not even exist structurally. The reason for this is that when we create the Maxwell-Rankine stress function this is essentially over the coned structure  $F_c(10, 30, 35, 15)$  for which  $q-p=6$ ; evidently the coned structure does not have any mechanisms and is rigid since  $e > 3v-6$ , as

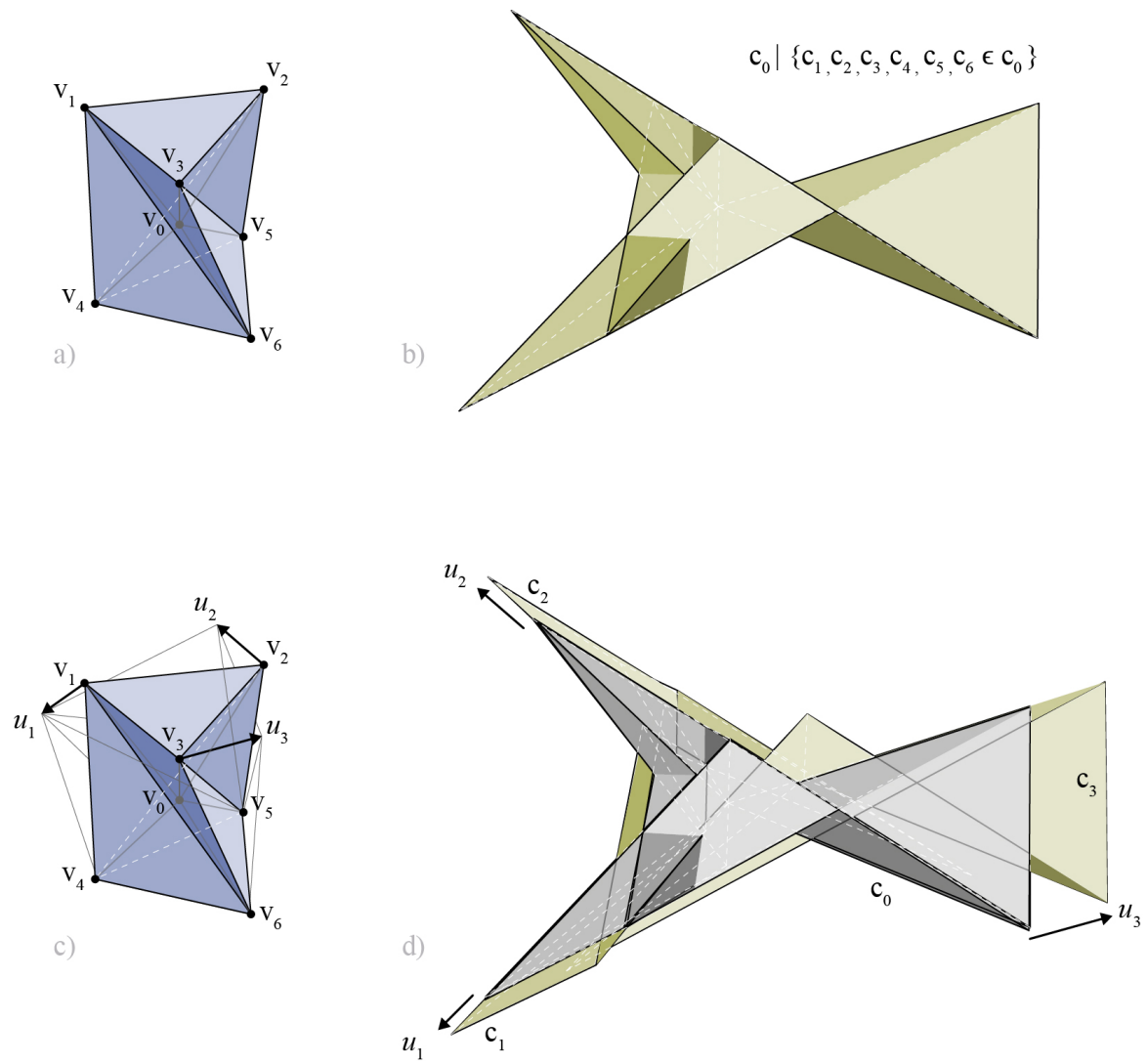


Fig. 6.8 Graphic statics and kinematics analysis of a 3-Prism tensegrity.

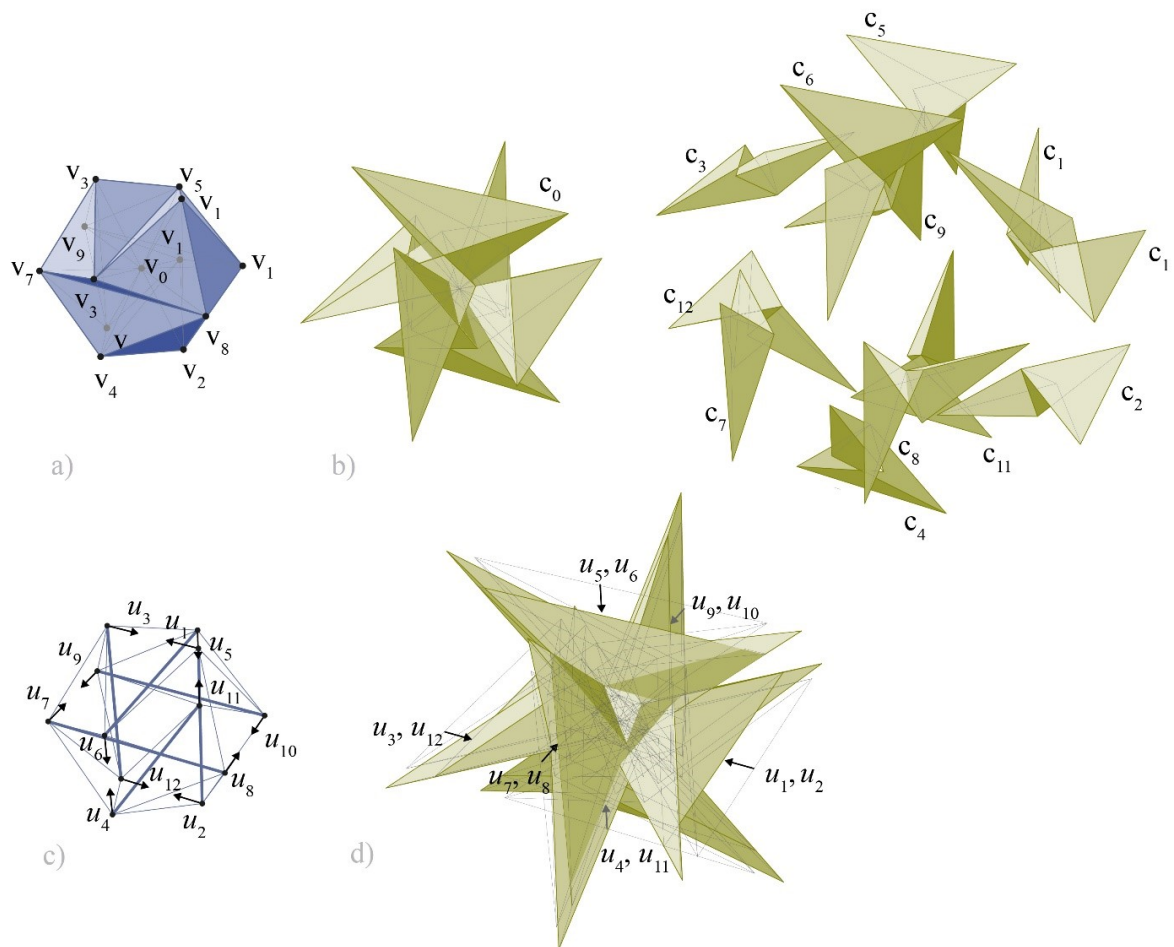


Fig. 6.9 Graphic statics and kinematics analysis of a Jessen icosahedron.

a result it has 6 states of self-stress. The 4D polarity used here maps the form cells to reciprocal vertices in a  $I-I$  fashion. Thus, for a structure which has more than one states of self-stress but only one linearly independent vertex which can be lifted to a Maxwell-Rankine stress function, we obtain only one of the possible Rankine reciprocals. In this way it is not possible to find a state of self-stress corresponding to the original - without internal spokes - Steffen polyhedron. A geometrical construction which provides the correct equilibrium analysis for this truss geometry has been developed in (McRobie, 2017b). This works by decomposing the polyhedron into two crinkles using a number of zero bars arranged to form zero cubes. However, this does not constitute a problem for the graphic kinematic analysis; since we can obtain one force reciprocal, we can still treat the internal spokes as having infinite flexibility and obtain the same, unique vectors of the finite mechanisms of the Steffen flexible polyhedron.

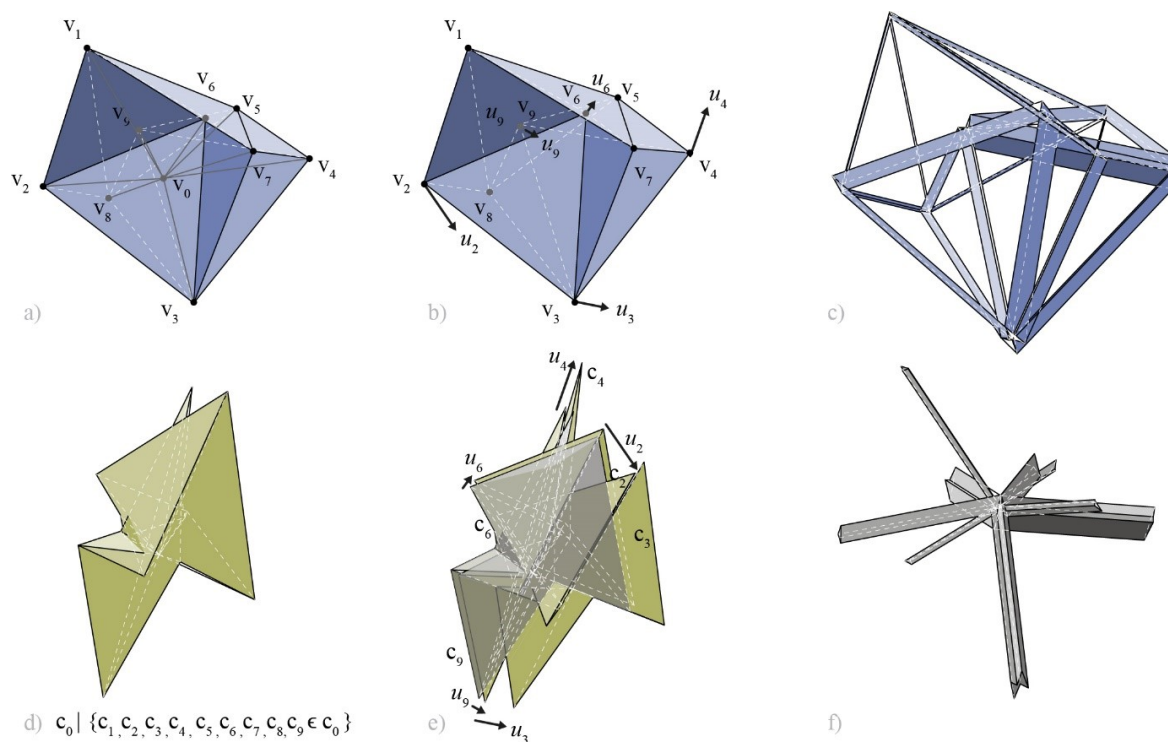


Fig. 6.10 Graphic statics and kinematics analysis for the Steffen flexible polyhedron.

### 6.1.3 Statically balanced tensegrity mechanisms

The 3-prism can be also an example of a statically balanced tensegrity mechanism if the tensioned members are substituted by zero free length springs (Schenk et al., 2007). In that case the hybrid structure will have zero-stiffness modes which correspond to a continuous



spectrum of configurations - on any one of which the structure is in static equilibrium. This category of structures is of interest in fields such as robotics, medical applications, architecture and generally where energy-efficient transformable design is a requirement (Schenk et al., 2007). It should be noted that even though the lengths of the compression members are fixed, the lengths of the tensioned members are not, thus, the 3-prism can change its shape considerably over large displacements without the corresponding motions being finite mechanisms (Schenk et al., 2007). The graphic static-kinematic analysis for every statically balanced configuration of this spectrum would reveal one state of self-stress and one infinitesimal mechanism for the corresponding conventional 3-prism. However, we observe that since the structure is continuously in static equilibrium it should have a dynamic Rankine reciprocal which gets continuously updated (Figure 6.11), giving an intuitive and visual inspection of the continuous reconfiguration of internal forces over the spectrum of movement. Thus, following equation (2.10), we define the dynamic Minkowski sum over the configuration space  $C$  to be:

$$\mathbf{A}_j + \mathbf{B}_j = \{a\mathbf{A}_{ij} + b\mathbf{B}_{ij} | \mathbf{A}_i \in \mathbf{A}, \mathbf{B}_i \in \mathbf{B}, a, b \text{ scalars}, j \in C\} \quad (6.1)$$

where  $\mathbf{A}$  and  $\mathbf{B}$  are two sets of vectors - for example, the set of form nodes and the set of force cells (see section 2.7).

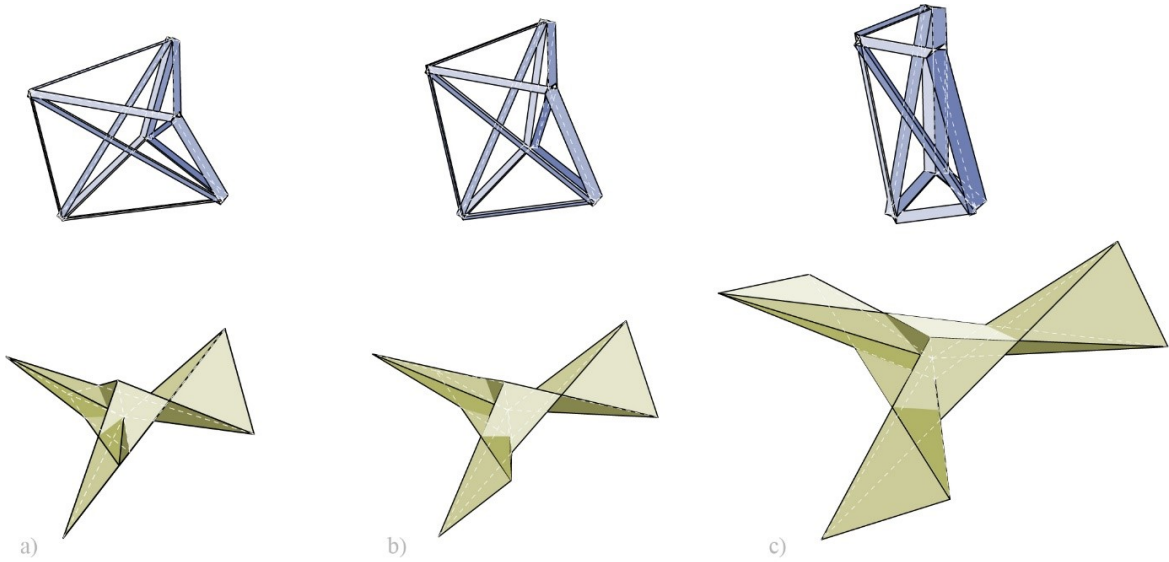


Fig. 6.11 Graphic statics analysis and dynamic Minkowski sums for a statically balanced tensegrity mechanism. Note that the Minkowski prisms of zero-bars have been omitted for visualisation purposes.

### 6.1.4 Large infrastructure: Towers

As discussed in Chapter 5, stress functions can be used as a tool for structural morphogenesis of forms in static equilibrium. Here we apply the theory of section 3.2.3 to design spatial trusses in the form of exoskeletons/ mega trusses of high-rise towers. As outlined above, the designer can start from the force diagram (Figure 6.13) - the topology and geometry of which will define the resulting spatial truss. Alternatively, the designer can choose to work straight in the form space. This particular geometry is essentially two interconnected envelopes. This is a direct application of Maxwell's Figure IV in the 4th dimension. Specifically, in Figure 2.12 we see how two planes intersect in 3-space to a line  $w$  and at the same time define a pyramid with a flat top - the projection of which is a truss in static equilibrium. In fact, the line  $w$  signifies the relative position of these two planes and is thus a design freedom with regards to the design of the 2D truss. Equivalently, if this construction is translated one dimension up in 4-space (Figure 6.12) then two hyperplanes will intersect to a plane  $w$  (which now signifies a design freedom), these two hyperplanes can be used to define a plane-faced 4D pyramid, the projection of which is thus guaranteed to be in static equilibrium. The lines of action of the external forces are added to the structural members resulting to an equivalent self-stressed truss which can be then be analysed.

By following this methodology and working solely in the form space a wide range of typologies for towers in static equilibrium can be generated as in Figure 6.14.

These geometries are self-stressed spatial systems comprising interconnected polyhedral truss envelopes. Each one of these systems will have a Rankine force reciprocal (Figure 6.13) which visualises the state of self-stress of the tower. The number of interconnected polyhedral envelopes can be decided by the designer based on the architectural brief. The geometry of Figure 6.13 was selected for developing a physical model of this tower typology. In collaboration with Dr. Masoud Akbarzadeh, Dr. Andrei Nejur and PhD students from the Polyhedral Structures Lab at UPenn, a computational and physical model was developed which comprised structural members of varying diameters and custom-made joints which connected to the edges. In particular, the structural members were timber rods whereas the joints were 3D-printed with flexible plastic material. The glass facade panels were laser-cut from perspex material and attached to the timber rods via 3D-printed rings. The finished model (Figure 6.15) is 1m high and has been exhibited at UPenn.

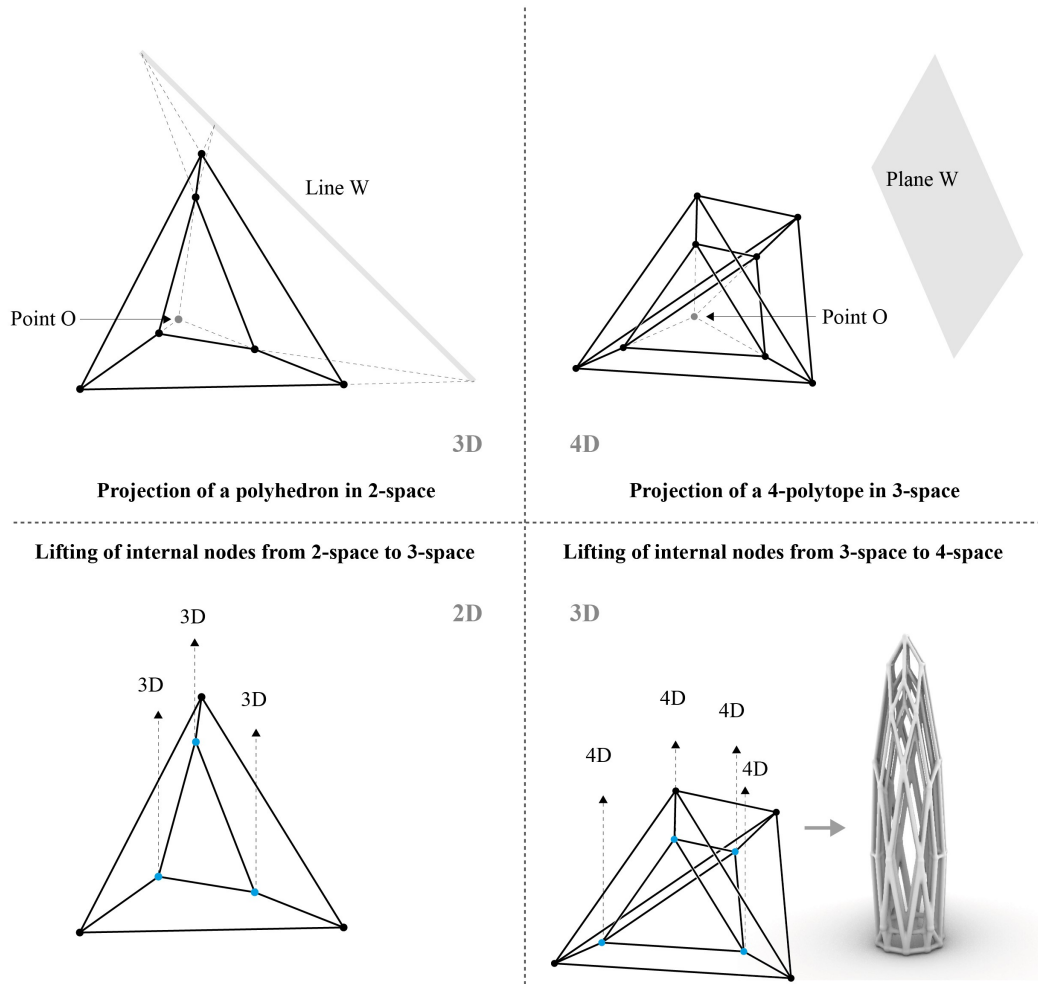


Fig. 6.12 Left-Top: Maxwell's Figure IV is a projection of a polyhedron where the position of line *w* signifies a design freedom; Left-Bottom: Polyhedral lifting of Maxwell's Figure IV; Right-Top: The 3D generalisation of Maxwell's Figure IV is a projection of a 4-polytope where the position of plane *w* signifies a design freedom; Right-Bottom: 4-polytopic lifting of the form diagram, showing the geometrical principles resulting in self-stressed spatial trusses in static equilibrium such as towers.

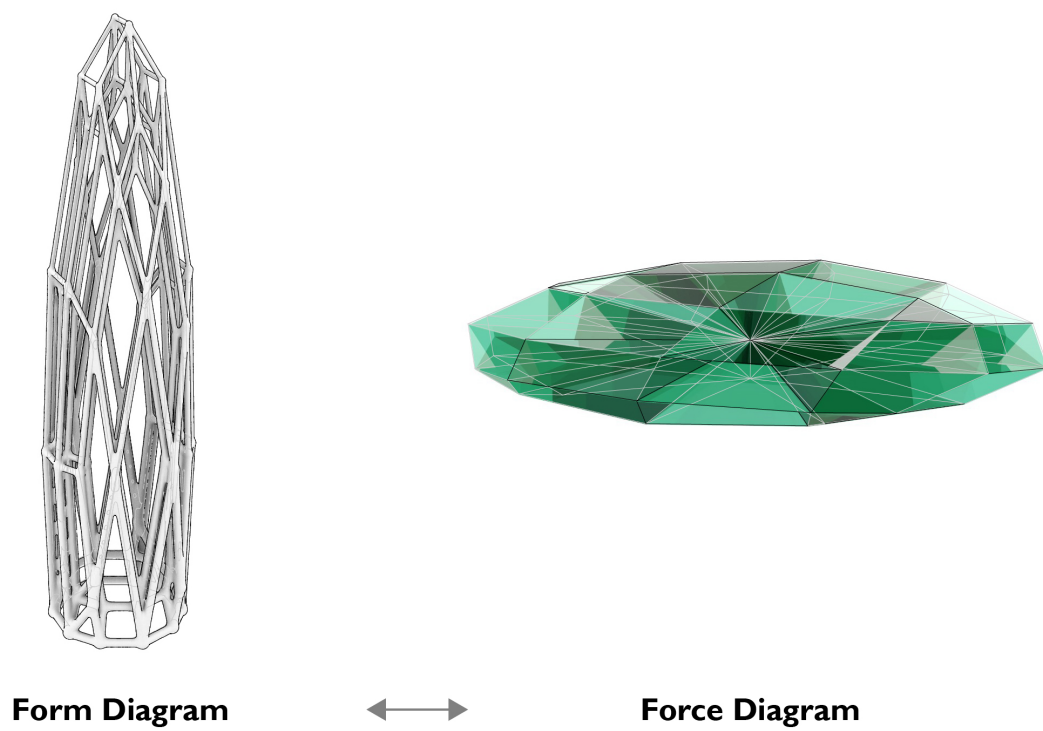


Fig. 6.13 Self-stressed mega truss of a tower in static equilibrium as a form diagram and its reciprocal Rankine 3D force diagram.

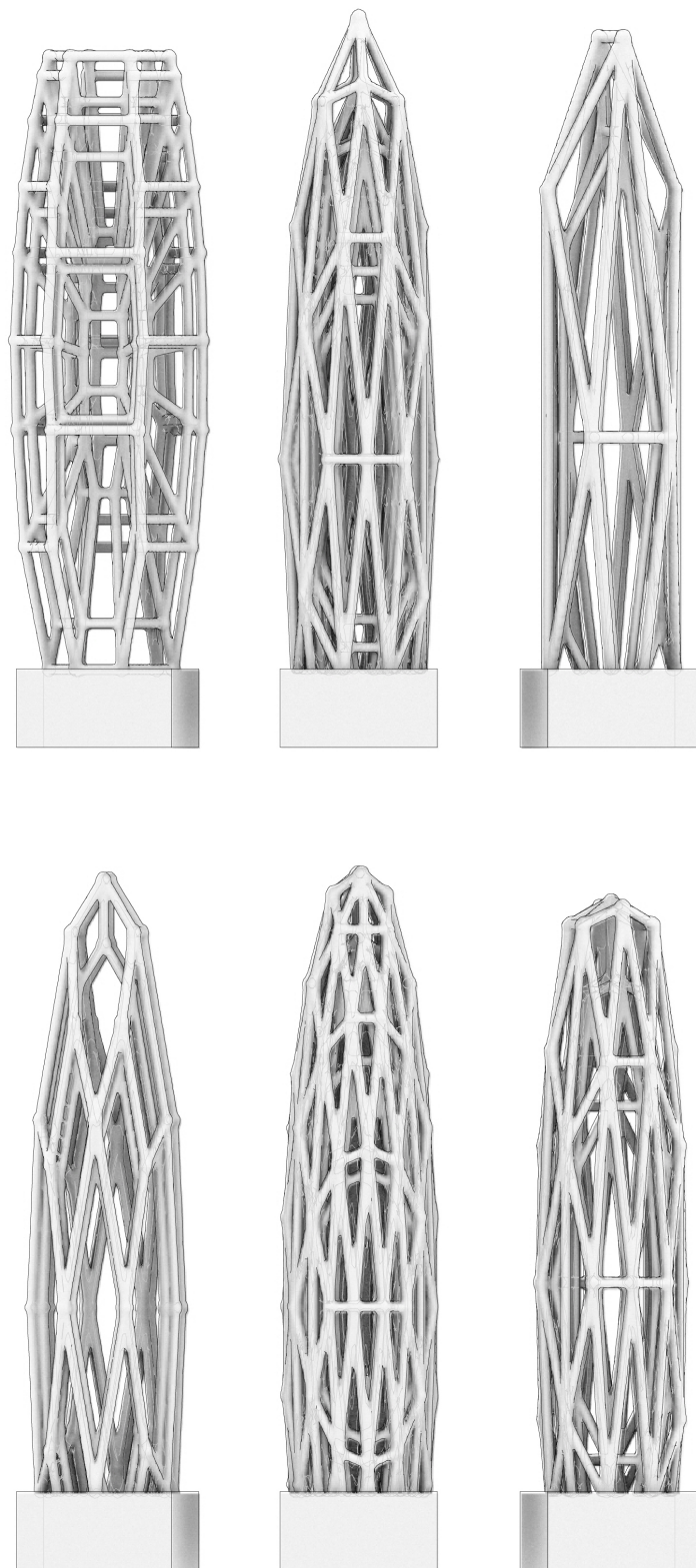


Fig. 6.14 Various typologies and heights of trusses of towers in static equilibrium.





Fig. 6.15 CAD and CAM produced physical model of the 4-polytopic tower typology.

### 6.1.5 Large infrastructure: Vaults, shells and grid-shells

The Airy stress function can be used in conjunction with the force density method as a form finding tool for compression-and-tension spatial structures while providing design and analysis freedoms. Specifically, for a tessellation given from a form diagram and for a given constant vertical load, different polyhedral liftings of the corresponding stress function result in different grid-shell forms in static equilibrium (Figure 6.19, Figure 6.20). The grid-shell model chosen here is a simplified version inspired from the Great Court roof of the British Museum. The latter, is an iconic structure designed by Foster + Partners and constructed by Buro Happold Engineering, and represents a great example of collaboration between architects and engineers where the structural analysis directly informed the geometry of the structure. In particular, the form-finding of the geometry was developed by Chris Williams of Bath University by using analytic and numerical methods - specifically the method of dynamic relaxation (Williams, 2001). The resulting structure is a grid-shell, the design load path of which includes bending action. It should be noted that in the methodology developed here the solutions are axial-only. Similar geometries have been designed and analysed in the literature using the RhinoVault framework (Rippmann et al., 2012); however, these explorations apply only to regular quad topologies and the resulting solutions are compression-only. Thus, they do not extend to tension-and-compression cases. In this section we design and analyse two different models of tension-and-compression grid-shells with an internal oculus, while exploring different solutions with regards to their load paths.

Firstly, a 2-connected polyhedral Airy stress function is developed for the topology of Figure 6.16 (top). The initial choice of the surface in space, on which the vertices that initially lie on the plane  $z = 0$  are mapped, results from wanting to create a smooth curvature while the surface intersects both boundary curves (the external rectangle  $C_1$  and the internal circle  $C_2$ ). To achieve this, we lift every non-fixed point  $P(x, y, 0)$  of the form diagram in the  $z$ -axis. Specifically, for every  $P(x, y, 0)$  with distance  $D_{P-C_1}, D_{P-C_2}$  from  $C_1, C_2$  respectively, we assign a  $z$ -coordinate using the equation:  $z = \min\{D_{P-C_1}, D_{P-C_2}\}lD_{P-C_2}$ , where  $l$  is a scalar. When the resulting polyhedron is mapped to its force reciprocal (Figure 6.21) and combined with force density it gives a valid solution for a spatial grid-shell in static equilibrium (Figure 6.19 (top)); however, the resulting load path is unorthodox - it comprises two tension hoops interconnected by tension and compression members (Figure 6.16 (top)). Also, the initial form has sharp angles between adjacent faces - should the designer want to smooth this, local transformations can be applied. In particular, by controlling the  $z$ -coordinates of some of the vertices in the Airy stress function, the curvature of the form can be altered resulting in a smoother roof shape (Figure 6.16 (bottom)), (Figure 6.22).

In order to design a more conventional load path - where an external tension ring encloses an internal compression ring through an interconnected truss - a second polyhedral Airy stress function is devised. This time we define this as an 1-connected polyhedron, the initial surface equation of which is: for every point  $P(x, y, z) : z = (x^2 - a^2)(y^2 - b^2)$  where  $a, b$  are the half dimensions of the external rectangle. This needs to be slightly altered near the oculus (internal ring) for this face to be plane. Also, for this topology we delete any 0-force edges near the external boundary. The resulting load path is indeed different (Figure 6.16 (bottom)). The resulting initial form also has some sharp edges which are smoothened through local transformations of sets of individual nodes resulting in a roof-like geometry (Figure 6.20 (top), Figure 6.24). We observe the 2D Minkowski sums of the two final grid-shell geometries (Figure 6.17, Figure 6.18). These show the primary trusses formed in the grid-shell by giving an intuitive and visual representation of the horizontal components of the axial forces and the force densities of each edge (through the aspect ratio of the corresponding parallelepiped).



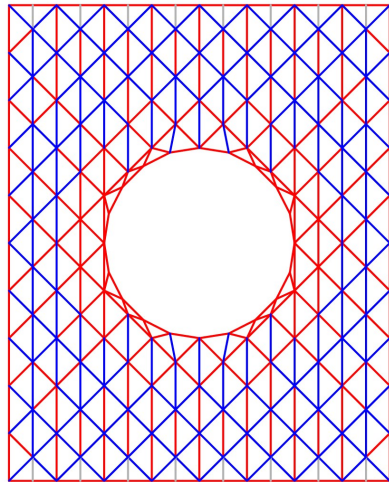
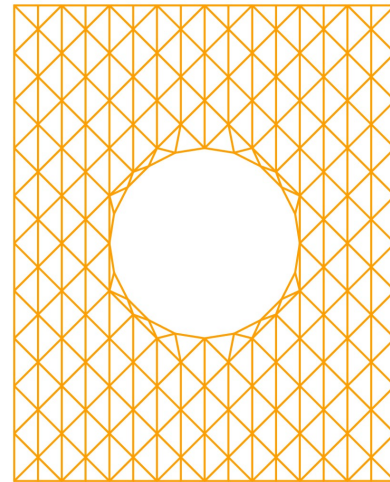
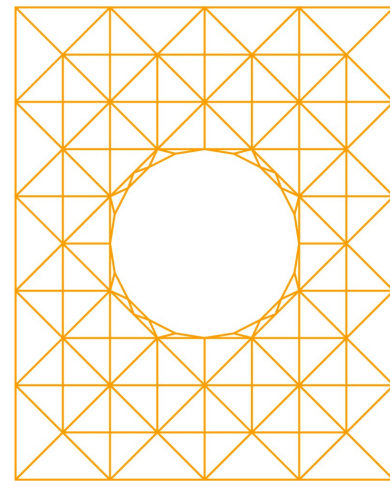
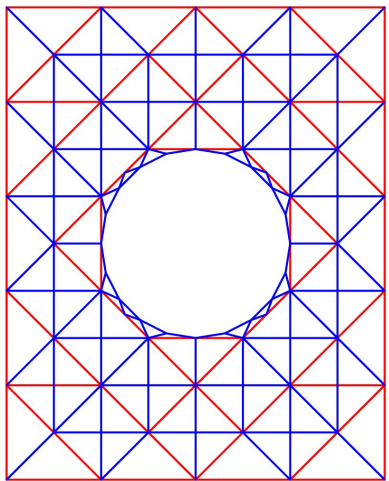
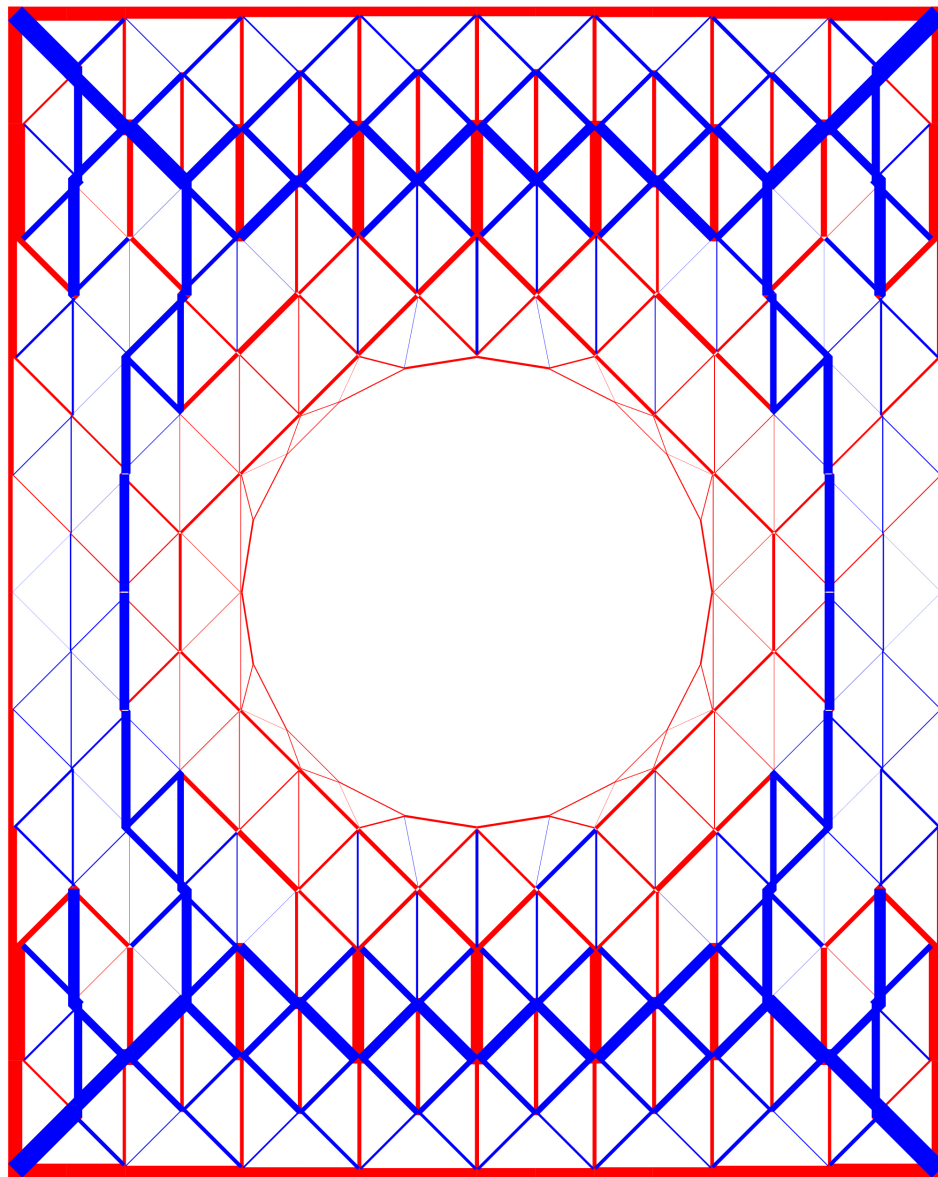
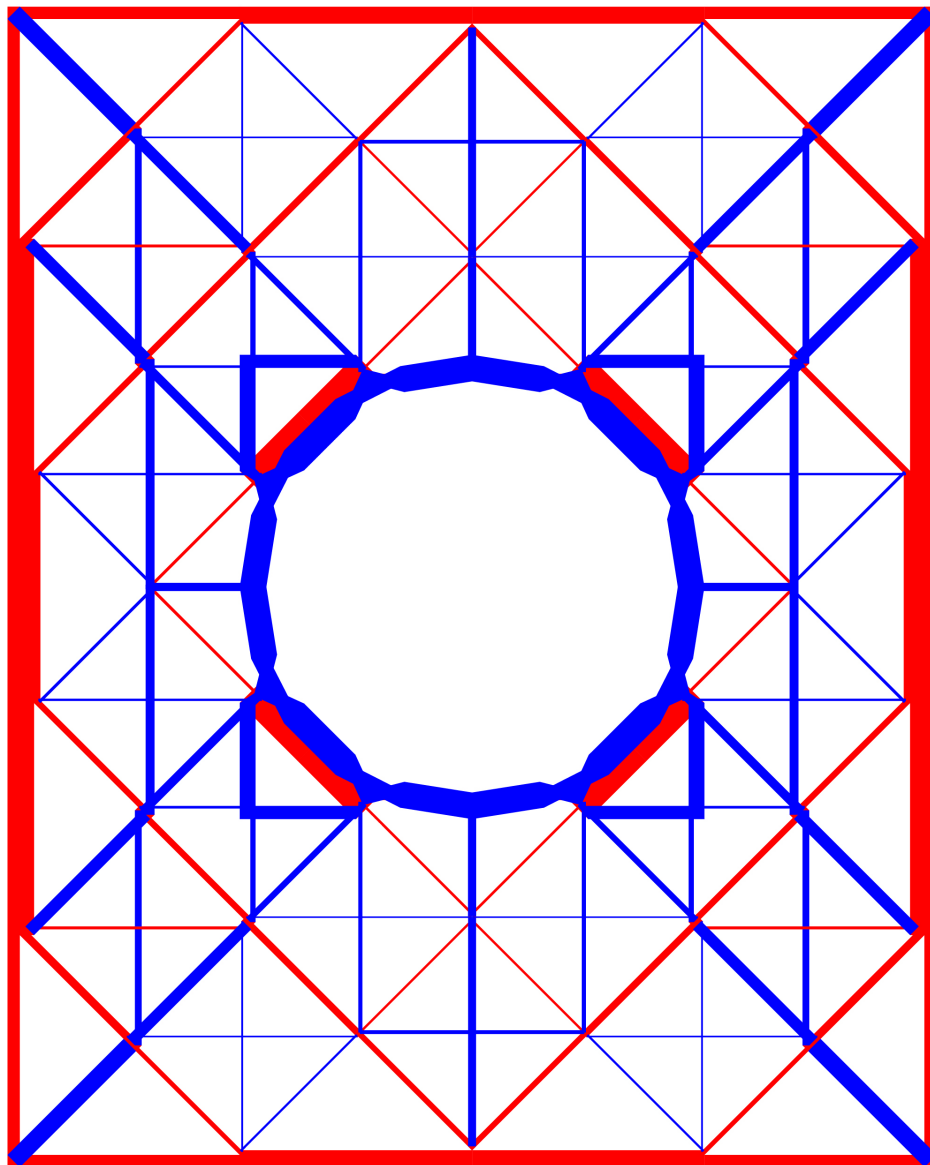
**Tension - Compression****Form Diagram**

Fig. 6.16 Top right: Form diagram of a 2-connected simplified model of the Great Court Roof of the British Museum; Top left: Form diagram with tension members in red, compression members in blue and 0-force members in grey; Bottom right: form diagram of a 1-connected simplified model of the Great Court Roof of the British Museum; Bottom left: Form diagram with tension members in red and compression members in blue



**2-connected Stress Function:  
Resulting Minkowski Sum - Visual Estimation of Force Density**

Fig. 6.17 Minkowski sum of a given grid-shell topology and for a 2-connected stress function: the primary truss of the load path can be observed (internal and external tension hoops interconnected through compression members) while the aspect ratio of the rectangles give the force density of the grid-shell edges



**2-connected Stress Function:  
Resulting Minkowski Sum - Visual Estimation of Force Density**

Fig. 6.18 Minkowski sum of a given grid-shell topology and for a 1-connected stress function: the primary truss of the load path can be observed (external tension hoop interconnected with an internal compression hoop) while the aspect ratio of the rectangles give the force density of the grid-shell edges

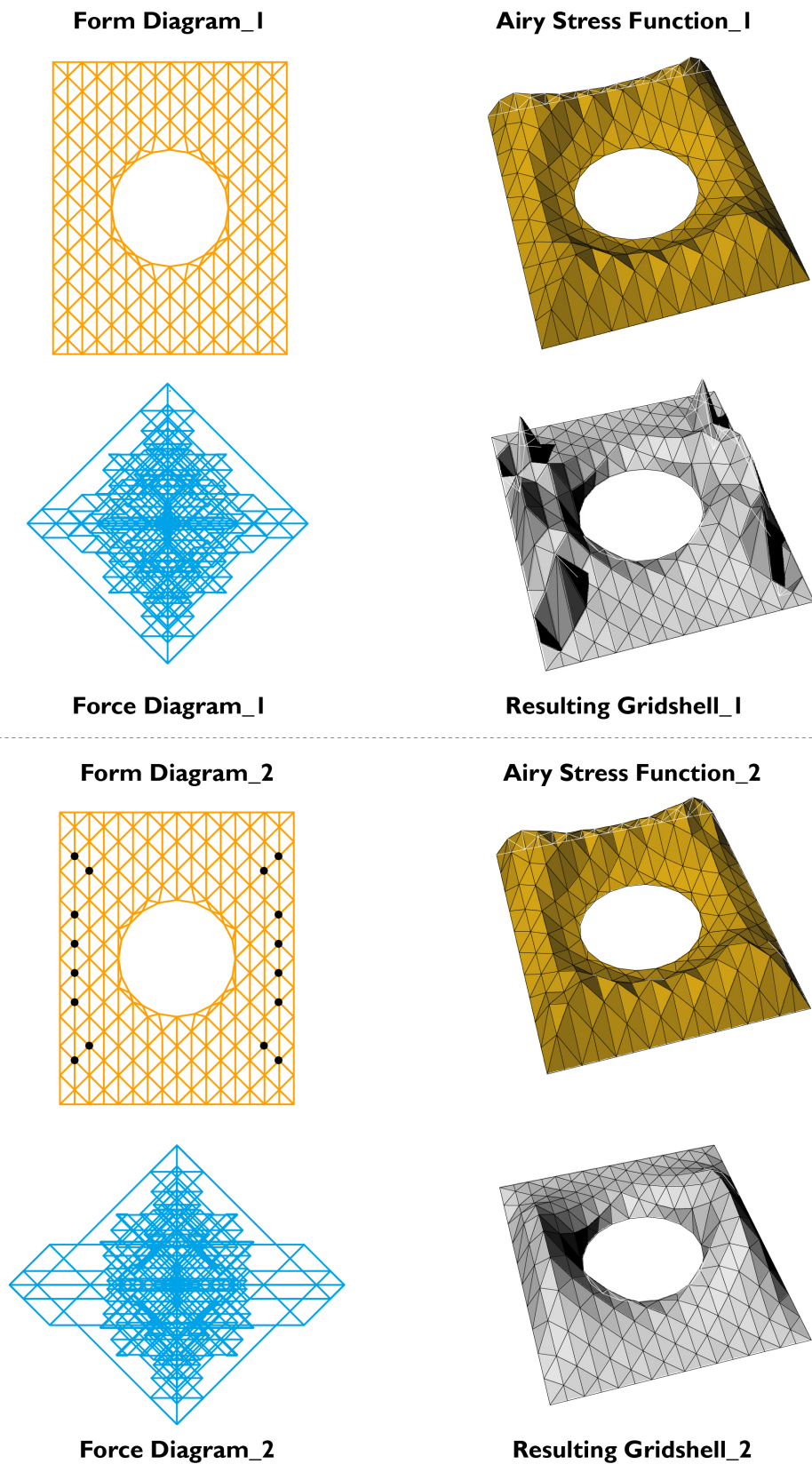


Fig. 6.19 Top: Initial grid-shell geometry resulting from a 2-connected polyhedral Airy stress function (right column); Corresponding form and force diagrams (left column). As the topology is triangulated there are infinite solutions of possible geometries/ states of self-stress/ design and analysis freedoms for the grid-shell; Bottom: Small changes in the initial geometry of the ASF/ state of self-stress result in a significantly different form (the nodes that have moved in the z-direction are indicated with dots on the form diagram).

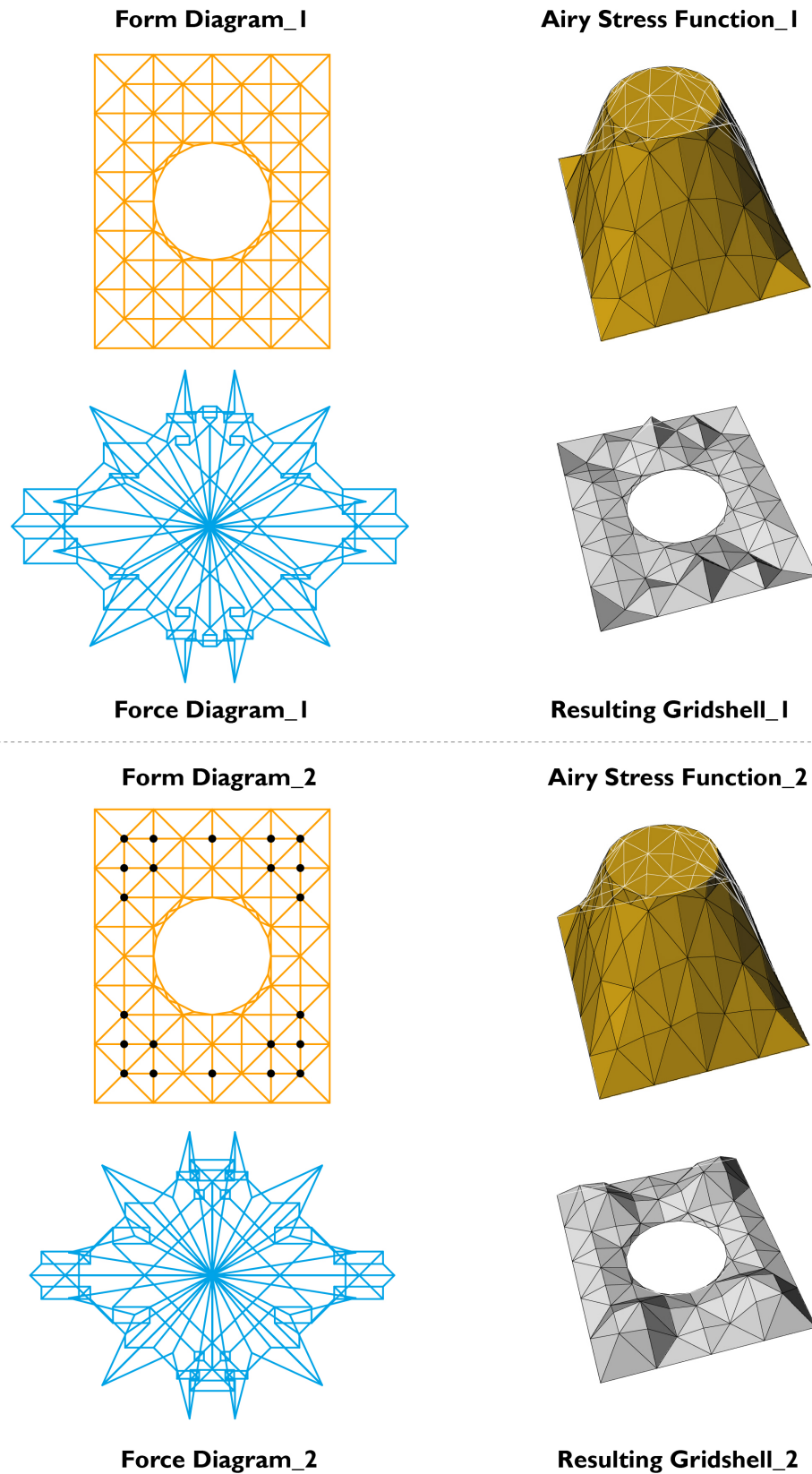


Fig. 6.20 Top: Initial grid-shell geometry resulting from a 1-connected polyhedral Airy stress function (right column); Corresponding form and force diagrams (left column). As the topology is triangulated there are infinite solutions of possible geometries/ states of self-stress/ design and analysis freedoms for the grid-shell; Bottom: Small changes in the initial geometry of the ASF/ state of self-stress result in a significantly different form (the nodes that have moved in the z-direction are indicated with dots on the form diagram).



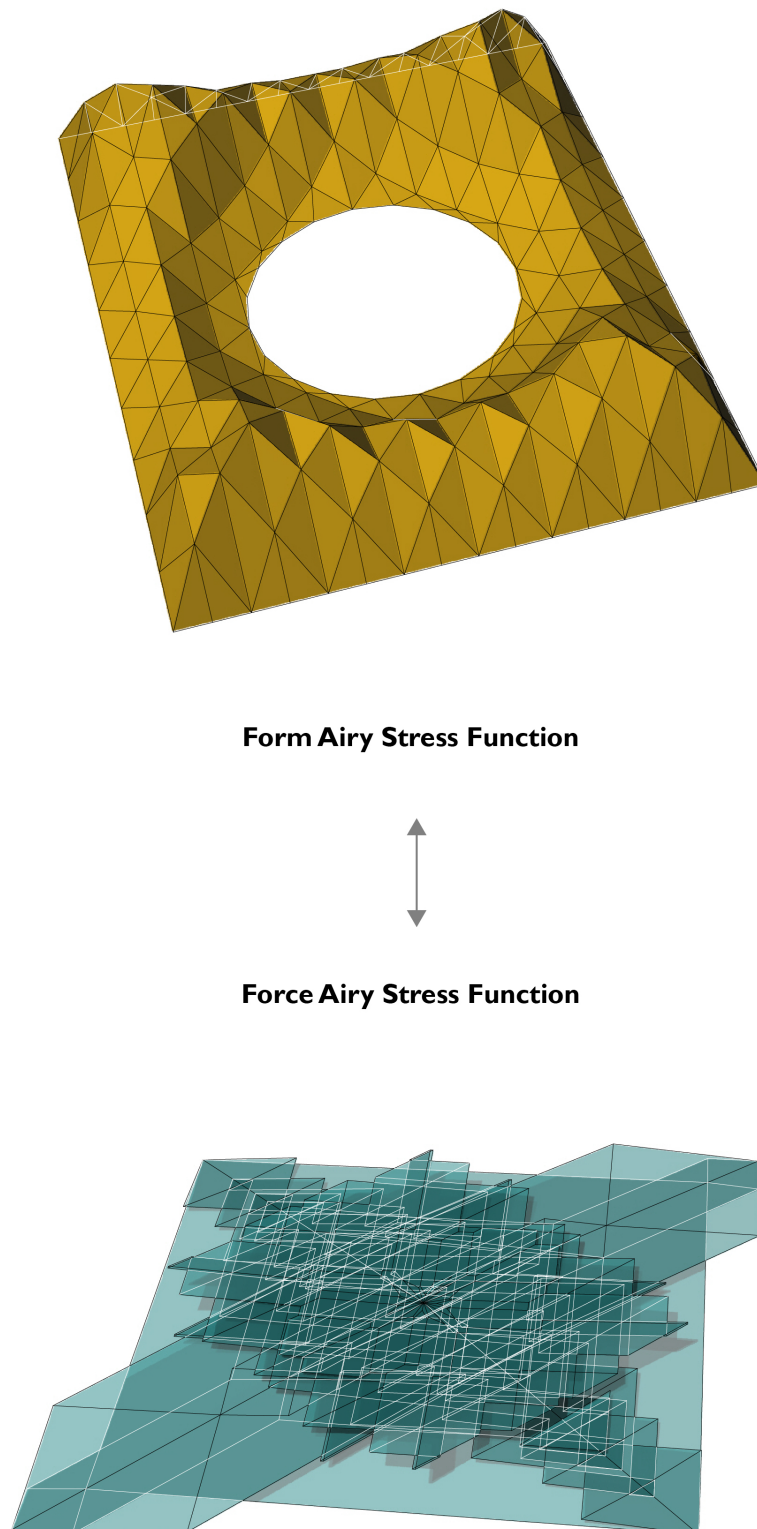


Fig. 6.21 Top: The 2-connected, polyhedral Airy stress function corresponding to the form diagram of the Great Court Roof; Bottom: Reciprocal polyhedral Airy stress function corresponding to the force diagram.

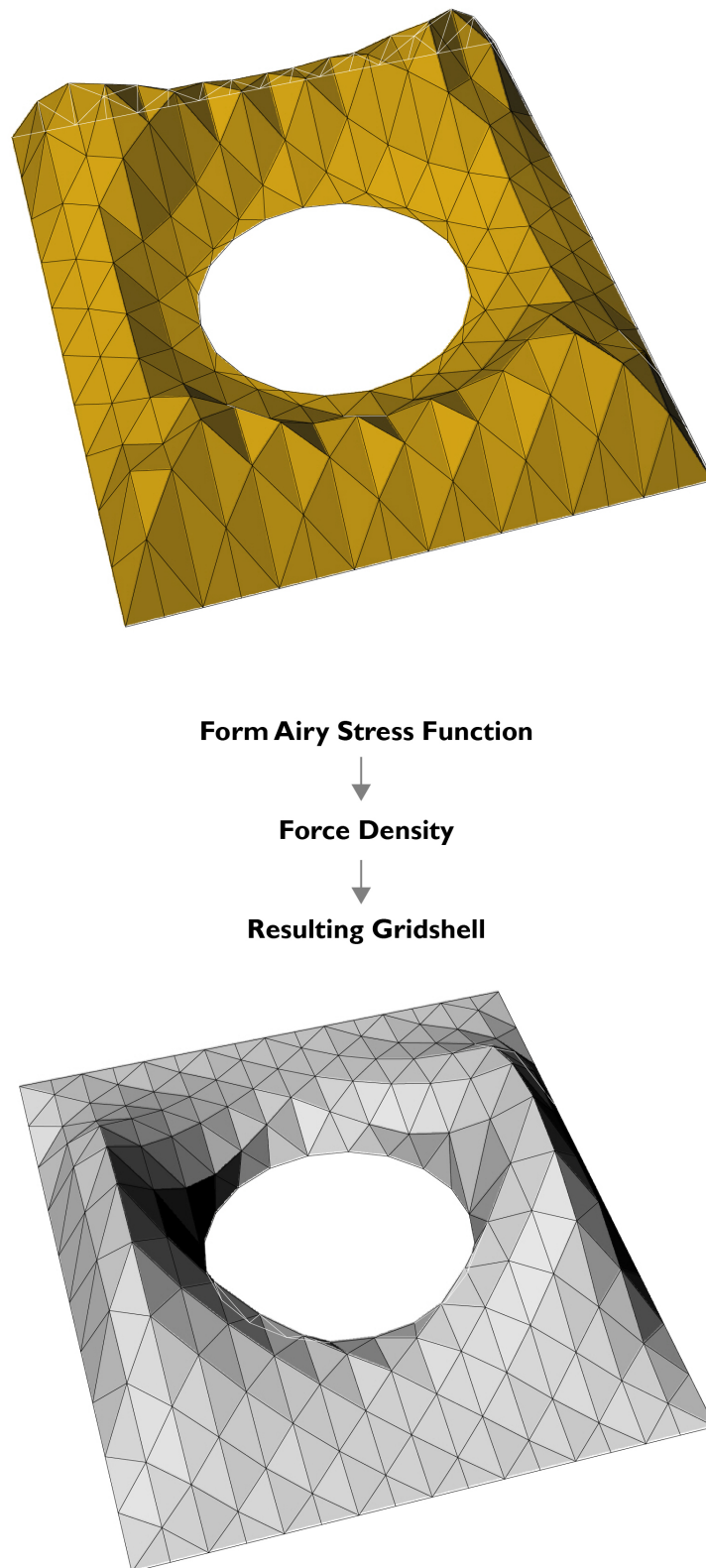


Fig. 6.22 The 2-connected polyhedral Airy stress function and the resulting smooth geometry of a grid-shell roof via the force density method.

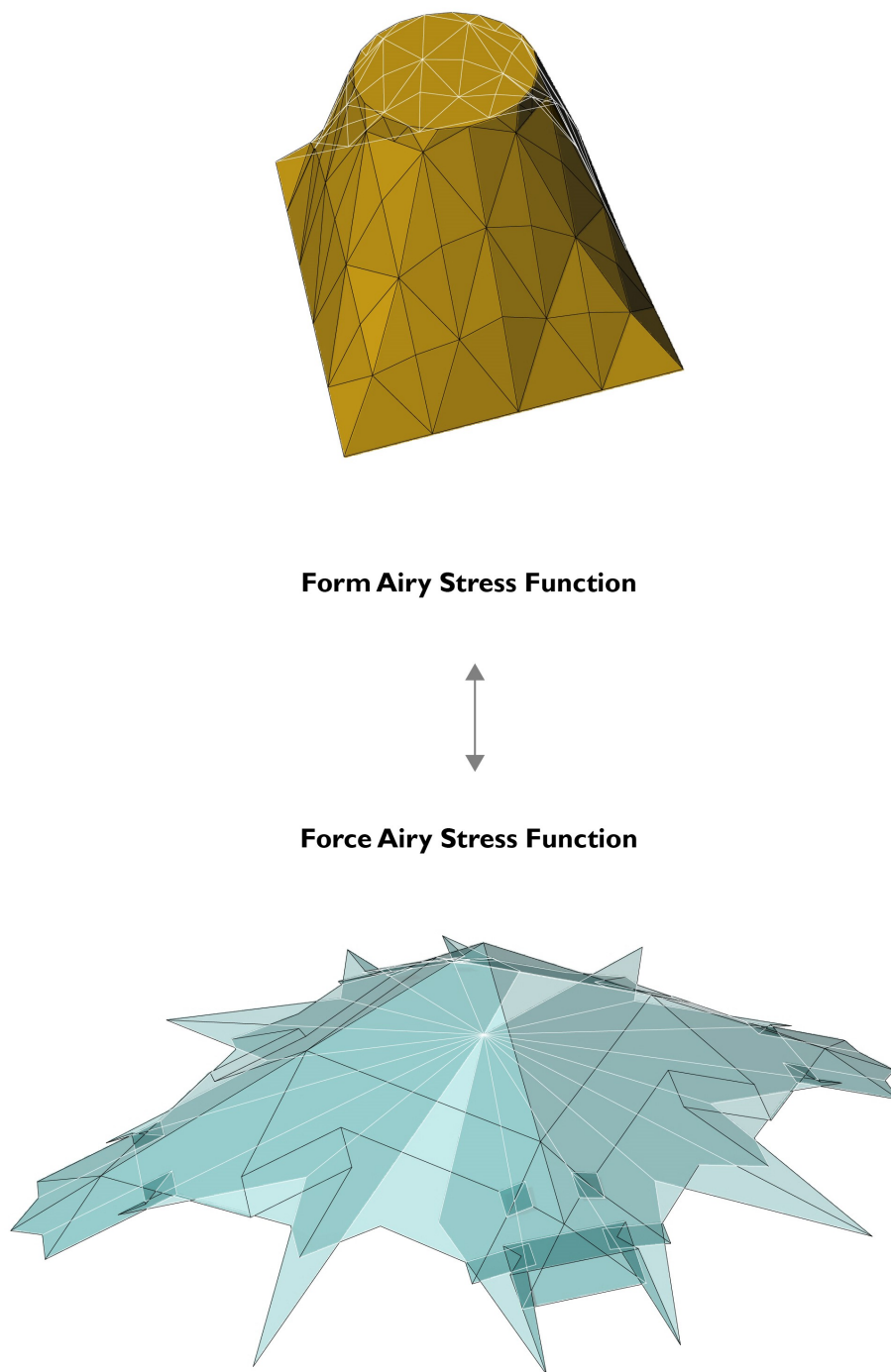


Fig. 6.23 Top: The 1-connected, polyhedral Airy stress function corresponding to the form diagram of the Great Court Roof; Bottom: Reciprocal polyhedral Airy stress function corresponding to the force diagram.



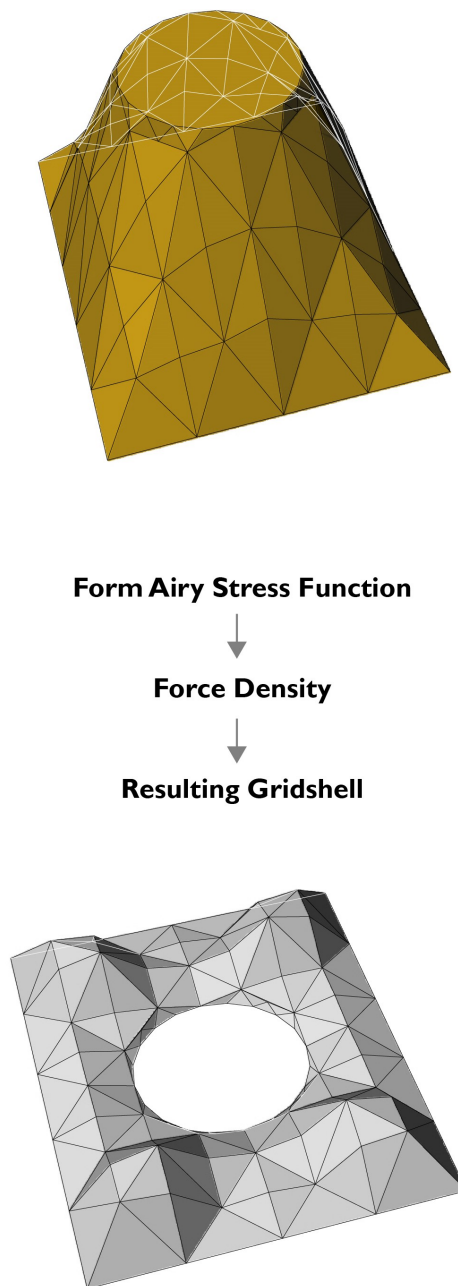


Fig. 6.24 The 1-connected polyhedral Airy stress function and resulting smooth geometry of a grid-shell roof via the force density method.

## 6.2 Summary

In this Chapter numerous applications and case studies of this PhD theory were presented.

We showed how by using a direct and unified graphic statics framework a designer can design, analyse, and transform 2D and 3D trusses within the equilibrium space.

We highlighted the graphic and kinematic analysis of spatial frameworks in a unified and purely geometrical basis. We showed that this twofold analysis can be applied to a wide variety of structures from trusses, to tensegrities, and flexible polyhedra; deriving Rankine reciprocals for frameworks which may or may not be projections of Maxwell-Rankine stress functions, using geometrical techniques like coning. Attention was restricted to special cases of ‘rare’ configurations of generically rigid frameworks in which the structures change their structural behavior by possessing mechanisms and states of self-stress. Specifically, we obtained accurately the nodal vector displacements of the Steffen flexible polyhedron and we generalised Minkowski sums to visualise the redistribution of internal forces in statically balanced tensegrity mechanisms; applicable to energy-efficient transformable design.

We showed how to design spatial trusses such as trusses of exoskeletons of towers in static equilibrium without having to start from subdivisions of the force diagram - in fact, structural morphogenesis can occur directly in the form space by obeying geometrical conditions of the corresponding stress function. Moreover, we showed how to design by analysis compression-and-tension shells, grid-shells, and vaults, such as the Great Court roof of the British Museum, by defining and sculpting stress functions. In particular, by sculpting the Airy stress function the designer can sculpt the form and design the load path - essentially shifting the method of *free-form* design from the form space to the force space. Any polyhedral stress function is an admissible self-stress - resulting in a different form.

In this way, the designer has explicit local and global control on the stress function and can choose: which members, or areas, are tension and which are compression; which members have axial forces and which do not (by imposing adjacent faces to lie on the same plane); which form areas of the shell need to be altered locally and impose the necessary alterations interactively while ensuring global equilibrium throughout the process. As the form and force reciprocal objects are interlinked the designer can also update the force diagram.

This method results in a truly interactive design and analysis process where the structural performance is a design freedom and the method is as meaningful as the output. In this framework the lower bound theorem not only ensures that a solution is admissible but it can also ensure this creative range of design and analysis freedoms.

# Chapter 7

## Impact study and cross-disciplinary applications

This Chapter discusses cross-disciplinary applications of this PhD research. In particular, it develops design and analysis applications on structural concrete, such as automatic generation of 2D and 3D discrete stress fields and geometrical criteria for admissibility of yield line patterns and geometrical representations of internal and external work. This work started as a collaboration with Dr. Pierluigi D'Acunto of ETH Zurich - Chair of Structural Design of Prof. Dr. Joseph Schwartz - during an academic secondment in December 2018. The results of this research will be presented in two conferences: Symposium for the International Association of Shell and Spatial Structures - Barcelona, October 2019 (Konstantatou et al., 2019a) and the International fib Symposium on Conceptual Design of Structures - Madrid, September 2019 (Konstantatou et al., 2019b).

### 7.1 Introduction

The reciprocity and duality of graphic statics is a fundamental notion that can be observed in many places around us. In particular, graphic statics is currently experiencing a renaissance for the analysis and design of structures in static equilibrium while also showing the potential of being applied to other fields such as structural concrete.

Methods such as stress fields and yield lines are valuable; however, their automation, generalisation in 3D cases, and geometrical admissibility are active research topics. In this Chapter, we introduce a twofold geometrical and interactive design and analysis methodology for: the generation of discrete stress fields of 2D and 3D reinforced concrete structures; the design and analysis of admissible yield line patterns in concrete slabs. This is based

on the polarities graphic statics framework. Specifically, on the construction of reciprocal stress functions and the interlink of form, force diagrams and Minkowski sums. Based on this proposed approach, for a given form diagram (which represents the topology of the strut-and-tie model), its polyhedral Airy stress function is transformed through a series of geometrical manipulations to produce a valid stress field that respects the specified topology of the strut-and-tie model, boundary constraints and applied external forces. This results not only to the generation of valid stress fields but also to the introduction of design and analysis freedoms on how to achieve this. Moreover, this methodology discusses yield line theory and how its fundamental principles (internal and external work) can be represented geometrically in an intuitive way. It is highlighted how both these applications are underpinned by the same fundamental geometry. Lastly, the application of these techniques has been also investigated in relation to cosmology (large-scale structure of the universe) and origami (Neyrinck et al., 2018). However, these areas will not be considered as part of this thesis.

## 7.2 Discrete stress fields in reinforced concrete

This section introduces a twofold geometrical methodology for generating valid 2D and 3D discrete stress fields in reinforced concrete structures and yield line patterns via the use of polyhedral stress functions in the context of graphic statics. This methodology contributes to more intuitive, visual and at the same time automated design and analysis of concrete structures which at the moment rely heavily on step-by-step calculations and experience. It discusses yield line theory and how its fundamental principles and notions can be represented geometrically in a clear and intuitive way. Moreover, it is highlighted how both these applications are underpinned by the same fundamental geometry which can be fine-tuned depending on the specific practical considerations of each one of them. This methodology is applied to 2D examples and is then generalised to 3D cases.

Strut-and-tie models and stress fields are useful tools for the design, analysis, and assessment of reinforced concrete structures. These two methods, which are both based on the lower bound theorem of plasticity theory, are complementary and closely related but do not coincide. Specifically, stress fields are a simplified version of strut-and-tie models, which can be obtained from the former by taking the stress resultants. As a result, different approaches and techniques may be followed with regards to each other (Muttoni et al., 2015). Strut-and-tie models are a consistent and rational design and analysis method for reinforced concrete structures. Strut-and-tie models were developed in Stuttgart (Schlaich et al., 1987) based on the earlier truss model. Before the introduction of computational

frameworks based on optimisation, the development of truss models for D-regions<sup>1</sup> was heavily based on experience, rules-of-thumb and intuition of practitioners. A method for deriving strut-and-tie models is by using the principal stress trajectories of linear elastic finite element models (Schlaich et al., 1987). However, there are still challenges and scope for improvement, particularly with regards to automation, selection, and refinement of the model (Tjhin and Kuchma, 2007). In response to that, several computational frameworks have been recently introduced such as (Tjhin and Kuchma, 2007). These are mostly based on topological optimisation of ground trusses (Ali and White, 2001; Liang et al., 2000) or finite element analysis approaches (Biondini et al., 2001; Muttoni et al., 2015). Stress fields on the other hand sprang out of the theory of plasticity based on the work of Gvozdev (Gvozdev, 1960) and Drucker (Drucker, 1961) and are useful design and analysis tools (Muttoni et al., 2015). Stress fields can be used for calculating the internal forces, the required reinforcement, and for describing the stress distribution with regards to the compression struts. Moreover, they are useful for dimensioning of members, detailing, and specifying the nodal geometries. However, their widespread use can be hampered by lack of automation. In recent years, research on this has been less extended in comparison to the strut-and-tie counterpart. An example based on stiffness can be found in (Kostic, 2006). However, currently there are no direct approaches which also generalise 2D discrete stress fields to 3D.

The concept of the strut-and-tie models was introduced in late 19<sup>th</sup> century through Ritter's and Mörsch's truss analogy. As mentioned in the seminal publication of Schlaich et al. (Schlaich et al., 1987), this was further developed by Leonhardt (Leonhardt, 1965), Rüsch (Rüsch, 1964), and Kupfer (Kupfer, 1964) and then formally defined and based on the theory of plasticity by Thürlimann (Thürlimann et al., 1983), Marti (Marti, 1985), and Müller (Müller, 1978) in Zürich. Other contributions include the work of Collins and Mitchell (Collins and Mitchell, 1980) who studied shear and torsion in relation to the deformations of the truss analogy model and of Leonhardt and Walther (Leonhardt and Walther, 1966), who showed the applicability and usefulness of this method to the design of reinforced concrete structures such as deep beams and corbels.

Strut and tie models for reinforced concrete are underpinned from plasticity theory (this implies a rigid-plastic material behavior, where everything is based on pure equilibrium solutions in compliance with the lower bound theorem). The crack pattern helps to describe load transfer in the member by means of forces that are concentrated in compressive struts and tensile loaded steel bars.

---

<sup>1</sup>D stands for discontinuity. Such regions can be found in areas where the strain distribution is non-linear. For example: corners, openings, and points of application of concentrated loads. Strut-and-tie models provide a good description of the flow of forces in these areas.

The lower bound, or safe, theorem and the upper bound, or unsafe, theorem are central to the theory of plasticity. The first theorem states that (Heyman, 2008): if a set of internal forces can be identified that satisfies both equilibrium and the yield criterion for a given set of external forces at a specific load factor, then this is less than or equal to the actual load factor of the structure. In other words, if the designer can find *an* equilibrium state for a structure which nowhere exceeds yield then, subject to various conditions such as ductility, the structure is safe. The upper bound theorem states that (Heyman, 2008): ‘if a plastic mode of deformation is assumed, and the work done by the external loads is equated to the internal work dissipated, then the resulting load factor  $\lambda$  is always greater than, or at best equal to, the true load factor  $\lambda_c$ . In other words, if there is a compatible collapse mechanism where the internal and external work are equal, then the structure will collapse at this or a lower load.

There are number of key publications from the late 1980s (Schlaich et al., 1987) and 90s (Muttoni et al., 1997; Schlaich and Schäfer, 1991) which have contributed to the development of this methodology. These aimed to provide a design concept for reinforced concrete structures, comprising both tension and compression elements, which was based on a generalization of the truss analogy in beams (Schlaich and Schäfer, 1991). Specifically, some of the main design principles of the strut-and-tie methodology are (Schlaich and Schäfer, 1991):

- In concrete stress fields, the struts will represent compression vectors in concrete and the ties, tension vectors in reinforcement.
- There is compliance with the lower bound theorem of plasticity.
- The ductility requirement is fulfilled and the resulting structure will conform with the hypothesized strut-and-tie model.
- Practical issues are taken in consideration when arranging the tensile reinforcement.
- The initial topology of the strut-and-tie model follows the results of an elastic theory analysis with regards to the force paths; however, unlike in the case of elasticity analysis, some ultimate load capacity is neglected.
- The strut-and-tie modelling concept equips the engineer with a level of design freedom, namely, a suitable solution can be tailor-made with regards to some specific requirements (cost, optimality, safety, etc).
- This method can also output and systemize detailing information related to the reinforcement layout, a process which is normally done based on experience in a ‘guess-work’ approach.

- The load paths subdivide and connect the D-regions in a consistent way while not overlapping each other.

The geometry of compression fields is much richer than the idealized rectangles used in the strut-and-tie approximation. Specifically, there are three main configurations that cover all the different cases (Schlaich and Schäfer, 1991): the fan-shape which has negligible curvature and no transverse stresses; the bottle-shape which has significant curvature and transverse stresses (which require tensile reinforcing); and the prismatic/ parallel-shape which is a common special case of the two aforementioned. However, it is this very characteristic of strut-and-tie models, namely, their simplified and understandable nature, that renders them a powerful method for designing reinforced concrete structures. The fact that the actual distribution of the stress fields differs in practice is not a problem following the applicability of the lower bound theorem and the theory of plasticity.

The stress distribution is also quite complicated at the nodes where the stress fields meet. However, there is a limited number of specific cases that are recurring in practice, the geometry of which is of particular interest. There are several rules for the design of these nodal geometries and detailing (Schlaich and Schäfer, 1991): the nodal geometry must comply with the incoming stress fields/ applied forces, specifically the height and location of tensile anchorage; safe anchorage is of paramount importance. Given a static equilibrium configuration for incoming stress fields at a node, its geometry can be altered to incorporate specific practical considerations. For example, the nodal geometry, which in fact is the reciprocal force polygon for this node of the strut-and-tie model, can be altered by re-distributing the edges of the force polygon in such a way that the tensile anchorage is in a convenient location from a practical point of view. In the case of compression-only nodes no further re-arrangement of the node is required. In other words, graphic statics gives a theoretically correct solution which may need to be altered to fit specific practical considerations depending on the particular application.

Discrete stress fields and strut-and-tie models are advantageous in early conceptual design phases, detailing, checking of the resulting design, as well as the education of engineers and architects. Through their simplified and fundamentally geometrical nature they can efficiently capture the flows of internal forces while at the same time providing valuable insight to detailing. (Schlaich and Schäfer, 1991). Moreover, if we compare them to Finite Element Analysis (FEA), FEA can be quite accurate and useful for substantiation and analysis, however, its accuracy is based on the accuracy of the material model and is generally less intuitive and suitable for design purposes. Moreover, it is computationally demanding and slow. On the other hand strut-and-tie because of its simplified and geometrical nature can be

more easily implemented in the CAD environment by designers, it is computationally much faster, and is more intuitive and visual - adding to its educational value.

### 7.2.1 Methodology

We discuss and interpret discrete stress fields and strut-and-tie models in reinforced concrete from a geometrical point of view based on graphic statics and the theory of plasticity. By using strut-and-tie models, we aim to automate the generation of stress fields within a given boundary of material and an initial input topology. The main tools we will use are the polyhedral Airy stress functions, reciprocal diagrams and the combination thereof in terms of Minkowski sums.

The general methodology is as follows:

- Input: Topology of strut-and-tie network, material boundaries, magnitude, direction and point of application of external forces (Figure 7.1).
- We choose an initial form diagram which has the same topology as the stress field/ Minkowski sum. For example, every node of this initial form diagram maps to a force polygon in the stress field/ reciprocal force diagram. We should note that both the geometry and topology of the final strut-and-tie model will differ.
- We replace the external forces in the geometry of the initial ‘form’ diagram with an auxiliary structure to produce an equivalent self-stressed truss (Figure 7.1).
- We lift this self-stressed truss to the 3-dimensional space to produce the polyhedral Airy stress function (Figure 7.1). We highlight that this lifting process of the form diagram will ensure that the corresponding strut-and-tie model is in static equilibrium by correcting any nodes of the initial chosen geometry (Vansice et al., 2018). Thus, the designer only needs to choose a topology and define an auxiliary geometry which then will be automatically corrected to one of a truss in static equilibrium. Another advantage of this approach is that the geometry of the polyhedral Airy stress function will automatically inform the designer as to which struts are compressive and which indicate tensile reinforcement.
- We then map the polyhedral stress function to its reciprocal polyhedron, which we then project one dimension down to obtain the force reciprocal in a Maxwell 2D configuration (Figure 7.1).
- The two diagrams are combined to a Minkowski sum, which is topologically the same as the stress field (Figure 7.1).



- We can freely apply affine transformations (1D Scaling) on the polyhedral Airy stress function, as well as translation of its planes, knowing that its orthographic projection (form diagram) is always in equilibrium as a consequence of the theory of Maxwell.
- This Minkowski sum is now a stress field for uniform hydrostatic stress-state under the given external forces (Figure 7.2). However, it corresponds to a case where the application points of the external forces may differ (but not their magnitude) (Figure 7.2).
- In order to fit the stress field within the material boundaries and to the specific points of application of the external forces we apply transformations on the polyhedral Airy stress function of the form diagram (Figure 7.3) until the Minkowski sum conforms to the geometrical requirements (Figure 7.2). In the general case, the way to relocate the force polygons of the stress field to the desired locations, without altering the direction of the lines of application and magnitude of external forces, is by parallel translations of the faces of the 3D form Airy stress function. As a result, the magnitudes of the external forces remain the same (the dihedral angles between the faces of the 3D form Airy stress function do not change) but their point of application changes in the stress field. In the simple but common 2D case where the applied loads are vertical, these operations can include global affine transformations such as 1D scaling - the force diagram can then be scaled uniformly to match the again the magnitude of the external forces.

Specifically, the way to relocate the force polygons of the stress field to the wanted locations is by parallel translations of the faces adjacent to the ‘form’ nodes. In the special case that affine transformations (1D scaling) and . As a result, the forces remain the same (the kink between faces does not change) but their point of application changes in the stress field.

- We should note that the resulting strut-and-tie network has more vertices than the initial ‘form’ diagram. That is, some of the nodes of the ‘form’ diagram, which corresponded to one force polygon were actually clusters of overlapping nodes that become distinct nodes in the new strut-and-tie network (Figure 7.2). This effect is due to a subtle difference between the Minkowski sum and the stress field. Namely, the initial Minkowski sum represents static equilibrium given a form diagram for which every  $n$ -sided force polygon corresponds to a node with  $n$  number of concurrent form edges (truss analogy). However, these form edges do not necessarily pass from the midpoint of the force edges – they are just perpendicular to them. As a result, the form

edges cannot be seen as the lines of action of the resultants. The force polygon is still in hydrostatic static equilibrium, but the resulting resultants are different.

- In the general case the stress fields in reinforced concrete can be diffused or non-perpendicular at the node as long as the stress resultant is kept constant in terms of location and magnitude. Consequently, along with the force diagram (which corresponds to static equilibrium of the resultants) we have the flexibility to define the ‘stress diagram’ which depicts the particular stress distribution given a static equilibrium of force resultants (Figure 7.4).

To sum up through the Minkowski sum we solve the topological problem of the stress field and we obtain a geometrical solution for one particular case. If our example differs geometrically from this solution the resulting stress field needs to be adapted through geometrical transformations of the polyhedral Airy stress function.

## 7.2.2 Practical interpretation and considerations

When a reciprocal diagram and a Minkowski sum are obtained for a strut-and-tie model, this is a valid solution from a theoretical standpoint (through the lower bound theorem of plasticity theory). Nonetheless, there are practical considerations that should be taken into account and the geometry may need to be refined, particularly in the nodal locations.

### Force polygon - nodal static equilibrium

If we assume hydrostatic pressure for each one of the nodes, then the method readily works for compression-only cases where the compressive struts do not overlap each other. However, geometrical changes need to be made at the corresponding force polygon in other cases where compressive struts meet with tensile reinforcement (compression and tension nodes) (Figure 7.2) for the theoretical solution to be applicable in this particular material (reinforced concrete). As a result, by rearranging the order of the edges of the force polygon which corresponds to a particular node, we can ensure appropriate anchorage of the tensile reinforcement as seen in literature (Muttoni et al., 1997).

### Stress field distribution

The stress fields in reinforced concrete are not always uniform: it is very common, particularly in cases of continuous, rather than point, loading for some of the fields to vary. In this case even though the direction, magnitude and point of application of the force resultant remains

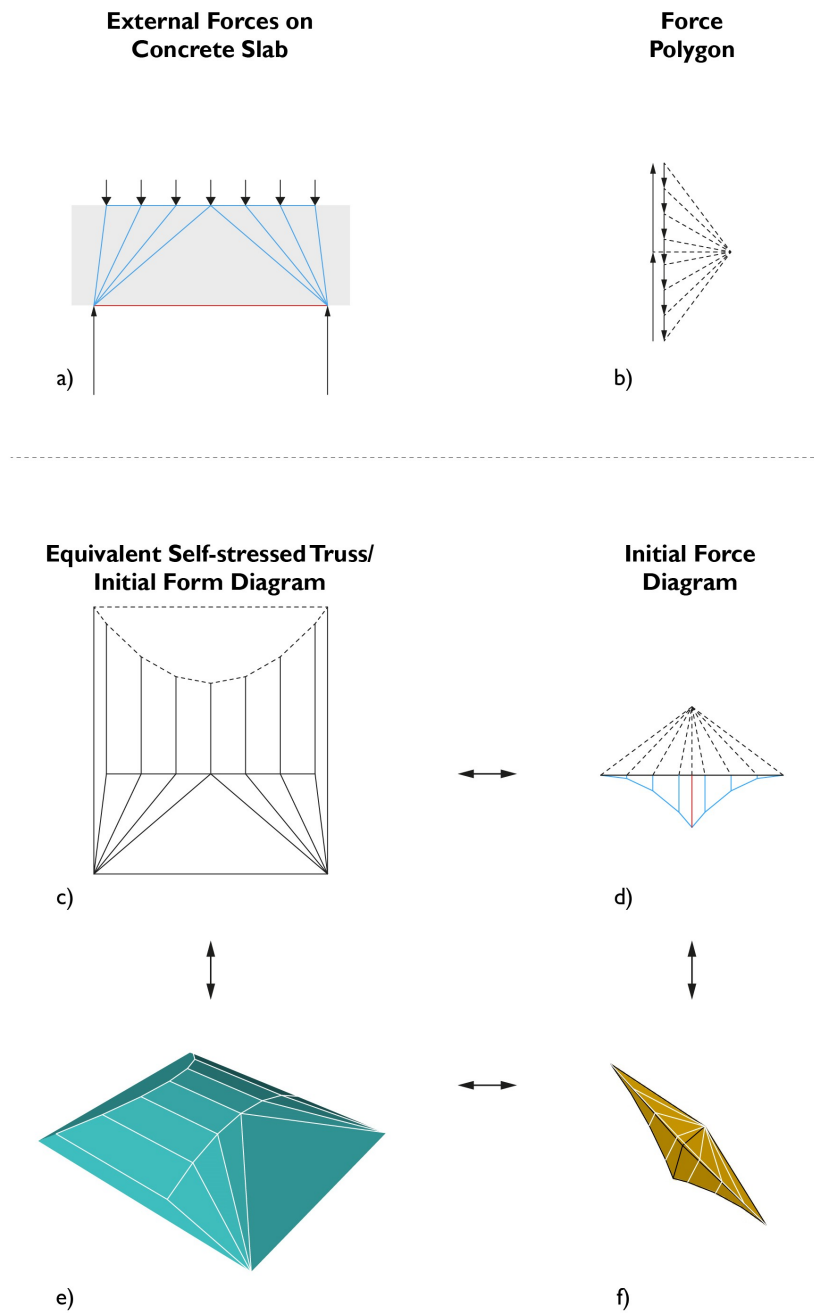


Fig. 7.1 a) External forces and reactions on a concrete slab; b) Force polygon; c) Equivalent geometry of a self-stressed truss including a funicular element deriving from the force polygon (initial form diagram); d) Reciprocal in a Maxwell 2D configuration (initial force diagram); e) Corresponding polyhedral Airy stress function of (c); f) Corresponding polyhedral Airy stress function of (d).

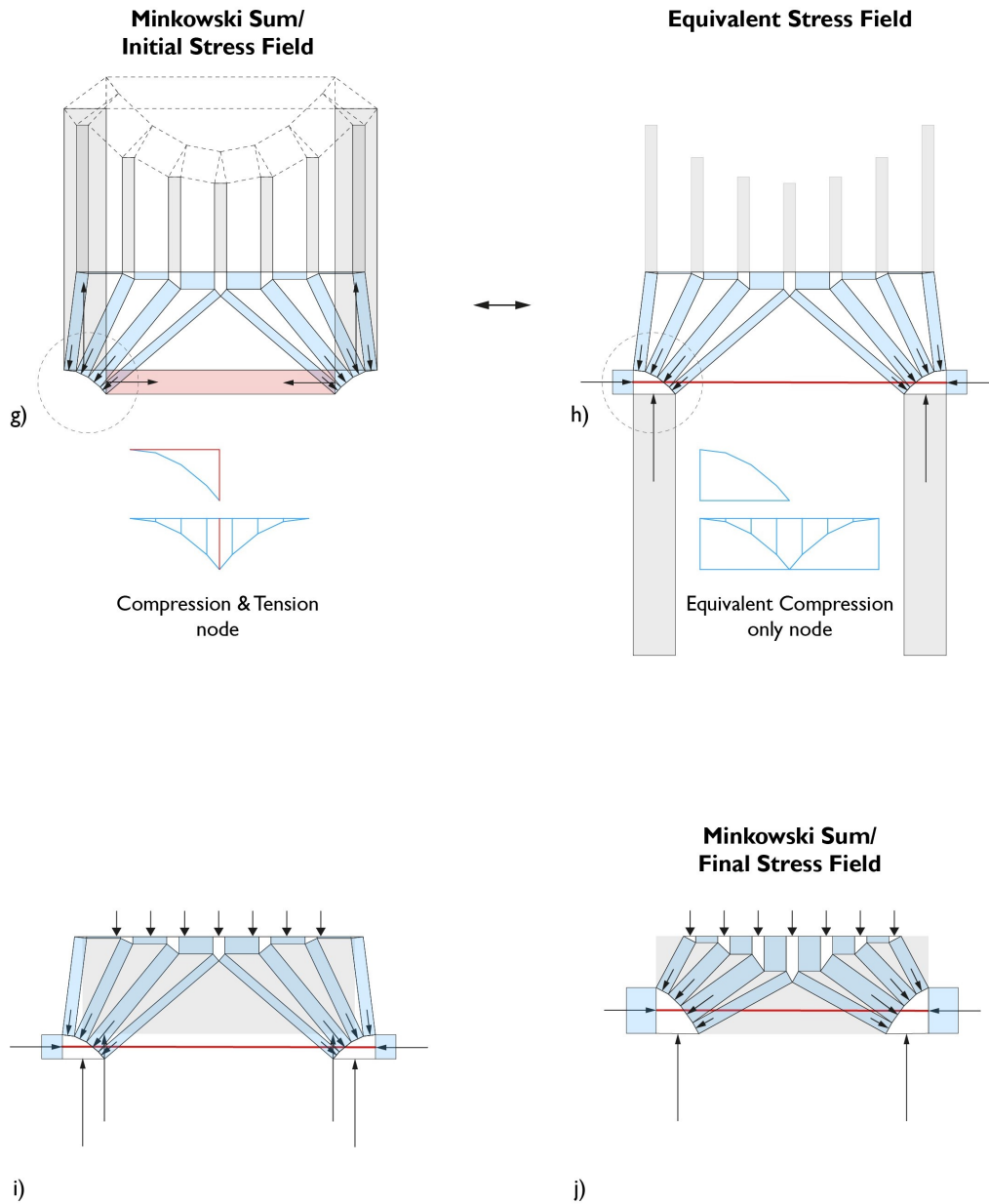


Fig. 7.2 g) Minkowski sum (initial stress field); h) Transformation of the nodal geometry to convert the force polygon into a compression only hydrostatic field; i) Superposition of the initial stress field with the boundaries of the slab show that this is not an acceptable solution; j) The final stress field coincides with the material boundary following transformations of (e).

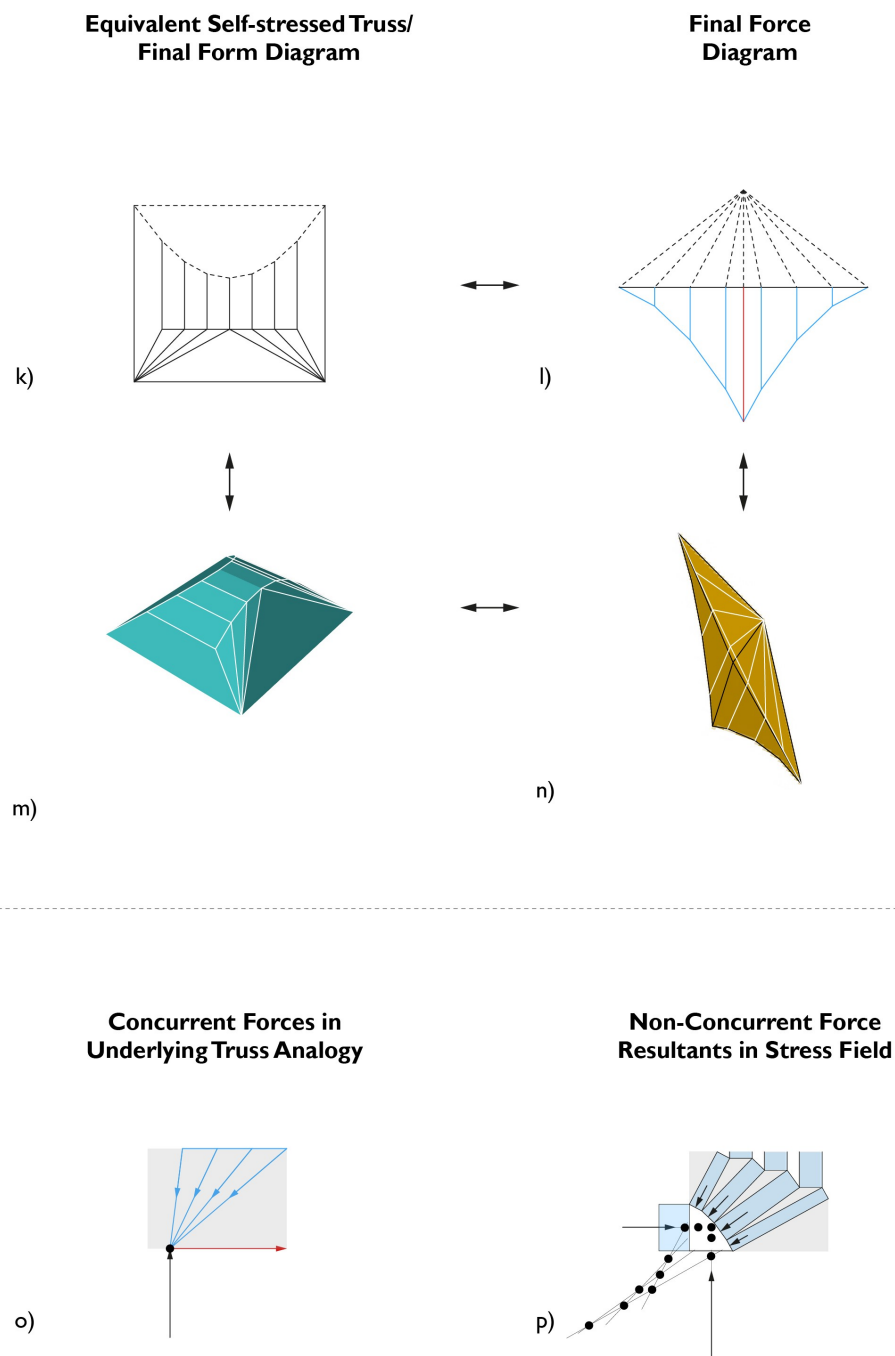


Fig. 7.3 k) Final form diagram; l) Reciprocal (final) force diagram; m) Final polyhedral Airy stress function after the transformations corresponding to the final stress field (j); n) Corresponding polyhedral Airy stress function of the final force diagram; o) The axial forces corresponding to the truss analogy are concurrent; p) The force resultants of the stress field are not concurrent.

the same, the corresponding stress field can be varied or spread with respect to a node in order to capture more accurately the structural behaviour of the concrete structure.

Taking as a starting point a valid stress field, which is uniform and hydrostatic, we can now scale some of the force polygons/ nodes of the stress field so as to correspond to continuous loading (Figure 7.4). For these force polygons we observe that the stress fields become non-uniform and non-hydrostatic. However, if the changes in the stress distribution are such that the force resultants remain the same, the static equilibrium is not violated. This also applies to the edges of the force polygon being curved rather than straight and perpendicular with respect to the underlying truss (form diagram). These transformations of the stress field distribution lead to a more nuanced representation of the force diagram which can also be seen as a ‘stress distribution’ diagram (Figure 7.4). This provides insight to the changes of stress distribution along a strut. It should be highlighted how the Airy stress function behaves geometrically differently in the two cases of discrete and continuous loading (Figure 7.4). In the case of discrete loading and uniform hydrostatic pressure the Airy stress function over the stress field comprises plane-faced rectangles connected to plane-faced force polygons. The change of slope between adjacent geometrical elements gives the magnitude of the force resultants and each of the rectangles represents a uniaxial stress of the material. In the limit of continuous loading the rectangles are no longer parallelepipeds and we have a non-uniform biaxial stress distribution. This applies to both regions of the stress field: the fans stemming from the force polygons of the bottom reactions towards the loading on the top edge of the slab, and of the triangular top region of the slab directly under the continuous loading. The biaxial non-uniform stress is translated in terms of geometry in these regions to be gauche. Also, at the continuous limit the numerous rectangles have merged to only three geometrical elements: the two fans and the triangular region connecting them with the loading. These three areas consist of closed polygonal loops in 3-space which do not lie on a plane and are spanned by doubly curved surfaces. Any such surface is admissible, and it will correspond to a different biaxial state of self-stress. Thus, the continuous limit introduces shear, where there were only axial forces in the discrete case. Special case is the circular symmetric fan with no transverse stresses.

At the continuous limit we end up with the general description of the Airy stress function as a surface  $\varphi$  (rather than the polyhedral version  $\mathbf{P}$  that we are using in graphic statics for trusses) for which we can calculate the Cauchy stress components as known:

$$\sigma_{xx} = \frac{\partial^2 \varphi}{\partial y^2}, \quad \sigma_{yy} = \frac{\partial^2 \varphi}{\partial x^2}, \quad \sigma_{xy} = -\frac{\partial^2 \varphi}{\partial x \partial y}$$

This framework of designing and analysing stress fields in reinforced concrete based on polyhedral Airy stress functions is also useful for optimisation purposes. Specifically, by

optimising the form diagram while its corresponding polyhedron remains plane-faced, the designer can be sure that the space of possible configurations corresponds to an admissible stress field in static equilibrium.

### 7.2.3 Implementation and results

We implement the above methodology to characteristic cases of stress fields found in the literature (Muttoni et al., 1997; Schlaich and Schäfer, 1991; Schlaich et al., 1987). For the 2D case, the initial topology of the strut-and-tie model, material boundary, and points of application of external forces are given. Then with simple transformations of the polyhedral Airy stress function a valid discrete stress field can be found (Figure 7.5, Figure 7.6, Figure 7.7) while automatically guaranteeing global static equilibrium throughout the process. It is shown how the force polygons at the nodes are converted to compression-only regions and the corresponding changes of the force reciprocal. Moreover, this process automates the geometry of the nodes where the stress fields intersect. There is no need for further calculations or special geometrical operations. When the stress field is found the stress resultants can be directly obtained to produce a valid and accurate geometry of the strut-and-tie network. 3D stress fields are not common in literature. However, using the polarities method which is unified for 2D and 3D cases we can obtain valid stress fields for known cases (Muttoni et al., 1997). In the 3D examples, the equivalent truss is lifted one dimension up to a plane-faced 4-polytopic stress function which when reciprocated and projected down gives a Rankine 3D reciprocal. Then by following the same methodology as in the 2D case the Minkowski sum provides a uniform hydrostatic stress field within the boundaries of the concrete wall.

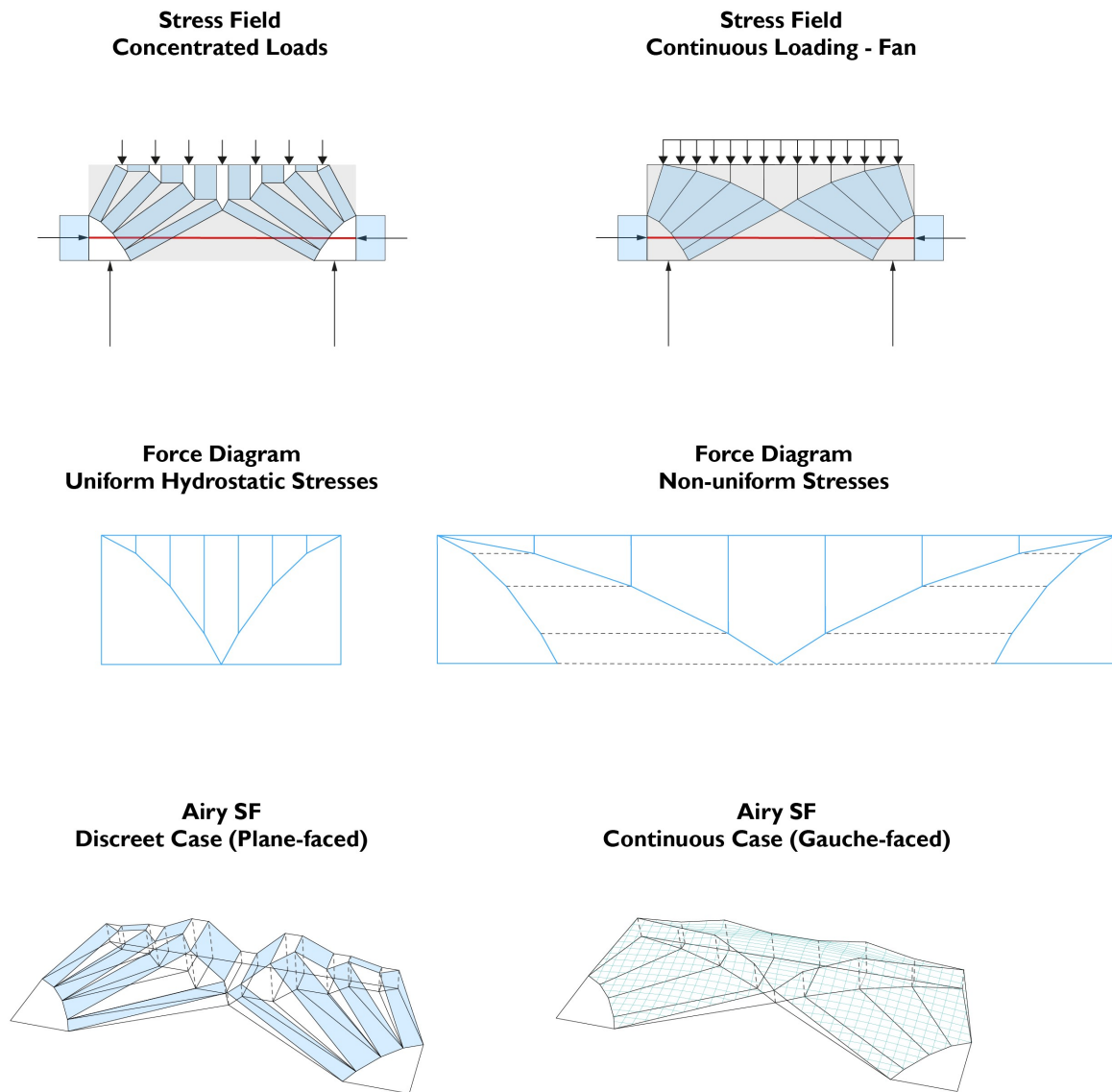


Fig. 7.4 Left) Stress field and corresponding force diagram for uniform hydrostatic stresses under point loading; Right) Stress field and corresponding force diagram for non-uniform stresses under continuous loading.



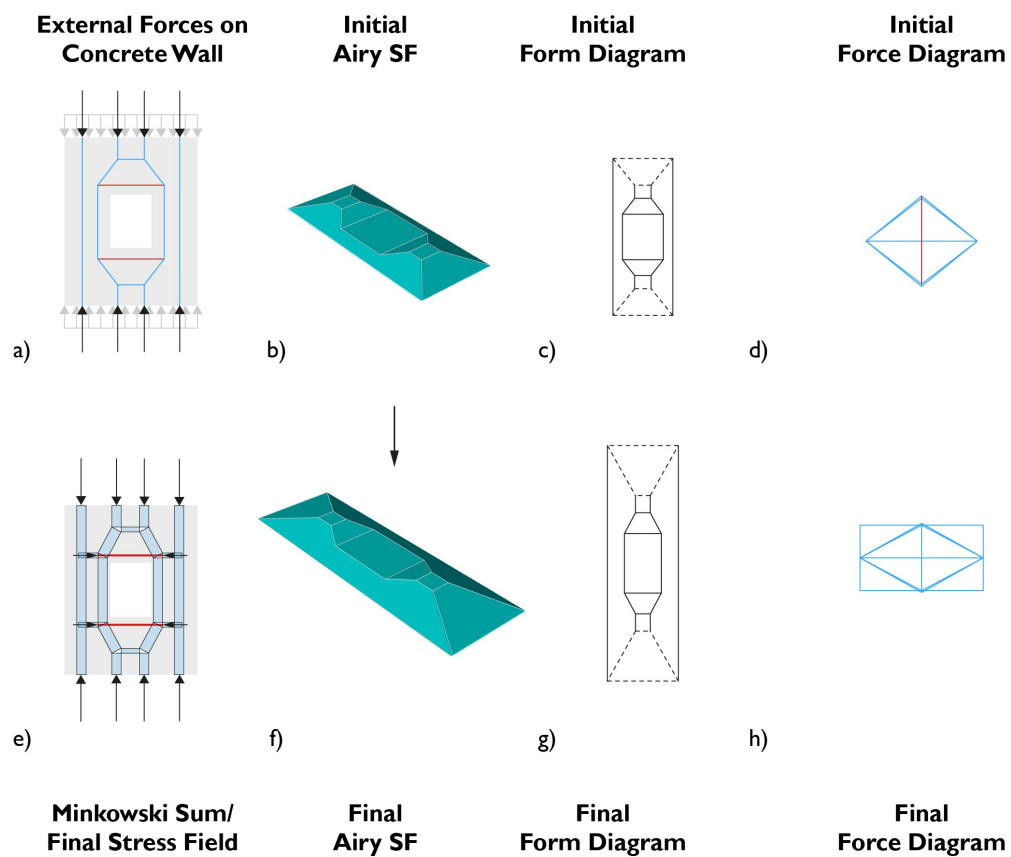


Fig. 7.5 Top) A common stress field case of a concrete wall with an opening is solved via the Airy stress function methodology. Simple geometrical manipulations of the polyhedron and changes in the resulting force diagram give a valid stress field with compression-only nodes.

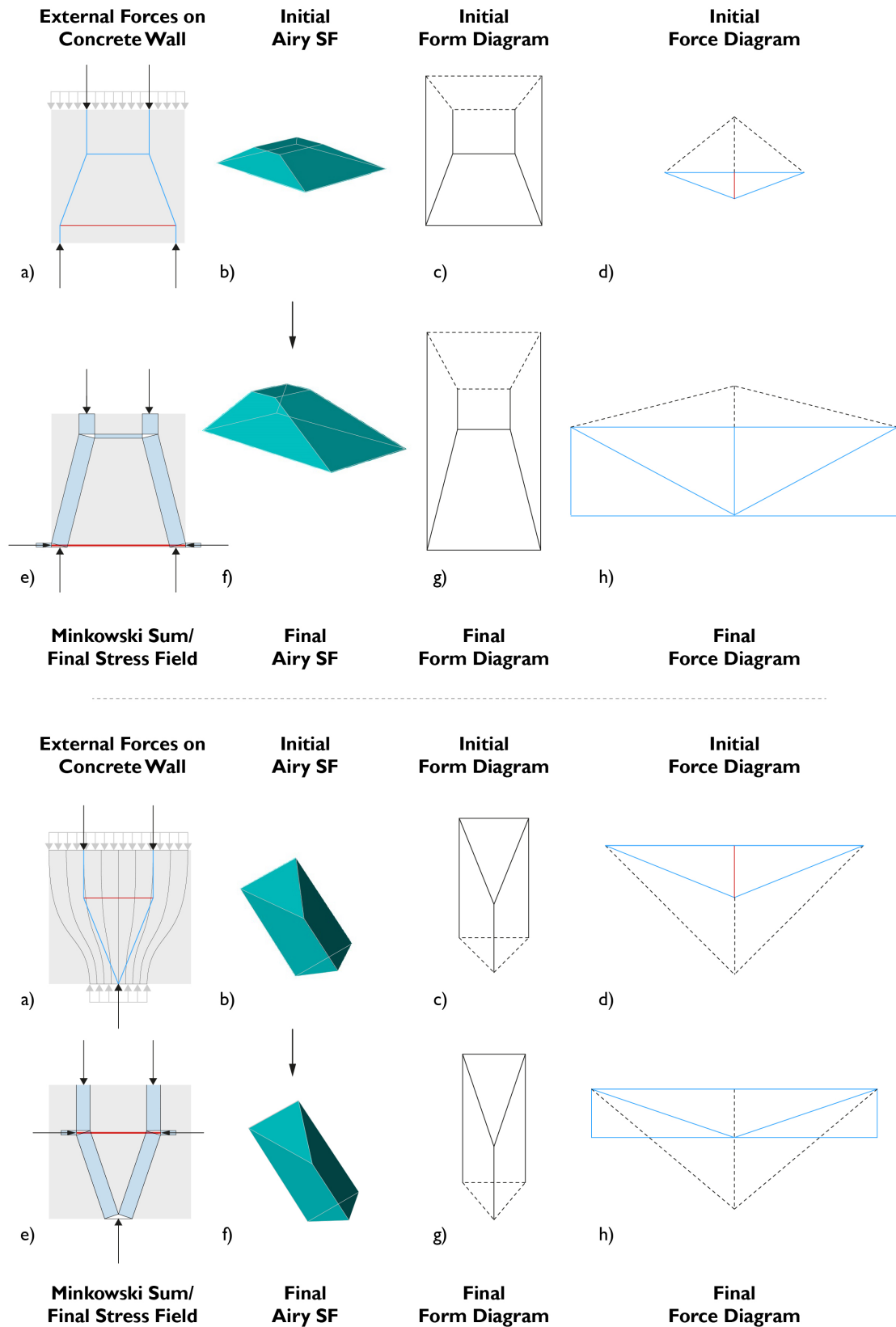


Fig. 7.6 Top and Bottom) Two common stress field cases are solved via the Airy stress function methodology. Simple geometrical manipulations of the polyhedron and changes in the resulting force diagram give a valid stress field with compression-only nodes.

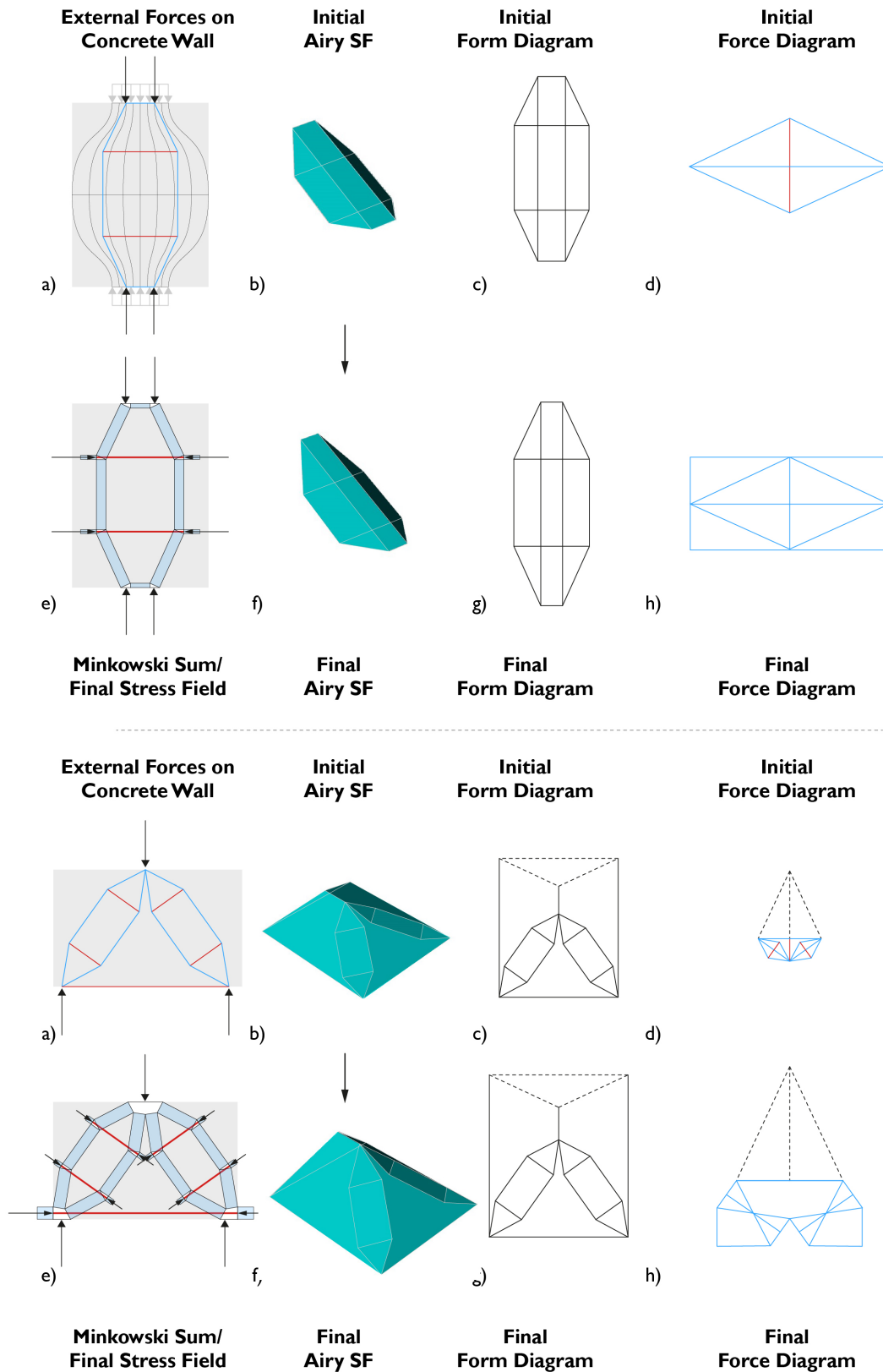


Fig. 7.7 Top and Bottom) Two common stress field cases are solved via the Airy stress function methodology. Simple geometrical manipulations of the polyhedron and changes in the resulting force diagram give a valid stress field with compression-only nodes.

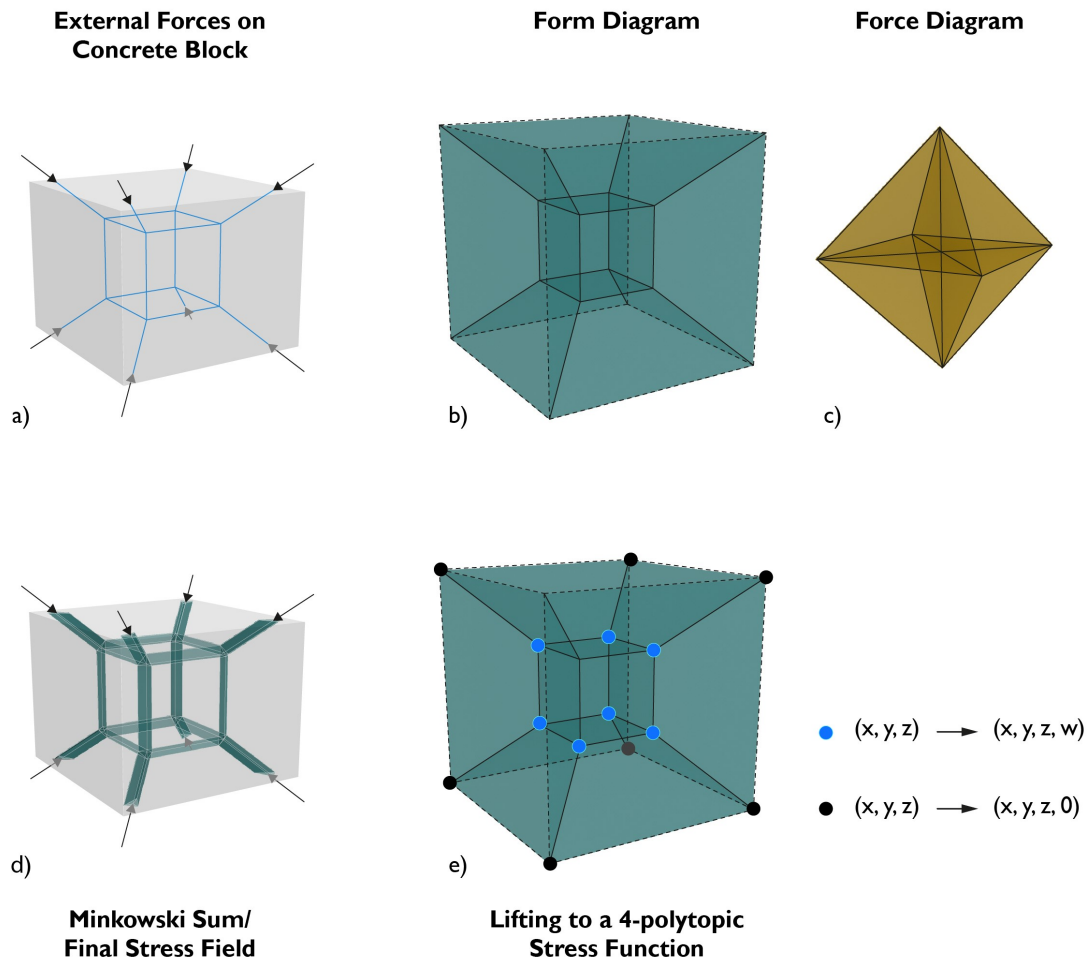


Fig. 7.8 a) A common strut-and-tie case for a cubic concrete block; b) The corresponding form diagram as a polyhedral spatial truss; c) The reciprocal Rankine 3D force diagram; d) The resulting discrete 3D stress field derived from a spatial Minkowski sum; e) The polyhedral form diagram is lifted to a 4-polytopic stress function by lifting the internal nodes in the 4th dimension.

### 7.3 Yield line mechanisms

Yield line analysis has been developed in the context of reinforced concrete slabs to identify their peak load capacity. Specifically, it follows the upper bound theorem in limit analysis and requires the postulation of compatible mechanisms consisting of rigid regions which intersect at yield lines. The yield lines are the axes along which rotation of the rigid regions can occur. The ultimate load can then be found by calculating the rate of internal energy dissipation of the yield lines and equating it to the rate of work resulting from the applied forces while the slab deforms in a specific mechanism (Denton, 2001). An issue of yield line theory is deciding whether a proposed mechanism is compatible or not (Moy, 1981). A systematic method has been proposed from (Denton, 2001) for the identification of compatible yield line mechanisms. Advantages of this approach include its applicability in cases where the concrete slabs have free edges and/or internal supports.

This method is based on the truss analogy, namely, on the analogy between a compatible yield line mechanism and a self-stressed truss the members/ edges of which lie on the mechanism's hinge lines. In particular, the yield lines are tensioned members  $e$  of the corresponding truss  $P(v, e, f)$  which meet at points which correspond to truss nodes  $v$ . Thus, a compatible mechanism of yield lines satisfies both requirements: rotational compatibility of the yield line mechanism and equilibrium of a corresponding self-stress truss. As a result, the compatibility of a yield line mechanism can be checked by examining the geometry of its corresponding truss. If the latter is self-stressed (without any external loads) and in static equilibrium, then the mechanism is compatible. Evidently, a self-stressed truss has at least one state of self-stress and the number of states of self-stress is equal to the number of degrees of freedom of the corresponding mechanism (Denton, 2001). Hence, a mechanism with one degree of freedom (DoF) corresponds to a truss with one state of self-stress. It follows from the upper bound theorem that the yield line mechanisms of concrete slabs that are of interest have  $DoF = 1$  (Denton, 2001). This is because if a mechanism has  $DoF > 1$  then it can never result in lower critical collapse loads compared to mechanisms with  $DoF = 1$ . Also, it suffices for the yield line mechanism to be a part or subset of a bigger truss for it to be compatible. As a result, the edges of the equivalent truss can expand beyond the boundaries of the slab. Consequently, the truss geometries that are of interest in this case are spiderwebs (see section 2.4) with one state of self-stress.

The truss analogy in the context of reinforced concrete slabs was explicitly highlighted by (Denton, 2001). Before that, it was discussed in more general terms from Calladine (Calladine, 1983) as part of the 'static-geometric analogies'. More recently, the truss analogy has been linked to graphic statics through the Airy stress function. Specifically, Williams and McRobie (Williams and McRobie, 2016) established that since a self-stress 2D truss is a

projection of a polyhedral Airy stress function then a yield line mechanism is compatible if it is a projection of a polyhedron. Moreover, since small deflections are assumed and small angle approximation for the relative rotational angle between slabs, compatible yield line mechanisms are equivalent to small-displacement origami patterns (Williams and McRobie, 2016).

We implement the above methodology to common cases of yield line patterns (Figure 7.9). For every one of those the equivalent truss geometry is found. Then the polyhedral Airy stress function checks for compatibility of the mechanism while giving a visual representation of the external work. By reciprocating, the Minkowski sum can be found which gives the visual representation of the internal work (assuming a uniform and isotropic plastic moment of resistance). It should be highlighted that if there are free edges only the regions of the polyhedron and Minkowski sum which correspond to the material boundary are taken into consideration for the geometrical assessment of internal/ external work.

### 7.3.1 Methodology

We analyse and design yield line mechanisms by using the polyhedral Airy stress function of the corresponding truss and the resulting Minkowski sum. This geometrical method can check for compatibility of the mechanism while providing an intuitive and simple representation of the internal and external work.

The general methodology is as follows:

- Input: the geometry of the hinge lines of the proposed mechanism which gives the underlying truss geometry  $P(v, e, f)$ .
- $P$  is lifted one dimension up and is checked whether it can form a plane-faced polyhedron for the specific nodal coordinates of  $v$ . If it does, it is a compatible yield line mechanism. If it does not and the designer wants to create one, then imposing the plane-faced condition in 3-spaces some of the nodal coordinates will be corrected and will result in a  $P'$  which represents a compatible mechanism (see section 5.1).
- We define the angles between adjacent faces of the polyhedral Airy stress function to be equal to the small rotational angles between adjacent rigid regions of the mechanism and we reciprocate to obtain a Minkowski sum. This will have dimensions of length of the yield lines multiplied by the corresponding rotational angle. Once multiplied by the plastic moment of resistance per unit length (which is here assumed to be uniform and isotropic), the areas of the rectangles in the Minkowski sum diagram give a geometrical representation of the internal work, where the blue internal rectangles denote the work

of compressive members enclosed from the red external rectangles denoting the work of tensile members (boundaries). The internal work in equation form (Moy, 1981) for the general case of reinforcement:

$$InternalWork = \sum \left[ \theta \int_S M_n ds \right]$$

is the integral over all lengths  $S$  of all yield lines of the rotation  $\theta$  of the yield line multiplied by the total plastic moment of resistance  $M$  transverse to the yield line.

- Also, for a uniformly distributed load  $q$ , the volume of the Airy stress function, when multiplied by  $q$ , is the external work, which in equation form is given as follows (Moy, 1981):

$$ExternalWork = \sum \left[ \int_A q \Delta dA \right]$$

where  $\Delta$  is the height of the stress function.

- Then the general expression of the work equation is:

$$\sum \left[ \int_A q \Delta dA \right] = \sum \left[ \theta \int_S M_n ds \right]$$

over all rigid regions and every yield line. So, the (weighted) volume of the Airy stress function is equated with (weighted) surface areas of rectangular regions of the Minkowski sum.

Generally concrete slabs have a 2-directional reinforcement which most commonly placed orthogonally. The equation of the plastic moment of resistance per unit length  $M_n$  is then given by (Moy, 1981):

$$M_n = M \sin^2 \theta' + \mu M \cos^2 \theta'$$

where  $\mu$  denotes different resistance moments and  $\theta'$  the angle of the yield line with respect to the direction of the reinforcement. If  $\mu = 1$  the reinforcement is isotropic and

$$M_n = M$$

In this case, the internal work is the same as the total surface area of the Minkowski sum rectangles multiplied by the scalar  $M$ . If  $\mu \neq 1$  then for the geometrical analogy between the

Minkowski sum and the internal work to hold, the rectangles should be scaled 1-dimensionally in the plane by a factor of  $\sin^2\theta' + \mu\cos^2\theta'$  and perpendicular to the yield lines.

### 7.3.2 Implementation and results

We apply the above methodology for common cases of yield line patterns found in the literature (Denton, 2001; Moy, 1981) and for isotropic reinforcement. In Figure 7.9 numerous patterns are shown on the left column - these geometries are compatible since they are projections of polyhedra and thus the corresponding truss is self-stressed. The corresponding polyhedral Airy stress function can be seen in the middle column. Up to a factor, this represents the external work. Through reciprocation the Minkowski sum can be created (right column) whose constituent rectangles represent (up to a factor) the internal work.

## 7.4 Summary

The methodologies and discussions presented here highlighted how graphic statics and Airy stress functions are valuable tools in other fields of engineering other than simple truss design. We showed how they can be used for the automatic generation of 2D and 3D discrete stress fields and geometries of strut-and-tie models given an initial topology. Moreover, they can be employed for the geometrical representation of internal/ external work and compatibility checking of yield line mechanisms, contributing towards a visual, geometrical, and intuitive analysis and design approach in these fields. The graphic statics framework developed in this PhD research proved to have a number of advantages with regards to these applications. Specifically, given that the method works in a unified way both for 2D and 3D cases, handles tension and compression, and is not limited to regular geometries/ topologies, the designer can start working from any one of the four reciprocal objects (form or force) thus allowing for a wide applicability of the method depending on the specific needs of the case-study. Most notably, the fact that it hinges on reciprocal stress functions results in a framework where the designer can interact at any step and is equipped with novel design and analysis freedoms. Moreover, the fact that this method is direct and analytical rather than based on iterative optimisation algorithms adds extra educational value.



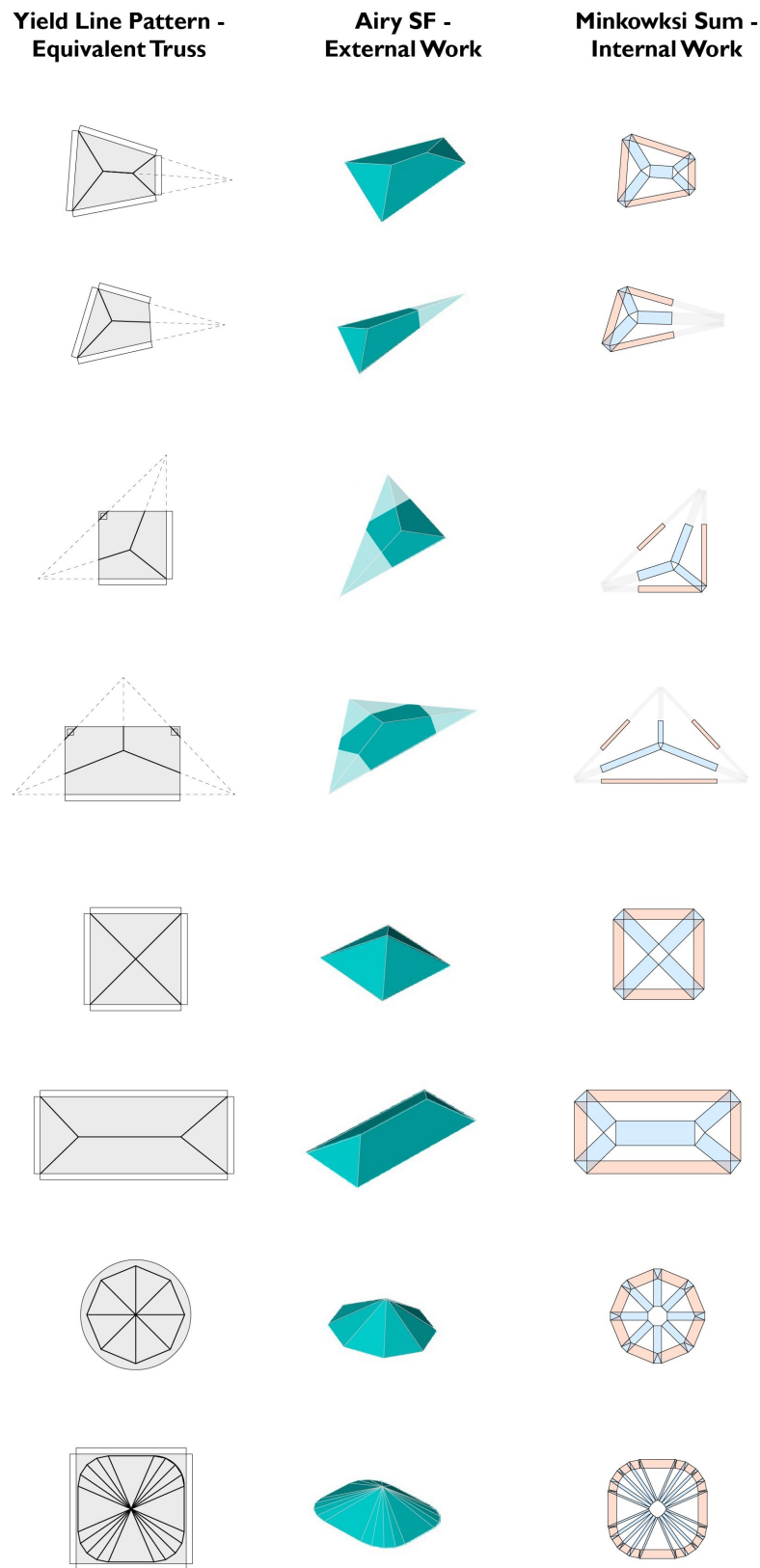


Fig. 7.9 Left) Common cases of yield line patterns; Middle) Their corresponding polyhedral Airy stress function checks for compatibility of the mechanism while providing a visual interpretation of the external work; Right) Their corresponding Minkowski sum gives an intuitive representation of the internal work and of compression-tension areas.

Stress fields are underpinned by the lower bound theorem whereas yield line theory uses the upper bound theorem, even though, the same fundamental geometry can be applied to both. The proposed approach is a general valid theoretical model, however, when it is applicable to specific materials (reinforced concrete for instance) there are a number of constraints and the theory needs to be adjusted to be useful to practitioners. These are specific to the application and change from one material to the other. In other words, we have a theoretical model which is universally valid but depending on the real-life case study may need to be refined following a set of constraints and rules specific to every one of the applications. Here we examined reinforced concrete and yield lines and we show how the same theory can be amended in different ways to satisfy both these fields of research.

# Chapter 8

## Conclusions

### 8.1 Discussion

This thesis described the development of geometry-based, direct, analytical and unified design and analysis methodologies for compression-and-tension 2D and 3D pin-jointed structures based on reciprocal stress functions, while introducing design and analysis freedoms in an interactive framework. These methodologies can tackle a wide range of structures in a unified way without the need for case-specific iterative algorithms. Moreover, this theory, through its elegant and abstract mathematical description, has a cross-disciplinary impact and contributes towards the educational value of graphic statics.

### 8.2 Contributions

This PhD research contributes to the field of contemporary graphic statics by creating and interpreting new knowledge on geometry-based structural and architectural design and analysis methods based on reciprocal stress functions. This is achieved by drawing insights from Maxwell's seminal, but largely unknown and inaccessible, 19<sup>th</sup> century work on graphic statics and connecting this knowledge to other fields of research, such as projective geometry and rigidity theory to develop new theory. Moreover, this theoretical acquisition of knowledge is combined with advanced CAD and visualisation tools to produce methods which are interactive and user-friendly within a computational framework but at the same time theoretically rigorous based on direct operations and elegant mathematical descriptions. Specifically, contributions developed in this research include:

- Explaining and visualising some of Maxwell's key contributions such as the idea of reciprocal polyhedral Airy stress functions, which through projection produce a pair of

form and force diagrams, as well as the idea of using geometrical properties, such as the states of self-stress, as design and analysis freedoms.

- Presenting research on Maxwell's comparatively unknown – but profound – impact on graphic statics in conjunction with his contemporary scientific context.
- Underpinning the fundamental role of polarities, or geometrical mappings, in a wide range of applications in structural analysis and design.
- Introducing a direct, unified, visual and intuitive graphic statics framework for global static equilibrium of 2D and 3D trusses which are projections of discrete stress functions by generalising Maxwell's reciprocal constructions in the 4th dimension (i.e., this method has an elegant, three-fold, equivalent mathematical description: purely geometrical construction, analytical description, and matrix representation; it applies to any 2D truss (resulting in Maxwell 2D/ Cremona 2D force reciprocals) and to polyhedral spatial trusses with plane faces (resulting in Rankine 3D force reciprocals); it works for any loading case (tension-, compression-only as well as for tension-and-compression structures) for self-stressed structures or equivalent ones with external loading).
- Within this context, developing novel design and analysis capabilities, specifically, through employing various states of self-stress, which through the lower bound theorem can equip designers with creative form-finding potential.
- Discussing how geometry optimisation based on minimising the load path, and thus the volume of the structure, can have a visual and intuitive geometrical interpretation through Minkowski sums.
- Presenting an interactive design and analysis method based on the reciprocity between stress functions where the designer operates within the equilibrium space without the need for iterative convergence after every step (i.e., all four reciprocal objects can be controlled and interlinked (form, force, or stress functions) while the user has the flexibility to start from any one of these; this method was developed for 2D and 3D trusses, as well as for tension-and-compression shells, grid-shells, and vaults, in the latter case, by combining global horizontal static equilibrium and the force density method).
- Highlighting how the stress function is useful not only for designing structures within static equilibrium but also as an intuitive and geometrical way of correcting form diagrams should the designer decide to start a free-form design exploration of the

geometry (form and force features can be introduced by sculpting, transforming, and carving locally and globally the polyhedral Airy stress function).

- Performing case studies of: tensegrities with infinitesimal mechanisms and flexible polyhedra with finite mechanisms (two-fold, purely geometrical static and kinematic analysis); dynamic Minkowski sums for statically balanced tensegrity mechanisms; the design and analysis of large infrastructure - tensile nets, shells, grid-shells and vaults; and the structural morphogenesis of large infrastructure - exoskeletons and trusses of towers.
- Proposing cross-disciplinary applications for the design and analysis of structural concrete: i.e., the automatic generation of 2D and 3D discrete stress fields; geometrical criteria for the admissibility of yield line patterns and geometrical representations of internal and external work achieved by developing an interactive framework where stress functions play the central role and provide the designer with design and analysis freedoms while operating within equilibrium space ( the method is unified both for 2D and 3D cases).

The method presented here is applicable to tension-and-compression pin-jointed structures of general geometry and topology in the 2D case. In the 3D case of polyhedral structures, the geometrical limitation is that they are plane-faced, and the topological limitation is that every face belongs to two cells – this covers a plethora of spatial structures but not all.

## 8.3 Impact

The impact of this PhD research is three-fold. Firstly, with regards to the contemporary research field of graphic statics, it is suggested that direct methods of global equilibrium can replace, where applicable, or be used in conjunction with conventional iterative node-by-node procedures to develop interactive design and analysis frameworks. Thus, algorithms could be simplified since there is no need for iterative convergence after every step. Related to this, stress functions embed rich information on the structural performance of the structure, whether tension-/compression-only or tension-and-compression, or whether self-stressed or externally loaded. Furthermore, users can start from any reciprocal object – form or force – and the method per se is more elegant mathematically, accessible to users, and adds educational value and intuitiveness. Secondly, with regard to practitioners since both the method and the output are geometrical, a wider range of users from different skill sets could benefit from understanding both aspects of the process. Specifically, designers could

benefit from simple geometrical rules and observations which reveal the structure's behaviour while equipping them with design and analysis freedoms for sculpting complex forms in static equilibrium. Lastly, the impact with regards to educational methods derives from the directness and fundamentally geometrical nature of the method. Specifically, as shown in the cross-disciplinary applications of Chapter 7 the notion of reciprocal stress functions and of duality can be applied to numerous different fields – providing a transferable theoretical framework.

## 8.4 Future work

As for where this piece of research is heading next, possible applications include material considerations and conservation of historic structures. Specifically, graphic statics are geometry-based and material properties are not considered. This is powerful since geometry has universal applicability for different materials. At the same time as shown in Chapter 7, the application of graphic statics to specific case studies needs to take materiality into consideration to refine and tailor the fundamental theory. Other examples or materials that could be investigated in the future based on this PhD research are: anisotropic natural materials such as timber and bamboo; sustainable materials such as adobe, bricks, and tiles. Moreover, the theory of reciprocal stress functions as a tool for assessing whether 2- and 3-dimensional trusses are in static equilibrium, as well as a tool for correcting them if they are not, could have applicability in the conservation of tension-and-compression spatial historic structures.

## 8.5 Personal Reflection

Coming from a maths and physics background I did not know much about architecture. This started to change when I went to the Architectural Association (AA) in London for a Master's degree in Emergent Technologies and Design. This predominantly form-centric school educated me and challenged my ideas on what contemporary architectural design is, and what it should be. I still remember one night at the beautiful AA library overlooking Bedford square I came across a book by Heinz Isler. I eagerly started reading about merging architectural and structural design, purity of concept, scientific rational and the form as an output rather as an input. I was attracted from the idea of elegant and bold, structurally expressive forms where the geometry manifests the forces. Of course, good architecture is not limited to this, but this felt like the right direction for me. I then knew that if I wanted to contribute towards good architectural design this had to be through a knowledge

of fundamental structural engineering theory. This is how I ended up at the University of Cambridge for a Master's in civil engineering and a subsequent PhD – unclear on what at that point. A direction was given during an unexpected encounter with Bill Baker who brought Maxwell's seminal, but largely unknown and inaccessible, 19<sup>th</sup> century graphic statics publications to my supervisor Allan McRobie. It was an eye-opener and I knew what my PhD would be. Since that moment, summer of 2014, a trip started on trying to decipher what Maxwell was saying and on who to generalise this and apply it to today's architectural and structural design. I was extremely lucky to be working with Allan and Bill for the last 5 years, I could not have found better mentors in every aspect. Their impact on my personal development has been tremendous and I am grateful for this. During my time at Cambridge I had the opportunity to travel and present my work to influential conferences such as the International Association for Shell and Spatial Structures (IASS) where I got useful input, met many colleagues, started fruitful long-standing collaborations and had a great time. As a result of the last five years I have come to appreciate forms which are conceptually pure and bold. The form though, not as a one-directional output of some algorithm in a generative sense, but rather as an output in conjunction with the designer's input and creativity in an interactive, bi-directional process. My hope is that this PhD research will contribute towards this direction.





# References

- Adriaenssens, S., Block, P., Veenendaal, D., and Williams, C. (2014). *Shell Structures for Architecture: Form Finding and Optimization*. Routledge, New York.
- Airy, G. B. (1862). On the Strains in the Interior of Beams. *Philosophical Transactions of the Royal Society of London*, 153:49–79.
- Akbarzadeh, M., Van Mele, T., and Block, P. (2015). On the equilibrium of funicular polyhedral frames and convex polyhedral force diagrams. *Computer-Aided Design*, 63(Supplement C):118–128.
- Ali, M. A. and White, R. N. (2001). Automatic Generation of Truss Model for Optimal Design of Reinforced Concrete Structures. *ACI Structural Journal*, pages 431–442.
- Allen, E. and Zalewski, W. (2010). *Forms and Forces*. John Wiley & Sons, New Jersey.
- Amir-Moez, A. R. (1973). The pole and polar with respect to a quadric. *Pi Mu Epsilon Journal*, 5(9):454–457.
- Baer, R. (1945). Null systems in projective space. *Bull. Amer. Math. Soc.*, 51(12):903–906.
- Bahr, M. (2017). *Form-finding and Analysis of Shells and Slabs Based on Equilibrium Solutions*. PhD thesis, ETH Zurich, Zurich.
- Baierlein, R. (1999). *Thermal Physics*. Cambridge University Press, Cambridge.
- Baker, W., Beghini, L., Mazurek, A., Carrion, J., and Beghini, A. (2013). Maxwell’s reciprocal diagrams and discrete Michell frames. *Structural and Multidisciplinary Optimization*, 48:267–277.
- Baker, W., Beghini, L., Mazurek, A., Carrion, J., and Beghini, A. (2015). Structural Innovation: Combining Classic Theories with New Technologies. *Engineering Journal*, 52:203–218.
- Barbaresco, F. (2018). Higher Order Geometric Theory of Information and Heat based on Poly-Symplectic Geometry of Souriau Lie Groups Thermodynamics and Their Contextures. *Preprint, 2018080196 (doi: 10.20944/preprints201808.0196.v1)*.
- Beghini, L., Carrion, J., Beghini, A., Mazurek, A., and Baker, W. (2014). Structural optimization using graphic statics. *Structural and Multidisciplinary Optimization*, 49(3):351–366.

- Biondini, F., Bontempi, F., and Malerba, P. (2001). Stress path adapting Strut-and-Tie models in cracked and uncracked R.C. elements. *Structural Engineering and Mechanics*, 12(6):685–698.
- Block, P. and Ochsendorf, J. (2007). Thrust Network Analysis: a new methodology for three-dimensional equilibrium. *Journal of the International Association for Shell and Spatial Structures*, 48(3).
- Bow, R. H. (1873). *Economics of Construction in relation to Framed Structures*. E. & F. N. Spon, London.
- Calladine, C. (1978). Buckminster Fuller's Tensegrity Structures and Clerk Maxwell's Rules for the Construction of Stiff Frames. 14:161–172.
- Calladine, C. R. (1983). *Theory of Shell Structures*. Cambridge University Press, New York.
- Callen, H. B. (1985). *Thermodynamics and an Introduction to Thermostatistics*. Wiley, second edition.
- Charlton, T. (1982). *A History of Theory of Structures in the 19th century*. Cambridge University Press, Cambridge.
- Chasles, M. (1875). *Aperçu Historique sur l'Origine et le Développement des Méthodes en Géométrie, particulièrement de celles qui se rapportent à la Géométrie Moderne*. Gauthier-Villars, Paris.
- Collins, M. and Mitchell, D. (1980). Shear and torsion design of prestressed and non prestressed concrete beams. *Journal of the Prestressed Concrete Institute*, 25(5):32–100.
- Connelly, R. (1993). Rigidity. In *Handbook of Convex Geometry*. Elsevier Science Publishers, Netherlands.
- Connelly, R. and Whiteley, W. (1996). Second-order Rigidity and Prestress Stability for Tensegrity Frameworks. *SIAM J. DISCRETE MATH*, 9(3):453–491.
- Coxeter, H. (1969). *Introduction to Geometry*. John Wiley & Sons, INC., New York, second edition.
- Coxeter, H. (1974). *Projective Geometry*. Springer-Verlag, New York, second edition.
- Crapo, H. (1979). Structural Rigidity. *Structural Topology*, 1:26–45.
- Crapo, H. and Whiteley, W. (1994). 3-Stresses in 3-Space and Projections of Polyhedral 3-surfaces: Reciprocals, Liftings and Parallel Configurations. *Preprint*.
- Cremona, L. (1872). *Le Figure Reciproche nella Statica Grafica*. Tipografia di Giuseppe Bernardoni, Milano, 1879 edition.
- Cremona, L. (1885). *Elements of Projective Geometry*. Clarendon Press, Oxford.
- Cremona, L. (1890). *Graphical Statics, two treatises on the Graphical Calculus and Reciprocal Figures in Graphical Statics*. Clarendon Press, Oxford.

- Cromwell, P. R. (1997). *Polyhedra*. Cambridge, cambridge university press edition.
- Culmann, K. (1875). *Die Graphische Statik*. Verlag von Meyer & Zeller, Zurich.
- D'Acunto, P., Jasienski, J.-P., Ohlbrock, P. O., and Fivet, C. (2017). Vector-Based 3d Graphic Statics: Transformations of Force Diagrams. In *International Association for Shell and Spatial Structures (IASS)*, Hamburg.
- D'Acunto, P., Jasienski, J.-P., Ohlbrock, P. O., Fivet, C., Schwartz, J., and Zastavni, D. (2019). Vector-based 3d graphic statics: A framework for the design of spatial structures based on the relation between form and forces. *International Journal of Solids and Structures*, 167:58–70.
- Denton, S. (2001). Compatibility requirements for yield-line mechanisms. *International Journal of Solids and Structures*, 38(18):3099–3109.
- Drucker, D. C. (1961). On Structural Concrete and the Theorems of Limit Analysis. *International Association for Bridge and Structural Engineering (IABSE)*, 21:49–59.
- Fivet, C. (2016). Projective transformations of structural equilibrium. *International Journal of Space Structures*, 31:135–146.
- Fraternali, F. (2010). A thrust network approach to the equilibrium problem of unreinforced masonry vaults via polyhedral stress functions. *Mechanics Research Communications*, 37:198–204.
- Fraternali, F. and Carpentieri, G. (2014). On the correspondence between 2d force networks and polyhedral stress functions. *International Journal of Space Structures*, 29:145–159.
- Gray, J. (2010). *Worlds Out of Nothing: A course in the History of Geometry in the 19th century*. SUMS. Springer, New York.
- Gvozdev, A. A. (1960). The determination of the value of the collapse load for statically indeterminate systems undergoing plastic deformation. *International Journal of Mechanical Sciences*, 1(4):322 – 335.
- Hablicsek, M., Akbarzadeh, M., and Guo, Y. (2019). Algebraic 3d graphic statics: Reciprocal constructions. *Computer-Aided Design*, 108:30–41.
- Harman, P. (1990). *The scientific Letters and Papers of James Clerk Maxwell*. Cambridge, cambridge university press edition.
- Harman, P. (1998). *The Natural Philosophy of James Clerk Maxwell*. Cambridge, cambridge university press edition.
- Harman, P. (2004). Maxwell, James Clerk (1831-1879), physicist. *Oxford Dictionary of National Biography*.
- Hemp, W. (1973). *Optimum Structures*. Clarendon Press, Oxford.
- Henneberg, L. (1911). *Die Graphische Statik der Starren Systeme*. Leipzig und Berlin, druck und verlag von b. g. teubner edition.

- Heyman, J. (1995). *The Stone Skeleton: Structural Engineering of Masonry Architecture*. Cambridge University Press, Cambridge.
- Heyman, J. (2008). *Basic Structural Theory*. Cambridge University Press, Cambridge.
- Houlsby, G. and Puzrin, A. M. (2007). *Principles of Hyperplasticity: An Approach to Plasticity Theory Based on Thermodynamic Principles*. Springer-Verlag, London.
- James, I. M. (1999). *History of Topology*. Elsevier, Great Britain.
- Jasienski, J.-P., D'Acunto, P., Ohlbrock, P. O., and Fivet, C. (2016). Vector-based 3d Graphic Statics (Part II): Construction of Force Diagrams. In *International Association for Shell and Spatial Structures (IASS)*, Tokyo.
- Konstantatou, M., D'Acunto, P., and McRobie, A. (2018). Polarities in structural analysis and design: n-dimensional graphic statics and structural transformations. *International Journal of Solids and Structures*, 152-153:272–293.
- Konstantatou, M., D'Acunto, P., McRobie, A., and Schwartz, J. (2019a). Application of Graphic Statics and Theory of Plasticity to the design of strut-and-tie models in reinforced concrete. In *International Association for Shell and Spatial Structures (IASS)*, Barcelona.
- Konstantatou, M., D'Acunto, P., McRobie, A., and Schwartz, J. (2019b). Applications of Graphic Statics to Design and Analysis of Structural Concrete: Strut-and-tie Models and Yield Line Theory. In *Proceedings of the International fib Symposium on Conceptual Design of Structures*, Madrid.
- Konstantatou, M. and McRobie, A. (2016). Reciprocal constructions using conic sections and Poncelet duality. In *International Association for Shell and Spatial Structures (IASS)*, Tokyo.
- Konstantatou, M. and McRobie, A. (2017). 3d Graphic statics and graphic kinematics for spatial structures. In *International Association for Shell and Spatial Structures (IASS)*, Hamburg.
- Konstantatou, M. and McRobie, A. (2018). Graphic statics for optimal trusses & Geometry-based structural optimisation. In *International Association for Shell and Spatial Structures (IASS)*, Boston.
- Kostic, N. (2006). Computer-based development of stress fields. In *6th International PhD Symposium in Civil Engineering*, Zurich.
- Kupfer, H. (1964). Erweiterung der Möhrsch'schen Fachwerkanalogie mit Hilfe des 'Prinzips vom Minimum der Formänderungsarbeit (Expansion of Möhrsch's truss analogy by application of the principle of minimum strain energy). *CEB Bulletin*, 40.
- Kurrer, K.-E. (2008). *The History of the Theory of Structures, From Arch Analysis to Computational Mechanics*. Ernst & Sohn, Germany.
- Lachauer, L. and Block, P. (2014). Interactive Equilibrium Modelling. *International Journal of Space Structures*, 29(1):25–37.

- Lachauer, L. S. (2015). *Interactive Equilibrium Modelling: A New Approach to the Computer-Aided Exploration of Structures in Architecture*. PhD thesis, ETH Zurich, Zurich.
- Laman, G. (1970). On Graphs and Rigidity of Plane Skeletal Structures. *Journal of Engineering Mathematics*, 4(4):331 – 340.
- Lee, J., Van Mele, T., and Block, P. (2018). Disjointed force polyhedra. *Computer-Aided Design*, 99:11–28.
- Leonhardt, F. (1965). Reducing the shear reinforcement in reinforced concrete beams and slabs. *Mag. Concrete Research*, 17(53):187.
- Leonhardt, F. and Walther, R. (1966). *Wandartige Träger (Deep Beams)*. Number Heft No.178 in DAFStb. Berlin, w. ernst & sohn edition.
- Lhuillier, G. (1812). Memoire sur la polyedrometrie. *Annales de Mathematiques pures et appliquees*, 3:169–189.
- Liang, Q. Q., Xie, Y. M., and Steven, G. P. (2000). Topology Optimization of Strut-and-Tie Models in Reinforced Concrete Structures Using an Evolutionary Procedure. *ACI Structural Journal*, 97(2):322–332.
- Loeb, A. (1991). Schlegel Diagrams. In *Space Structures*, Design Science Collection. Boston, birkhäuser edition.
- Malerba, P., Patelli, M., and Quagliaroli, M. (2012). An Extended Force Density Method for the form-finding of cable systems with new forms. *Structural Engineering and Mechanics*, 42(2):191–210.
- Marti, P. (1985). Basic tools of reinforced concrete beam design. *American Concrete Institute (ACI) Journal*, 82(1):46–56.
- Maxwell, J. (1855). On Faraday’s Lines of Force. *Transactions of the Cambridge Philosophical Society*, X:156–229.
- Maxwell, J. (1864a). On Reciprocal Figures and Diagrams of Forces. *Philosophical Magazine and Journal of Science*, 26:250–261.
- Maxwell, J. (1864b). On the calculation of equilibrium and the stiffness of frames. *The London, Edinburgh, and Dublin Philosophical Magazine and Journal of Science*, XXVII:294–299.
- Maxwell, J. (1867). On the Application of the theory of reciprocal polar figures to the construction of diagrams of forces. *The Engineer*, 24:402.
- Maxwell, J. (1870). On Reciprocal Figures, Frames, and Diagrams of Forces. *Transactions of the Royal Society of Edinburgh*, 7:160–208.
- Mazurek, A. (2012). Geometrical Aspects of Optimum Truss Like Structures for Three-force Problem. *Struct. Multidiscip. Optim.*, 45(1):21–32.
- Mazurek, A., Baker, W., and Tort, C. (2010). Geometrical aspects of optimum truss like structures. *Structural and Multidisciplinary Optimization*, 43:231–242.

- Mazurek, A., Beghini, A., Carrion, J., and Baker, W. F. (2016). Minimum weight layouts of spanning structures obtained using graphic statics. *International Journal of Space Structures*, 31(2-4):112–120.
- McClure, M. (2005). Steffen’s flexible polyhedron. *Preprint version of a “Mathematical graphics” column from Mathematica in Education and Research*, 10(4).
- McRobie, A. (2016). Maxwell and Rankine reciprocal diagrams via Minkowski sums for two-dimensional and three-dimensional trusses under load. *International Journal of Space Structures*, 31(2-4):203–216.
- McRobie, A. (2017a). The geometry of structural equilibrium. *Royal Society Open Science*, 4(3):10.1098/rsos.160759.
- McRobie, A. (2017b). Graphic analysis of 3d frames: Clifford algebra and Rankine Incompleteness. In *International Association for Shell and Spatial Structures (IASS)*, Hamburg.
- McRobie, A., Baker, W., Mitchell, T., and Konstantatou, M. (2015). Mechanisms and states of self-stress of planar trusses using graphic statics, Part III: Applications and extensions. In *International Association for Shell and Spatial Structures (IASS)*, Amsterdam.
- McRobie, A., Baker, W., Mitchell, T., and Konstantatou, M. (2016). Mechanisms and states of self-stress of planar trusses using graphic statics, Part II: Applications and extensions. 31(2):102–111.
- McRobie, A., Konstantatou, M., Athanasopoulos, G., and Hannigan, L. (2017). Graphic kinematics, visual virtual work and elastographics. *Royal Society Open Science*, 4(5):170–202.
- Micheletti, A. (2008). On generalized reciprocal diagrams for self-stressed networks. *International Journal of Space Structures*, 23:153–166.
- Michell, A. (1904). The Limits of Economy of Material in Frame-structures. *Philosophical Magazine*, 8(47):589–597.
- Miki, M., Igarashi, T., and Block, P. (2015). Parametric Self-supporting Surfaces via Direct Computation of Airy Stress Functions. *ACM Trans. Graph.*, 34(4):89:1–89:12.
- Miki, M. and Kawaguchi, K. (2010). Extended force density method for form-finding of tension structures. *Journal of the International Association for Shell and Spatial Structures*, 51(4):291–303.
- Mitchell, T., Baker, W., McRobie, A., and Mazurek, A. (2016). Mechanisms and states of self-stress of planar trusses using graphic statics, part I: The fundamental theorem of linear algebra and the Airy stress function. *International Journal of Space Structures*, 31(2-4):85–101.
- Müller, P. (1978). Plastische Berechnung von Stahlbetonscheiben und Balken (Plastic analysis of reinforced concrete deep beams and beams). *Presentation for Bericht No. 83, Institut für Baustatik und Konstruktion, ETH Zürich*.

- Motro, R. (2003). *Tensegrity Structural Systems for the Future*. Butterworth-Heinemann, London.
- Moy, S. S. J. (1981). *Plastic Methods for Steel and Concrete Structures*. The MacMillan Press Ltd, Hong Kong.
- Muttoni, A., Fernández, R. M., and Niketic, F. (2015). Design versus Assessment of Concrete Structures Using Stress Fields and Strut-and-Tie Models. *ACI Structural Journal*, 112(5):605–616.
- Muttoni, A., Schwartz, J., and Thürlimann, B. (1997). *Design of Concrete Structures with Stress Fields*. Birkhaeuser, Basel.
- Muttoni, A. (2011). *The Art of Structures: Introduction to the Functioning of Structures in Architecture*. EPFL Press.
- Neyrinck, M. C., Hidding, J., Konstantatou, M., and van de Weygaert, R. (2018). The cosmic spiderweb: Equivalence of cosmic, architectural and origami tessellations. *Royal Society Open Science*, 5(4):171582.
- Ohlbrock, P. O., D’Acunto, P., Jasienski, J.-P., and Fivet, C. (2017). Constraint-Driven Design with Combinatorial Equilibrium Modelling Vector-Based 3d Graphic Statics: Transformations of Force Diagrams. In *International Association for Shell and Spatial Structures (IASS)*, Hamburg.
- Ohlbrock, P. O. and Schwartz, J. (2016). Combinatorial equilibrium modeling. *International Journal of Space Structures*, 31(2-4):177–189.
- Pellegrino, S. (1993). Structural Computations with the Singular Value Decomposition of the Equilibrium Matrix. *International Journal of Solids and Structures*, 30(21):3025–3035.
- Poincare, M. H. (1895). Analysis Situs. *Journal de L’Ecole Polytechnique*, pages 1–50.
- Poncelet, J. V. (1822). *Traité des propriétés projectives des figures*, volume 1. Bachelier, Paris.
- Rankine, M. (1864). Principle of the equilibrium of polyhedral frames. *Philosophical Magazine*, 27:92.
- Rankine, W. (1858). *A Manual of Applied Mechanics*. Richard Griffin and Company, Glasgow.
- Rippmann, M. and Block, P. (2013). Funicular Shell Design Exploration. In *Adaptive Architecture*, Waterloo/ Buffalo/Nottingham.
- Rippmann, M., Lachauer, L., and Block, P. (2012). Interactive Vault Design. *International Journal of Space Structures*, 27(4):219–230.
- Rosenfeld, B. (1988). *A History of non-Euclidean Geometry, Evolution of the Concept of a Geometric Space*. Number 12 in Studies in the History of Mathematics and Physical Sciences. Springer-Verlag, New York.

- Rüsch, H. (1964). Über die Grenzen der Anwendbarkeit der Fachwerkanalogie bei der Berechnung der Schubfestigkeit von Stahlbetonbalken (On the limitations of applicability of the truss analogy for the shear design of RC beams). *Lecture for Festschrift F. Campus 'Amici et Alumni', Université de Liège*.
- Sauer, R. (1970). *Differenzengeometrie*. Springer-Verlag, Berlin/Heidelberg.
- Schek, H. J. (1974). The force density method for form finding and computation of general networks. *Computer Methods in Applied Mechanics and Engineering*, 3(1):115–134.
- Schenk, M., Guest, S., and Herder, J. (2007). Zero stiffness tensegrity structures. *International Journal of Solids and Structures*, 44:6569–6583.
- Schlaich, J. and Schäfer, K. (1991). Design and detailing of structural concrete using strut-and-tie models. *The Structural Engineer*, 69(6):113–125.
- Schlaich, J., Schäfer, K., and Jennewein, M. (1987). Toward a Consistent Design of Structural Concrete. *Technical report in PCI Journal*.
- Shell, M. S. (2015). *Thermodynamics and Statistical Mechanics: An Integrated Approach*. Cambridge Series in Chemical Engineering. Cambridge University Press, Cambridge.
- Smith, C. (1886). *Elementary Treatise on Solid Geometry*. Macmillan and Co., London.
- Tachi, T. (2012). Design of infinitesimally and finitely flexible origami based on reciprocal figures. *J. Geom. Graph.*, 16:223–234.
- Tarnai, T. (1989). Duality between plane trusses and grillages. *International Journal of Solids and Structures*, 25(12):1395–1409.
- Thürlimann, B., Marti, P., Pralong, J., Ritz, P., and Zimmerli, B. (1983). Vorlesung zum Fortbildungskurs für Bauingenieure (Advanced lecture for Civil Engineers). *Institut für Bautechnik und Konstruktion, ETH Zürich*.
- Tjhin, T. N. and Kuchma, D. A. (2007). Integrated analysis and design tool for the strut-and-tie method. *Engineering Structures*, 29:3042–3052.
- Vaisman, I. (1997). *Analytical Geometry*, volume 8 of *Series on University Mathematics*. World Scientific Publishing Co. Pte. Ltd., Singapore.
- Vansice, K., Kulkarni, A., Hartz, C., Baker, W. F., and Konstantatou, M. (2018). A 3d Airy Stress Function Tool for Reciprocal Graphic Statics. In *International Association for Shell and Spatial Structures (IASS)*, Boston.
- Varignon, P. (1725). *Nouvelle Mécanique ou Statique*. Claude Jombert, Paris.
- Wallner, J. and Pottman, H. (2008). Infinitesimally flexible meshes and discrete minimal surfaces. *Monat. Math.*, 153:347–365.
- Wester, T. (1989). The Dualistic Symmetry between Plane- and Point-based Spatial Structures. In *Symmetry of Structure*, Hungary.



- Wester, T. (2011). 3-D Form and Force Language Proposal for a Structural Basis. *International Journal of Space Structures*, 26(3).
- Whiteley, W. (1982). Motions and Stresses of Projected Polyhedra. *Structural Topology*, 7:13–38.
- Whiteley, W. (1987). Rigidity and Polarity I: Statics of Sheet Structures. *Geometriae Dedicata*, 22:329–362.
- Whiteley, W., Ash, P. F., Bolker, E., and Crapo, H. (2013). Convex Polyhedra, Dirichlet Tessellations, and Spider Webs. In *Shaping Space: Exploring Polyhedra in Nature, Art, and the Geometrical Imagination*. Springer-Verlag, New York.
- Williams, C. (2001). *The Analytic and Numerical definition of the Geometry of the British Museum Great Court Roof*, pages 434–440. Deakin University, Geelong, Victoria 3217, Australia.
- Williams, C. and McRobie, A. (2016). Graphic statics using discontinuous Airy stress functions. *International Journal of Space Structures*, 31(2-4):121–134.
- Wolfe, W. S. (1921). *Graphical Analysis: A Text Book on Graphic Statics*. McGraw-Hill Book Company, Inc., New York.
- Zalewski, W. and Allen, E. (1998). *Shaping Structures, Statics*. John Wiley & Sons, INC., Unites States of America.
- Zanni, G. and Pennock, G. R. (2009). A unified graphical approach to the static analysis of axially loaded structures. *Mechanism and Machine Theory*, 44(12):2187–2203.
- Zhang, J. Y. and Ohsaki, M. (2006). Adaptive force density method for form-finding problem of tensegrity structures. *International Journal of Solids and Structures*, 43(18):5658 – 5673.



# Appendix A

## Algebraic description of Lemma.01

Two planes  $\pi_1$ ,  $\pi_2$  intersect in a line  $l_3$  on which points  $\mathbf{P}_1 = [x_1, y_1, z_1]'$ ,  $\mathbf{P}_2 = [x_2, y_2, z_2]'$  lie on. The projection of this line ( $l_{3pr}$ ) is given by the two fixed points:  $\mathbf{P}_{1pr} = [x_1, y_1, 0]'$ ,  $\mathbf{P}_{2pr} = [x_2, y_2, 0]'$ . Given that the planes go through the given lines  $l_1$ ,  $l_2$  respectively, we find the  $z$ -coordinate of the point  $\mathbf{P}_1$  which satisfy the fixed elements:  $l_1$ ,  $l_2$ ,  $\mathbf{P}_{1pr}$  and  $\mathbf{P}_{2pr}$ .

We express line  $l_1$  as:

$$l_1 = \mathbf{A}_1 + \mathbf{B}_1 t$$

and line  $l_2$  as:

$$l_2 = \mathbf{A}_2 + \mathbf{B}_2 t$$

as a result,

$$\mathbf{n}_1 = \mathbf{B}_1 \times (\mathbf{A}_1 - \mathbf{P}_1)$$

and

$$\mathbf{n}_2 = \mathbf{B}_2 \times (\mathbf{A}_2 - \mathbf{P}_2)$$

Then the equations of planes  $\pi_1$ ,  $\pi_2$  are respectively:

$$\mathbf{n}_1 \cdot \mathbf{X} = D_1$$

and

$$\mathbf{n}_2 \cdot \mathbf{X} = D_2$$

where  $\mathbf{X} = [x, y, z]'$

Given that points  $\mathbf{P}_1, \mathbf{P}_2$  belong to both planes  $\pi_1, \pi_2$ , that  $x_1, y_1, x_2, y_2$  are known and only the  $z$ -coordinates  $z_1, z_2$  remain to be found, we substitute the coordinates of  $\mathbf{P}_1, \mathbf{P}_2$  in the above two equations to find the two unknowns.